

# Offshore Pipeline Flotation during Sand Backfilling with a TSHD

An Experimental Study

**P.M.A. Eikhout**

**MSc. Thesis Geo-Engineering**  
Delft University of Technology  
Faculty of Civil Engineering and Geosciences



# Offshore Pipeline Flotation during Sand Backfilling with a TSHD

## An Experimental Study

by

P.M.A. Eikhout

to obtain the degree of Master of Science  
at the Delft University of Technology,  
to be defended publicly on Monday January 25, 2021.

Student number:	4396081	
Date:	January 18, 2021	
Thesis committee:	Dr. F. Pisanò,	TU Delft, chair
	Dr. ir. A.M. Talmon,	TU Delft, supervisor
	Dr. ir. W. Broere,	TU Delft, supervisor
	Ir. W.J. Karreman,	Van Oord, supervisor
	Ir. E.F. Uelman,	Van Oord, supervisor

An electronic version of this thesis is available at <http://repository.tudelft.nl/>.



# Abstract

Offshore pipelines represent major items in the oil and gas industry nowadays. These submarine pipelines are usually covered with backfill for protection and a well-known method for this is sand backfilling with a trailing suction hopper dredger (TSHD). Although pipeline installation with a TSHD is a developed technique, there are still some challenges regarding uplift movements of the pipeline during the backfill procedure. This action is called pipeline flotation, which is a frequently occurring problem during the sand backfilling process and the costs for repair measures afterwards are very expensive. Accurate modelling of the sand backfilling process over a pipeline can lead to significant cost reductions by optimising the sand backfilling technique.

Pipeline flotation is induced by the development of upward buoyancy forces from the sand-water mixture on the pipeline. If the weight of the pipeline is not sufficient enough, it will experience uplift movements during the backfilling process. The purpose of this research is to develop a better understanding of the mechanism of pipeline flotation. Due to a lack of available field data, it is anticipated that a set of laboratory experiments will provide a better insight into the parameters involved in pipeline flotation during sand backfilling.

This research builds on the study of Yang (2020), in which a small-scale set-up and 2D calculation model are designed to perform experiments concerning pipeline flotation during sand backfilling [20]. A total amount of 50 experiments is performed with Geba Weiss sand in four different stages, so experiments are performed with: horizontal discharge, vertically upward discharge, elevated initial pipe positions and increased pipe specific weights. The set of experiments have provided better insight into physical processes that influence pipeline flotation during sand backfilling.

The discharge of the sand-water mixture is dominated by its sedimentation and dispersion, so the model is based on empirical equations and the sedimentation theory. The main conclusion regarding the static force balance on the pipe is that the degree of pipe embedment influences the magnitude of an additional frictional force working downwards on the pipe body. A new approach for assessing this frictional downward force, due to the presence of sand that has deposited, is described and added to the model. In the small-scale experiments, this influence plays a significant role in pipe flotation triggering. An undesirable result from the small-scale experiments are the additional hydrodynamic effects from the fluid in the experimental tank, which are induced by the geometrical constraints.

A pipe flotation limit was found in the parameter of sand volume concentration in the surroundings of the pipe. This flotation limit was defined at a domain concentration of approximately 7.5% for the experiments with a pipe specific gravity of 1.03. The boundary of flotation for heavier pipes was not achieved in this research, but evidence points towards a significantly higher flotation limit. The discharge flow rate and the total discharged sand volume are the key factors for development of domain concentration in the small-scale experiments.

With the acquired data as a strong foundation, additional research regarding pipe flotation during sand backfilling is recommended. As there is still a strong variation in several important input parameters in the small-scale experiments, a Computational Fluid Dynamics (CFD) analysis is suggested to relate the domain concentration to the input parameters at every moment in time. Additional 3D experiments on a larger scale are also recommended to optimise the sand backfilling process and validate the CFD analysis. From this analysis, a prediction can be made regarding the boundary of pipeline flotation on the seabed when discharging with a TSHD. Moreover, additional research regarding the stress and drainage conditions underneath the pipe is proposed to validate the cause and accuracy of the relatively high friction coefficients. Finally, a model could be built to examine the friction force generated on the pipe due to its embedment. With this method, the suggested approach of the frictional resistance due to pipe embedment could be further analysed.



# Preface

This thesis describes the process of a small-scale experimental study regarding offshore pipeline flotation during sand backfilling with a TSHD. This research is part of the MSc. programme Geo-Engineering at the faculty of Civil Engineering and Geosciences at Delft University of Technology, and has been conducted in collaboration with Van Oord.

First of all, I would like to thank the chair of my thesis committee Dr. Federico Pisanó for his great guidance and support during this research. Furthermore, my gratitude goes out to Ir. Wouter Karreman and Ir. Evert Uelman from Van Oord for their advice and for the weekly meetings that helped me through my work. I would also like to thank my other supervisors Dr. ir. Arnold Talmon and Dr. ir. Wout Broere for their insightful help and for keeping me attentive at all times. It has all been very much appreciated.

A word of thanks to Kaiyue Yang for starting this research and for always being available to help me understanding every part of the experimental set-up. Moreover, I would like to express my gratitude to Ed Stok and Andre van den Bosch, who have helped me with the experimental set-up in the laboratory from the first moment I got there, for always being there for me and for thinking along.

Finally, I would like to thank my family and friends for their endless support and patience, not only during this research, but over the entire course of my studies.

I hope you enjoy your reading,

*Pippi Eikhout*  
January 18, 2021



# Contents

<b>List of Tables</b>	<b>ix</b>
<b>List of Figures</b>	<b>xi</b>
<b>Nomenclature</b>	<b>xiii</b>
<b>1 Introduction</b>	<b>1</b>
1.1 Background . . . . .	1
1.2 Problem Description . . . . .	2
1.3 Research Questions . . . . .	2
1.4 Assumptions and limitations . . . . .	3
1.5 Outline . . . . .	3
<b>2 Literature Review</b>	<b>5</b>
2.1 TSHD Sand Backfilling Process . . . . .	5
2.2 Sedimentation Process . . . . .	7
2.3 Pipe-Soil Interaction . . . . .	7
<b>3 Small-Scale Physical Modelling of Pipe Flotation</b>	<b>11</b>
3.1 Experimental Set-Up . . . . .	11
3.2 Experimental Procedure . . . . .	14
3.2.1 Stage 1: Discharging horizontal and checking the spatial variability. . . . .	14
3.2.2 Stage 2: Discharging upwards. . . . .	15
3.2.3 Stage 3: Increasing the pipe elevation . . . . .	15
3.2.4 Stage 4: Increasing the pipe specific gravity . . . . .	16
3.2.5 Testing Programme. . . . .	16
3.3 Measurements and Data Processing . . . . .	19
3.3.1 Sand concentration. . . . .	19
3.3.2 Sedimentation . . . . .	20
3.3.3 Discharge conditions . . . . .	21
3.3.4 Pressure increments . . . . .	22
3.3.5 Specific gravity . . . . .	23
3.3.6 Pipe displacements. . . . .	26
<b>4 Experimental Parametric Studies</b>	<b>29</b>
4.1 Influence of Domain Concentration . . . . .	29
4.2 Influence of Pipe Embedment . . . . .	31
4.3 Influence of Hydrodynamic Effects . . . . .	36
4.4 Influence of Pipe Specific Gravity . . . . .	38
<b>5 Discussion</b>	<b>41</b>
<b>6 Conclusion and Recommendations</b>	<b>43</b>
6.1 Conclusion . . . . .	43
6.2 Recommendations . . . . .	44
<b>Bibliography</b>	<b>45</b>
<b>A Force Meter Data</b>	<b>47</b>
<b>B Experimental Data</b>	<b>49</b>



# List of Tables

3.1	Overview prototype and laboratory set-up parameters . . . . .	13
3.2	Geba Weiss sand properties . . . . .	13
3.3	Technical specifications of the sensors . . . . .	13
3.4	Overview of all performed experiments with the input parameters . . . . .	18
4.1	Normal stress and friction values for the different pipes used in this research . . . . .	33
B.1	Numerical overview of the results of all experiments performed in this research . . . . .	50



# List of Figures

1.1	An example concept picture of a TSHD from Van Oord and its workings during sand backfilling of an offshore pipeline [11] . . . . .	1
2.1	Schematic drawing of a one-dimensional section of the pipeline, which is partially buried and fully surrounded by a sand-water mixture . . . . .	6
2.2	Schematisation of the pipe-soil contact stress parameters . . . . .	8
2.3	Difference between the shear strength failure envelope with the assumption of constant friction (MC) with a typical friction angle of 30 degrees or with a sigma-dependant friction . . . . .	9
3.1	A schematic overview of the laboratory set-up . . . . .	12
3.2	Schematic overview of sensors in the experimental tank, slightly different from Yang (2020) [20] . . . . .	14
3.3	The V-shaped design of the structure and the method to elevate the pipe during the experiments . . . . .	16
3.4	The development of sand concentration in time and space during Test VNL15 . . . . .	20
3.5	Comparison between the direction of discharge during the small-scale experiments . . . . .	21
3.6	The development of DP net increment over time, together with the pipe displacements from Test VNL12 . . . . .	23
3.7	The development of specific gravity over time, together with the pipe displacements from Test VNL12 . . . . .	25
3.8	An overview of the maximum pipe displacement over the maximum domain concentration of all experiments performed in this research with the same pipe specific gravity of 1.03 . . . . .	27
4.1	Overview of the obtained maximum domain concentrations at the corresponding average discharge flow rate during all performed experiments with a pipe specific gravity of 1.03 . . . . .	30
4.2	Schematic drawing of the forces on a one-dimensional section of the pipeline, which is partially buried and fully surrounded by a sand-water mixture, and the corresponding parameters . . . . .	32
4.3	Influence of the pipe embedment on the downward working friction force . . . . .	33
4.4	Determination of the start of flotation based on buoyant specific gravity on the pipe and based on the normalised force balance in Test VNL15 . . . . .	35
4.5	Determination of the start of flotation based on buoyant specific gravity on the pipe and based on the normalised force balance in Test VNL13 . . . . .	35
4.6	Overview of the obtained maximum domain concentrations at the corresponding average discharge flow rate during the experiments with both horizontal discharge and vertical discharge and where the pipe, of specific gravity 1.03, initially lays on top of the sand bed . . . . .	37
4.7	Determination of the start of flotation based on buoyant specific gravity on the pipe and based on the normalised force balance in Test VNL14 . . . . .	37
4.8	Overview of the obtained maximum domain concentrations at the corresponding average discharge flow rate during the experiments with vertical discharge and where the pipe, with a varying specific gravity, initially lays on top of the sand bed . . . . .	39
A.1	An indication of the influence of pipe embedment on the force needed to lift the pipe from the tests with a force meter in the small-scale experiments . . . . .	47



# Nomenclature

## Abbreviations

*CFD* Computational Fluid Dynamics

*DP* Differential pressure sensor

*MC* Mohr-Coulomb

*SOD* Stand-off distance

*TSHD* Trailing suction hopper dredger

## Symbols

$\beta$  Semi-angle subtended by the contact surface of the sedimentation front

$\Delta h$  Cover sand layer thickness

$\Delta h_p$  Cover sand layer thickness in the prototype

$\Delta P_{DP,80}$  Pressure increment at a height of 80 cm measured by a DP

$\Delta P_{DP,h+\Delta h,net}$  Net pressure increment at height  $h + \Delta h$  measured by a DP

$\Delta P_{DP,h,net}$  Net pressure increment at height  $h$  measured by a DP

$\Delta P_{DP,h}$  Pressure increment at height  $h$  measured by a DP

$\mu$  Friction coefficient

$\nu$  Kinematic viscosity of sand

$\phi$  Friction angle

$\phi_{int}$  Interface friction angle between pipe and soil

$\psi$  Angle of dilation

$\rho_m$  Density of the sand-water mixture around the pipe

$\rho_p$  Density of the empty pipe

$\rho_s$  Density of a sand particle

$\rho_w$  Density of pure water

$\rho_{p,p}$  Density of the pipe in the prototype

$\rho_{seawater}$  Density of the seawater

$\sigma'_r$  Normal stress on the pipe-soil contact surface

$\sigma'_{r,avg}$  Average normal stress on the pipe-soil contact surface

$\tau$  Shear stress on the pipe-soil contact surface

$\theta$  Inclination from the vertical

$A_p$  Cross-sectional area of the pipe

---

$A_{dis,p}$	Cross-sectional area of the suction pipe in the prototype
$A_{eff,i}$	Effective area of the pipe in the subordinate area of the $i^{th}$ conductivity probe
$A_{eff}$	Effective area of the pipe; the area that is above the sedimentation front
$C_1$	Constant for particle settling velocity
$C_2$	Shape factor for particle settling velocity
$C_D$	Non-dimensional drag coefficient
$C_s$	Sand volume concentration
$C_u$	Uniformity coefficient
$C_{bed}$	Volume concentration of the sand bed
$C_{dis,avg}$	Average discharge sand volume concentration
$C_{dis,p}$	Discharge sand volume concentration in the prototype
$C_{dis}$	Discharge sand volume concentration
$C_{max}$	Maximum sand volume concentration in the domain around the pipe
$C_{s,h}$	Sand volume concentration at height $h$
$D$	Diameter of the pipe
$d$	Diameter of a sand particle
$D_p$	Diameter of the pipe in the prototype
$d_{10}$	Cumulative 10% of the diameter of the sand particles
$d_{50,p}$	Median diameter of a sand particle in the prototype
$d_{50}$	Median diameter of the sand particles
$d_{60}$	Cumulative 60% of the diameter of the sand particles
$D_{dis,p}$	Diameter of the suction pipe in the prototype
$Dis_{max}$	Maximum displacement of the pipe
$ds$	Infinitesimal part along the pipe-soil contact surface
$dT$	Elementary vertical force due to friction
$F$	Total friction force per unit of length on the pipe
$F_{down}$	Downward force generated on the pipe
$F_p$	Force generated on the pipe
$F_{up}$	Upward force generated on the pipe
$g$	Gravitational acceleration
$h$	Height
$h_{eff,i}$	Effective height of the pipe in the subordinate area of the $i^{th}$ conductivity probe
$h_{eff}$	Effective height of the pipe; the part of the pipe diameter that is above the sedimentation front
$L_p$	Length of the pipe

$n$	Sedimentation coefficient
$n_{bed}$	Porosity of the sand bed
$n_{max}$	Maximum porosity of the sand
$n_{min}$	Minimum porosity of the sand
$p_{atm}$	Atmospheric pressure
$q$	Resultant force per unit of length on the pipe
$q_n$	Normalised resultant force on the pipe
$Q_{cal}$	Average discharge flow rate
$Q_{dis}$	Discharge flow rate
$r$	Radius of the pipe
$Re$	Reynolds number
$s_i$	Specific gravity of the sand-water mixture measured by the $i^{th}$ conductivity probe
$s_p$	Specific gravity of the pipe
$s_s$	Specific gravity of sand particles
$s_w$	Specific gravity of pure water
$s_{con,a,max}$	Maximum value of the average specific gravity of the sand-water mixture around the pipe estimated by concentration without considering the shape effect
$s_{con,avg}$	Average specific gravity of the sand-water mixture around the pipe estimated by concentration without considering the shape effect
$s_{con,h}$	Specific gravity of the sand-water mixture estimated by the conductivity probe at height $h$
$s_{con,p}$	Average specific gravity of the sand-water mixture around the pipe estimated by concentration after considering the shape effect
$s_{DP,avg}$	Average specific gravity of the sand-water mixture around the pipe estimated by the DP's
$s_{DP,max}$	Maximum value of the average specific gravity of the sand-water mixture around the pipe estimated by the DP's
$SOD_p$	Stand-off distance in the prototype
$T$	Friction force per unit of length
$t_{dis}$	Time of discharge
$u_{dis,p}$	Discharge speed of the TSHD in the prototype
$V$	Buoyant weight of the pipe
$v_p$	Fall velocity of a sand particle for different flow conditions
$v_{trail,p}$	Trailing speed of the TSHD in the prototype
$w$	Embedment of the pipe
$w_0$	Fall velocity of a sand particle
$W_p$	Weight of the pipe
$w_s$	Hindered fall velocity of a sand particle in a suspension



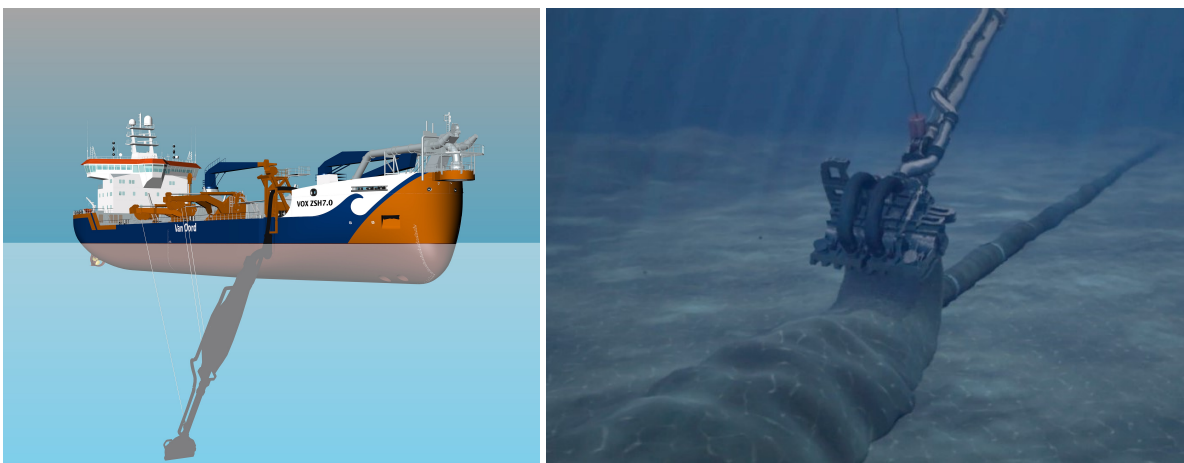
# Introduction

## 1.1. Background

The offshore industry has evolved tremendously in the previous decades. Nowadays, offshore pipelines in the seabed are essential to transport resources to land, especially in the oil and gas industry. Submarine pipelines are usually placed in trenches and covered with backfill to protect them against physical damage and to provide an increased thermal insulation. Furthermore, the backfill cover provides lateral resistance and thus restrains the pipelines from upheaval buckling. This final feature of backfilling stresses the importance of the mechanical properties of the backfill material.

Material for the burial of offshore pipelines can originate from a different site or from the excavated spoil from the trench itself. The most prevailing types of soil used as backfill material are rock and sand [12]. Since pipelines in the oil and gas industry are usually relatively light, sourcing and depositing rock to cover entire pipelines is rather expensive compared to using sand as backfill.

There are different techniques for trenching and backfilling pipelines in subsea environments with sand. A well-known method to trench and cover offshore pipelines is with a trailing suction hopper dredger (TSHD). Large and powerful pumps enable a TSHD to perform dredge, storage and backfill operations in the subsea. During backfilling, the TSHD pumps a sand-water mixture through a suction pipe over the pipeline in a pre-dredged trench. An example concept picture of a TSHD from Van Oord and the sand backfilling process over a pipeline in submarine environments are shown in Figure 1.1.



(a) An example concept picture of a TSHD from Van Oord

(b) Backfilling sand over an offshore pipeline with a TSHD suction pipe

Figure 1.1: An example concept picture of a TSHD from Van Oord and its workings during sand backfilling of an offshore pipeline [11]

## 1.2. Problem Description

Although submarine pipeline installation with a TSHD is a developed technique, there are still some challenges in this field. Multiple incidents have occurred in which the pipeline experiences excessive vertical displacements during the backfilling process [8]. The term used for this mechanism is pipeline flotation, which could lead to unprotected or even damaged offshore pipelines. As the offshore industry utilises relatively more light-weighted pipelines nowadays, the assessment of the pipeline flotation risk during backfilling has become increasingly prevalent.

As shown in Figure 1.1, in order to bury an offshore pipeline with a TSHD, a sand-water mixture is deposited by a draghead over the pipeline. The draghead, which is connected to a suction pipe, slowly trails over the pipeline with the purpose of covering its entire surface. During the backfilling process, the discharge rate of the soil-water mixture is larger than the sedimentation rate of its sand particles, which causes the mixture to build up a suspension around the pipeline. This suspension behaves like a dense slurry and generates buoyancy forces around the pipeline. If this buoyancy reaches a value larger than the specific gravity of the pipeline, it is prone to flotation. Considering that the offshore pipelines are currently composed of much lighter materials for economic reasons, the effect of buoyancy is even more critical.

Therefore, the most important aspects in this research are the properties of the pipeline itself and the properties regarding the developed buoyancy around this pipeline. However, there are other mechanisms during the backfilling process that are of great importance for the analysis of pipeline flotation. The sedimentation process of sand particles is the reason for the development of a dense suspension above the seabed, which inflicts buoyancy on the pipeline. The sedimentation rate of the sand particles depends on the soil properties of the backfill material. In addition, the soil properties of the seabed, on which the pipeline is positioned, are significant as the backfilling process could cause disturbances at the surface. One of the potential hazards in the submarine environment is the instability of the sand bed due to liquefaction. If liquefaction occurs, the pipeline may experience even more displacements than it is designed to withstand and failure could occur.

The parameters that influence the flotation potential of offshore pipelines can be divided in three different categories. They depend on: (1) the specifications of the pipeline, (2) the conditions of the draghead and (3) the composition of both the backfill material and the seabed. Parameters included in these categories are the pipe specific weight, the discharge rate of the draghead and the concentration of the sand-water mixture used as backfill.

A majority of the influential parameters are predetermined factors in the backfilling process. However, the distinct trigger of offshore pipeline flotation during the sand backfilling process is still unknown. In order to get insight into the exact mechanisms that influence the process, this research concerns the analysis of submarine pipeline flotation during sand backfilling.

## 1.3. Research Questions

A substantial amount of knowledge has been accumulated on the influence of liquefaction on buried offshore pipelines, and an effort has been made to study the influence of the specific weight of pipelines on pipeline flotation, but no conclusions can yet be drawn regarding pipeline flotation during the sand backfilling process of a TSHD. The purpose of this research is to develop a better understanding of the mechanism of pipeline flotation, which is induced by the development of buoyancy during the sand backfilling process. In order to achieve this insight, the following research questions need to be addressed:

- 1. How does buoyancy develop in the surroundings of the pipeline during sand backfilling?**
- 2. What is the boundary of reaching pipeline flotation for the different parameters involved during backfilling?**
- 3. How can pipeline flotation during TSHD sand backfilling be predicted?**

It is anticipated that a set of laboratory experiments will provide a better insight into the parameters involved in pipeline flotation during sand backfilling. Due to the lack of available data, Yang (2020) developed a 2D model to carry out experiments on a small scale with the purpose of investigating the development of buoyancy around a pipeline during backfilling [20]. The current research extends this study of Yang and his 2D experimental model is used, analysed and optimised. A series of multiple experiments with different implementations and varying input parameters is conducted in this composed laboratory set-up.

## 1.4. Assumptions and limitations

To translate the 3D sand backfilling process with a TSHD into a 2D small-scale experiment, several assumptions are made and some limitations can be identified. First of all, the pipe is simulated by a finite rigid body, for which any horizontal displacements are prevented from taking place. This way, local bending of the pipeline due to possible unequal loading is disregarded. Despite this event being excluded from the current research, in reality this local bending is still a structural problem in the offshore pipeline industry [8].

Mobile and irregular loading can be caused during backfilling with a TSHD, because the ship discharges the sand-water mixture while moving with a constant speed over the pipeline. To eliminate this 3D irregularity in the model, the mobile discharge in the field is simulated by a stationary line discharge in the experiment over the entire rigid body.

Additionally, the turbulence caused by the mobile TSHD suction pipe and by the discharge of the backfill material is ignored and thus the potentially developed whirling motions of the mixture are also not taken into account in this research. The degree of turbidity of the mixture depends on the specifications of the draghead of the TSHD and on the background currents present in the sea during backfilling. As the TSHD backfilling situation is translated to 2D small-scale experiments, these factors are not taken into account in the model.

The sedimentation mechanism is a very significant factor during these backfilling operations, so it is thoroughly observed in the experiments. The opposite mechanism of sedimentation, erosion, could also occur due to the disturbance of the sand bed when backfilling in the field. However, the effects of erosion are not considered in this model and they are avoided as much as possible in the experiments. The effects of erosion on pipeline flotation could be computed in further research, once there is a proper understanding of the sedimentation process and the buoyancy development around the pipe.

Finally, to simplify this research, the influence of thermal changes, natural infill and background flow are neglected. These simplifications are applied to focus exclusively on the development of buoyancy due to the backfilling process itself, disregarding these potential external influences for now.

## 1.5. Outline

This study continues with a brief literature study in Chapter 2. In Chapter 3, the experimental framework for this research is explained. The specifications of the physical modelling are described here. Chapter 4 describes the experimental parametric studies, in which the most influential mechanisms regarding pipeline flotation during sand backfilling are evaluated. Subsequently, all relevant parameters and assumptions concerning the pipe flotation model are discussed in Chapter 5 and finally, this research is concluded and recommendations for future research are included in Chapter 6.



# 2

## Literature Review

The mechanism of offshore pipeline flotation during TSHD sand backfilling is relatively unknown. Extended research has been done regarding pipeline flotation caused by the mechanical backfill method called ploughing and regarding pipeline behaviour during its service period. The study concerning pipeline behaviour during its service period focuses on the effects on the already buried pipeline during soil liquefaction due to disturbance, for example caused by currents, tidal waves or earthquakes. However, research regarding the mechanisms in the surroundings of the pipeline during the sand backfilling process has not been conducted yet.

This literature review comprises the TSHD sand backfilling process, the sedimentation process of sand particles and the pipe-soil interaction stresses. First, the process of sand backfilling with a TSHD and its corresponding studies respecting pipeline flotation are discussed. An important aspect during this sand backfilling process with a TSHD is the sedimentation activity itself. Thereupon, the sedimentation theory and its influential parameters are explained in this section as well. Finally, the stresses generated on the pipe-soil contact surface, due to the partial embedment of the pipeline, are discussed.

### 2.1. TSHD Sand Backfilling Process

The technique of backfilling sand with a TSHD is discharging a sand-water mixture from a suction pipe at a certain distance above the pipeline. This vertical distance between the suction head, also known as the point of discharge, and the sand bed is called the stand-off distance (SOD). According to Burgmans (2005), the magnitude of this SOD has a significant influence on the backfilling process [3]. Apart from the SOD, other influential parameters during TSHD sand backfill are the trailing speed of the suction head, the discharge rate, the mixture density and the sand characteristics.

Another important aspect of backfilling with a suction pipe, is the behaviour of the discharge jet. De Nijs (2009) explained this behaviour in two different fluxes: the momentum flux and the buoyancy flux [6]. The momentum flux is also known as the jet behaviour right after the point of discharge and the plume behaviour after this is the buoyancy flux. The initial characteristics of the jet and plume behaviour and the exit geometry influence the trajectory and mixing of the discharge. These properties can be classified with length scales, which can be made non-dimensional with the SOD. This causes the ability to evaluate the relative importance of the individual physical processes to the dynamics of buoyant jets.

In order to prevent pipeline flotation during sand backfilling, a method of backfilling in thin layers has been developed by Van Oord [3]. To assess the potential flotation of a pipeline, Burgmans (2005) analysed the one-dimensional section of a pipeline on the seabed. This 1D static model estimates which maximum backfill layer thickness can be used without the occurrence of pipeline flotation. The moment when the discharge has stopped above the pipe, but the sand particles have not settled yet, is defined as the most critical state during the backfilling process. In this phase, a sand-water mixture suspends above the sand bed and the specific weight of this layer is of great importance. The buoyancy force directing upwards from this suspended layer is balanced against the specific weight of the pipeline. The maximum layer thickness can be derived from this balance to avoid pipeline flotation.

The main downward force in this model consists of the weight of the pipe. This force ensures that the pipe will remain on the sand bed if the conditions are at rest. Accordingly, the pipe should be designed in a way that its specific gravity is sufficiently larger than the specific gravity of water, but that it is still economically attractive.

The upward buoyant forces are divided in two parts: the buoyancy induced by pure water and the buoyancy generated on the pipe by the suspended sand particles in the domain. Although the discharge rate of the sand-water mixture during backfilling is larger than the sedimentation rate, sedimentation around the pipeline does take place during backfilling. The sedimentation causes the pipeline to become embedded in the newly settled sand layer, of which the top is called the sedimentation front. As the settled sand below the sedimentation front is considered to have the same pressure gradient as water, the buoyancy induced by pure water works on the entire area of the pipeline during the full extent of the backfilling process. On the other hand, the buoyancy produced by the suspension in the domain surrounding the pipeline, only works on the part of the pipe that is above the sedimentation front, which is called the effective area of the pipeline (see Figure 2.1). Naturally, the effective area of the pipeline decreases while sedimentation takes place. Consequently, over the course of discharging backfill material, the suspension in the domain surrounding the pipeline will build up, increasing the magnitude of the buoyancy on the pipeline. However, at the same time the sedimentation will decrease the effective area of the pipeline, causing the buoyancy to have a reduced impact. If the local upward buoyant forces from the mixture in the domain are larger than the forces working downwards on the pipeline, the pipeline will start to float. In a static vertically oriented force balance, Equations 2.1 and 2.2 are representations of the gravitational and buoyancy forces working on the pipeline [3]. The positive direction of forces is considered to be downwards.

$$W_p = A_p \rho_p g L_p \quad (2.1)$$

$$F_b = -A_p \rho_w g L_p - A_{eff} (\rho_m - \rho_w) g L_p \quad (2.2)$$

where  $W_p$  is the weight of the pipeline, which is based on the design properties  $A_p$ ,  $\rho_p$  and  $L_p$  of the pipeline, respectively its surface area, density and length. Furthermore, the equation for the upward buoyancy forces working on the pipeline (Eq. 2.2) depends on the density of pure water  $\rho_w$  and the density of the suspended sand particles in the domain due to discharge  $\rho_m$ . The effective surface area of the pipeline  $A_{eff}$  is considered as well and the forces are multiplied with the gravitational acceleration  $g$ . An overview of these forces on a one-dimensional section of the pipeline, partially embedded in the seabed, is given in Figure 2.1. This figure also displays the influence of the pipe embedment on the effective area of the pipe and therefore on the buoyancy during the sand backfilling process.

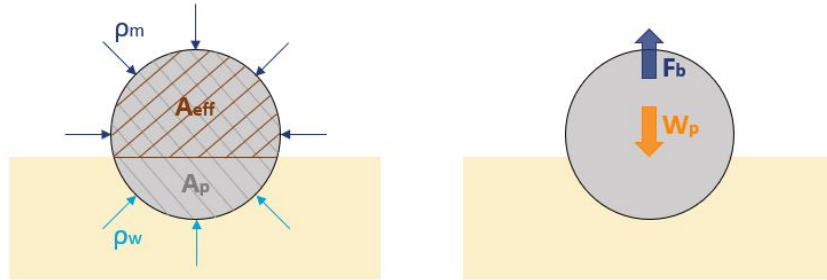


Figure 2.1: Schematic drawing of a one-dimensional section of the pipeline, which is partially buried and fully surrounded by a sand-water mixture

To evaluate the resultant force ( $q$ ) on the pipeline in a one-dimensional spectrum, the mass per unit of length can be determined with Equation 2.3 [3]:

$$q = \frac{\sum F_p}{g L_p} \quad (2.3a)$$

$$q = A_p (\rho_p - \rho_w) - A_{eff} (\rho_m - \rho_w) \quad (2.3b)$$

In this model, the sedimentation process that takes place during sand backfilling and the hydrodynamic forces that are present, are not considered. However, this is expected to have an influence on the force balance of the pipe body.

## 2.2. Sedimentation Process

The sand sedimentation process is a significant aspect of the sand backfilling technique of a submarine pipeline. The discharge of a sand-water mixture over a pipeline is dominated by the sedimentation process. During the sedimentation process, the fall velocity of an individual sand particle in water is the basis. This fall velocity is influenced by the properties of the individual sand particles, by the concentration of sediment and by the fluid dynamic drag force. The fall velocity of a sand particle can be expressed as Equation 2.4 [7]:

$$w_0 = \sqrt{\frac{4(\rho_s - \rho_w)gd}{3\rho_w C_D}} \quad (2.4)$$

where  $w_0$  is the fall velocity of a sand particle,  $d$  is the sand particle diameter, and  $g$  is the gravitational acceleration.  $C_D$  is the non-dimensional drag coefficient, which depends on the Reynolds number and a shape factor and is equal to approximately 0.4 in the case of turbulence. However, the flow conditions during the sand backfilling process are difficult to assess and an approximation for the fall velocity of a sand particle for different flow conditions ( $v_p$ ) from Ferguson and Church (2004) is considered as well (Eq. 2.5) [7]:

$$v_p = \frac{\frac{\rho_s - \rho_w}{\rho_w} g d^2}{C_1 \nu + \sqrt{0.75 C_2 \frac{\rho_s - \rho_w}{\rho_w} g d^3}} \quad (2.5)$$

where  $\rho_s$  is the density of a sand particle,  $C_1$  and  $C_2$  are constants of the values 18 and 1 respectively and  $\nu$  is the kinematic viscosity of sand.

The sand volume concentration of sediment influences the fall velocity of a single sand particle. An increase in sediment concentration causes a lower fall velocity of a single particle, which is called hindered settling. If a sand particle is present in a concentrated suspension, the shear stresses are larger and hindered settling occurs. According to Richardson and Zaki (1997), the fall velocity present in a suspension of a certain concentration can be expressed with Equation 2.6 [16].

$$w_s = v_p (1 - C_s)^n \quad (2.6)$$

where  $w_s$  is the reduced fall velocity in a suspension with a volume concentration of  $C_s$ . The factor  $n$  is a coefficient which depends on the Reynolds number ( $Re$ ) and its determination is given in Equation 2.7:

$$n = \frac{4.7 + 0.41 Re^{0.75}}{1 + 0.175 Re^{0.75}} \quad (2.7)$$

The discharge of the sand-water mixture during sand backfilling with a TSHD is dominated by the sand sedimentation and dispersion. For this reason, the 2D calculation model is based on empirical equations and the sedimentation theory as explained in this section. The previously described equations are applicable to a suspension of sand particles of the same grain size diameter. A variation in grain size diameters has an influence on the hindered settling velocity [9]. However, in this research the sand particles of the Geba Weiss sand are approximated with the mean grain size diameter so the specifications of Equation 2.6 are applied in the 2D calculation model in this research.

## 2.3. Pipe-Soil Interaction

An understanding of the interaction between the pipe material and the seabed is of the utmost importance for the assessment of pipeline flotation. The stress conditions on the pipe body depend on the specifications of the pipeline and on the positioning of the pipeline on the seabed. These interaction stresses are generally much lower than in conventional geotechnical processes. According to White and Randolph (2007), an assumption can be made that the normal stress on the pipe-soil contact depends on the amount of embedment of the pipe and varies for each inclination from the vertical  $\theta$ , following the elastic solution for a line load acting on a half-space (Figure 2.2). The normal stress on the pipe-soil contact surface,  $\sigma'_r$ , can be approximated by the Equation 2.8 [19].

$$\sigma'_r = \frac{V}{D} \frac{2 \cos \theta}{\beta + \sin \beta \cos \beta} \quad (2.8)$$

where  $V$  is the buoyant weight of the pipe and  $D$  is the pipe diameter. The inclination from the vertical is indicated with  $\theta$  and  $\beta$  is the semi-angle subtended by the contact surface of the sedimentation front (Figure 2.2).

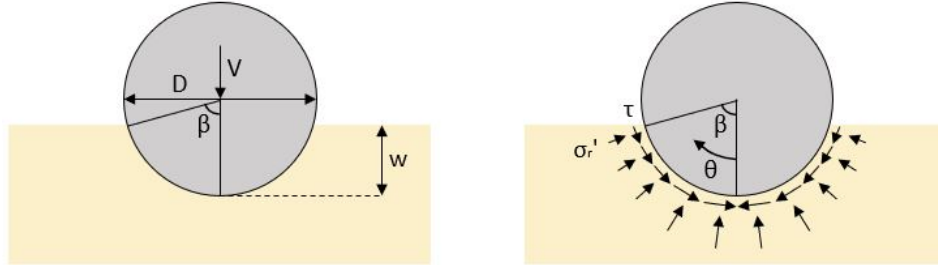


Figure 2.2: Schematisation of the pipe-soil contact stress parameters

To evaluate the shear stresses at the pipe-soil contact surface, the linear relationship between the normal stresses and the friction coefficient is considered. The friction coefficient is based on the on-bottom pipe-soil interface friction angle ( $\phi_{int}$ ), which is equal to the arctangent of the shear stress over the normal stress. However, the contact stresses between the pipe and the soil are much lower than in conventional geotechnical studies and therefore the friction angles are much higher than expected. White and Randolph (2007) derived the residual friction coefficient at these low stress levels with Equation 2.9 [19]:

$$\mu = 0.25 - 0.3 \log \left( \frac{\sigma'_r}{p_{atm}} \right) \quad (2.9)$$

where  $\sigma'_r$  is the normal effective stress, which is normalised by the atmospheric pressure  $p_{atm}$ . This determines a friction coefficient of approximately 0.75 for a corresponding effective stress of 2 kPa, which is representative for pipe-soil interaction during axial movements of a pipeline at full scale that is partially buried in the seabed [19]. However, experimental data does show that the rate and magnitude of pipe displacements influence the friction coefficient [15].

With the known relationship between normal and shear stresses, the shear stress ( $\tau$ ) at every infinitesimal part of the contact surface can be determined by Equation 2.10:

$$\tau = \sigma'_r \mu \quad (2.10)$$

In this equation, both parameters can be determined with the previously described equations in this section: the normal effective stress  $\sigma'_r$  with Equation 2.8 and the friction coefficient  $\mu$  with Equation 2.9. These pipe-soil interaction parameters at low stress levels are significant for the assessment of pipeline flotation in this research.

The very low stress levels at the pipe-soil interface, generates unusual high friction coefficients. This could be explained by the formulation of a failure envelope in the normal-shear stress plane for the pipe-soil interface at low stress levels. A simplification for approximating this shear failure envelope, is with the method of Mohr-Coulomb (MC), where a constant friction angle ( $\phi$ ) is assumed [18]. However, in reality, the friction angle does depend on the stress levels and the shear failure envelope is slightly curved, which is shown for low stress levels in Figure 2.3. This figure shows an evident difference in friction angle between the two methods. At very low stress levels, the friction angle of a sigma-dependant method shows larger values than according to the commonly known Mohr-Coulomb method. This explains the unusually high friction angles, and therefore friction coefficients, at the very low stress levels on the pipe-soil interface.

The determination of the normal stresses and friction coefficients on the pipe-soil contact surface in this section (Equations 2.8 and 2.9) were derived by White and Randolph (2007) based on experiments with clay samples [19]. However, in this research, the seabed and backfill material are simulated with sand particles. Nevertheless, these equations are considered to represent the pipe-soil interaction stresses reasonably well, as the small-scale experiments cause very low stress levels, and are therefore assumed in this research.

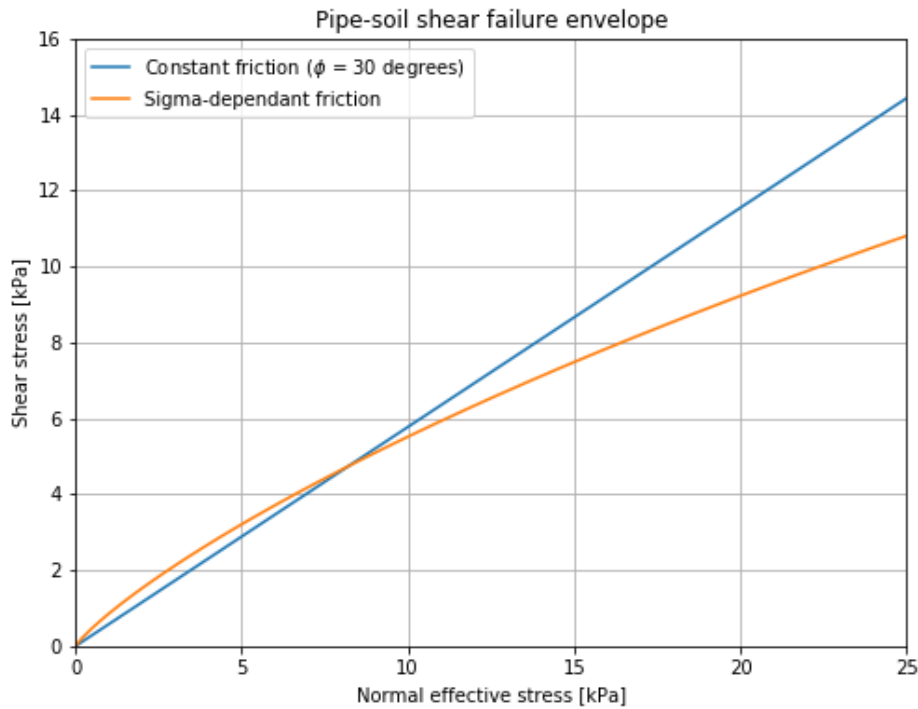


Figure 2.3: Difference between the shear strength failure envelope with the assumption of constant friction (MC) with a typical friction angle of 30 degrees or with a sigma-dependant friction



# 3

## Small-Scale Physical Modelling of Pipe Flotation

It is valuable to know exactly what parameters are responsible for the pipeline flotation during sand backfilling with a TSHD, so it can be prevented but the method for backfilling offshore pipelines can still be implemented as economically attractive as possible. In order to achieve this knowledge, the development of buoyancy and the sedimentation process during sand backfilling need to be investigated thoroughly. Due to the lack of available field data regarding these mechanisms, this research focuses on the use and analysis of the existing 2D experimental model from Yang (2020) [20]. This research is based on a series of small-scale experiments in order to interpret the developments in the surroundings of a pipeline during a simplified sand backfilling process.

A detailed description of the laboratory set-up used in this research is given. The different types of experiments that are conducted are explained in this section and an overview of all experiments with their input parameters is given as well. Furthermore, the steps undertaken during each experiment are elaborated in the testing programme. Finally, in Section 3.3, the means of measuring during the experiments and the data processing are discussed.

### 3.1. Experimental Set-Up

The aim of this research is to develop an understanding of the mechanism of pipeline flotation during sand backfilling. The laboratory set-up, designed by Yang (2020), simulates the sand backfilling process on a small scale with a stationary discharge of a sand-water mixture over a rigid pipe [20]. Similar as with a sand backfilling process with a TSHD, the discharge rate of the mixture in the domain is larger than the sedimentation rate of the sand particles. This causes a suspension to develop in the domain surrounding the pipe. The development of concentration of this suspended mixture over the course of an experiment can be determined. Some other measurements are the pressure increments in the domain due to the discharged material and the displacements of the pipe. In Section 3.3 a more extensive description of the measurements during the experiments is given. From these measurements, the forces generated on the pipe, can be determined at the moment of flotation. With this approach, a relationship between pipeline flotation due to buoyancy and the responsible parameters can be derived.

The laboratory set-up consists of two perspex tanks: the mixture tank and the experimental tank. The mixture tank is used to evenly distribute the sand-water mixture before discharging it into the experimental tank. The mixing is done with a Homa mixture pump and the Einhell GE-DP 7935 pump discharges the mixture into the experimental tank. With the help of a T-valve between the mixture and experimental tank, the mixing can also be enhanced by a backflow circuit. The discharge rate can be regulated by a control valve and a flow meter. The pipe flotation tests take place in the experimental tank, which consists of two equal compartments with a bottom area of 72.5 cm by 74.5 cm and a height of 85.0 cm. One compartment serves as body for the experiments, while the other one collects the overflow from the experimental compartment in order to keep its water level constant. A schematic overview of the complete set-up is shown in Figure 3.1.

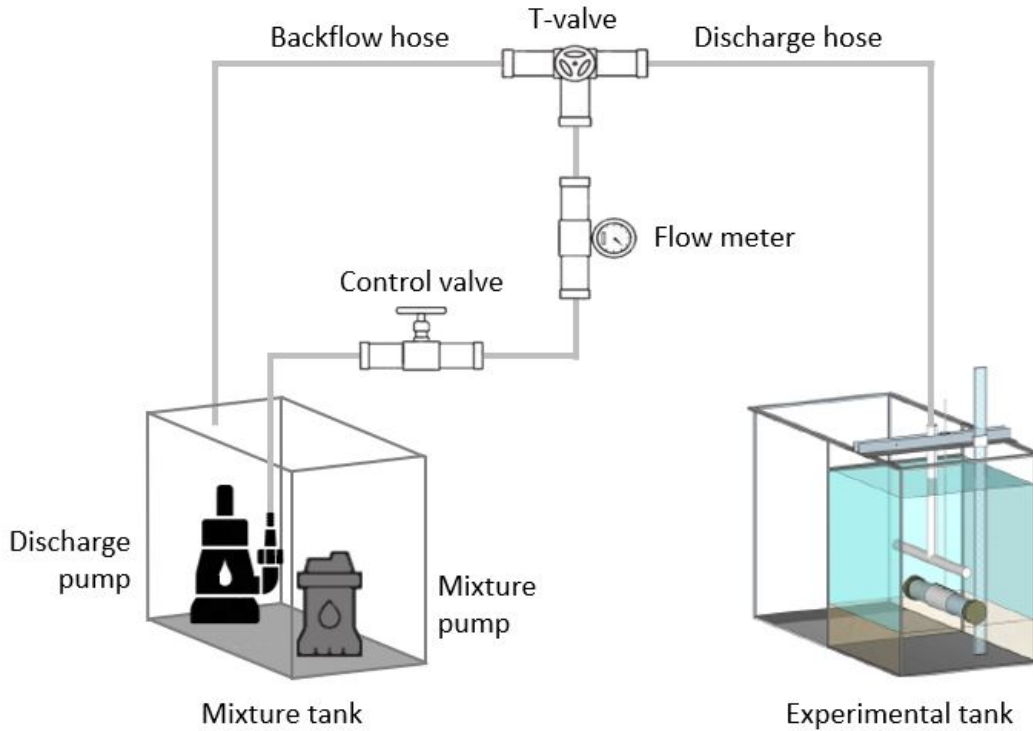


Figure 3.1: A schematic overview of the laboratory set-up

A prototype backfilling process with a TSHD and its properties can be derived from the experience of projects from Van Oord [10] [13]. The most significant prototype TSHD properties for the current research are the stand-off distance  $SOD_p$ , the discharge speed  $u_{dis,p}$ , the volume concentration of sand in the mixture  $C_{dis,p}$ , the median diameter of the sand backfill particles  $d_{50,p}$  and the diameter  $D_{dis,p}$  and area  $A_{dis,p}$  of the suction pipe. The empty pipeline density  $\rho_{p,p}$  and outside diameter  $D_p$ , the seawater density  $\rho_{seawater}$  and the sand cover thickness  $\Delta h_p$  are also of great importance. Some properties that are ignored in this research, but do contribute to the backfilling process in the field, are the trailing speed  $v_{trail,p}$  and the trench bottom width and slope. Some relevant characteristic values of the prototype are given in Table 3.1, together with the properties applied in the experimental set-up.

The design criteria for the laboratory set-up are explained by Yang (2020) [20]. From the geometrical limitations of the laboratory tank, Yang derived a scaling ratio of 1:12 for the experimental set-up. At this scale, the experimental compartment is too small to simulate a trench with such gentle slopes, so the pipe is laid directly on the 20 cm thick horizontal sand bed. The pipe itself is simulated with a rigid body with a diameter of 10 cm and its specific gravity can be regulated from 1.03 to 1.97 by attaching ballast steel rods on the inside of the pipe. The pipe is prevented from making any horizontal movements by a vertical guiding rod, connected to the top of the pipe at the centre, and two separate vertical rods next to the pipe on both sides of the experimental tank.

The discharge of the sand-water mixture on the pipe is simulated with a reversed T-junction with holes in it. Two interchangeable T-junctions are used in this research, one with holes in the sides for horizontal discharge and one with holes at the top for discharging upwards. To minimise the water head drop in the T-junction, the total area of all discharge holes is kept constant to the cross-section of the T-junction itself. Some minor differences can be identified between the two T-junctions. The mixture is discharged horizontally through 14 holes on both sides of the T-junction with a diameter of 8 mm. To achieve a vertical discharge of the sand-water mixture, this T-junction contains 12 holes at the upper side with a diameter of 12 mm. The T-junction is positioned in the middle of the tank and the holes are uniformly allocated to evenly distribute the discharge in the experimental compartment. The height of the T-junction above the sand bed, and thus the SOD in the experimental set-up, is set to 25 cm [20]. In order to prevent the T-junction to overlap with the pipe guiding rod, the pipe is located 7 cm to one side.

Table 3.1: Overview prototype and laboratory set-up parameters

Prototype		Laboratory set-up	
Parameter	Value	Parameter	Value
$u_{dis,p}$	5 m/s	$Q_{dis}$	2 L/s
$C_{dis,p}$	30%	$C_{dis}$	30%
$SOD_p$	5 m	$SOD$	0.25 m
$D_p$	1.2 m	$D$	0.10 m
$\rho_{p,p}$	1.3 t/m <sup>3</sup>	$s_p$	1.03 - 1.97

The sand used in the experiment for the sand bed and the backfill material is the well sorted Geba Weiss sand. Yang (2020) performed multiple soil tests and an overview of the acquired Geba Weiss sand properties is given in Table 3.2 [20], which involve the cumulative grain diameters at 10%, 50% and 60%, respectively, the uniformity coefficient and the maximum and minimum porosity.

The amount of Geba Weiss sand needed for the sand bed is approximately 152 kg and the sand bed is re-prepared before each experiment. The amount of sand needed in the mixture tank depends on different parameters, such as the discharge rate, discharge concentration and cover layer thickness. Based on a discharge rate of 2 L/s, a discharge sand concentration of 30% and a cover layer thickness of 10 cm, the amount of sand needed in the mixture tank is approximately 118 kg. This leads to a total amount of approximately 270 kg of Geba Weiss sand needed during the experiments.

Table 3.2: Geba Weiss sand properties

$d_{10}$ [ $\mu\text{m}$ ]	$d_{50}$ [ $\mu\text{m}$ ]	$d_{60}$ [ $\mu\text{m}$ ]	$C_u$ [-]	$n_{max}$ [-]	$n_{min}$ [-]
92	125	133	1.45	0.51	0.37

The experiments are measured with various instruments to monitor the fluid conductivity, pressure, flow volume and pipe displacements. The flow rate and volume are monitored with a flow meter and the vertical displacements of the pipe are measured with a ZWS-70 ultrasonic sensor.

The conductivity of the fluid is of importance to understand the development of mixture specific gravity in space and time and it is measured by a composed conductivity bar [20]. This conductivity bar consists of 16 pairs of conductivity probes at different heights and it measures the potential difference between the pairs of probes. One pair of conductivity probes consists of two electrodes with each a diameter of 3 mm, which have a spacing of 7 mm. With this approach, the density of the mixture at the different heights can be back-calculated, based on the electrical resistivity of the fluid between the electrodes. The conductivity bar is positioned on the bottom of the experimental compartment, at a distance of 9 cm from the centre of the pipe.

The water pressure is measured at different heights with three Model 1151 Alphaline differential pressure transmitters (DP). The DP's measure the relative head difference in the domain. During the experiments, the sand particles from the discharged mixture attribute to the mixture density in the domain and hence an increase in water pressure is anticipated. To measure this development of the mixture around the pipe, the DP's are attached to the conductivity bar at the same height of the bottom and top of the pipe. The water level in the experimental compartment is kept constant as much as possible by the overflow of water in the adjacent empty compartment, but for reference one DP sensor is located near the top of the tank as well. The locations of the pressure sensors in the experimental tank attached to the conductivity bar are displayed in Figure 3.2. The technical specifications of the ZWS-70 ultrasonic displacement sensor and of the DP sensors are given in Table 3.3.

Table 3.3: Technical specifications of the sensors

	DP	ZWS-70
Range	0 - 7.46 kPa	120 - 700 mm
Accuracy	0.1%	1%
Connection	Stiff hose	Electrical wire

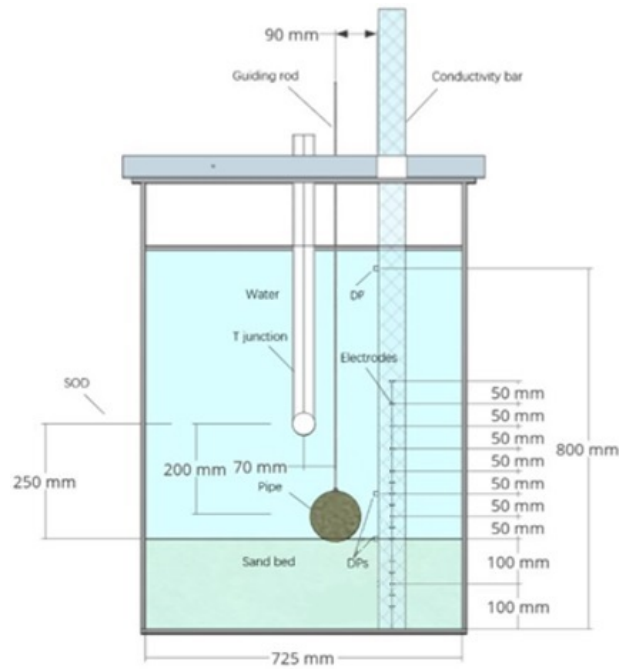


Figure 3.2: Schematic overview of sensors in the experimental tank, slightly different from Yang (2020) [20]

## 3.2. Experimental Procedure

To establish an understanding in the mechanism of pipeline flotation during sand backfilling and to develop answers to the research questions from Section 1.3, multiple experiments with different implementations are performed in the previously described laboratory set-up. The experimental procedure for these implementations is divided in four different stages. First, multiple experiments are executed as designed by Yang (2020) [20]. During this stage, the spatial variability of the discharge process in the experimental tank is examined as well. In the second stage, the direction of discharge is modified and analysed. Subsequently, the pipe, originally positioned on top of the sand bed, is elevated to different heights. In the final stage, the influence of the specific gravity of the pipe is investigated. The detailed specifications of these four different stages are described in the following sections. Furthermore, the general testing programme for a single experiment is reported and an overview of all performed experiments in this research is given.

### 3.2.1. Stage 1: Discharging horizontal and checking the spatial variability

In the first stage, the laboratory set-up from Yang (2020) is rebuilt and multiple experiments are performed to obtain more data for the developed 2D model [20]. To analyse the mechanisms inside the experimental compartment during discharge, the input parameters for each experiment are kept as constant as possible. Before starting the discharge, the pipe with a fixed specific gravity of 1.03 is positioned on top of the sand bed. The tests in this stage are performed with a discharge of the sand-water mixture directed horizontally at a set distance above the pipe.

The development of the specific gravity of the mixture is based on the measurements carried out with a conductivity bar. It measures the conductivity of the fluid with 16 pairs of electrodes at different heights and demonstrates how the density of the mixture changes in space and time. The conductivity bar is positioned at one specific location in the experimental compartment and therefore it only measures the development of the mixture at this singular horizontal distance from the pipe. However, the development of the specific gravity of the mixture in the surroundings of the pipe is a very significant parameter in the pipeline flotation analysis. To monitor if there are any critical spatial differences in the experimental tank during the experiments, the conductivity bar is placed at different locations with various horizontal distances from the pipe.

### 3.2.2. Stage 2: Discharging upwards

Yang (2020) designed a T-junction with horizontal discharge to prevent the effects of erosion at the sand bed [20]. However, there were still some circular flow streams and signs of erosion visible during these experiments. As erosion is not included in the model, these effects should be eliminated as much as possible. In this stage, the initial horizontal discharge is substituted by a vertically upward discharge from the stationary T-junction. This upwards release of the sand-water mixture is the exact opposite of the TSHD sand backfilling process, but the focus of this research is on the development of buoyancy around the pipe as the sand-water mixture starts to settle. With a vertical discharge, the sedimentation process and the build-up of mixture density in the domain are even more accurately simulated than with a horizontal discharge. Multiple experiments with the vertical discharge are performed. The erosion and the turbulence due to the influence of the sidewalls of the experimental tank on the flow streams are expected to be significantly less prominent during these experiments. These beneficial effects of the vertical discharge induce the alternative T-junction to stay during the following stages of performing experiments.

### 3.2.3. Stage 3: Increasing the pipe elevation

In a previous research, some difficulties with the relatively large sedimentation rate compared to the pipe dimensions were encountered in the experiments [20]. The dimensions of the sand particles are approximately the same in the small-scale experiments as in the field, while the simulated pipe is significantly scaled down. Therefore, the relatively large sedimentation rate reduces the effective area of the pipe substantially before flotation occurs, which both reduces the buoyancy forces working on the pipe and increases the embedment of the pipe. The initial reduction in effective area of an offshore pipeline in the field is negligible, which causes the analysed risk of flotation to be underestimated in the small-scale experiments.

The influence of the relatively large sedimentation rate is analysed by changing the initial position of the pipe from directly on top of the sand bed to slightly elevated above the sand bed. This prevents the reduction in effective area of the pipe due to sedimentation in the first seconds of the experiment. The experiments are conducted with the vertical discharge from Stage 2 and an effort has been made to maintain all other input parameters constant.

A structure based on a pipe cradle is used in the experiments to elevate the pipe. This structure to lift the pipe is a V-shaped metal plate, which rests on the bottom of the experimental tank. The design of the structure and the method to elevate the pipe from the surface are shown in Figure 3.3. Two constructions like this at both edges of the pipe are used, so the structure barely influences the sedimentation process and it gives as little friction as possible on the pipe. However, the open space created between the pipe and the sand bed facilitates the flow of the sand-water mixture underneath the pipe. The changes in drainage paths and hydrodynamic forces have additional effects on the experiments, which should be taken into account in the analysis. To investigate the influence of an elevated pipe in the experiments, the pipe is elevated to three different heights. The heights to which the pipe is elevated is restrained by the T-junction above the pipe in the experimental tank, so the pipe is only elevated 1 cm, 2 cm and 4 cm.

The sedimentation velocity of the Geba Weiss sand during the experiments of a previous research is measured to be approximately 2 mm/s at the end of discharge and approximately 1 mm/s at the end of the entire experiments [20]. With a pipe diameter of 10 cm, and an even lower cover thickness after the experiments, the sedimentation process ends relatively fast. By elevating the pipe 4 cm, even the relatively large sedimentation rate barely causes a reduction in the effective area of the pipe over the time of discharge. The elevations of 1 cm and 2 cm are generally passed by the sedimentation front within the course of discharge, but the start of reduction in the effective area of the pipe is somewhat delayed.



(a) V-Shaped design to elevate the pipe



(b) The small-scale pipe on top of the two structures for elevation

Figure 3.3: The V-shaped design of the structure and the method to elevate the pipe during the experiments

### 3.2.4. Stage 4: Increasing the pipe specific gravity

In the final stage of performing experiments in this research, the specific gravity of the pipe is varied. The moment of pipe flotation is shifted with heavier pipes and the influence of the pipe specific gravity is of great importance. Therefore, this implementation is applied to verify the conclusions regarding a potential pipe flotation limit during sand backfilling for different pipes. The pipe specific gravity is increased by adding extra weights to the initial pipe, which has a pipe specific gravity of 1.03. This added ballast to increase the total weight of the pipe, is done by attaching solid weights inside the pipe, making sure no movements are allowed. Based on the total buoyancy reached during the experiments with this initial pipe, the influence of an increased pipe specific gravity of 1.08 and 1.12 is investigated. All experiments in this stage are conducted with the vertically upward discharge and with the pipe positioned directly on the sand bed.

### 3.2.5. Testing Programme

Although the experiments in this research are performed with different implementations, the general testing programme for each individual experiment is identical. The testing programme is similar to the procedure described by Yang (2020) [20], but a different approach is used to prepare the sand bed before the start of the experiments. The preparation of the sand bed as proposed by Yang was very time-consuming, so a different method was integrated. Instead of emptying the experimental tank completely and discharging it back again, the sand bed was remoulded. As the measurements after discharging the sand bed and after remoulding the sand bed were very similar, the time-consuming method is adopted. The steps to perform an experiment in this research are as follows:

#### Preparations

1. Take the pipe out of the experimental tank.
2. Only in Stage 1, replace the conductivity bar to another position in the tank.
3. Pump the sand from the experimental tank back to the mixture tank, until the sand bed of 20 cm in the experimental tank is reached.
4. Remould the remaining sand in the experimental tank and let the sand particles settle again to the 20 cm sand bed (and in Stage 3: position the structures for the elevation of the pipe).
5. Adjust the amount of water in the mixture tank to ensure the right concentration of the mixture.
6. Take the air out of the DP transmitters, check the sensors on the conductivity bar and the displacement sensor.
7. Measure for 5 minutes, to check if the measurements are stationary.
8. Lay the pipe on the sand bed and check whether the pipe is free to float.

**Experiment**

1. Start the measurements and recordings
2. Mix the sand and water in the mixture tank with means of the mixture pump and the backflow from the discharge pump.
3. Adjust the control valve until the flow meter reaches the desired value.
4. Switch the T-valve from the mixture tank to the experimental tank to start the discharge.
5. End the discharge by switching the T-valve again, when the desired discharge volume is reached.
6. Stop the measurements after 10 minutes, as the data is already stationary after this amount of time.

A total amount of 50 experiments, divided over the four different stages, is executed in this research. An overview of all performed experiments is given in Table 3.4 with the corresponding input parameters. A single experiment can be influenced by the following relevant specifications: the direction of discharge of the sand-water mixture, the initial pipe position, the specific gravity of the pipe ( $S_p$ ), the duration of discharge ( $t_{dis}$ ) and the discharged sand cover layer thickness ( $\Delta h$ ). The performed experiments in this research are coded with a name consisting of three letters and a number, from which three specifications can be read. The first letter in the code symbolises the direction of discharge during the experiments, which could be:

- H for horizontal discharge
- V for vertical discharge

The second parameter in the code suggests the initial position of the pipe, for which the options are:

- N for not elevated, where the pipe lays on top of the sand bed
- S for slightly elevated, where the pipe is elevated for 1 cm
- M for medium elevated, where the pipe is elevated for 2 cm
- V for very elevated, where the pipe is elevated for 4 cm

Finally, the third symbol represents the specific gravity of the pipe and it can be described by one of the following letters:

- L for lightweight pipe, with a specific gravity of 1.03
- W for weighted pipe, with a specific gravity of 1.08
- H for heavyweight pipe, with a specific gravity of 1.12

Table 3.4: Overview of all performed experiments with the input parameters

Experiment	Input Parameters				
	Direction of discharge	Initial pipe position	Sp [-]	t <sub>dis</sub> [s]	Δh [cm]
HNL1	Horizontal	On the sand bed	1.03	51	4.3
HNL2	Horizontal	On the sand bed	1.03	48	4.4
HNL3	Horizontal	On the sand bed	1.03	52	4.3
HNL4	Horizontal	On the sand bed	1.03	38	6.8
HNL5	Horizontal	On the sand bed	1.03	46	6.1
HNL6	Horizontal	On the sand bed	1.03	54	3.9
HNL7	Horizontal	On the sand bed	1.03	42	6.0
HNL8	Horizontal	On the sand bed	1.03	34	5.2
HNL9	Horizontal	On the sand bed	1.03	48	6.8
HNL10	Horizontal	On the sand bed	1.03	56	5.7
HNL11	Horizontal	On the sand bed	1.03	51	5.3
VNL12	Vertical	On the sand bed	1.03	60	6.6
VNL13	Vertical	On the sand bed	1.03	39	8.0
VNL14	Vertical	On the sand bed	1.03	37	5.9
VNL15	Vertical	On the sand bed	1.03	45	5.9
VNL16	Vertical	On the sand bed	1.03	44	4.8
VNL17	Vertical	On the sand bed	1.03	43	6.3
VNL18	Vertical	On the sand bed	1.03	43	6.1
VNL19	Vertical	On the sand bed	1.03	60	4.7
VNL20	Vertical	On the sand bed	1.03	23	4.9
VNL21	Vertical	On the sand bed	1.03	45	6.8
VNL22	Vertical	On the sand bed	1.03	31	5.8
VNL23	Vertical	On the sand bed	1.03	41	4.5
VSL24	Vertical	Elevated 1 cm	1.03	56	6.6
VSL25	Vertical	Elevated 1 cm	1.03	55	6.8
VSL26	Vertical	Elevated 1 cm	1.03	46	6.4
VSL27	Vertical	Elevated 1 cm	1.03	58	6.1
VSL28	Vertical	Elevated 1 cm	1.03	40	4.7
VML29	Vertical	Elevated 2 cm	1.03	55	5.5
VML30	Vertical	Elevated 2 cm	1.03	49	7.7
VML31	Vertical	Elevated 2 cm	1.03	29	5.8
VML32	Vertical	Elevated 2 cm	1.03	43	6.0
VML33	Vertical	Elevated 2 cm	1.03	38	7.0
VML34	Vertical	Elevated 2 cm	1.03	53	6.0
VVL35	Vertical	Elevated 4 cm	1.03	53	6.1
VVL36	Vertical	Elevated 4 cm	1.03	43	6.7
VVL37	Vertical	Elevated 4 cm	1.03	58	6.1
VVL38	Vertical	Elevated 4 cm	1.03	66	6.4
VVL39	Vertical	Elevated 4 cm	1.03	67	7.3
VVL40	Vertical	Elevated 4 cm	1.03	34	6.4
VVL41	Vertical	Elevated 4 cm	1.03	60	7.1
VNW42	Vertical	On the sand bed	1.08	32	4.7
VNW43	Vertical	On the sand bed	1.08	25	4.4
VNW44	Vertical	On the sand bed	1.08	26	4.3
VNW45	Vertical	On the sand bed	1.08	30	5.1
VNW46	Vertical	On the sand bed	1.08	30	5.7
VNH47	Vertical	On the sand bed	1.12	26	4.6
VNH48	Vertical	On the sand bed	1.12	30	5.0
VNH49	Vertical	On the sand bed	1.12	26	5.1
VNH50	Vertical	On the sand bed	1.12	44	5.1

### 3.3. Measurements and Data Processing

This research revolves around the parameters involved in pipeline flotation during sand backfilling. The data that is analysed is acquired from measurements taken during the experiments. The measuring instruments used during the experiments consist of a flow meter, conductivity probes, differential pressure sensors and an ultrasonic displacement sensor. Each measuring device delivers a different type of data and the processing of this data is elaborated in this section.

#### 3.3.1. Sand concentration

During the experiments, the focus lies on the development of the density of the mixture in the surroundings of the pipe over time and on the simultaneous sedimentation that takes place. As explained in Section 3.1, the conductivity bar in the experimental tank measures the potential difference between 16 pairs of electrodes, positioned at different heights within the domain. The average concentration of sand particles at these 16 heights is based on the change in electrical resistance between the electrodes at each moment in time over the course of the experiment [17]. For the analysis of the concentration developments in the domain, the Maxwell equation is adopted in the calibration of the conductivity bar, which is further elaborated by Yang (2020) [20]. The knowledge of the development of sand concentration over time during discharge is important for the determination of the density of the suspension around the pipe. According to Archimedes' law, the mixture in the domain produces uplift forces on the pipe equal to the weight of the fluid displaced [4]. With a denser mixture, the magnitude of these buoyant forces will increase.

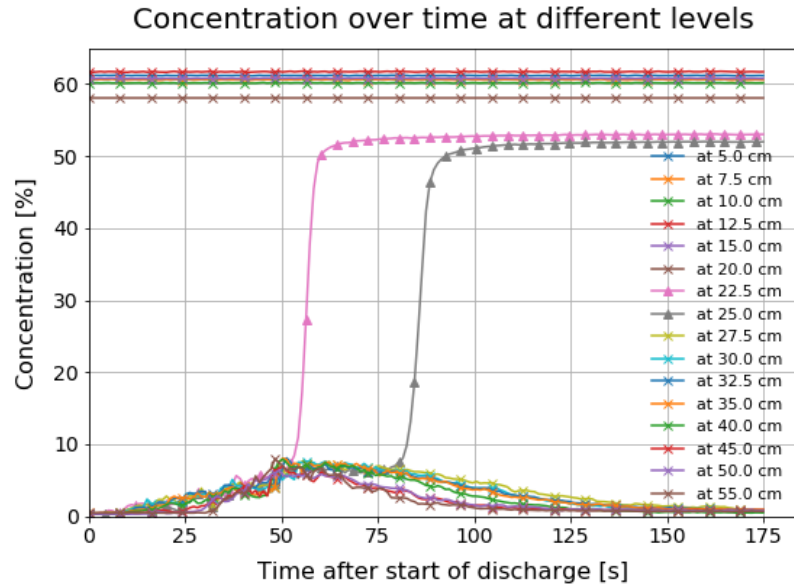
Figure 3.4a demonstrates the development of concentration of solids over time at various heights during Test VNL15 (see Table 3.4). Figure 3.4b displays the same data, but now with the concentration on the horizontal axis and the height on the vertical axis. The different curves in this figure show the development at various times, which are also known as the concentration isochrones. Figure 3.4b only shows the concentration isochrones when the concentration is increasing over time, so they stop at the moment the maximum sand concentration is reached. The sand concentration at every 2.5 cm or 5 cm in height is determined. The height of the sand bed before the start of the experiment is 20 cm. Therefore, the sensors below this level show a steady concentration of approximately 60%, which corresponds well with the determined porosity of the sand bed ( $n_{bed}$ ) of approximately 40% ( $C_{bed} = 1 - n_{bed}$ ) [20]. The measurements at all levels above the sand bed are fixed at 0% concentration before the start of the experiment. As soon as the discharge starts, a gradual increment in concentration is visible until they reach approximately the same maximum value, creating a homogeneous domain around the pipe. The build-up of mixture density in the entire domain strongly depends on the height and direction of discharge and on the discharge flow rate. The results in Figure 3.4, are from an experiment that is performed with a vertical discharge for approximately 50 seconds.

The increase in sand concentration just above the sand bed happens relatively simultaneous at all heights, because of gravitational and dispersion effects when the mixture leaves the T-junction at a height of 45 cm. The maximum sand concentration reached in the domain, without settling of the sand particles, is an important parameter in the analysis of pipeline flotation. This parameter is called the maximum domain concentration  $C_{max}$  and is a key factor in the critical buoyancy forces working on the pipe.

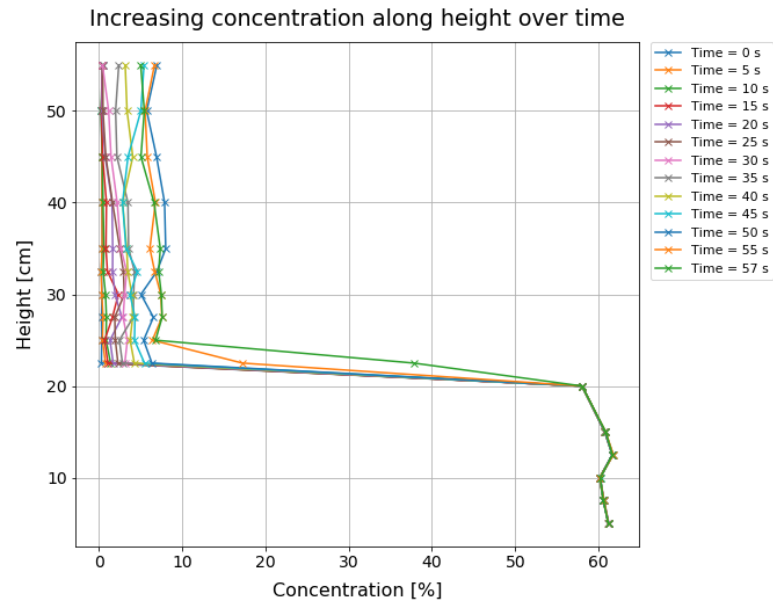
After the discharge has stopped, the sand particles in the domain gradually sink towards the sand bed, in which a distinction from the highest sensor downwards is visible. The sensors at higher levels are the first to be clear of sand particles, which corresponds with the laws of gravity.

Experiments with a horizontal direction of discharge achieve slightly different concentration developments. During these experiments, barely any sand particles reach above the discharge height, so no concentration increases are visible in the upper two sensors. Nevertheless, in general the concentration developments in the surroundings of the pipe are comparable in experiments with horizontal and vertical discharge.

In Stage 1 (see Section 3.2.1), the spatial variability of the concentration in the domain during the experiments is examined, by positioning the conductivity at different positions in the experimental tank. This variation in position of the conductivity bar demonstrates insignificant spatial differences in the direct surroundings of the pipe. Some differences in the differential pressure measurements near the sidewalls of the experimental tank can be recognised, but in general the concentration developments due to discharge in the vicinity of the pipe are relatively homogeneous.



(a) The development of sand concentration in the experimental tank over time at different heights during Test VNL15



(b) The development of sand concentration in the experimental tank with elevation at different times during Test VNL15

Figure 3.4: The development of sand concentration in time and space during Test VNL15

### 3.3.2. Sedimentation

From Figure 3.4, the concentration developments can also be translated to the ongoing sedimentation that is taking place during the experiments. When the sedimentation front reaches the height of a sensor, the concentration measurements jump up to a sand concentration of approximately 48% and afterwards gradually increase to approximately 52%. The sedimentation speed during the experiments is deduced by interpolating between the heights and moments in time when such a jump occurs. This sedimentation speed not only varies slightly between experiments, but a decrease or increase can also be recognised during one single experiment. This indicates that the sedimentation rate depends on the concentration of sand present in the domain, which is also proven with column sedimentation tests by Yang (2020), and therefore on the discharge conditions [20].

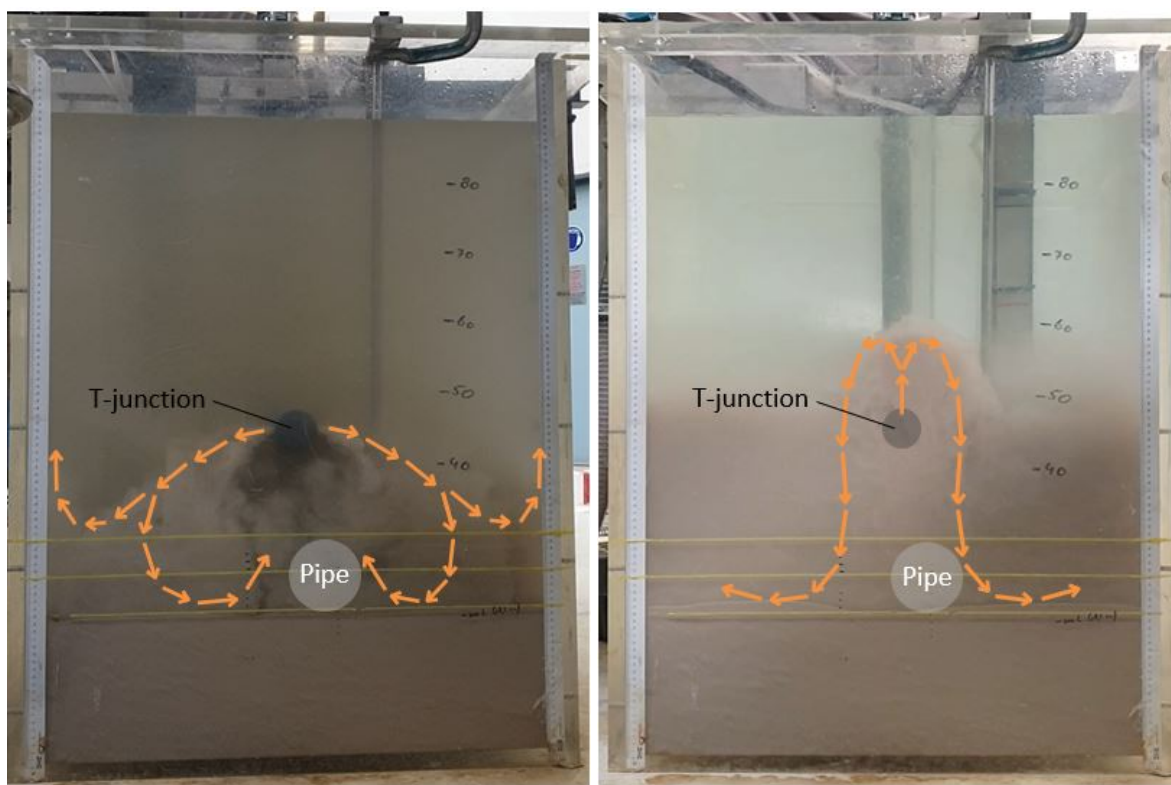
An expression to determine the sedimentation rate, based on the domain concentration, is derived by Yang (2020) as well [20]. The measured sedimentation rates during the experiments in this research, suggest reliable values according to this equation and the sedimentation theory from the literature.

The sedimentation during the experiments is of great importance for the calculation of forces generated on the pipe before flotation occurs. Evidently, the sedimentation reduces the effective area of the pipe on which the upward buoyancy applies and it increases the embedment of the pipe before flotation occurs.

### 3.3.3. Discharge conditions

The discharge conditions are significant input parameters of the backfilling process. The direction of discharge in the experiments is either horizontal or vertically upwards. The flow conditions around the pipe are influenced by this direction of discharge. With horizontal discharge, dominant circular motions are observed in the experimental tank. The horizontal discharge flow from the two sides of the T-junction eventually falls down due to gravity, but still contains a horizontal acceleration. This property directs the stream over the sand bed towards the middle of the tank, where the flow from the two sides creates turbulence in the domain of the pipe on the sand bed. The perceived flow during horizontal discharge is schematically shown in Figure 3.5a.

In Figure 3.5b, the global direction of flow during an experiment with vertically upward discharge is displayed. With this method, the sand-water mixture is pushed upwards from the T-junction and almost immediately falls down again due to gravity. Some signs of erosion of the sand bed are still visible directly below the T-junction, which is visible in Figure 3.5b by the gradually increasing level of the sand bed towards the sides of the experimental tank.



(a) The direction of flow with horizontal discharge from the T-junction (b) The direction of flow with upward discharge from the T-junction

Figure 3.5: Comparison between the direction of discharge during the small-scale experiments

Furthermore, two other discharge conditions that are taken into account are the discharge flow rate and the discharge concentration during the experiments. As all input parameters, these conditions are preferably kept constant for the analysis of pipeline flotation. However, this is more difficult to maintain in the small-scale experiments than anticipated beforehand.

A discharge flow rate of 2 L/s is determined to approximate the TSHD sand backfilling process on a small scale [20]. A flow meter is attached to the experimental set-up to maintain and monitor this fixed flow rate. To deliver this constant flow rate immediately from the start of the experiment, the flow meter is positioned before the T-valve (see Figure 3.1). However, after the T-valve is switched to start the discharge, the flow is divided in two different directions: towards the experimental tank for discharge and back to the mixture tank to stimulate the homogeneous mixing. Although the flow rate, measured before the T-valve, still measures the constant flow rate of 2 L/s, the actual discharge flow rate can vary significantly over the course of the experiment. An average discharge flow rate ( $Q_{cal}$ ) can be calculated by the total discharged volume at the end of the experiment and the duration of discharge. This determined  $Q_{cal}$  shows a wide variety of values for the experiments, ranging from 0.90 to 2.18 L/s.

However, this is an average value over the entire duration of discharge and not completely representative for every moment in time. The trend in concentration and pressure developments depend on the discharge flow rate, so from the individual experiments the variation in  $Q_{cal}$  can be estimated.

Similarly, the concentration of the discharged mixture differs for each experiment and fluctuates over the duration of discharge. To simulate the TSHD sand backfilling process, a constant discharge concentration of 30% is preferred, but this parameter is relatively difficult to control over the course of the experiments. The sand and water levels in the experimental tank, mixture tank and overflow container are measured before and after the experiments, so again an estimation can be made regarding the average discharge concentration ( $C_{dis,avg}$ ). The average discharge concentration for each experiment is based on three different methods, which are calculated with: (1) the total volume of sand and water discharged from the mixture tank, (2) the new sand bed in the experimental tank and the total volume of water in the overflow container and (3) the new sand bed in the experimental tank and the total discharged volume from the mixture tank.

In general, the different calculation methods produce a similar discharge concentration, but some differences are possible. These differences can be caused by measuring the sand and water levels on the sidewalls of the experimental set-up. It is most likely that the sand layers are not entirely equally distributed, so the volume calculation has some uncertainty. For this reason, the value chosen for the average discharge concentration is the average of all three calculations. This determined average discharge concentration shows a relatively confined range of values for all experiments between approximately 20% and 30%.

### 3.3.4. Pressure increments

The addition of a sand-water mixture during an experiment increases the pressure in the domain around the pipe in the experimental tank. This change in pressure is measured by three differential pressure transmitters (DP's), which are attached to the conductivity bar at several heights (see Figure 3.2). The differential pressures are measured at the same height of the bottom of the pipe (at 20 cm) and of the top of the pipe (at 30 cm). The water table in the experimental tank is maintained at the same level due to the allowance of water in the adjacent overflow container, but some global water head increment was still found during discharge [20]. Therefore, the final DP is located near the top of the tank (at 80 cm) as reference for the net pressure increment ( $\Delta P_{DP,h,net}$ ) in the domain due to the discharge (Eq. 3.1):

$$\Delta P_{DP,h,net} = \Delta P_{DP,h} - \Delta P_{DP,80} \quad (3.1)$$

where  $\Delta P_{DP,h}$  is the measured global pressure increment at height  $h$  and  $\Delta P_{DP,80}$  is the pressure increment measured by the DP at the top of the tank.

An example of the DP net pressure increments over the course of an experiment, together with the corresponding pipe displacements, is shown in Figure 3.6 with the results from Test VNL12. The net pressure increments due to discharge show a smooth increase until the end of discharge, which is at 60 seconds in the example from Test VNL12. The bottom DP measures higher pressures than the DP located 10 cm above it. This is because the bottom DP has an additional 10 cm of domain in which the sand particles stay suspended and increase the measured pressures. After the discharge has stopped, the net pressure increments gradually return back to zero, when all the suspended sand particles have settled again.

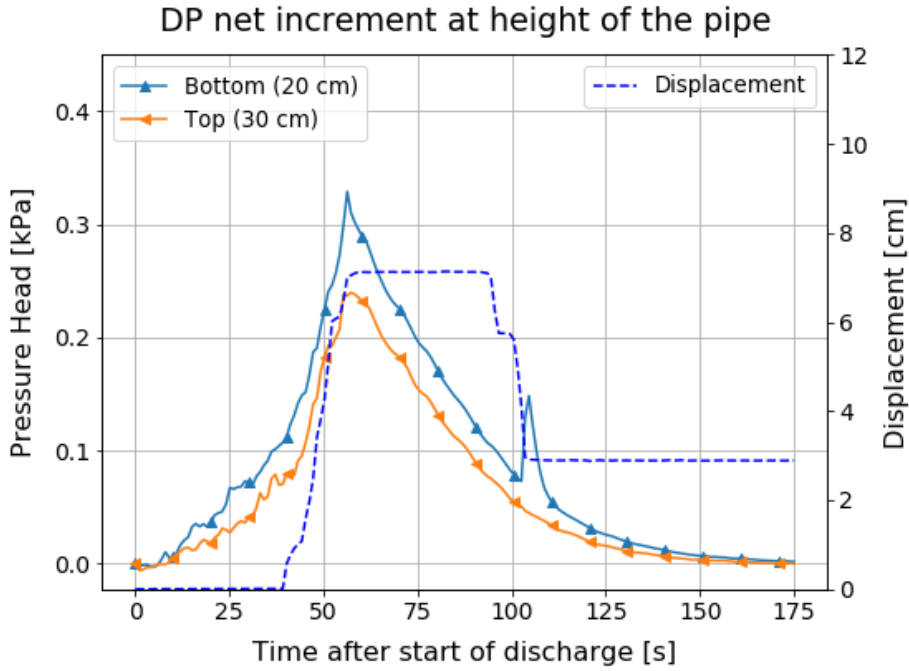


Figure 3.6: The development of DP net increment over time, together with the pipe displacements from Test VNL12

The pressure increments are produced by the sand particles in the discharge during an experiment and therefore depend on the discharge conditions. The total discharged volume and the maximum domain concentration are directly correlated to the maximum net pressure increments. Furthermore, the discharge flow rate influences the slope of the increment in net pressures. In the example in Figure 3.6, with the increasing slope at approximately 40 seconds after the start of discharge, a distinct increase in discharge flow rate is noticed.

If pipe flotation has occurred during the experiment, the pipe eventually starts to sink again and it lands on the new sand bed. If the impact of the pipe on the recently settled and relatively loose sand is large enough, it causes a sudden increase in pressure measured by the DP inside the sand bed (at 20 cm). This increase in pressure is due to the local excessive water pressure, induced by the shear forces from the pipe impact. The DP at 30 cm does not measure this increment, because the sedimentation front is still below this level. In Figure 3.6 this impact is visible just after 100 seconds after the start of discharge.

### 3.3.5. Specific gravity

The specific gravity of the mixture in the domain is used to signify the buoyancy generated on the pipe. This parameter can be estimated based on two different measurements: the concentration developments, derived with the conductivity bar or the differential pressure measurements. For the analysis of pipeline flotation in this research, both methods are included and the results are compared.

The concentration development of the mixture in the domain over time and at each height, as shown in Figure 3.4, can also be expressed as the evolution of the specific gravity of the mixture at these particular heights ( $s_{con,h}$ ). The method to convert these parameters is given in Equation 3.2:

$$s_{con,h} = s_w(1 - C_{s,h}) + s_s C_{s,h} = 1 + 1.65C_{s,h} \quad (3.2)$$

where  $s_w$  is the specific gravity of water and  $s_s$  is the specific gravity of a sand particle, which are 1 and 2.65, respectively. The sand volume concentration at height  $h$  is represented by  $C_{s,h}$ .

Equation 3.2 determines the specific gravity of the mixture at one specific height. The specific gravity of the mixture that is producing buoyancy on the pipe body can be estimated by the weighed average from the specific gravity at each height directly around the pipe [20]. As the pipe diameter in this research is 10 cm, the amount of sensors directly surrounding the pipe in the initial position on top of the sand bed is five (from 20 to 30 cm height). Therefore, the diameter of the pipe is divided in five weighed heights around these sensors. Once the sedimentation starts and the sedimentation front develops over the area of the pipe, the total effective height of the pipe ( $h_{eff}$ ) decreases. The specific gravity of the sand layer underneath the sedimentation front is set equal to the specific gravity of water. The subordinate effective heights of the individual sensors ( $h_{eff,i}$ ) are also influenced if the sedimentation front reaches their zone. The weighed average specific gravity on the pipe ( $s_{con,avg}$ ) is approximated by the measurements from these subordinate sensors, their corresponding effective heights and the location of the sedimentation front (Eq. 3.3). The details regarding this calculation are demonstrated by Yang (2020) [20].

$$s_{con,avg} = \frac{s_w(D - h_{eff}) + \sum(s_i h_{eff,i})}{D} \quad (3.3)$$

where  $s_i$  is the specific gravity calculation of the mixture at the subordinate sensor with its corresponding effective heights ( $h_{eff,i}$ ). If this equation is applied to a situation where no sedimentation has occurred (yet), the effective height of the pipe is equal to the pipe diameter, and the first term in the numerator becomes zero. The weighed average of the specific gravity is obtained by rounding the sum of these calculations over the full pipe diameter. With this approach, the average specific gravity producing buoyancy on the pipe can be compared to the specific gravity of the pipe weight.

This average specific gravity of the mixture in the domain is based on the effective height of the weighed sensors in the domain, but the circular shape of the pipe surface has an additional influence on this calculated buoyancy. Hence, the second method is based on the weighed average of the measured specific gravity of the mixture on the effective area of the pipe ( $s_{con,p}$ ). A difference with the previously described method is that the shape effect is taken into account here. The buoyancy approximation on the pipe can be calculated with Equation 3.4 [20]:

$$s_{con,p} = \frac{\sum(s_i A_{eff,i})}{A_p} \quad (3.4)$$

where the effective area of each subordinate sensor ( $A_{eff,i}$ ) is used, instead of the effective height in Equation 3.3. For this reason, the numerator in this case is rounded over the total pipe surface area ( $A_p$ ), instead of over the pipe diameter. The width of the pipe increases from the bottom towards the middle and decreases again after the middle of the pipe has been reached. This causes the minor difference between  $s_{con,avg}$  and  $s_{con,p}$ . Before the sedimentation front has extended to the middle of the pipe,  $s_{con,p}$  is slightly larger than  $s_{con,avg}$ , while the reverse is true after the sedimentation front exceeds the middle of the pipe.

To verify the reliability of the system, the net pressure increments in the system can also be translated to the specific gravity of the mixture producing buoyancy on the pipe. The net pressure increments come from differential pressure transmitters, measuring the difference between pure water before the start of the experiment and an increased amount of sand in the water during the experiment. These measurements are used to estimate the specific gravity of the mixture at the height of the pipe. The average specific gravity of the mixture between two measurement points is derived from net pressure increments measured at two different heights.

$$s_{DP,avg} = s_w + \frac{\Delta P_{DP,h+\Delta h,net} - \Delta P_{DP,h,net}}{gh} \quad (3.5)$$

where  $\Delta P_{DP,h,net}$  and  $\Delta P_{DP,h+\Delta h,net}$  are the net pressure increments from Equation 3.1 at height  $h$  and height  $h + \Delta h$  respectively. The average specific gravity of the mixture ( $s_{DP,avg}$ ) is determined between these two measurement points. As the two main DP's are positioned at the initial bottom and top levels of the pipe, the average buoyancy from the mixture on the pipe is determined at the middle of the pipe before flotation occurs, which is at a height of 25 cm in the experimental tank.

The previously explained approaches to estimate the buoyant specific gravity of the mixture on the pipe, return similar results. An example of the development of specific gravity of the mixture during an experiment is shown in Figure 3.7. The specific gravity of the pipe is constant during the entire experiment and is displayed with the horizontal red dotted line. The blue dashed line represents the displacements of the pipe due to the backfilling process. If progressive flotation takes place, which is usually the case if the pipe experiences any uplift at all, the DP measurements still demonstrate the average buoyant specific gravity from 20 cm to 30 cm height. This calculation is not representative for the specific gravity of the mixture around the pipe anymore. However, this research especially focuses on the start of flotation, which does agree with the measurements.

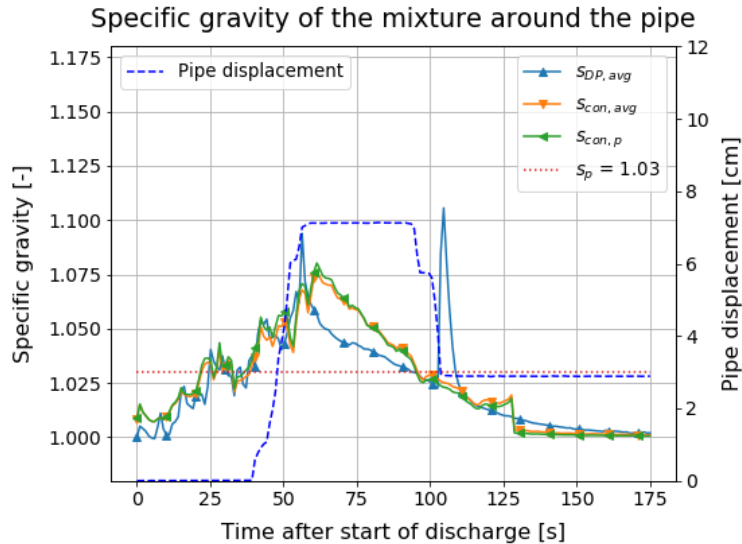


Figure 3.7: The development of specific gravity over time, together with the pipe displacements from Test VNL12

The specific gravity of the mixture determined by the conductivity bar,  $s_{con,avg}$  and  $s_{con,p}$ , are very similar. This is plausible, as the only difference in approach of these two calculations is the shape effect of the pipe surface. The difference with the specific gravity based on the pressure increments ( $s_{DP,avg}$ ) is slightly larger. In general, the different approaches still approximate the same value of specific gravity of the mixture, as is evident in the part of Figure 3.7 with the increasing specific gravity values.

The maximum mixture density in every experiment is obtained when the discharge is stopped or right after this moment. At this maximum mixture density, the maximum amount of sand particles is present as a suspension in the domain and therefore this is the most critical moment in time regarding buoyancy. In Test VNL12 in Figure 3.7, this maximum is visible around 60 seconds after the start of discharge.

In some experiments, one or two large peaks in  $s_{DP,avg}$  are noticeable: one at the end of discharge and/or one at the moment the pipe hits the sand bed after it sank again. The peak at the end of discharge is caused by the disturbance of the stiff hose, which is connected to the bottom DP, when the T-valve is switched off. Furthermore, directly after the end of discharge or after the pipe starts to float progressively, in some experiments a larger difference is recognised between the methods based on the conductivity bar and the DP's. In Figure 3.7, this phenomenon is visible between approximately 60 and 90 seconds after the start of discharge. This wider scatter between the two approaches is more evident with upwards discharge than with horizontal discharge. This is caused by the higher concentration developments in the sensors above the top DP sensor. The DP increments do not take these measurements into account, but the conductivity bar is capable of including these developments.

After the end of discharge, the sedimentation continues until all sand particles in the domain have settled. At the end of the sedimentation process, the sedimentation front ceases at a certain level. If the end level of the sedimentation front is right between two pairs of conductivity probes, the sensors experience difficulties with this data processing. The discontinuity in effective height causes a jump in the specific gravity calculations. In Figure 3.7, this jump is visible at 130 seconds, right at the end of sedimentation.

### 3.3.6. Pipe displacements

Once the discharge for an experiment starts, the sand-water mixture in the domain blocks the view from the pipe in the experimental tank. Therefore, the vertical displacements of the pipe are measured with an ultrasonic displacement sensor, positioned on top of the tank. The pipe is attached to a vertical guiding rod with a steel plate secured to it, right above the ultrasonic sensor. With this approach, the displacement sensor can measure the vertical movements of the pipe during the experiments. These results are compared to the forces working on the pipe, so conclusions regarding pipeline flotation can be drawn.

Unfortunately, the measurements from the ultrasonic displacement sensor do not always agree with the displacements visible in the recordings and often show (much) lower values than expected. The minimum distance between the sensor and the steel plate to measure properly, is actually larger than anticipated beforehand. For this reason, the movements of the pipe at the lowest elevations are not always included in the measured values. Hence, the pipe displacement values in the experimental results do not always show the correct values. Therefore, the maximum pipe displacement values ( $Dis_{max}$ ) used in the analysis of pipeline flotation are estimated with the movements of the steel plate in the video recordings. This parameter is now based on a visual inspection, but due to the clearly visible movements of the steel plate, the estimation of the maximum pipe displacements is still very accurate.

The start of pipe flotation is a significant observation during the experiments. Despite the lower maximum pipe displacements measured by the displacement sensor, the moment of flotation is generally correctly measured by this sensor due to the relatively fast uplift of the pipe. So in the graphic visualisations of the results, the start and end of flotation for most experiments are properly shown in the displacements, while the height of the pipe uplift is generally lower. In some experiments, the pipe actually started to float before the sensor registered or there were pipe displacements, while the sensor did not show any movements. In these cases, the actual start (and sometimes end) of flotation is added to the graphical results with vertical lines at these times (see Appendix B). Moreover, in many experimental results, the pipe displacements return to zero after the end of flotation. However, this is a consequence of the false measurements of the displacement sensor. In reality, sedimentation takes place during pipe flotation and the sedimentation front has risen several centimetres before the pipe hits the soil again, so the end position of the pipe is always higher than before flotation.

When flotation occurs, the maximum pipe displacement is an interesting parameter. An overview of the maximum pipe displacements over the maximum domain concentrations reached in all experiments performed in this research with the same pipe specific gravity of 1.03, is displayed in Figure 3.8. Generally, if the pipe experiences any uplift in the experiments, it floats up until it reaches the T-junction used for discharge. These maximum pipe displacements to the top vary from 7 cm to 14 cm, but this is due to the initial elevation of the pipe in some experiments (see Section 3.2) and due to the different alignment of the pipe compared to the T-junction. The experiments with this pipe uplift to the top are shown with the green circles in Figure 3.8 and the red coloured circles display the experiments without any pipe flotation. Some experiments are exceptions to this assumption. The two grey data points are unreliable, due to some external disturbances in the laboratory where the experiments were conducted. In the set of orange experiments, the pipe does experience flotation, but not to its maximum potential. A further analysis of these noticeable experiments is given in Chapter 4.

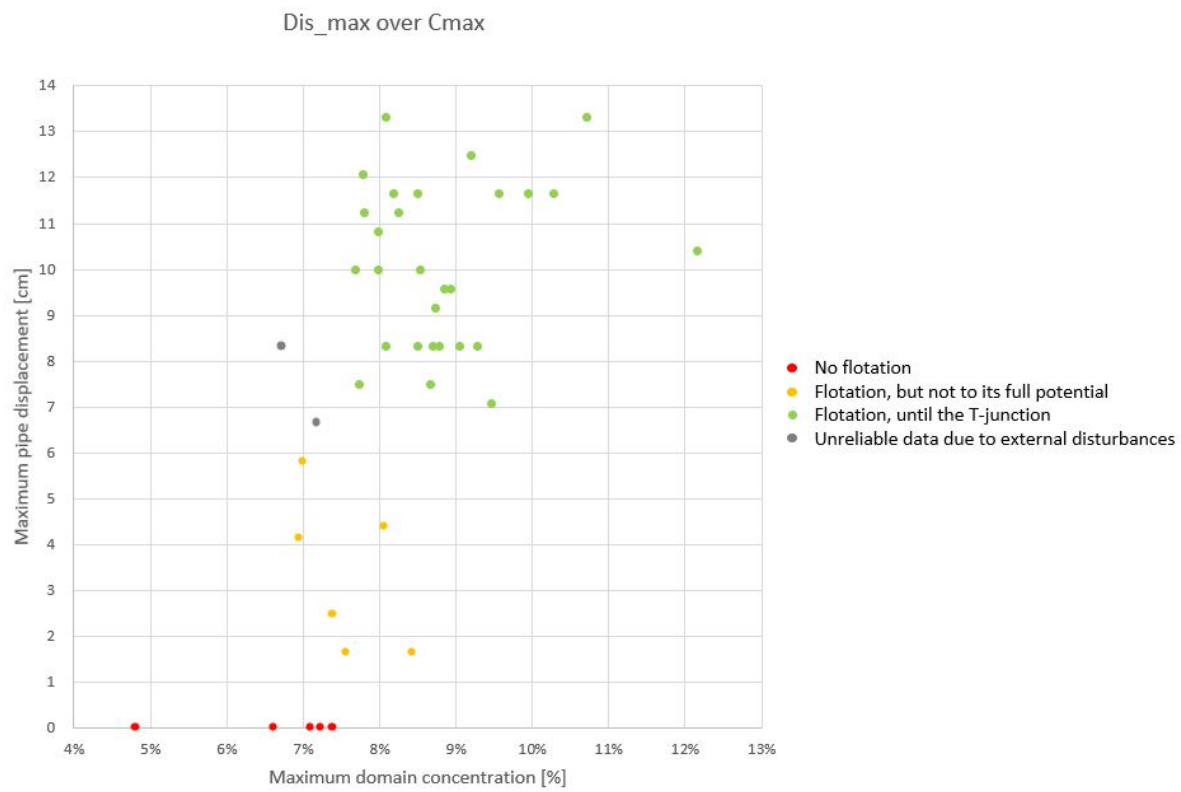


Figure 3.8: An overview of the maximum pipe displacement over the maximum domain concentration of all experiments performed in this research with the same pipe specific gravity of 1.03



# 4

## Experimental Parametric Studies

The desired outcome of this research is to find the critical state of pipeline flotation during sand backfilling on a small scale for the different parameters involved in this process. From these results, a prediction of the mechanisms during a TSHD sand backfilling process on offshore pipelines could be derived in the future. A total amount of 50 experiments is executed, divided over the four different stages from Section 3.2 and the steps in the testing programme from Section 3.2.5 are followed during each experiment. An overview of the most significant parameters and results from each individual experiment is given in Appendix B. The data from three specific experiments (Test VVL37, VVL38 and VNH48), is considered unreliable due to external disturbances in the laboratory during the experiments.

Considering the four stages of the experimental procedure (see Section 3.2), a division of the experiments is made in these categories. Experiments HNL1 to HNL11 are all performed in Stage 1, where the pipe with a constant specific gravity of 1.03 is situated on top of the sand bed and it experiences horizontal discharge. All tests after this stage are performed with a vertically upward discharge. Experiments with codes VSL, VML and VVL are used to investigate the initial pipe elevations of different heights from Stage 3 and experiments with codes VNW and VNH are executed with an increased pipe specific gravity (Stage 4).

The most significant parameters and mechanisms found in this research during a sand backfilling process are the developments of the concentration of mixture surrounding the pipe, the continuous sedimentation during discharge, and therefore the pipe embedment before the start of flotation, and the pipe specific gravity. The hydrodynamic effects during discharge also prove to have an important influence in the small-scale experiments.

### 4.1. Influence of Domain Concentration

The development of the sand volume concentration in the domain is one of the most influential parameters in the pipeline flotation analysis. This concentration build-up in the surroundings of the pipe produces the buoyancy forces and thus the potential uplift of the pipe is a direct cause of this parameter. The maximum concentration that is reached in the suspension around the pipe during an experiment, without the sand particles to settle, is the most critical value for potential pipe flotation. This parameter depends on the total amount of discharged volume and therefore varies with different input parameters. From the experimental results, with a relatively constant average discharge concentration between 20% and 30%, the input variable with the most influence on the trend of the domain concentration is the discharge flow rate. The larger this discharge flow rate, the more rapid the domain concentration increases. The only known variable is the average discharge flow rate over the entire duration of discharge, but a variation in speed of domain concentration developments indicates a changing discharge flow rate over the course of the experiment.

In Figure 4.1, two of the most important parameters in the analysis of pipeline flotation are plotted against each other for all experimental data with the same pipe specific gravity: the maximum domain concentration that is reached during the experiment ( $C_{max}$ ) versus the average discharge flow rate over the entire duration of discharge ( $Q_{cat}$ ).

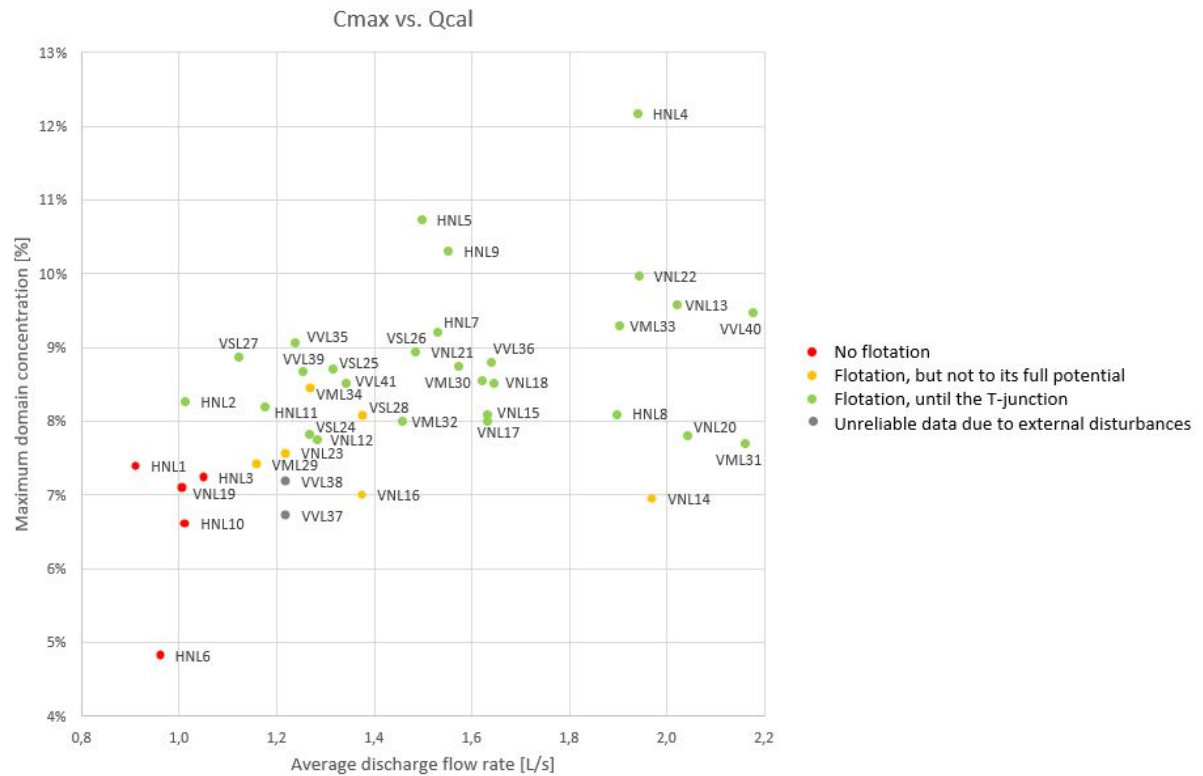


Figure 4.1: Overview of the obtained maximum domain concentrations at the corresponding average discharge flow rate during all performed experiments with a pipe specific gravity of 1.03

The results in Figure 4.1 are based on experiments with a pipe specific gravity of 1.03, which includes all experiments from the first three stages explained in Section 3.2. The data points are therefore labelled with the name of the corresponding experiment, in which the direction of discharge and the initial positioning of the pipe for that specific experiment can be recognised. The experiments with the increased pipe weight are not featured in Figure 4.1, due to the different behaviour in this stadium.

An approximate correlation between the average discharge flow rate, the maximum domain concentration and the moment of flotation can be recognised. The test results where the pipe remains on the sand bed during the entire experiment, all show a low average discharge flow rate and a relatively low maximum domain concentration. A distinction is made between the experiments with flotation, where the pipe floats up until it hits the T-junction positioned above the pipe, and where the pipe does show some uplift reactions, but not to its full potential. In general, the experiments with maximum flotation are obtained when a relatively high maximum domain concentration is approached. An apparent limit of pipe flotation can be recognised at a maximum domain concentration of approximately 7.5%, regardless in which stage the experiment is performed. In general, this flotation limit does not seem to depend on the average discharge flow rate. However, the discharge flow rate is correlated to the maximum domain concentration: with a lower discharge flow rate, the maximum sand volume concentration around the pipe generally reaches lower values and is therefore more prone to stay below the pipe flotation limit.

The experiments with some moderate signs of pipe uplift are visible with the orange coloured dots in Figure 4.1. These results show exceptions to the pipe flotation limit. In experiments VNL14 and VNL16, a relatively low maximum domain concentration of 7% is obtained, but the pipe still experiences some uplift. In both experiments the start of pipe flotation is at a point in time where the domain concentrations briefly jump up, so a very high momentary discharge flow rate is identified (the graphical illustrations of the results can be found in Appendix B). Experiment VNL14 even has a very high flow rate over the entire duration of discharge. Experiments VNL23 and VML29 are exactly around the pipe flotation limit of 7.5%, but also experience a sudden increase in discharge flow rate at the moment of some signs of uplift.

Contrarily, in experiments VSL28 and VML34 a relatively high maximum domain concentration is achieved, but only minor pipe uplift movements are visible. From the recordings and the measurements from Test VSL28, it is clear that the discharge flow rate fluctuates heavily from very low to very high in a pulsating manner. This could induce some hydrodynamic streams, which influence the pipe uplift movements. Furthermore, in both experiments the initial position of the pipe was elevated 1 cm or 2 cm above the sand bed, so other hydrodynamic effects may be of influence here as well. The influential hydrodynamic effects during the experiments are further discussed in Section 4.3.

In conclusion, the maximum domain concentration is a key factor in determining the pipe flotation limit. However, this parameter is difficult to measure during TSHD sand backfilling on the seabed. To stay below the critical domain concentration in the field, a prediction of the relation between the input parameters and the maximum domain concentrations should be made. As there is still a strong variation in several input parameters in the small-scale experiments, a Computational Fluid Dynamics (CFD) analysis is suggested to relate the domain concentration to the input parameters over time.

## 4.2. Influence of Pipe Embedment

During the experiments, the ongoing sedimentation influences the behaviour of the pipe. The height of the sedimentation front, compared to the total pipe diameter leads to the embedment ratio of the pipe ( $w/D$ ) at each moment in time during the experiments. The pipe embedment affects the forces generated on the pipe body, due to its decreasing consequence on the effective area of the pipe surface: the larger the pipe embedment, the smaller the pipe effective area becomes, on which buoyancy from the mixture applies. It is plausible to assume that the sedimentation of the sand particles around the pipe not only reduces the effective area of the pipe on which the mixture induces buoyancy, but that it also creates some additional resistance towards flotation. This resistance can be translated to a downward force on the pipe, of which the magnitude depends on the height of the sedimentation front around the pipe. No explicit formula has yet been defined for this friction force, due to the presence of sand that has deposited around the pipe, that counteracts its vertical uplift.

In this research, the additional downward working force is approximated by the shear stresses on the curved edge of the pipe due to the deposited sand around it (Eq. 2.10). These shear stresses can be approximated with the normal stress acting on the pipe surface (Eq. 2.8) and the corresponding friction coefficient at low stress levels (Eq. 2.9) from White and Randolph (2007) [19]. The equations are considered in the analysis of this research, but in reality this method was developed for the approximation of pipe-soil contact stresses in clay. The application of these equations for the small-scale experiments with sand is considered to be acceptable, but it still causes some uncertainties.

When considering this method, the elementary force due to friction perpendicular to the surface at every infinitesimal part along the pipe-soil contact surface can be obtained by multiplying the shear stresses by the length of this small arc. For the one-dimensional assessment of pipeline flotation in this research, only the vertical components of the friction force are taken into account. The elementary vertical force due to friction can be determined with Equation 4.1.

$$dT = \sin \theta \tau ds \quad (4.1)$$

To approximate the total vertical friction force, an integral is taken along the pipe surface from the bottom of the pipe to the contact surface of the sedimentation front ( $\beta$ ). For symmetry reasons, the equation needs to be multiplied by 2 to get the total friction force. Combining equations 2.8, 2.9, 2.10 and 4.1, and taking the integral in polar coordinates leads to the calculation of vertical friction force  $T$  per unit length as shown in Equation 4.2.

$$T = 2 \int_0^\beta \sin \theta \sigma'_r \mu r d\theta \quad (4.2a)$$

$$T = 2 \int_0^\beta \sin \theta \left( \frac{V}{D} \frac{2 \cos \theta}{\beta + \sin \beta \cos \beta} \right) \left( 0.25 - 0.3 \log \left( \frac{\frac{V}{D} \frac{2 \cos \theta}{\beta + \sin \beta \cos \beta}}{p_{atm}} \right) \right) r d\theta \quad (4.2b)$$

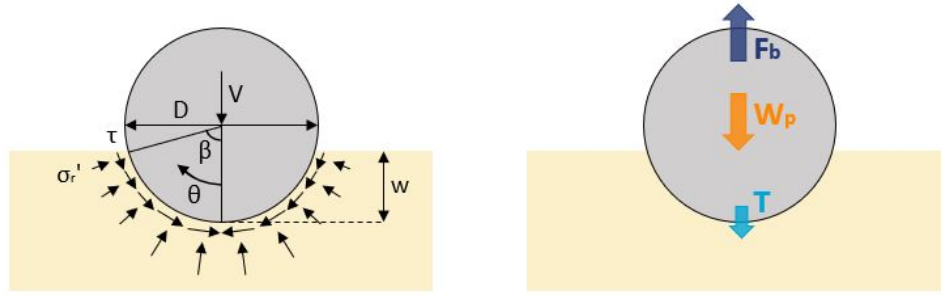


Figure 4.2: Schematic drawing of the forces on a one-dimensional section of the pipeline, which is partially buried and fully surrounded by a sand-water mixture, and the corresponding parameters

A schematic drawing of the forces on a one-dimensional section of a partially buried pipe and the corresponding parameters are shown in Figure 4.2. Equation 4.2 accurately approximates the friction force only when the pipe is buried for (less than) half of its diameter due to trigonometric constraints of the formula. To simplify the equation and to derive the friction force analytically, the friction coefficient  $\mu$  is approximated as a constant and not depending on the pipe embedment. With a constant friction coefficient, the parameter  $\mu$  can be taken out of the integral and the vertical friction force per unit length due to burial of the pipe can be approximated as follows:

$$T = \mu V \frac{\sin^2 \beta}{\beta + \sin \beta \cos \beta} \quad (4.3)$$

Equation 4.3 describes the friction force  $T$  as a function of a constant friction coefficient, the pipe buoyant weight and the pipe embedment. When the discharge continues over the course of an experiment, the pipe becomes more embedded, which increases parameter  $\beta$  and therefore the friction force. This equation accurately approximates the vertical friction force only if a representative friction coefficient is applied, which can be determined by a representative normal stress on the pipe-soil contact surface.

The normal effective stress can be derived by Equation 2.8 and depends on the pipe buoyant weight, the pipe diameter and the amount of pipe embedment [19]. As this research focuses on small-scale experiments with a very low pipe weight, the normal stresses at the pipe-soil contact surface obtain very low values. The pipes with a specific gravity of only 1.03 to 1.12 in this research cause normal effective stresses underneath the pipe between 0 and 100 Pa, instead of in the order of  $10^2$  kPa in conventional geotechnical studies. The corresponding friction coefficients in the current research are therefore much higher than the known friction coefficient of approximately 0.30 to 0.45 between pipe material and sand [1]. For the determination of a representative normal stress for the experiments in this research, the integral mean of the normal stresses is calculated over the embedded contact surface between the pipe and the sand:

$$\sigma'_{r,avg} = \frac{1}{\beta - 0} \int_0^\beta \sigma'_r d\theta \quad (4.4a)$$

$$\sigma'_{r,avg} = \frac{V}{\beta D} \frac{2 \sin \beta}{\beta + \sin \beta \cos \beta} \quad (4.4b)$$

The average normal stresses ( $\sigma'_{r,avg}$ ) for the different pipe weights used in this research are approximated with Equation 4.4 and the results are given in Table 4.1. The corresponding friction coefficients, calculated with Equation 2.9, are given in this table as well. Furthermore, the pipe-soil interface friction angle  $\phi_{int}$  can be determined with the friction coefficient ( $\mu = \tan(\phi_{int})$ ).

In this specific small-scale research, the corresponding interface friction angles are approximately  $50^\circ$ , instead of the more common value of  $30^\circ$  [14]. This unusually high friction angle is related to the particularly low stress situation underneath the pipe, as explained in Section 2.3, and can be recognised as a peak friction angle. The exact stress situation underneath the pipe is unknown, but the presence of shear stresses is likely to enhance a change in the volume of sand, which is represented by the angle of dilation ( $\psi$ ). This angle of dilation becomes more prevalent if the normal stresses are low, as is explained by Bolton (1986) [2].

This peculiarly low stress situation is found in the small-scale experiments in this research, therefore the presence of large dilatancy is expected underneath the pipe. In a fully drained condition, a large friction angle is caused by this large dilatancy underneath the pipe. On the other hand, in undrained conditions, the soil below the pipe can develop pore underpressures and some effects of suction could be accounted for. Yang (2020) indicated that excess pore pressures in the newly deposited sand around the pipe slightly build up during the experiment, but dissipate again relatively fast [20]. By this observation, a condition of partial drainage is likely to be assumed underneath the pipe in the small-scale experiments. With this assumption, the large friction angle (and therefore the large friction coefficient) in this research could be explained by a combination of high dilatancy and possible pore underpressures underneath the pipe. However, this hypothesis cannot be validated due to the lack of knowledge of the stress situation underneath the pipe and further research is recommended.

Table 4.1: Normal stress and friction values for the different pipes used in this research

$s_p$ [-]	$\sigma'_{r,avg}$ [kPa]	$\mu$ [-]	$\phi_{int}$ [°]
1.03	0.019	1.368	54
1.08	0.047	1.250	51
1.12	0.074	1.191	50

When assuming these relatively large friction coefficients from Table 4.1 for the analysis of pipe flotation in this research, the influence of the pipe embedment on the friction force  $T$  is shown in Figure 4.3. The resistance is normalised to the vertical contact force on the sand bed ( $V$ ), which is the pipe submerged weight. The difference between the calculation of the friction force with the assumption of a representative constant value or with a more accurate friction coefficient that varies over the course of an experiment, is shown in Figure 4.3. In general, these differences are very small. Hence, the calculation of the friction force can be approximated by a constant friction coefficient, as long as there is a good impression of the normal stresses present underneath the pipe. As the implementation of a single and constant friction coefficient shows reliable results for multiple experiments with the same input parameters, the sedimentation mechanisms are considered similar in all these experiments.

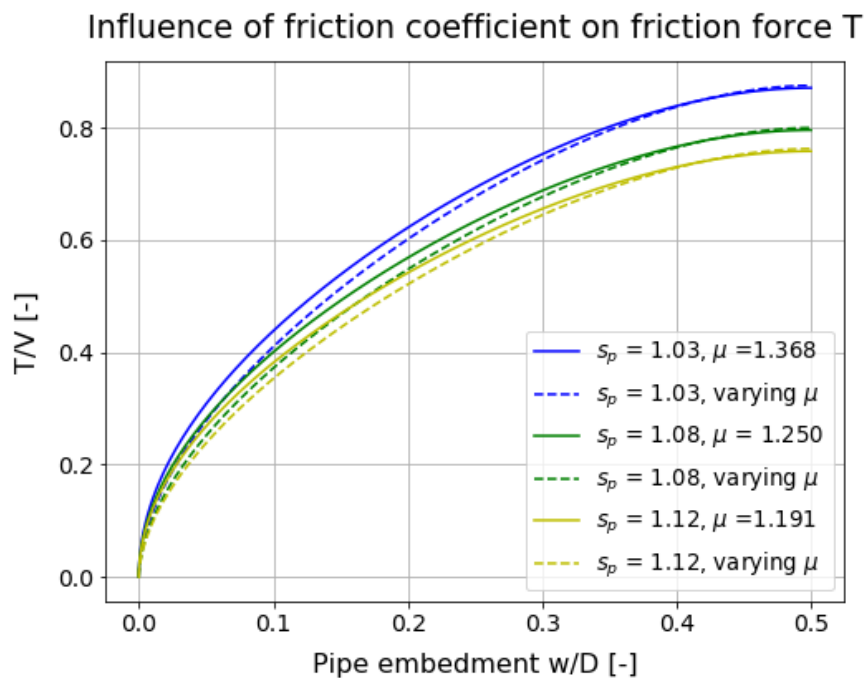


Figure 4.3: Influence of the pipe embedment on the downward working friction force

The ratio of the friction force over the buoyant pipe weight, results in a dimensionless relationship that gradually increases with an increasing embedment of the pipe (Figure 4.3). If the pipe lays directly on top of the sand bed, the friction force is equal to zero. However, if the sedimentation buries half of the pipe ( $w/D = 0.5$ ), the friction force approaches a magnitude that ranges around 75% to 90% of the pipe buoyant weight. This variation in friction is related to the different pipe weights used in the experiments. The lightest pipe, with a specific gravity of 1.03, shows the largest influence from the friction coefficient. This is because the friction coefficient increases as the normal stresses at the pipe-soil contact surface decrease (see Equation 2.8).

Flotation triggering of the pipe during discharge, can be assessed by considering a one-dimensional section of the pipe. The static force balance from Burgmans (2005), as explained in Section 2.1, can now be extended [3]. Taking the additional downward friction force (Eq. 4.2) into account in the static force balance per unit of length of the pipe, together with the pipe weight and the upward buoyancy forces, the resultant force per unit length of the pipe  $q$  converts from Equation 2.3 to Equation 4.5:

$$q = A_p(\rho_p - \rho_w) + T - A_{eff}(\rho_m - \rho_w) \quad (4.5)$$

The sign of the resultant force working on the pipe is relevant for the analysis of pipeline flotation. If the pipe weight and the friction force due to pipe embedment together are dominant, the pipe will stay on the sand bed. On the other hand, if the resultant force is negative due to the dominating buoyancy forces on the pipe, it will start to float. To evaluate flotation triggering during the sand backfilling process, the normalised force balance in Equation 4.6 is applied at multiple points in time during the experiments.

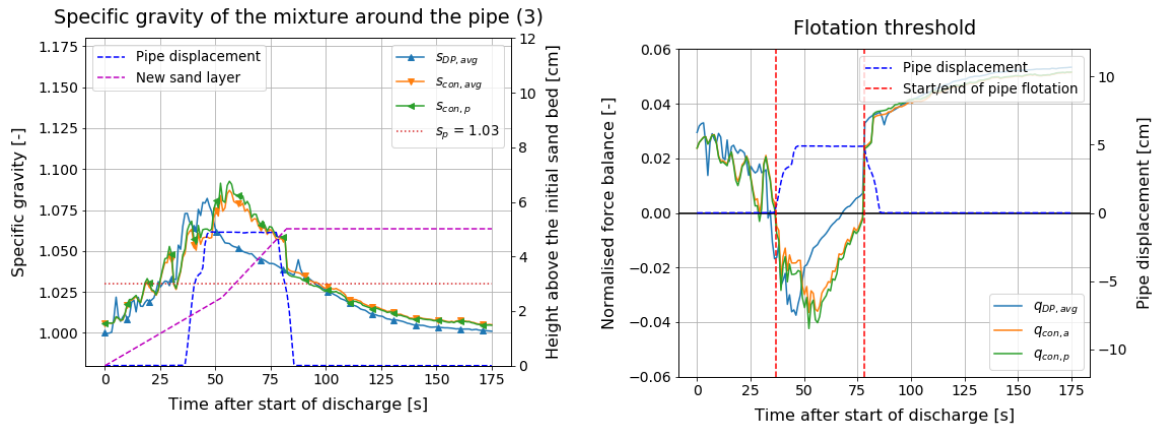
$$q_n = \frac{\sum F_{down} + \sum F_{up}}{\sum F_{down}} \quad (4.6a)$$

$$q_n = \frac{A_p(\rho_p - \rho_w) + T - A_{eff}(\rho_m - \rho_w)}{A_p\rho_p + T} \quad (4.6b)$$

The moment the normalised resultant  $q_n$  changes from positive to negative, the pipe will start to float. Including the friction force in the force balance, which is directed downwards and is therefore positive, increases the total resultant force and thus predicts a later moment of pipe flotation in the small-scale experiments. The actual magnitude of the friction force depends on the pipe weight and the sedimentation rate during an experiment: with a large sedimentation rate, the pipe embedment rapidly increases and the difference in resultant force when including the friction force in the force balance, becomes larger. If the pipe experiences enough uplift to completely separate itself from the sedimentation front, the resisting force  $T$  will evidently disappear.

The pipe embedment influences the average buoyant specific gravity of the mixture on the pipe. A decrease in effective area of the pipe, reduces the surface on which buoyancy is generated and thus decreases the total buoyant force on the pipe. This reducing effect is taken into account in the flotation assessment of all experiments and Figure 4.4a shows the build-up of buoyancy on the pipe from one specific experiment (Test VNL15), together with the constant pipe specific gravity of 1.03. The pipe displacements and the height of the developing sedimentation front are included in this figure with the dashed lines. This figure evidently shows that the buoyancy from the mixture increases rapidly after the start of discharge and it exceeds the pipe specific gravity at approximately 30 seconds after the start of discharge. Hence, without friction from pipe embedment, this moment in time should indicate the theoretical flotation triggering. Nevertheless, any uplift movements from the pipe are absent until approximately 37 seconds after the start of discharge.

The delay in pipe flotation from Figure 4.4a can be explained by the friction force generated by the pipe embedment. The sedimentation around the pipe develops instantly after the start of discharge and the pipe is already embedded 2 cm before flotation occurs. The resistance against pipe flotation due to its embedment is included in the force balance in Figure 4.4b, together with the pipe weight and the buoyancy forces on the pipe, so a theoretical flotation threshold is visible. A distinction can be made between the three different calculation methods for the buoyancy from the mixture on the pipe: based on the DP measurements and based on the conductivity bar measurements with the effective height or with the effective area.

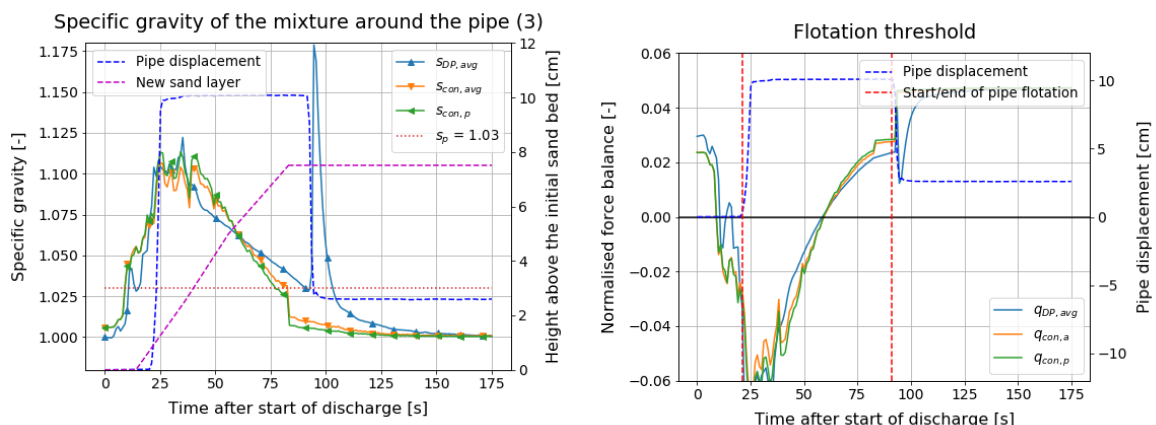


(a) Build-up of buoyant specific gravity on the pipe, compared to the pipe specific gravity from Test VNL15 (b) Normalised force balance on the pipe from Test VNL15

Figure 4.4: Determination of the start of flotation based on buoyant specific gravity on the pipe and based on the normalised force balance in Test VNL15

If the normalised force balance is positive, the downward forces on the pipe dominate and the pipe stays on the sand bed. Once this value becomes negative, the buoyancy forces from the mixture prevail and the pipe experiences flotation. In Figure 4.4b, this theoretical flotation limit matches well with the measured pipe displacements. The normalised force balance from Equation 4.6 is applied to all experiments (see Appendix B) and in general, the theory approximates the start of flotation adequately. The three different calculation methods show similar results, but in some experiments either one method works better than the others.

Moreover, in several experiments the force balance indicates negative values before the actual pipe displacements take place or even without any uplift over the course of the experiment. This is due to the fixed initial sand bed at 20 cm in the calculation model. According to the new sand layer measurements, indicated with the purple dashed line in Figure 4.5a, there is no sedimentation in the first 15 seconds. In reality, the initial sand bed height is just below 20 cm and sedimentation does take place from the beginning, but without these measurements being registered as the new sedimentation front in the calculations for the friction force. Therefore, the influence of the friction force is not taken into account in the initial stadium of the experiment and the normalised force balance is more negative than expected before the pipe movements occur (see Figure 4.5b).



(a) Build-up of buoyant specific gravity on the pipe, compared to the pipe specific gravity from Test VNL13 (b) Normalised force balance on the pipe from Test VNL13

Figure 4.5: Determination of the start of flotation based on buoyant specific gravity on the pipe and based on the normalised force balance in Test VNL13

However, the results of a few experiments still show a slight delay in physical flotation compared to the theoretically defined moment of flotation. This could indicate that apart from the friction due to pipe embedment, suction is also playing a role in the pipe flotation mechanism in these small-scale experiments. For a rough indication of the influence of pipe embedment on the force needed to lift the pipe in the small-scale experiments, simple tests with a force meter are performed. The results from these uplift tests are explained in Appendix A. Unfortunately, no conclusions could be drawn from these uplift tests and more research regarding the possible influence of suction underneath the pipe, is suggested.

### 4.3. Influence of Hydrodynamic Effects

The TSHD process of sand backfilling a pipeline on the seabed is translated to a small-scale experiment with a ratio of approximately 1:12 in this research. A secondary influence of downscaling the process to a relatively small experimental tank is the emergence of hydrodynamic effects. The flow of a sand-water mixture from the discharge is influenced by the sidewalls from the experimental tank, which could cause erosion and additional hydrodynamic and drag forces.

Initially, horizontal discharge was maintained during the experiments, but dominant circular motions were observed with this method and additional erosion and hydrodynamic forces on the pipe body were recognised. Due to the generated turbulence at the sand bed, the pipe body was prone to experience hydrodynamic forces, the most critical in this research being uplift forces at the bottom of the pipe. In a later stage, the vertically upward discharge was applied in the small-scale experiments. This vertical direction of discharge shows promising results regarding a less prevalent influence of the sidewalls of the tank and a more accurate approximation of the TSHD discharge action in the field. Nevertheless, some signs of erosion of the sand bed were still visible directly below the T-junction, specifically with a relatively large discharge flow rate. Although the dominant circular motions in flow are significantly reduced with the vertical discharge, some effects of erosion still remain in the experiments. These minor erosion effects are not considered in the calculation model.

The magnitude of the discharge conditions, the discharge flow rate and the concentration of discharge, are the most significant parameters for these additionally encountered hydrodynamic effects. As the concentration of discharge is approximately constant over the course of an experiment and stays between 20% and 30% volume concentration for all tests, the most influential parameter is the discharge flow rate.

In general, the direction of discharge does not influence the moment or magnitude of pipe uplift. In Figure 4.6, a clear pipe flotation limit is visible at a domain concentration of approximately 7.5% for the small-scale experiments, despite the direction of discharge. However, the magnitude of the discharge flow rate does seem to play a significant role in the uplift movements of the pipe. A fierce stream of sand is expected to separate during backfilling and sub-currents of various concentrations are created, as was observed by Cathie, Barras and Machin (1998) as well [5]. Backfilling with a very high discharge flow rate is proven to induce oscillating movements of the pipe in multiple experiments and in the orange coloured results in Figure 4.6 even some uplift of the pipe was created.

In Figure 4.6, Tests VNL14, VNL16 and VNL23 achieve a relatively low domain concentration, below or exactly around the flotation limit, but still some uplift is recognised. All three experiments experience a very high discharge flow rate at the moment of the recorded displacements, which confirms the presence of hydrodynamic uplift forces on the pipe caused by the turbulence at the sand bed. The precise influence of the hydrodynamic forces cannot be derived from the experiments in this research and a Computational Fluid Dynamics (CFD) analysis is recommended.

The developments in buoyancy on the pipe and the normalised force balance from Test VNL14 are shown in Figure 4.7. The normalised force balance in Figure 4.7b shows an approach of the flotation threshold by the conductivity bar measurements, but they only graze the flotation limit for a very brief moment in time. At 36 seconds, the sedimentation front has reached a height of approximately 2.5 cm on the pipe surface and a sudden increase in discharge flow rate is perceived. The fact that the pipe displacements occur at this exact moment in time and the maximum displacement does not even reach 2 cm, shows that local liquefaction of the newly laid sand layer is caused by the impact from the high discharge flow rate.

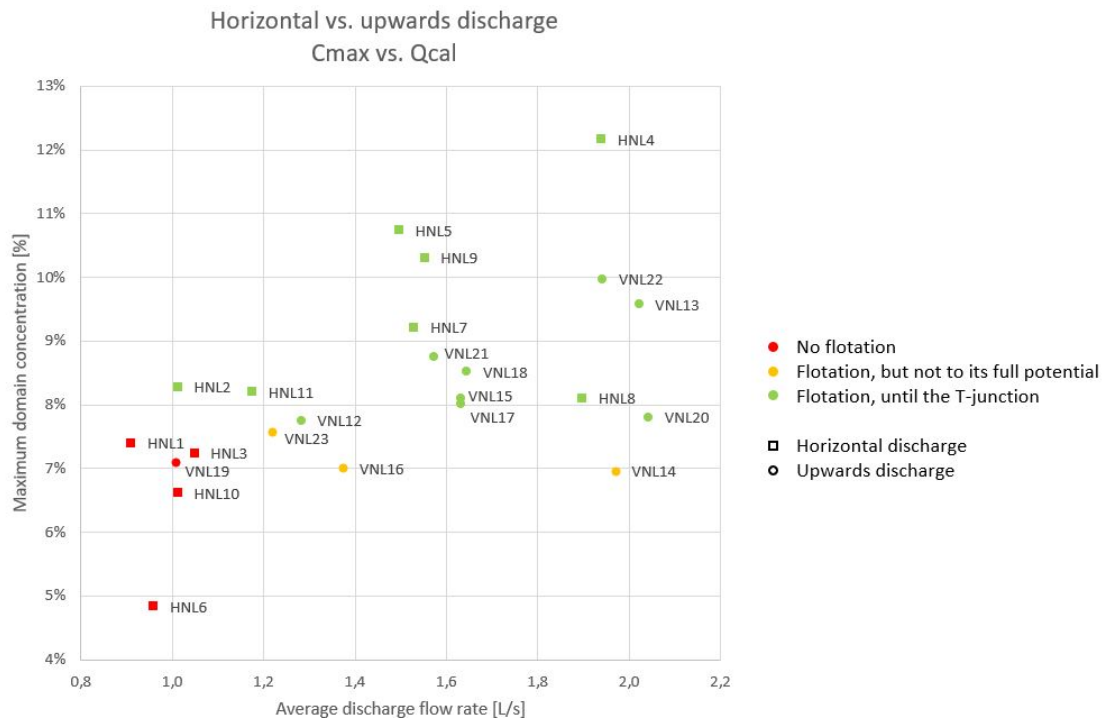
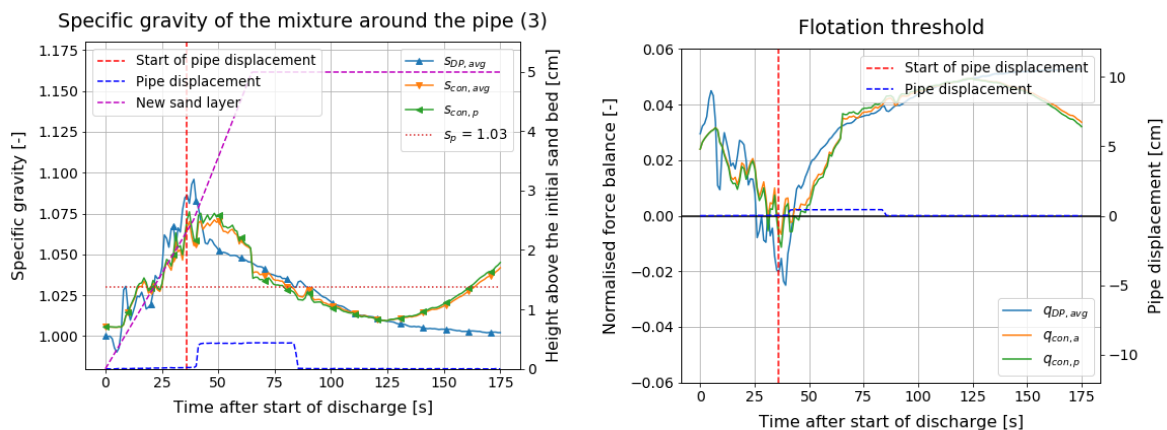


Figure 4.6: Overview of the obtained maximum domain concentrations at the corresponding average discharge flow rate during the experiments with both horizontal discharge and vertical discharge and where the pipe, of specific gravity 1.03, initially lays on top of the sand bed



(a) Build-up of buoyant specific gravity on the pipe, compared to the pipe specific gravity from Test VNL14

(b) Normalised force balance of the pipe from Test VNL14

Figure 4.7: Determination of the start of flotation based on buoyant specific gravity on the pipe and based on the normalised force balance in Test VNL14

To reduce the effect of sedimentation on the potential pipe flotation, experiments are conducted with an initial elevation at different heights of the pipe (Tests VSL, VML and VVL in Appendix B). The influence of the friction force due to pipe embedment is reduced or even completely diminished to zero, depending on the elevation height and sedimentation speed, and the only forces on the pipe are expected to be from the pipe specific weight and the buoyancy from the mixture. When only comparing these two forces, the pipe should start to float when the buoyant specific gravity exceeds the pipe specific weight, as happens at approximately 25 seconds in Figure 4.7a. Nevertheless, a delay in physical pipe flotation is again recognised during the experiments. This indicates that the elevation causes another hydrodynamic effect, which should be taken into account in the analysis of pipeline flotation during discharge.

The elevation of the pipe above the sand bed, causes a fixed opening between the pipe and the sand bed before the start of sedimentation. The discharged sand-water mixture is prone to flow over the sand bed through this opening and the hydrodynamic effects on the pipe are completely different from the experiments with the pipe directly on the sand bed. Specifically with the vertical discharge, the mixture flows downwards from the middle of the tank and the collision with the sand bed pushes the mixture towards the sides. If the pipe is positioned directly on the sand bed, the flow comes across the pipe and the speed is significantly reduced around the pipe. On the other hand, if the pipe is initially elevated above the sand bed, the flow underneath the pipe could create a change in behaviour of the hydrodynamic forces on the bottom side of the pipe. The horizontal constraints on pipe displacements prevent the pipe from sliding towards the sides due to this drag effect.

Three noticeable results with the elevated pipe experiments were found. Tests VSL28, VML29 and VML34 indicate some pipe uplift, but not to the full potential in terms of displacements, while the achieved domain concentrations are relatively high (see Figure 4.1). The opening between the pipe and the sand bed due to the elevations in these experiments and a very high but temporary discharge flow rate, could explain these relatively low pipe displacements with the hydrodynamic forces on the bottom of the pipe. The mixture flowing underneath the pipe, while the flow at the top of the pipe is relatively stationary, could induce means to keep the pipe down. However, the exact specifications of these hydrodynamic effects cannot be determined with the current experiments and additional research is necessary.

#### 4.4. Influence of Pipe Specific Gravity

Finally, the influence of the pipe weight is of great importance in the flotation limit. To bury an offshore pipeline with a TSHD sand backfilling process, it is beneficial to make the pipe as heavy as possible so there will be no risk of flotation. However, the offshore pipelines are often included in the oil and gas industry and a much lighter pipeline can be used for its service period. Therefore, it is beneficial for economic reasons to know the influence of the pipe specific weight on the pipeline flotation limit.

In this research, certain small-scale experiments are executed with a different pipe specific weight. The largest amount of experiments include a pipe with a constant specific gravity of 1.03, while in the final stage of experimenting, some tests with a pipe specific gravity of 1.08 and 1.12 are conducted. The specific weights of these heavier pipes are chosen based on a dichotomy search performed by Yang (2020) [20]. The average buoyancy of the mixture on the pipe occasionally approaches or even exceeds these specific weights during discharge, so a potential crossing of the pipe flotation limit was expected. However, in this prediction the resisting force due to pipe embedment was not taken into account, so the downward forces were underestimated.

Pipe flotation was not achieved in any of the experiments with approximately the same input parameters as all other experiments, except for a larger pipe specific gravity. In Figure 4.8, the maximum domain concentrations are shown for all experiments with vertical discharge and the initial pipe positioning on top of the sand bed, which makes the pipe specific gravity the main variable. In all tests with a heavier pipe, the normalised force balance does not approximate the pipe flotation limit and the pipe evidently remains on the sand bed while it becomes embedded for approximately half of the pipe diameter. Most of the experiments with the heavier pipes achieve a maximum domain concentration between 7% and 8%, but Tests VNW46 and VNH49 even pass a maximum domain concentration of 8.5% during discharge. With a pipe specific gravity of 1.03, a domain concentration this high consistently leads to pipe flotation. The average discharge flow rate in nearly all experiments with heavier pipes was very large. Nevertheless, even the additional hydrodynamic effects due to this large discharge flow rate, as explained in the previous section, were not enough to cause pipe flotation. Therefore, an increase in pipe specific weight leads to a significant increase in resistance towards uplift and an (undefined) increase in the pipe flotation limit regarding domain concentrations.

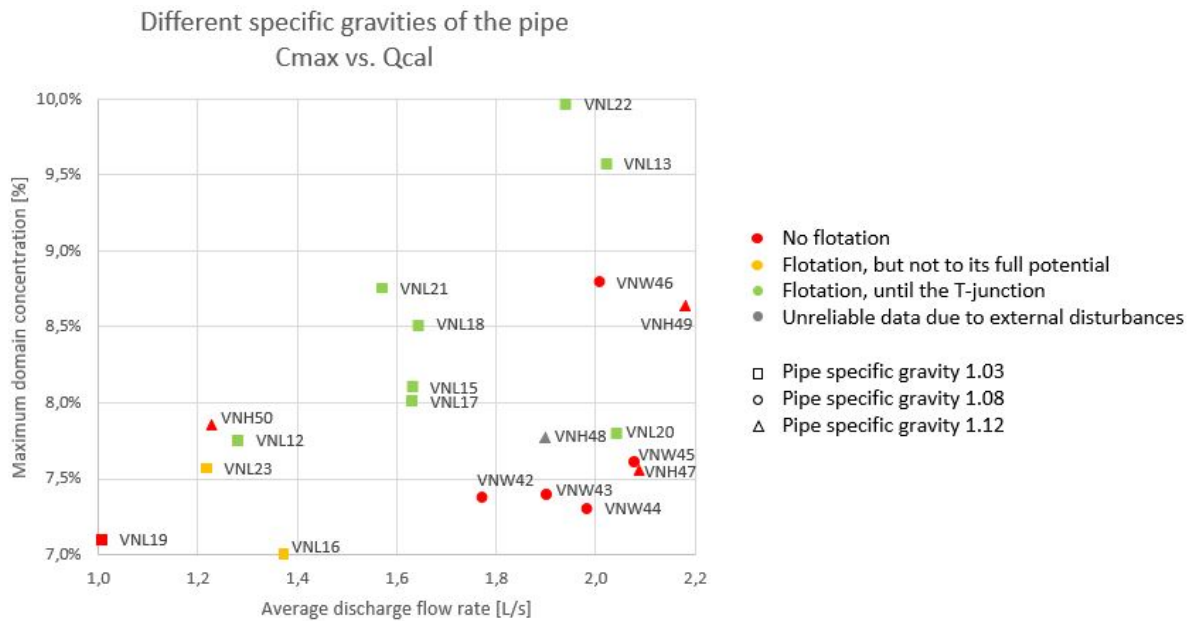


Figure 4.8: Overview of the obtained maximum domain concentrations at the corresponding average discharge flow rate during the experiments with vertical discharge and where the pipe, with a varying specific gravity, initially lays on top of the sand bed

The increase in pipe specific weight from 1.03 to 1.08 was too coarse for relevant conclusions in this research regarding the pipe flotation threshold and the corresponding influential parameters for the heavier pipes. A hypothesis is suggested that an increase in pipe specific weight to 1.08 is a step of more than twice the buoyant pipe weight compared to the initial pipe specific gravity of 1.03. The pipe flotation limit at 7.5% domain concentration for a pipe weight of 1.03, potentially needs at least a multiplication by two to obtain the domain concentration needed for flotation of a pipe with specific gravity of 1.08. This prediction has been tested theoretically, based on the calculation model, for a pipe with a specific gravity of 1.08 and a concentration of 15% in the entire domain around the pipe. The sedimentation front is set at 2.5 cm and the normalised force balance is calculated for this static moment in time. This estimation demonstrates that the normalised force balance is approximately at the flotation threshold for an experiment with a pipe specific gravity of 1.08. However, this is a very rough estimation; the evidence of this hypothesis is outside the scope of the current research and further investigation is needed to prove this.



# 5

## Discussion

This chapter discusses the most relevant mechanisms and problems that were encountered during the experimental study regarding pipeline flotation during sand backfilling, and provides a critical review on the interpretation of the findings.

The measurements during the experimental study have provided better insight into physical processes which govern offshore pipeline flotation during sand backfilling with a TSHD. The mechanisms during backfilling in the field are investigated by a series of small-scale experiments. The downward forces on the pipe in the model provide a desire for the pipe to maintain on the sand bed and to be buried by the discharged sand volume. These downward forces consist of the pipe specific weight and the friction due to sedimentation around the pipe. Contrarily, the discharge of sand in the domain creates buoyant upward forces on the pipe, in correspondence with Archimedes' law. An undesirable effect from the small-scale experiments are the additional hydrodynamic forces from the fluid on the pipe, of which the exact influences on the pipe are not entirely known yet.

In the small-scale experiments with a pipe with a relatively low buoyant pipe weight, an apparent pipe flotation limit was found in the parameter of sand volume concentration in the domain. This pipe flotation limit was defined at a maximum achieved domain concentration of approximately 7.5% for experiments with a pipe specific weight of 1.03. This flotation limit was regardless of the direction of discharge and the initial position of the pipe. This pipe flotation limit of the experiments performed on a small scale could be translated to critical domain concentrations in the field, under which the suspension concentrations must remain to prevent pipeline flotation. However, this parameter is difficult to measure during TSHD sand backfilling on the seabed. To stay below the critical domain concentration in the field, a prediction of the relation between the input parameters and the maximum domain concentrations should be made. As there is still a strong variation in several important input parameters in the small-scale experiments, a Computational Fluid Dynamics (CFD) analysis is suggested to relate the maximum domain concentration to the input parameters at every moment in time.

Some exceptions to this flotation limit were recognised in the experiments and the driving factor behind these irregularities is the discharge flow rate. An average discharge flow rate can be determined over the course of the entire experiment, but only an indication regarding the momentary discharge rates can be made. The unexpected large variation in this parameter complicates the pipe flotation analysis, but estimations respecting the discharge flow rate at each moment in time are based on the concentration and pressure developments. Modifications to the experimental set-up can be made to monitor this discharge flow rate or to maintain it constant over the course of the experiment. An additional flow meter just before the point of discharge in the experimental tank could be added to measure the fluctuation of the discharge flow rate over time. To fix this parameter to a constant value during the entire discharge, the T-valve between the mixture tank and the experimental tank should contain an L-bend instead of a T-bend. The current T-bend splits the flow into the discharge flow to the experimental tank and a backflow to the mixture tank to favour further mixing. If this T-bend is replaced with an L-bend, and the full mixture flow is discharged to the experimental tank, the discharge flow rate will maintain a more constant value over the duration of discharge. However, to fully understand the influence of this parameter in the sand backfilling process, further research and 3D computational modelling is recommended.

Furthermore, the influence of the pipe embedment on the potential of pipe flotation is considered in this research. This parameter has a much larger influence than anticipated beforehand and therefore only considering the pipe weight and buoyancy is not sufficient for the analysis of pipe flotation in the small-scale experiments. To include the frictional force due to the sedimentation around the pipe, a theory based on the pipe-soil interaction stresses is applied in the analysis. The very low stress conditions underneath the pipe in the small-scale experiments lead to exceptionally high friction angles and friction coefficients. This high level of friction is likely to be related to the drainage conditions below the pipe and could be caused by a combination of dilation and pore underpressures that have formed underneath the pipe. The downward friction force is approximated by this friction coefficient and the shear stresses around the pipe-soil interface. However, the calculation of the friction force is based on equations that were originally derived from clay samples, while the experiments take place with a sandy soil. The peculiarly low stress situation in the small-scale experiments is very unfamiliar in the literature and these equations are assumed to be acceptable for the analysis in this research. Moreover, the exact drainage conditions underneath the pipe are not measured, so the magnitude of potential dilatancy and pore underpressures is unknown. Nevertheless, the results from a normalised force balance, including the resisting downward force from frictional calculations, show a good approximation for the moment of flotation. In order to confirm the validity of the application of this theory in the analysis of pipe flotation, further research is recommended where the focus lies on the mechanisms at the pipe-soil interface and in the deposited sand around the pipe.

Burgmans (2005) described in a technical report of Van Oord about the static force balance on a pipe in different stages of the sand backfilling process with a TSHD [3]. This approximation of the force balance does not take the influence of sand sedimentation into account, while the pipe embedment is proven to have quite some influence in this research. However, the sedimentation rate is much more significant in the small-scale experiments than in the field. The ratio of a sand particle diameter over the pipe diameter is much smaller in the small-scale experiments than with an actual offshore pipeline. The sedimentation resistance during a TSHD sand backfilling process will most likely enhance the downward forces on the pipe, so the static force balance from Burgmans (2005) underpredicts the flotation resistance slightly. Nevertheless, due to the deficient knowledge of the mechanisms during sand backfilling with a TSHD, this model still provides a safe prediction to prevent pipeline flotation.

An additional force in the experimental tank is due to the hydrodynamic effects from the discharged sand-water mixture. These are induced by the geometrical constraints of the experimental tank and play a much more significant role in the small-scale experiments than in the TSHD sand backfilling processes in the field. The exact direction and magnitude of this hydrodynamic force on the pipe body is not fully determined yet. However, an estimation can be made based on several exceptional results of the experiments, where some pipe uplift displacements were measured but not to the full potential. With a large discharge rate, the mixture flows are prone to induce movements of the pipe, even when the flotation threshold has not been exceeded yet.

The influence of erosion is not considered in the 2D model for pipeline flotation analysis, but there are still some signs of erosion visible during the experiments. The direction of discharge portrays a significant influence on these hydrodynamic effects. The vertically upward discharge in the small-scale experiments showed a decrease in circular motions of the flow and a better approximation of the TSHD sand backfilling process in the field.

The experiments with an elevated pipe are conducted for the analysis of flotation without the immediate sedimentation around the pipe. These results still show some resistance in pipeline flotation after the buoyancy exceeds the pipe specific weight and no conclusions concerning pipe flotation with the diminished friction forces can be deduced. An interesting event in the case of pipe elevation is the possibility of the mixture to flow over the sand bed underneath the pipe to the sides of the experimental tank. This flow underneath the pipe is likely to change the behaviour of the hydrodynamic forces on the bottom of the pipe, but additional research with CFD is recommended to verify this hypothesis.

Finally, an attempt has been made to investigate the influence of the pipe specific gravity on the flotation threshold. However, the variation in pipe specific gravity was too coarse to obtain relevant conclusions about this parameter in the experimental set-up used in this research. A much higher concentration is needed in the domain around the pipe to obtain flotation for the investigated heavier pipes. Additional experiments are suggested for this research with a higher discharge flow rate and a higher total discharged volume.

# Conclusion and Recommendations

This chapter concludes on the current knowledge with respect to pipe flotation due to sand backfilling in small-scale experiments and provides suggestions and recommendations for further developments.

## 6.1. Conclusion

This research built on the study of Yang (2020), in which a small-scale set-up is designed to perform experiments concerning pipe flotation during sand backfilling [20]. A total amount of 50 experiments was performed with Geba Weiss sand in four different stages, so experiments were performed with: horizontal discharge, vertically upward discharge, elevated initial pipe positions and increased pipe specific weights. The set of experiments have provided better insight into physical processes that influence pipeline flotation during sand backfilling.

During the discharge of a sand-water mixture over a pipe, the development of buoyancy was induced by the increase in concentration in the domain surrounding the pipe. The buoyancy created uplift forces on the pipe, which could be estimated accurately in the small-scale experiments, and the pipe weight produced gravity forces in the opposite direction. The main conclusion regarding the one-dimensional force balance on the pipe is that the degree of pipe embedment influences the magnitude of an additional frictional force working downwards on the pipe body. A suggestion to approximate the friction force due to pipe embedment with the stresses on the pipe-soil contact surface, based on the low stress friction coefficient, is made and verified in this research. In the small-scale experiments, this influence played a significant role in the determination of the start of flotation. When backfilling with a TSHD in the field, this influence is less dominant due to the much smaller ratio of sand particles over the pipe diameter. In the static force balance from Burgmans (2005), the resistance generated by the deposited soil is not taken into account [3], therefore it overestimates the uplift potential of the pipelines. Nevertheless, due to the deficient knowledge of the mechanisms during sand backfilling with a TSHD on the seabed, this model still provides a safe prediction to prevent pipeline flotation.

A pipe flotation limit was found in the parameter of sand volume concentration in the surroundings of the pipe. This flotation limit was defined at a domain concentration of approximately 7.5% for the experiments with a pipe specific gravity of 1.03. The boundary of flotation for heavier pipes was not achieved in this research, but evidence points towards a significantly higher flotation limit. The flotation limit of 7.5% domain concentration is regardless of the direction of discharge and the initial height of the pipe above the sand bed. The discharge flow rate and the total discharged sand volume are the key factors for development of domain concentration in these small-scale experiments.

An undesirable result from the small-scale experiments are the additional hydrodynamic effects from the mixture in the experimental tank, which are induced by the geometrical constraints. The exact direction and magnitude of this hydrodynamic force on the pipe body is not determined yet, but the influence was clearly visible in several small-scale experiments. With a large discharge rate, the mixture flows are prone to induce movements of the pipe, even when the flotation threshold has not been exceeded yet. When the position of the pipe before the start of the experiment is elevated to a certain height, the mixture can flow between the sand bed and the pipe, changing the hydrodynamic forces on the pipe body.

## 6.2. Recommendations

The processes during discharge over the pipe in the small-scale experiments are relatively well understood. However, additional research regarding pipe flotation during sand backfilling is recommended. As there is still a strong variation in several important input parameters in the small-scale experiments, a CFD analysis is suggested to relate the domain concentration to the input parameters at every moment in time. From this analysis, a prediction can be made regarding the boundary of pipeline flotation on the seabed when discharging with a TSHD. Moreover, the experimental set-up could be modified so the average discharge rate at every moment in time can be monitored. This could be achieved by adding a second flow meter to the discharge hose, but now between the T-valve and the T-junction.

The suggested CFD analysis for future assessments of pipeline flotation during sand backfilling can be compared to the analytical analysis from the current research. Furthermore, the computation of 3D experiments on a larger scale is recommended for a final validation of the model. The geometrical constraints of the current experimental tank and the relatively fast burial of the pipe due to the small pipe diameter cause difficulties in the simulation of the TSHD sand backfilling process on a small scale. The present hydrodynamic effects could be more reduced in experiments on a larger scale and the backfilling process in the field could be better approximated. The mechanisms that were found in this research form a good foundation for the type of measurements needed in future experiments. In this larger 3D model, the exact influence of the pipe specific weight on the flotation threshold could be investigated as well. For the determination of the flotation limit of heavier pipes, more experiments in the current laboratory set-up could also be executed with a pipe specific gravity varying between 1.03 and 1.08.

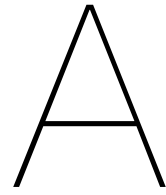
Additionally, pressure sensors could be added to the experimental set-up at the bottom of the pipe and in the upper layer of the sand bed. These sensors could deliver more knowledge about the conditions right underneath the pipe at the start of flotation and could give more insights into the drainage conditions and the potential pore underpressures or suction effects that influence the pipeline triggering. The knowledge of the stress and drainage conditions at the pipe-soil interface is of importance to validate the hypothesis of the relatively large friction coefficients and the use of the equations for the determination of normal stresses and friction coefficients at the pipe-soil contact surface, originally derived from clay samples, in the pipe flotation analysis.

Moreover, a model could be built to analyse the friction force generated on the pipe due to its embedment. The idea of the performed pull-out experiments from Appendix A can be expanded and executed in a more advanced method. In the current research, the pulling action is done manually, but a structure could be formed around the experimental tank so the pipe can be pulled out of the sand bed with a more accurate mechanism and with more sensors underneath the pipe. With this method, the suggested theory about the friction force  $T$  could be further analysed.

# Bibliography

- [1] A.I. Al-Mhaidib. Shearing Rate Effect on Interfacial Friction Between Sand and Steel. *The International Society of Offshore and Polar Engineers*, 2005.
- [2] M.D. Bolton. The strength and dilatancy of sands. *Geotechnique*, 1986.
- [3] S.H. Burgmans. Backfillen met de Volvox Asia. *Van Oord, Technical Report*, 2005.
- [4] D.N. Cathie, J. Machin, and R. Overy. Engineering Appraisal of Pipeline Floatation During Backfilling. *Offshore Technology Conference*, 1996.
- [5] D.N. Cathie, S. Barras, and J. Machin. Backfilling Pipelines: State of the Art. *Offshore Technology Conference*, 1998.
- [6] M.A.J. de Nijs, R. van der Hout, J. Peters, and J. Haverkamp. Laboratory Experiments on the Effect of Suction Head Modifications on Spill of Backfill. *Van Oord, Technical Report*, 2009.
- [7] R. Ferguson and M. Church. A simple universal equation for grain settling velocity. *Journal of sedimentary Research*, 2004.
- [8] M. Finch. Upheaval Buckling and Floatation of Rigid Pipelines: The Influence of Recent Geotechnical Research on the Current State of the Art. *Offshore Technology Conference*, 1999.
- [9] S. Mirza and J.F. Richardson. Sedimentation of suspensions of particles of two or more sizes. *Chemical Engineering Science*, 1979.
- [10] MRP. Trench Backfilling Arkutun Dagi. *Van Oord, Technical Report*, 2010.
- [11] Van Oord. Van oord strengthens dredging fleet with third new hopper. URL <https://www.vanoord.com/news>. (accessed: 06.09.2020).
- [12] A.C. Palmer and R.A. King. *Subsea Pipeline Engineering*. PennWell Corporation, 2008.
- [13] PRQ. Work visit report: 31.3824 KNPC NRP5 Backfilling - TSHD Rotterdam. *Van Oord, Technical Report*, 2018.
- [14] V.S. Quinteros, R. Dyvik, and N. Mortensen. Interface friction angle from Ring Shear tests on offshore North Sea sands. *Geotechnical Frontiers*, 2017.
- [15] M.F. Randolph and S.M. Gouvernec. *Offshore Geotechnical Engineering*. Taylor & Francis, 2011.
- [16] J. Richardson and W. Zaki. Sedimentation and fluidisation: Part i. *Chemical Engineering Research and Design*, 1997.
- [17] F. van Grunsven and A.M. Talmon. Local Anomalies in Slip for Slurry Flow within Pipes near the Deposit Limit Velocity. *CEDA Dredging Days*, 2012.
- [18] A. Verruijt. *Soil Mechanics*. 2001.
- [19] D.J. White and M.F. Randolph. Seabed Characterisation and Models for Pipeline-Soil Interaction. *International Society of Offshore and Polar Engineers, ISOPE-I-07-098*, 2007.
- [20] K. Yang. Physical Modelling of Offshore Pipeline Flotation during TSHD Sand Backfill. Master's thesis, Delft University of Technology, 2020.





## Force Meter Data

The data from the force meter measurements are shown here. For these tests, the pipe was laid on top of the sand bed or partially buried into the sand bed with a varying embedment in the experimental tank. With a force meter, the pipe was manually pulled vertically out of the sand bed, while all other parameters were kept constant. Furthermore, there was no discharge during these tests, so the (partially embedded) pipe was surrounded by pure water. The maximum force needed to pull the pipe out of the sand bed was recorded. If no other effects are taken into consideration, this total force recorded should be equal to the summation of the pipe buoyant weight ( $V$ ) and an additional friction force ( $F$ ) due to the pipe embedment. As the pipe buoyant weight can be calculated, the ratio of this friction force to the pipe buoyant weight ( $F/V$ ) is determined and shown in Figure A.1 as a function of pipe embedment.

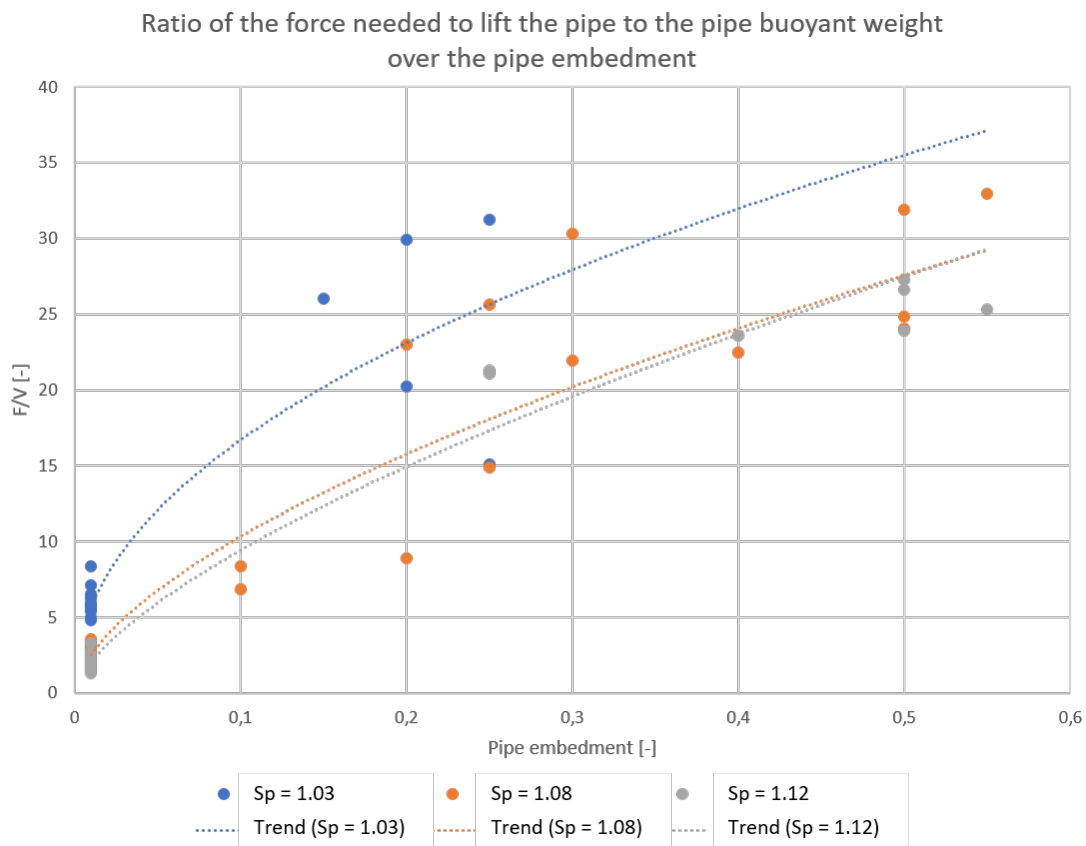


Figure A.1: An indication of the influence of pipe embedment on the force needed to lift the pipe from the tests with a force meter in the small-scale experiments

The ratio of  $F/V$  depends on the friction coefficient and the pipe embedment, so Figure A.1 should show similar results as displayed in Figure 4.3. Unfortunately, the forces present during the pulling tests are much larger than in the discharge experiments. The results in Figure A.1 do not seem to correlate with the theory and an assumption is made that the manual execution of these tests have influenced the results. In these pulling tests the method of burying the pipe was done in a different manner than during the discharge experiments with sedimentation (the sand was 'pushed' manually around the pipe and did not settle as with normal discharge). Furthermore, during the pulling tests it was evident that a relatively large force was needed for a very brief moment in time, to lift the pipe from the sand bed. This could mean the presence of some suction effects underneath the pipe, while pulling it up vertically. Nevertheless, the forces needed to lift the pipe in the pulling tests are still much larger than in the discharge experiments. Moreover, the ratio  $F/V$  should mainly depend on the pipe embedment and the friction coefficient. Therefore, the displayed dotted trend lines of the pipes with a various specific gravity should be more aligned. The overall shape of these trend lines does seem to coincide with each other and with the lines in Figure 4.3, but the values are much too large to be reasonable in the small-scale set-up.

Evidently, the force meter data is very rough and does not support the other obtained and processed data in this research. As there were no pressure sensors present underneath the pipe, the exact influence and magnitude of potential suction mechanisms on the pipe uplift activity cannot be known in this stage.

# B

## Experimental Data

This section shows all data obtained from the pipe flotation tests that were performed in the small-scale experimental set-up. The sequence from Table 3.4 is maintained. In Table B.1, the numerical results from all experiments are given. In the following pages, the results of each experiment is graphically presented, one experiment per page.

Table B.1: Numerical overview of the results of all experiments performed in this research

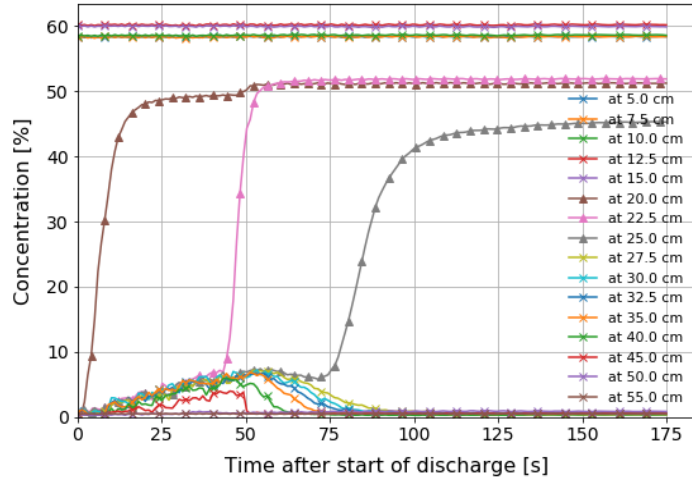
Test	Qcal [L/s]	t <sub>dis</sub> [s]	Δ h [cm]	c <sub>dis</sub> [%]	c <sub>max</sub> [%]	S <sub>dp,max</sub> [-]	S <sub>con,a,max</sub> [-]	Flotation	dis <sub>max</sub> [cm]
HNL1	0,91	51	4,33	23,4	7,4	1,162	1,083	No	0
HNL2	1,01	48	4,40	24,6	8,3	1,134	1,082	Yes	11,2
HNL3	1,05	52	4,33	22,0	7,2	1,066	1,085	No	0
HNL4	1,94	38	6,75	27,5	12,2	1,145	1,124	Yes	10,4
HNL5	1,50	46	6,13	25,4	10,7	1,124	1,099	Yes	13,3
HNL6	0,80	54	3,85	26,2	4,7	1,089	1,037	No	0
HNL7	1,53	42	6,00	27,0	9,2	1,190	1,097	Yes	12,5
HNL8	1,90	34	5,17	23,5	8,1	1,151	1,094	Yes	13,3
HNL9	1,55	48	6,75	26,1	10,3	1,159	1,086	Yes	11,6
HNL10	1,01	56	5,65	28,2	6,6	1,104	1,068	No	0
HNL11	1,18	51	5,25	25,3	8,2	1,152	1,086	Yes	11,6
VNL12	1,28	60	6,60	25,0	7,8	1,094	1,076	Yes	7,5
VNL13	2,02	39	8,03	30,2	9,6	1,122	1,107	Yes	11,6
VNL14	1,97	37	5,85	22,9	7,0	1,096	1,071	Semi	4,2
VNL15	1,63	45	5,85	23,8	7,7	1,082	1,087	Yes	8,3
VNL16	1,37	44	4,80	23,7	7,0	-	1,076	Semi	5,8
VNL17	1,63	43	6,30	24,9	8,0	1,092	1,081	Yes	10,8
VNL18	1,65	43	6,13	25,2	8,5	1,086	1,093	Yes	11,6
VNL19	1,01	60	4,70	21,9	7,1	1,108	1,083	No	0
VNL20	2,04	23	4,90	29,7	7,8	1,904	1,986	Yes	12,0
VNL21	1,57	45	6,83	27,8	8,8	1,106	1,090	Yes	9,1
VNL22	1,94	31	5,78	26,9	10,0	1,113	1,115	Yes	11,6
VNL23	1,22	41	4,45	25,8	7,6	1,057	1,084	Semi	1,7
VSL24	1,27	56	6,55	25,8	7,8	1,100	1,088	Yes	11,2
VSL25	1,32	55	6,83	26,7	8,7	1,079	1,081	Yes	8,3
VSL26	1,49	46	6,38	26,5	8,9	1,084	1,086	Yes	9,5
VSL27	1,12	58	6,05	26,0	8,9	1,087	1,085	Yes	9,5
VSL28	1,38	40	4,68	24,0	8,1	1,079	1,077	Semi	4,4
VML29	1,16	55	5,50	24,4	7,4	1,084	1,086	Semi	2,5
VML30	1,62	49	7,68	27,5	8,6	1,101	1,079	Yes	10,0
VML31	2,16	29	5,78	25,9	7,7	1,087	1,100	Yes	10,0
VML32	1,46	43	5,95	26,8	8,0	1,081	1,082	Yes	10,0
VML33	1,90	38	6,95	27,0	9,3	1,107	1,093	Yes	8,3

VML34	1,27	53	6,03	25,4	8,4	1,077	1,075	Semi	1,7
VVL35	1,24	53	6,08	26,1	9,1	1,081	1,089	Yes	8,3
VVL36	1,64	43	6,68	26,5	8,8	-	1,091	Yes	8,3
VVL37	1,22	58	6,13	24,6	6,7	1,092	1,057	Yes	8,3
VVL38	1,22	66	6,40	22,3	7,2	1,091	1,055	Yes	6,6
VVL39	1,25	67	7,28	24,7	8,7	1,118	1,078	Yes	7,5
VVL40	2,18	34	6,38	24,4	9,5	1,073	1,117	Yes	7,1
VVL41	1,34	60	7,10	24,7	8,5	1,095	1,082	Yes	8,3
VNW42	1,77	32	4,68	22,9	7,4	1,072	1,101	No	0
VNW43	1,90	25	4,35	25,9	7,4	1,068	1,098	No	0,4
VNW44	1,98	26	4,30	23,1	7,3	1,080	1,095	No	0
VNW45	2,08	30	5,10	23,2	7,6	1,079	1,087	No	0,4
VNW46	2,01	30	5,65	26,5	8,8	1,097	1,106	No	0
VNH47	2,09	26	4,55	24,0	7,6	1,072	1,083	No	0
VNH48	1,90	30	5,00	24,3	7,8	1,086	1,094	No	0
VNH49	2,18	26	5,08	24,8	8,6	1,076	1,105	No	0
VNH50	1,23	44	5,08	26,4	7,9	1,125	1,084	No	0

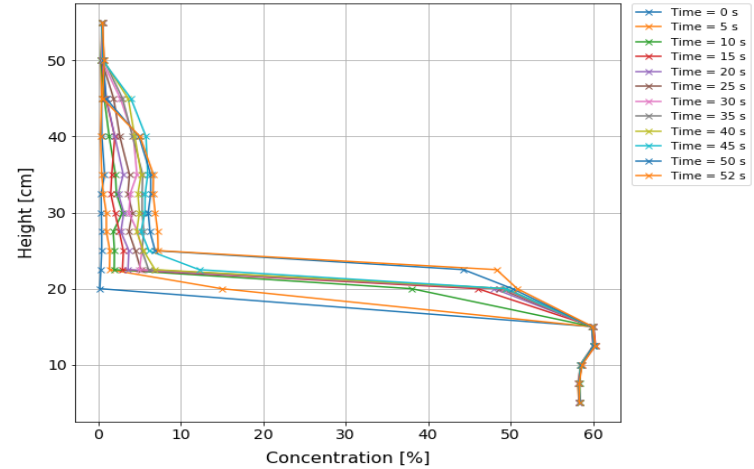
Test	Qcal [L/s]	t <sub>dis</sub> [s]	Δh [cm]	c <sub>dis</sub> [%]	c <sub>max</sub> [%]	S <sub>pipe</sub>	S <sub>dp</sub>	S <sub>con,a</sub>	Flotation	dis,max [cm]	ΔP <sub>dp,bottom</sub> [kPa]	ΔP <sub>dp,top</sub> [kPa]
HNL1	0,91	51	4,33	23,4%	7,4%	1,03	1,162	1,083	No	0	0,247	0,097

Horizontal discharge  
No elevation  
SG<sub>p</sub> = 1.03

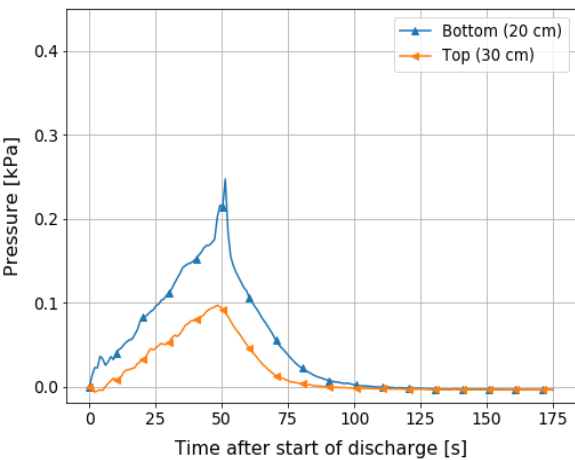
Concentration over time at different levels



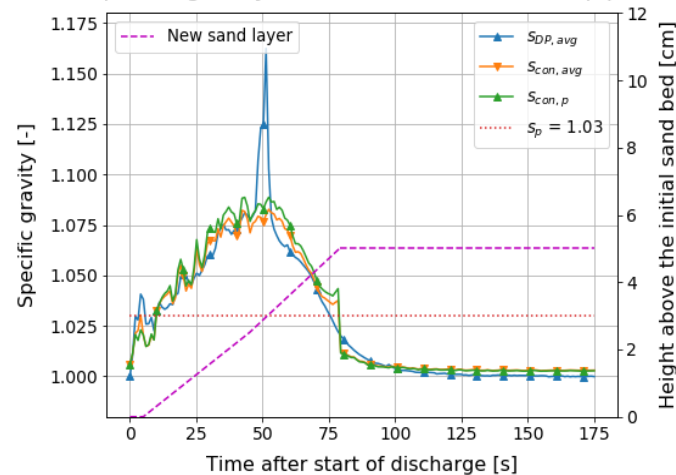
Increasing concentration along height over time



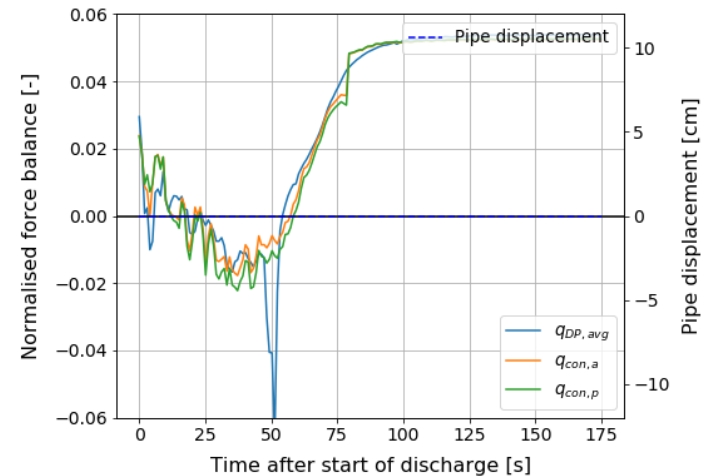
DP net increment at height of the pipe



Specific gravity of the mixture around the pipe



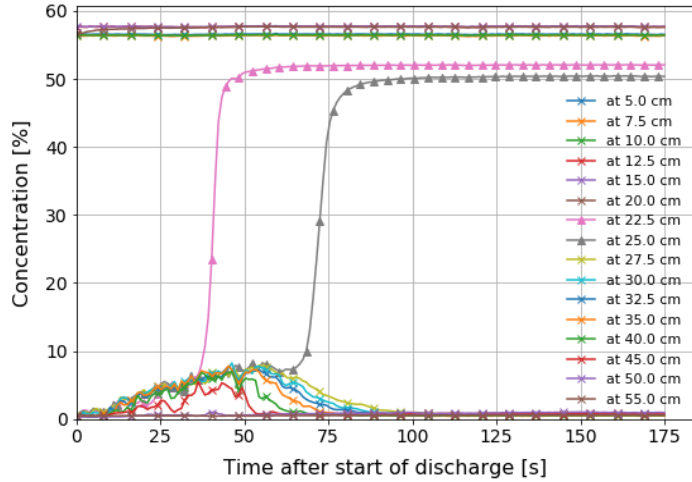
Flotation threshold



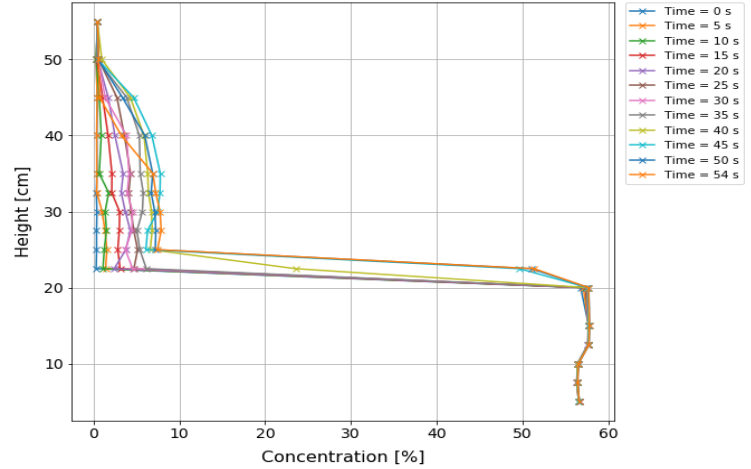
Test	Qcal [L/s]	t <sub>dis</sub> [s]	Δh [cm]	c <sub>dis</sub> [%]	c <sub>max</sub> [%]	S <sub>pipe</sub>	S <sub>dp</sub>	S <sub>con,a</sub>	Flotation	dis,max [cm]	ΔP <sub>dp,bottom</sub> [kPa]	ΔP <sub>dp,top</sub> [kPa]
HNL2	1,01	48	4,40	24,6%	8,3%	1,03	1,134	1,082	Yes	11,2	0,238	0,109

Horizontal discharge  
No elevation  
SG<sub>p</sub> = 1.03

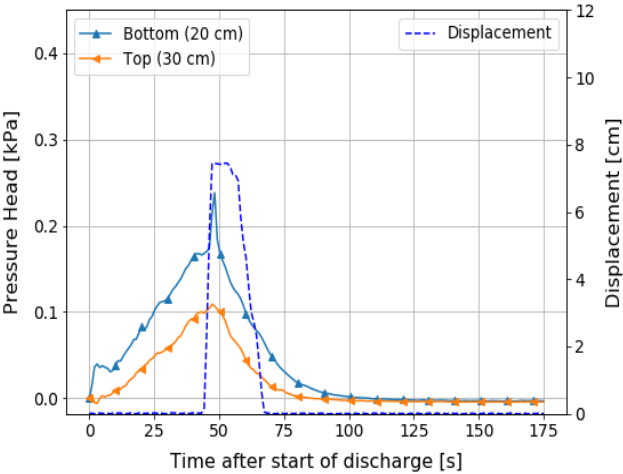
Concentration over time at different levels



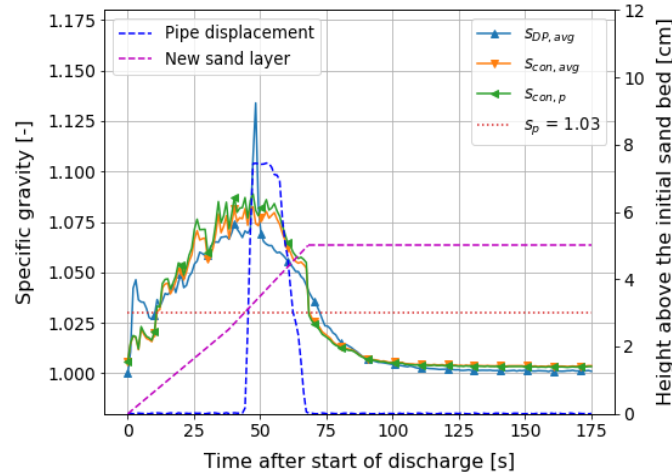
Increasing concentration along height over time



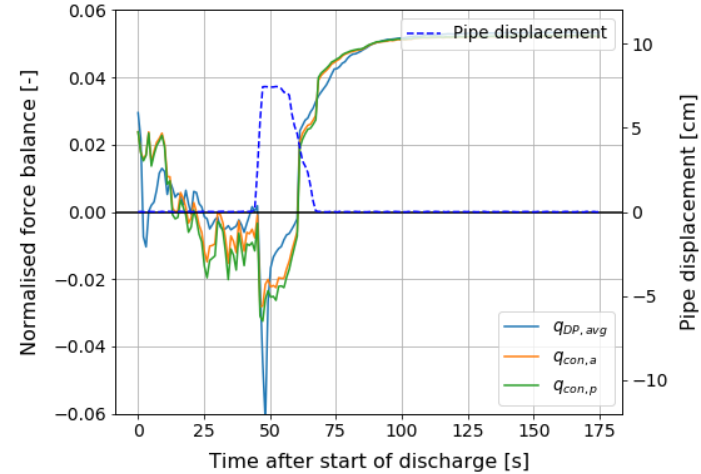
DP net increment at height of the pipe



Specific gravity of the mixture around the pipe (3)



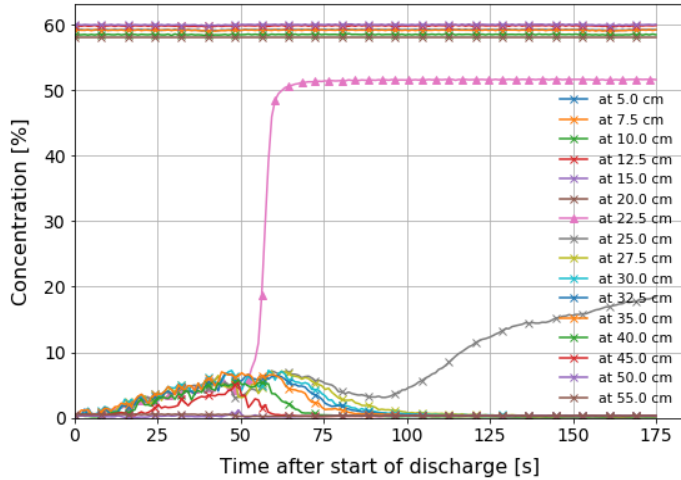
Flotation threshold



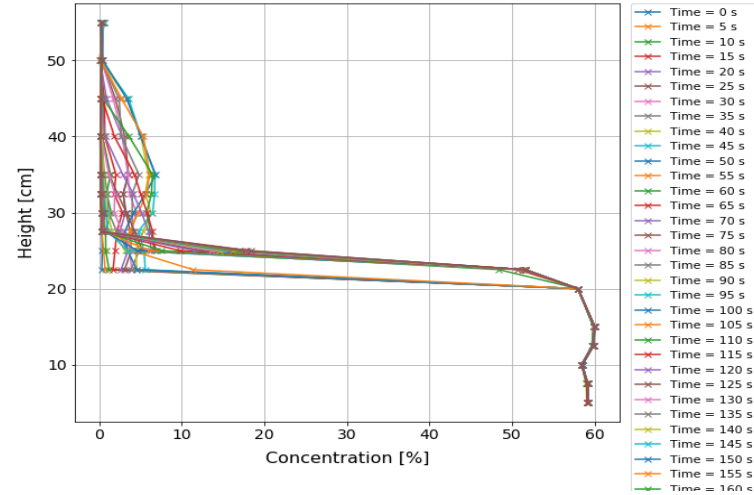
Test	Qcal [L/s]	t <sub>dis</sub> [s]	Δh [cm]	c <sub>dis</sub> [%]	c <sub>max</sub> [%]	S <sub>pipe</sub>	S <sub>dp</sub>	S <sub>con,a</sub>	Flotation	dis,max [cm]	ΔP <sub>dp,bottom</sub> [kPa]	ΔP <sub>dp,top</sub> [kPa]
HNL3	1,05	52	4,33	22,0%	7,2%	1,03	1,066	1,085	No	0	0,176	0,123

Horizontal discharge  
No elevation  
SG<sub>p</sub> = 1.03

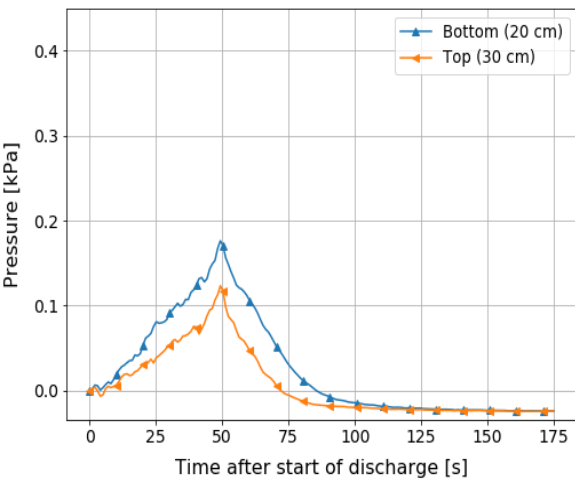
Concentration over time at different levels



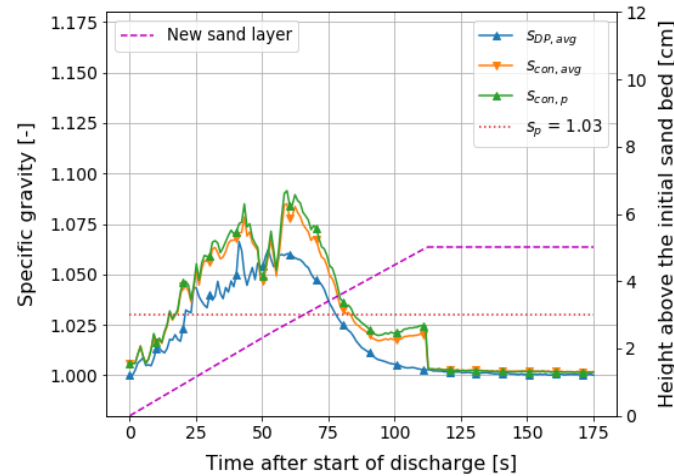
Increasing concentration along height over time



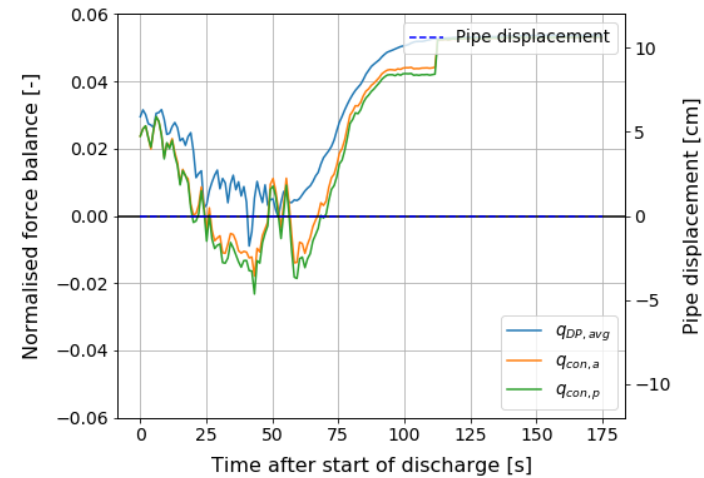
DP net increment at height of the pipe



Specific gravity of the mixture around the pipe



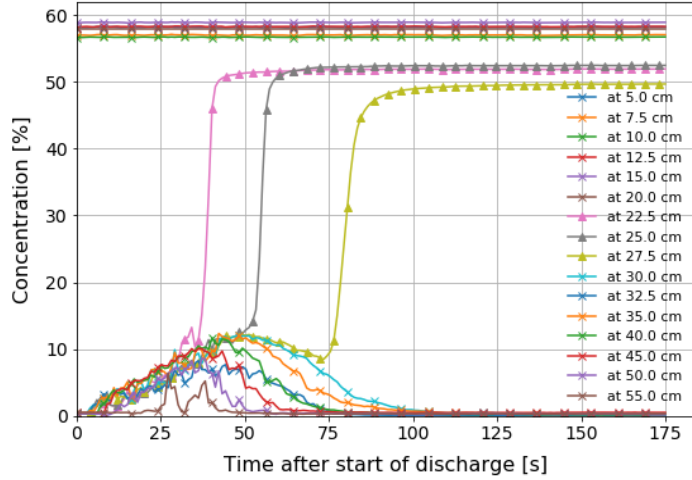
Flotation threshold



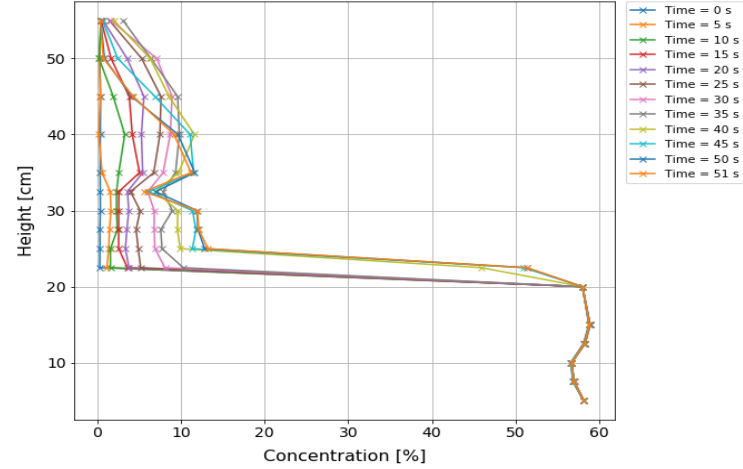
Test	Qcal [L/s]	t <sub>dis</sub> [s]	Δh [cm]	c <sub>dis</sub> [%]	c <sub>max</sub> [%]	S <sub>pipe</sub>	S <sub>dp</sub>	S <sub>con,a</sub>	Flotation	dis,max [cm]	ΔP <sub>dp,bottom</sub> [kPa]	ΔP <sub>dp,top</sub> [kPa]
HNL4	1,94	38	6,75	27,5%	12,2%	1,03	1,145	1,124	Yes	10,4	0,420	0,298

Horizontal discharge  
No elevation  
SG<sub>p</sub> = 1.03

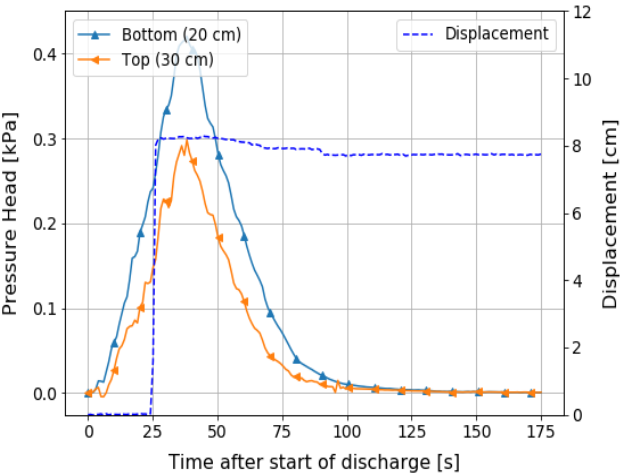
Concentration over time at different levels



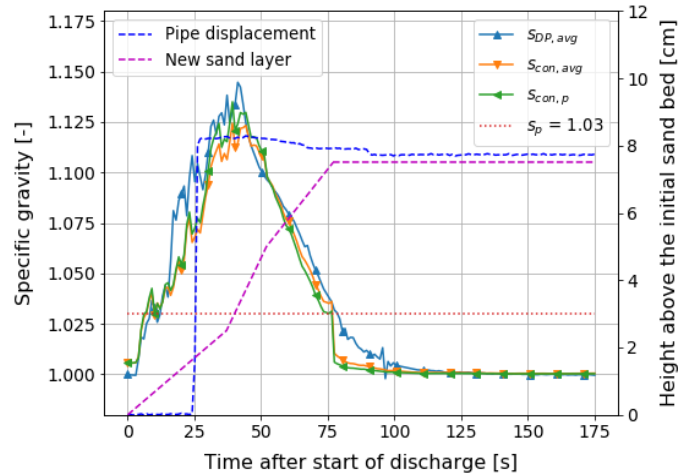
Increasing concentration along height over time



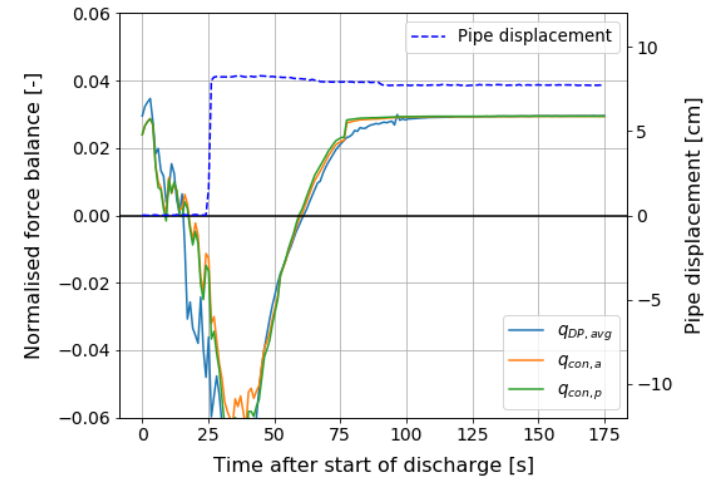
DP net increment at height of the pipe



Specific gravity of the mixture around the pipe (3)



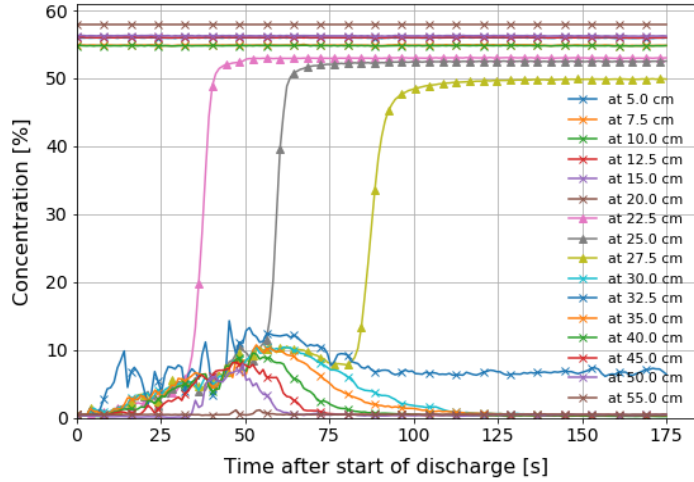
Flotation threshold



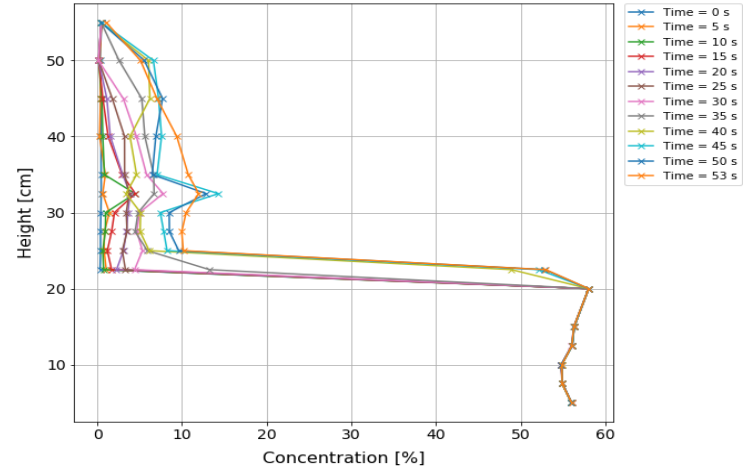
Test	Qcal [L/s]	t <sub>dis</sub> [s]	Δh [cm]	c <sub>dis</sub> [%]	c <sub>max</sub> [%]	S <sub>pipe</sub>	S <sub>dp</sub>	S <sub>con,a</sub>	Flotation	dis,max [cm]	ΔP <sub>dp,bottom</sub> [kPa]	ΔP <sub>dp,top</sub> [kPa]
HNL5	1,50	46	6,13	25,4%	10,7%	1,03	1,124	1,099	Yes	13,3	0,331	0,210

Horizontal discharge  
No elevation  
SG<sub>p</sub> = 1.03

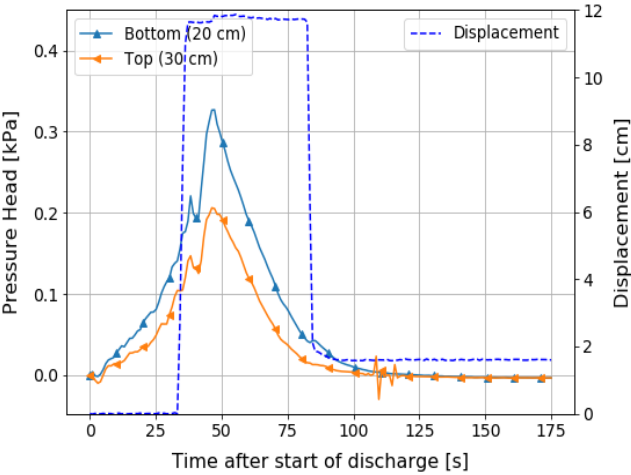
Concentration over time at different levels



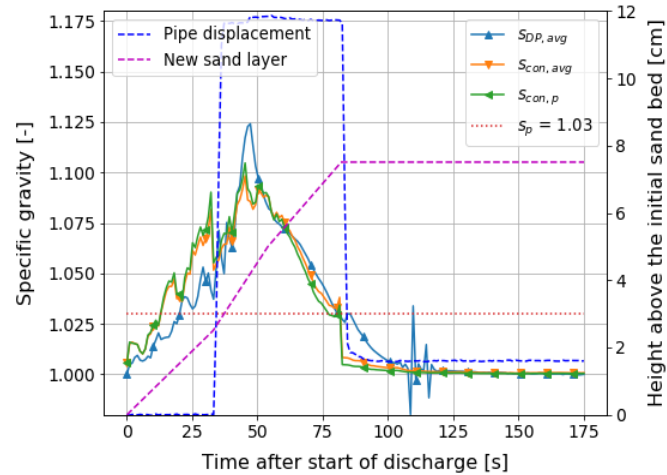
Increasing concentration along height over time



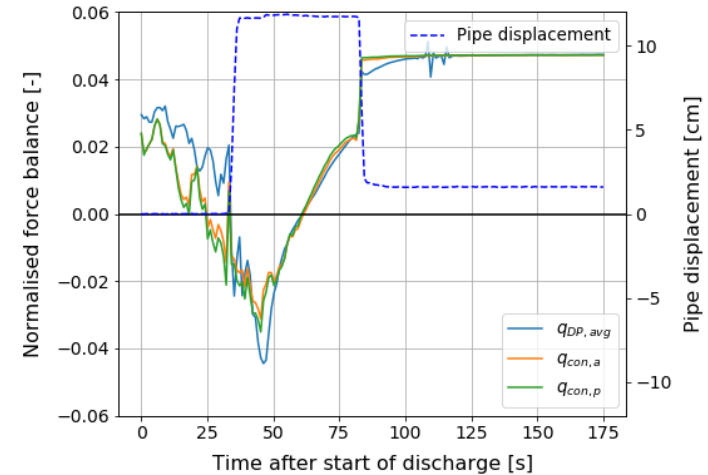
DP net increment at height of the pipe



Specific gravity of the mixture around the pipe (3)



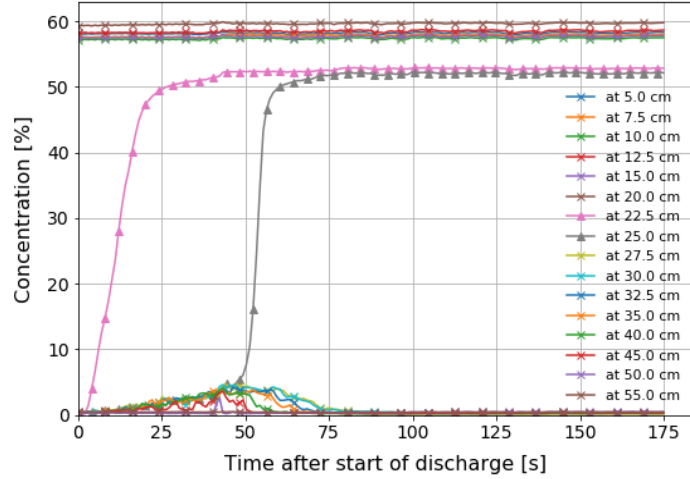
Flotation threshold



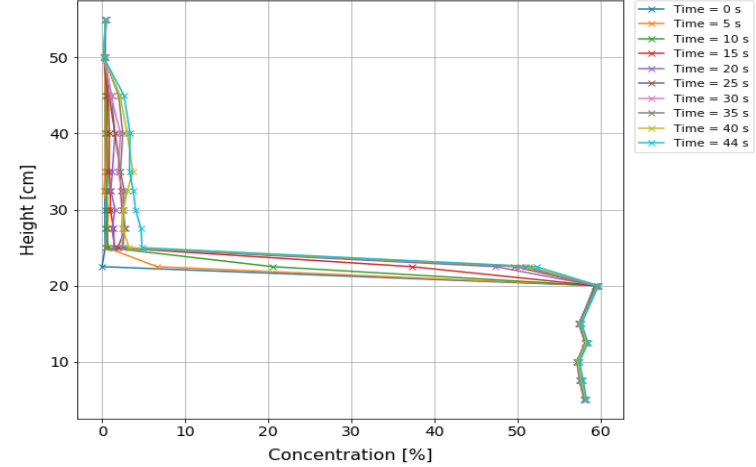
Test	Qcal [L/s]	t <sub>dis</sub> [s]	Δh [cm]	c <sub>dis</sub> [%]	c <sub>max</sub> [%]	S <sub>pipe</sub>	S <sub>dp</sub>	S <sub>con,a</sub>	Flotation	dis,max [cm]	ΔP <sub>dp,bottom</sub> [kPa]	ΔP <sub>dp,top</sub> [kPa]
HNL6	0,80	54	3,85	26,2%	4,7%	1,03	1,089	1,037	No	0	0,163	0,094

Horizontal discharge  
No elevation  
SG<sub>p</sub> = 1.03

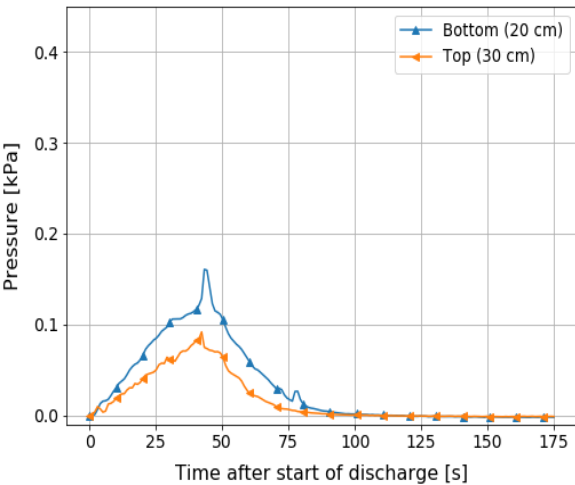
Concentration over time at different levels



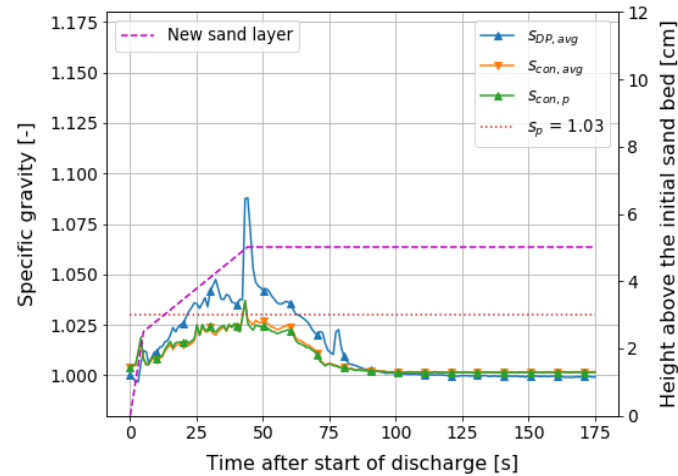
Increasing concentration along height over time



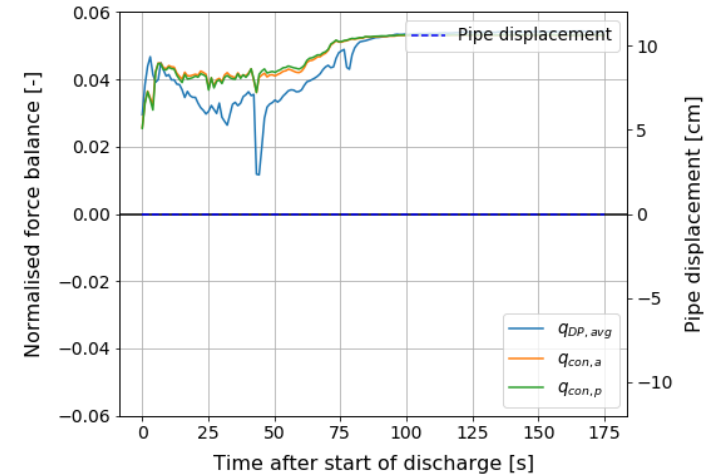
DP net increment at height of the pipe



Specific gravity of the mixture around the pipe



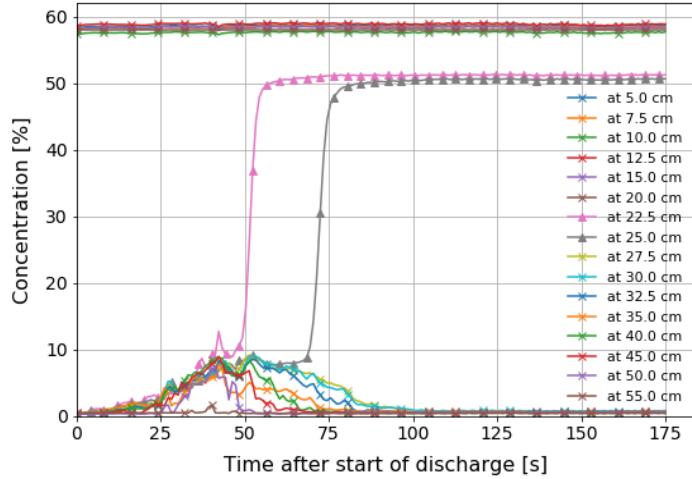
Flotation threshold



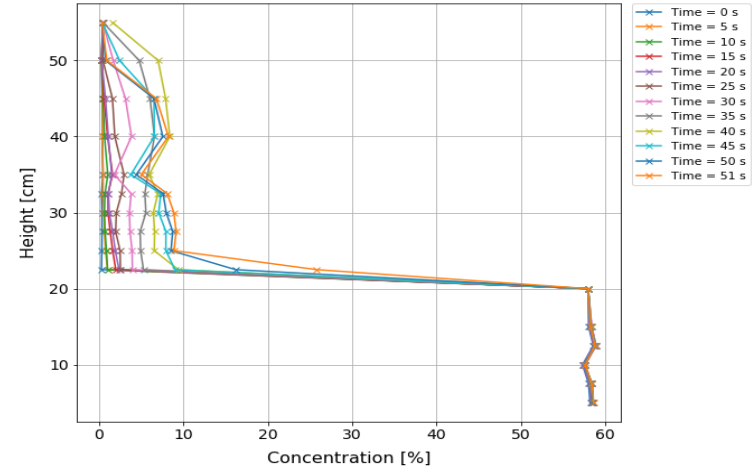
Test	Qcal [L/s]	t <sub>dis</sub> [s]	Δh [cm]	c <sub>dis</sub> [%]	c <sub>max</sub> [%]	S <sub>pipe</sub>	S <sub>dp</sub>	S <sub>con,a</sub>	Flotation	dis,max [cm]	ΔP <sub>dp,bottom</sub> [kPa]	ΔP <sub>dp,top</sub> [kPa]
HNL7	1,53	42	6,00	27,0%	9,2%	1,03	1,190	1,097	Yes	12,5	0,386	0,227

Horizontal discharge  
No elevation  
SG<sub>p</sub> = 1.03

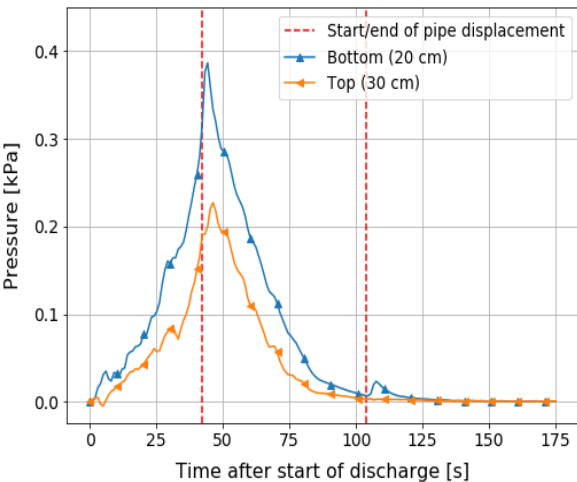
Concentration over time at different levels



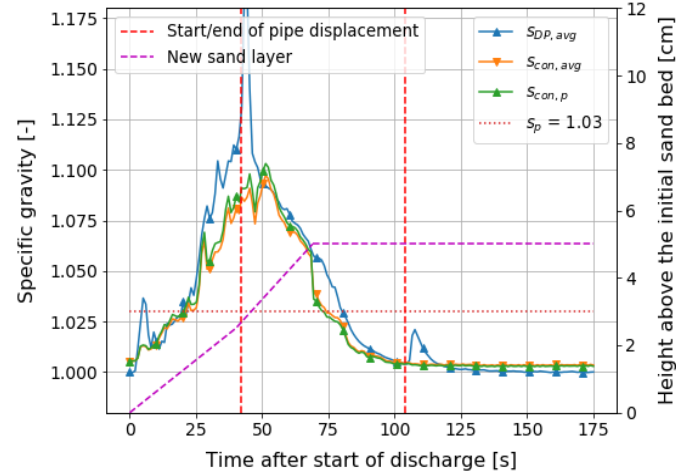
Increasing concentration along height over time



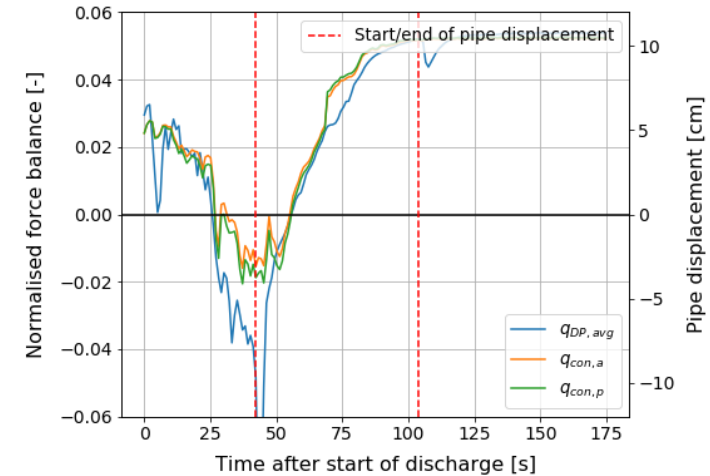
DP net increment at height of the pipe



Specific gravity of the mixture around the pipe



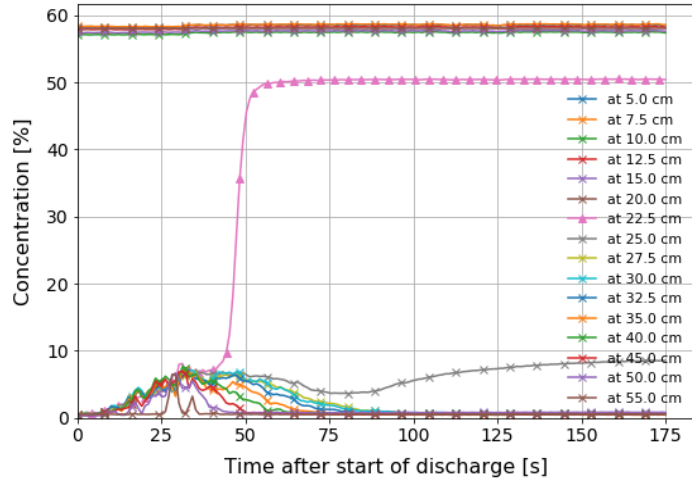
Flotation threshold



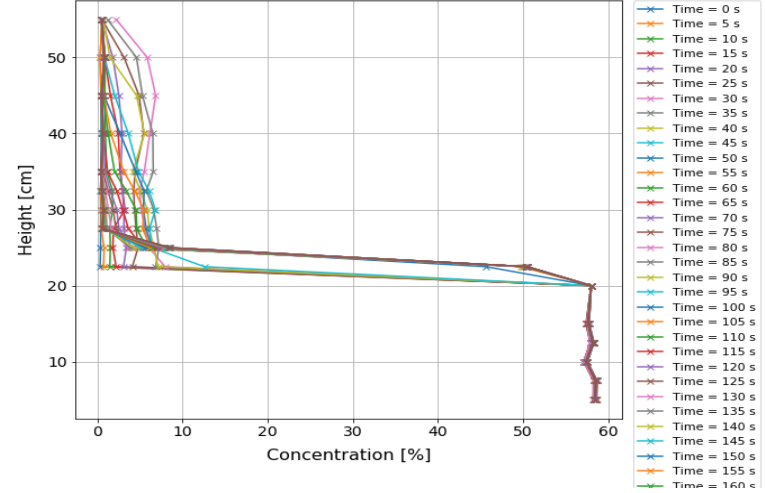
Test	Qcal [L/s]	t <sub>dis</sub> [s]	Δh [cm]	c <sub>dis</sub> [%]	c <sub>max</sub> [%]	S <sub>pipe</sub>	S <sub>dp</sub>	S <sub>con,a</sub>	Flotation	dis,max [cm]	ΔP <sub>dp,bottom</sub> [kPa]	ΔP <sub>dp,top</sub> [kPa]
HNL8	1,90	34	5,17	23,5%	8,1%	1,03	1,151	1,094	Yes	13,3	0,283	0,158

Horizontal discharge  
No elevation  
SG<sub>p</sub> = 1.03

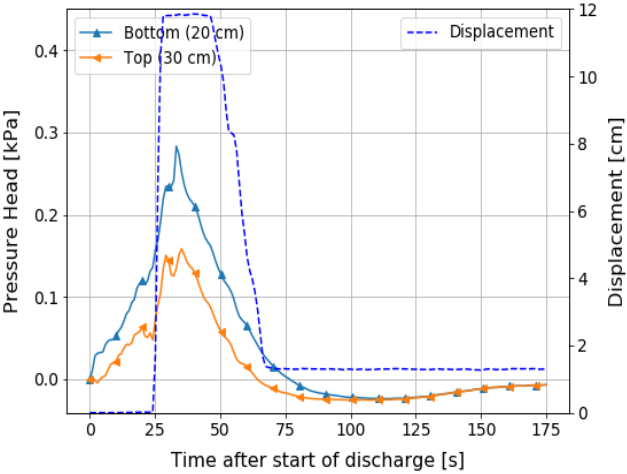
Concentration over time at different levels



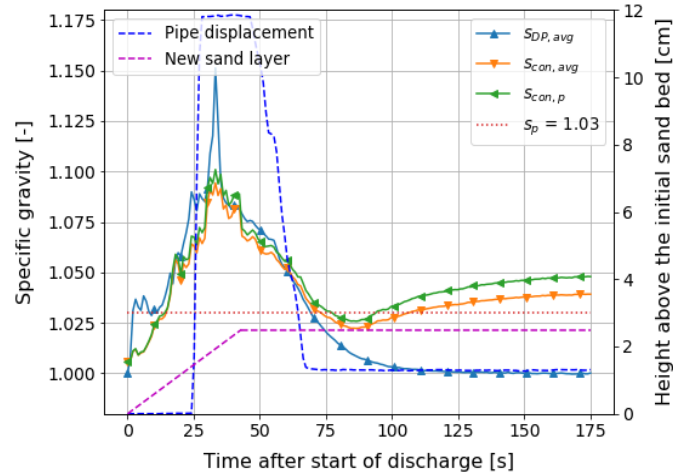
Increasing concentration along height over time



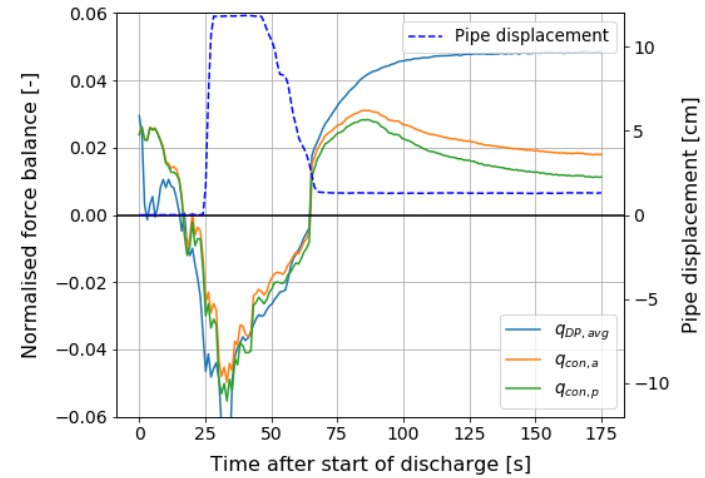
DP net increment at height of the pipe



Specific gravity of the mixture around the pipe (3)



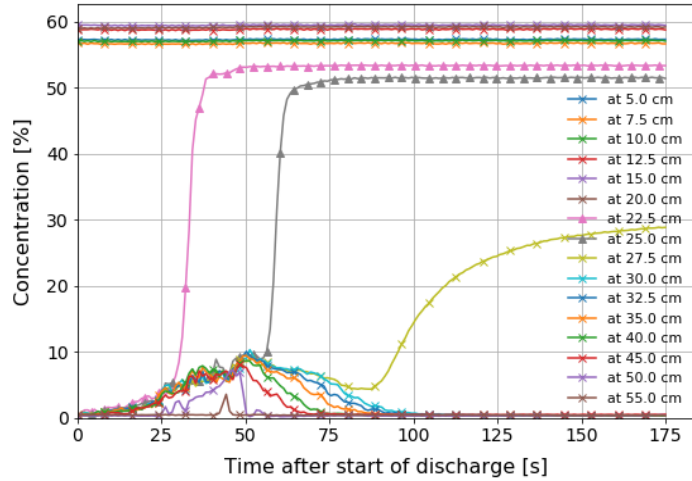
Flotation threshold



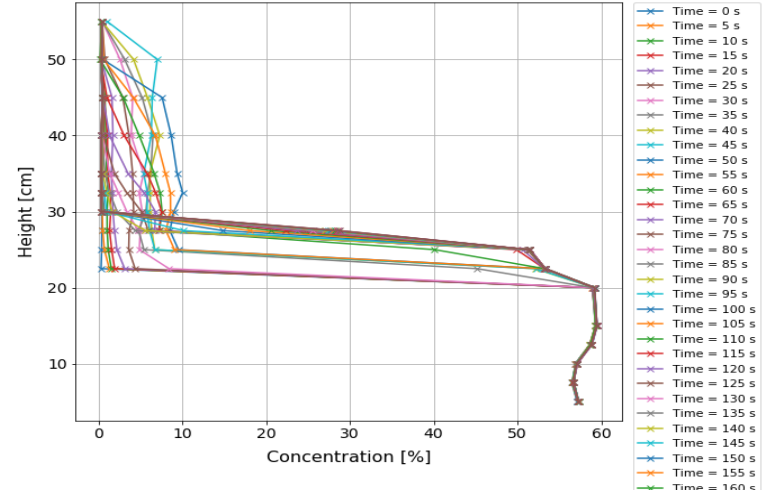
Test	Qcal [L/s]	t <sub>dis</sub> [s]	Δh [cm]	c <sub>dis</sub> [%]	c <sub>max</sub> [%]	S <sub>pipe</sub>	S <sub>dp</sub>	S <sub>con,a</sub>	Flotation	dis,max [cm]	ΔP <sub>dp,bottom</sub> [kPa]	ΔP <sub>dp,top</sub> [kPa]
HNL9	1,55	48	6,75	26,1%	10,3%	1,03	1,159	1,086	Yes	11,6	0,407	0,275

Horizontal discharge  
No elevation  
SG<sub>p</sub> = 1.03

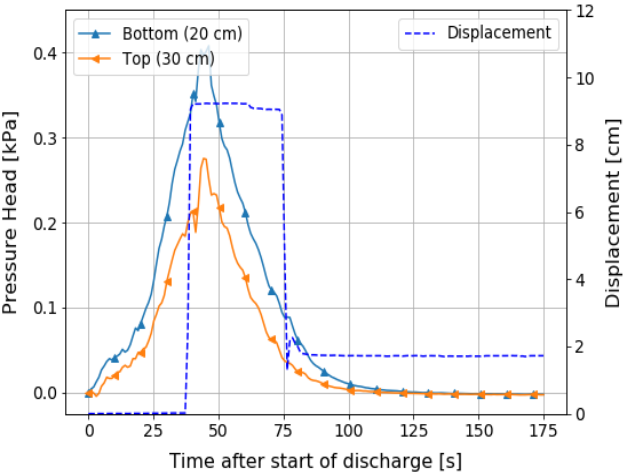
Concentration over time at different levels



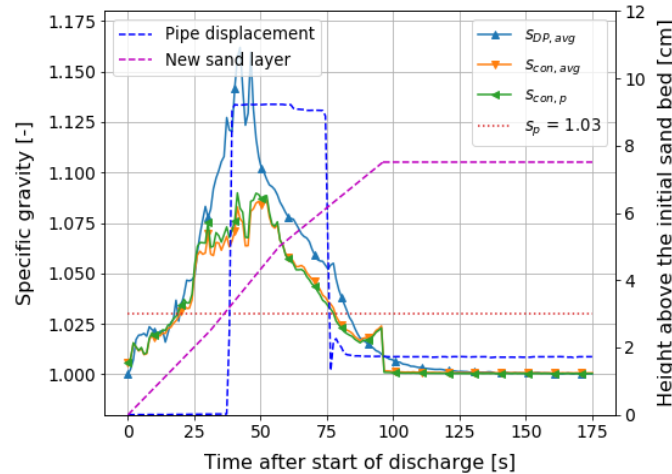
Increasing concentration along height over time



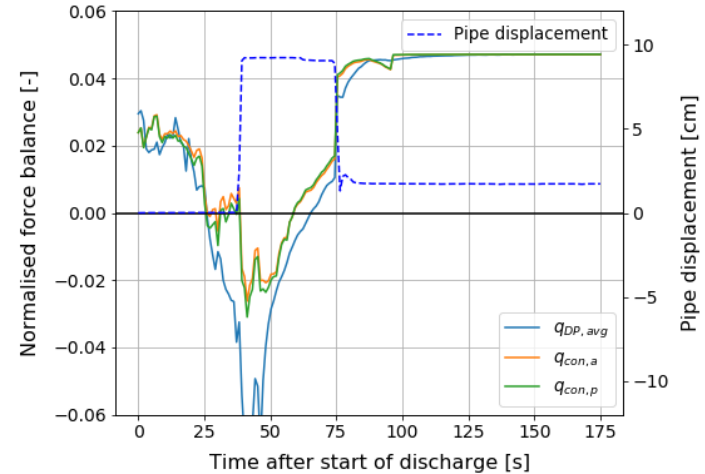
DP net increment at height of the pipe



Specific gravity of the mixture around the pipe (3)



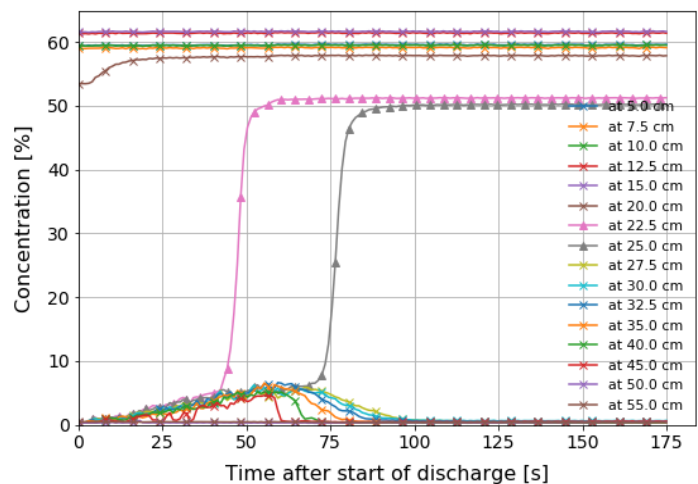
Flotation threshold



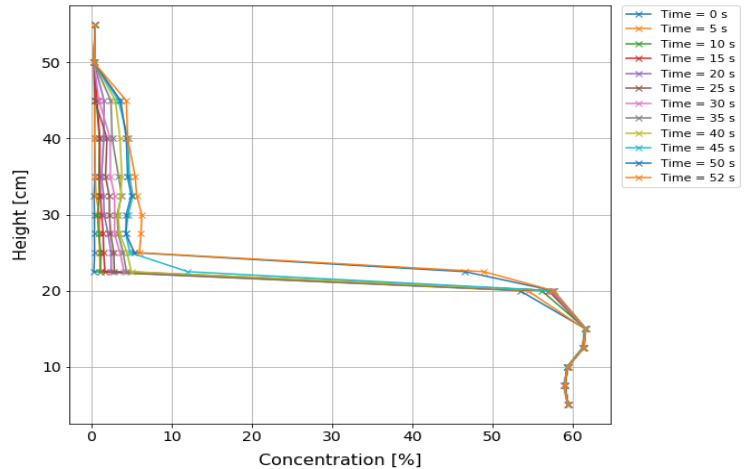
Test	Qcal [L/s]	t <sub>dis</sub> [s]	Δh [cm]	c <sub>dis</sub> [%]	c <sub>max</sub> [%]	S <sub>pipe</sub>	S <sub>dp</sub>	S <sub>con,a</sub>	Flotation	dis,max [cm]	ΔP <sub>dp,bottom</sub> [kPa]	ΔP <sub>dp,top</sub> [kPa]
HNL10	1,01	56	5,65	28,2%	6,6%	1,03	1,104	1,068	No	0	0,232	0,129

Horizontal discharge  
No elevation  
SG<sub>p</sub> = 1.03

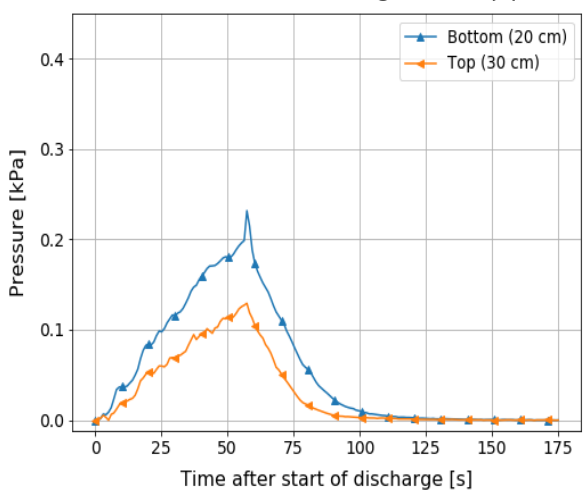
Concentration over time at different levels



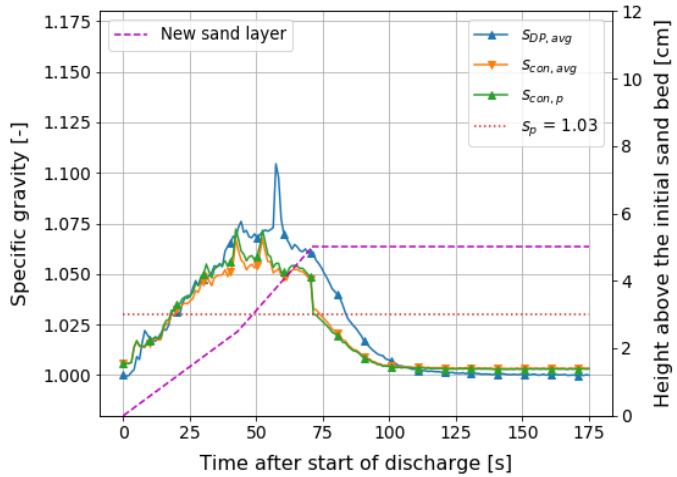
Increasing concentration along height over time



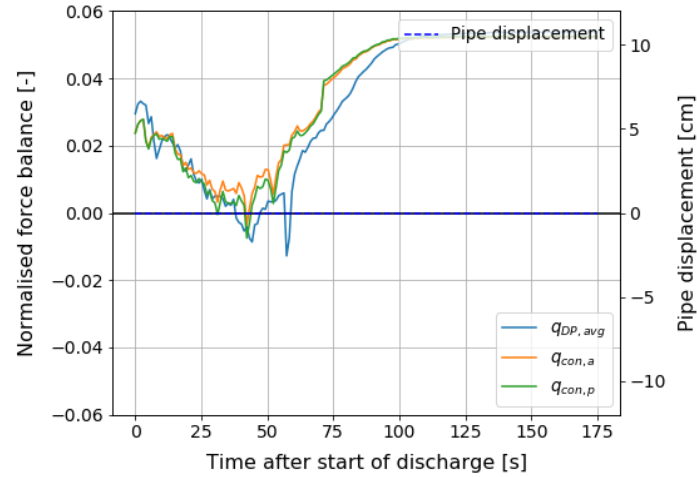
DP net increment at height of the pipe



Specific gravity of the mixture around the pipe

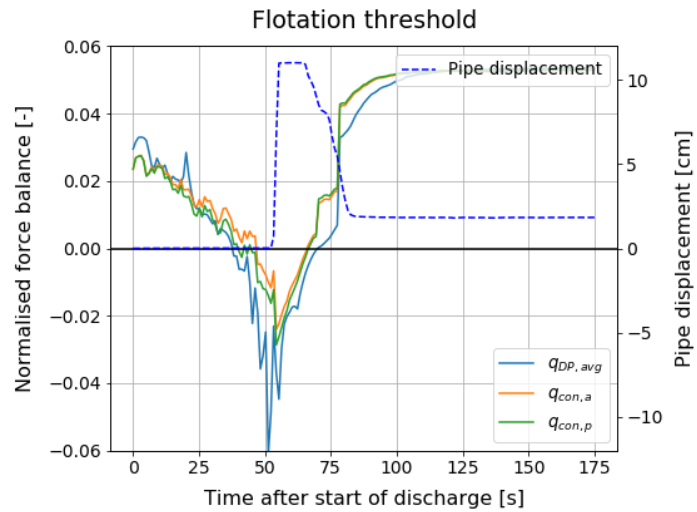
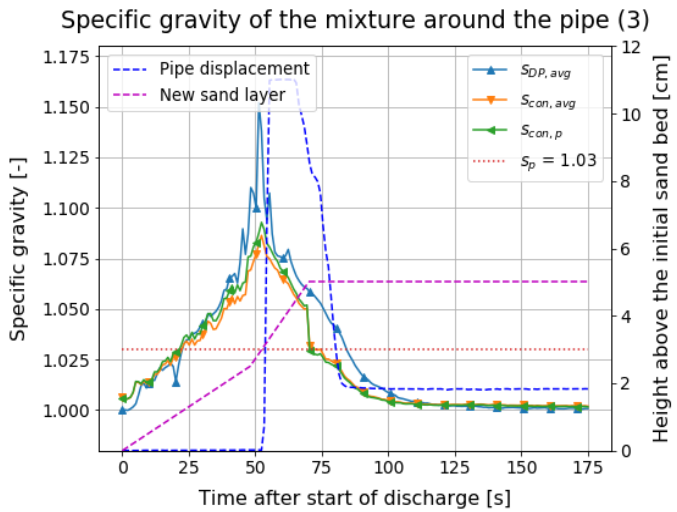
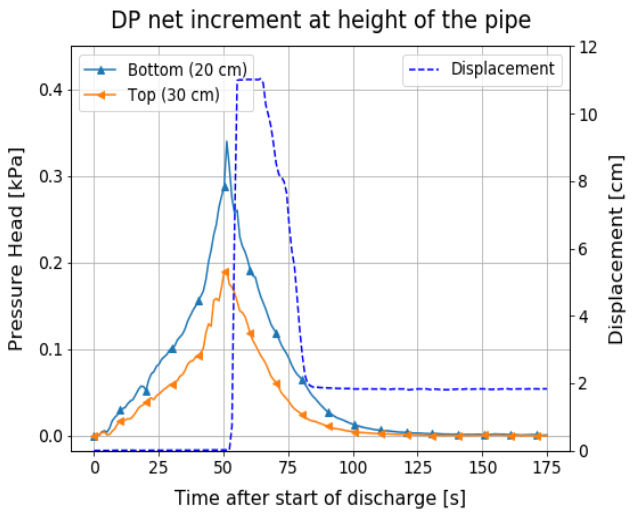
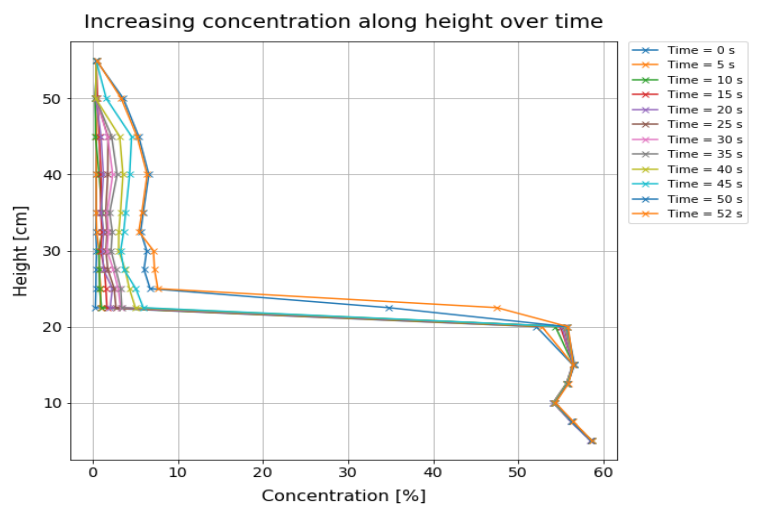
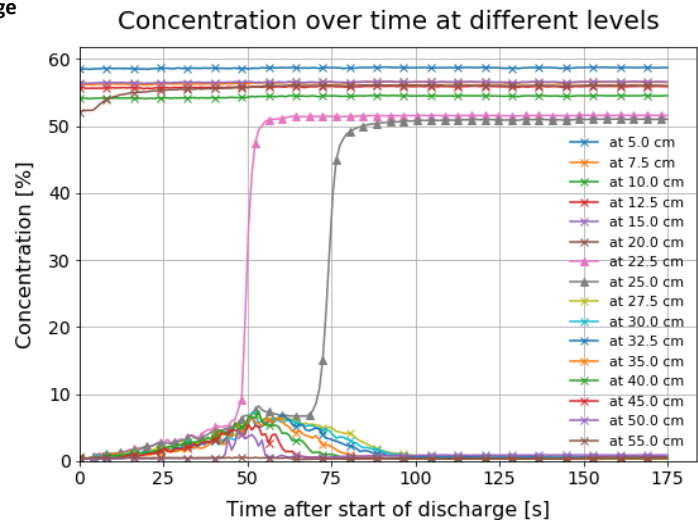


Flotation threshold



Test	Qcal [L/s]	t <sub>dis</sub> [s]	Δh [cm]	c <sub>dis</sub> [%]	c <sub>max</sub> [%]	S <sub>pipe</sub>	S <sub>dp</sub>	S <sub>con,a</sub>	Flotation	dis,max [cm]	ΔP <sub>dp,bottom</sub> [kPa]	ΔP <sub>dp,top</sub> [kPa]
HNL11	1,18	51	5,25	25,3%	8,2%	1,03	1,152	1,086	Yes	11,6	0,340	0,191

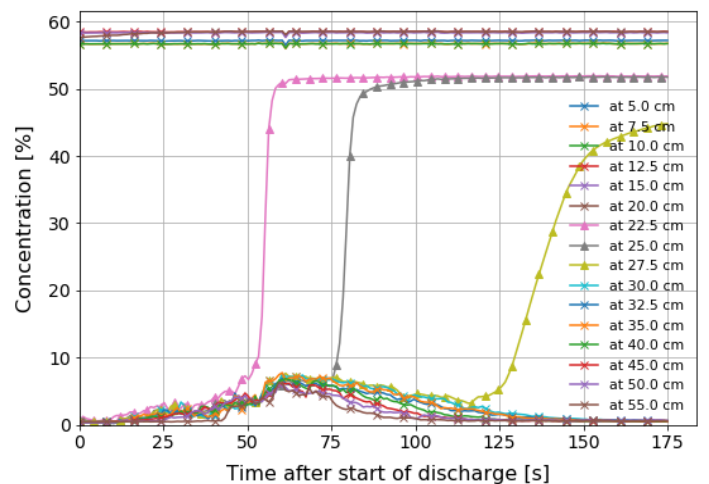
Horizontal discharge  
No elevation  
SG<sub>p</sub> = 1.03



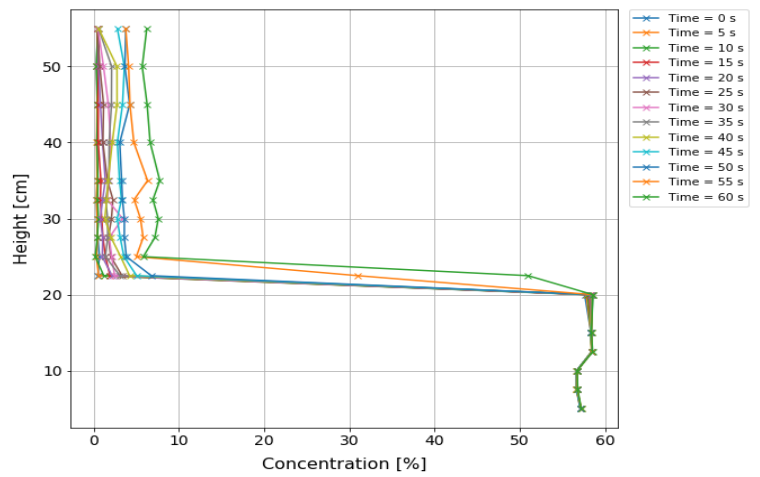
Test	Qcal [L/s]	t <sub>dis</sub> [s]	Δh [cm]	c <sub>dis</sub> [%]	c <sub>max</sub> [%]	S <sub>pipe</sub>	S <sub>dp</sub>	S <sub>con,a</sub>	Flotation	dis,max [cm]	ΔP <sub>dp,bottom</sub> [kPa]	ΔP <sub>dp,top</sub> [kPa]
VNL12	1,28	60	6,60	25,0%	7,8%	1,03	1,094	1,076	Yes	7,5	0,329	0,240

Upwards discharge  
No elevation  
SG<sub>p</sub> = 1.03

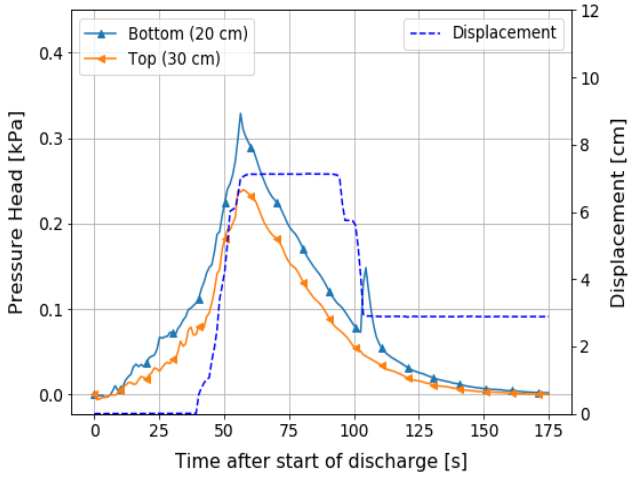
Concentration over time at different levels



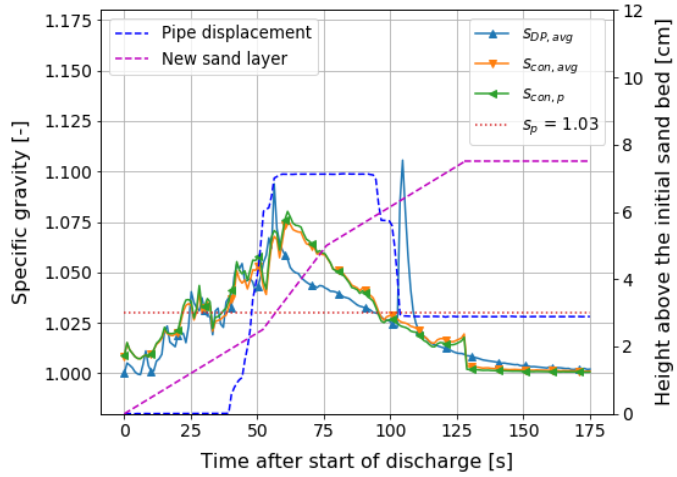
Increasing concentration along height over time



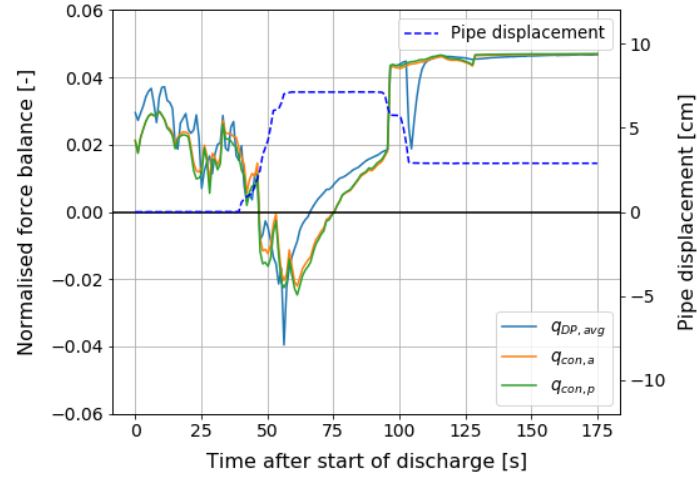
DP net increment at height of the pipe



Specific gravity of the mixture around the pipe (3)

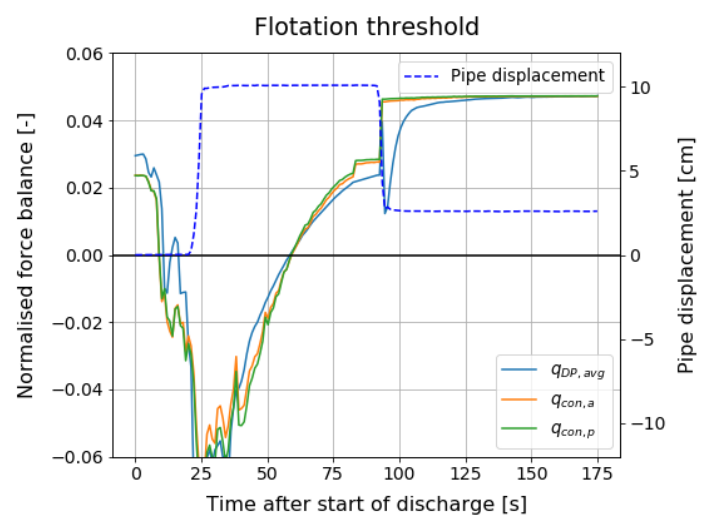
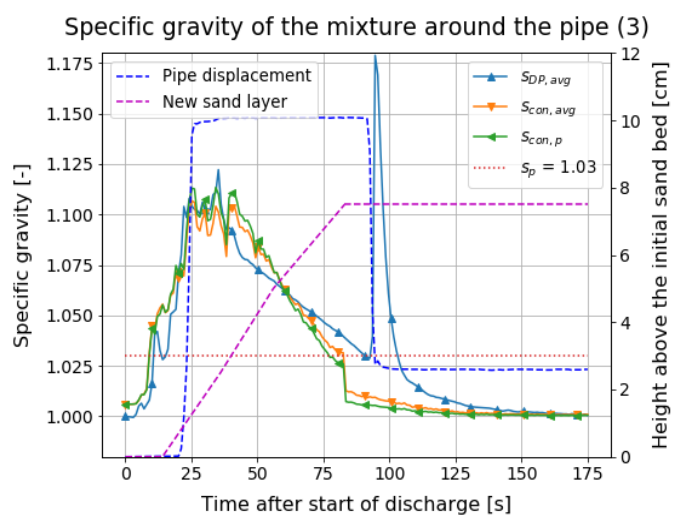
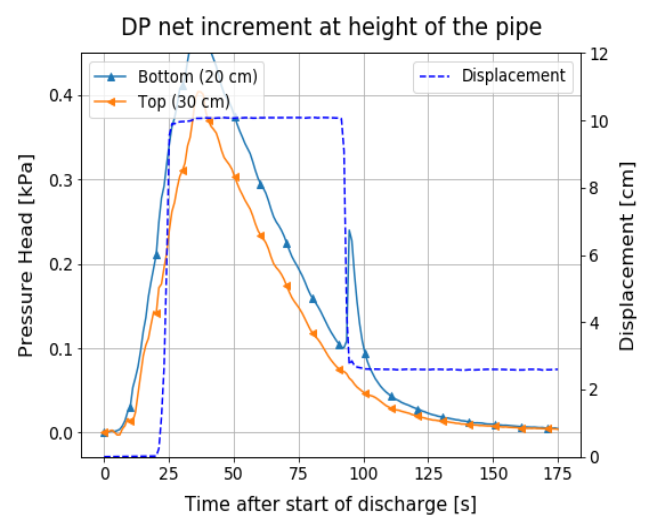
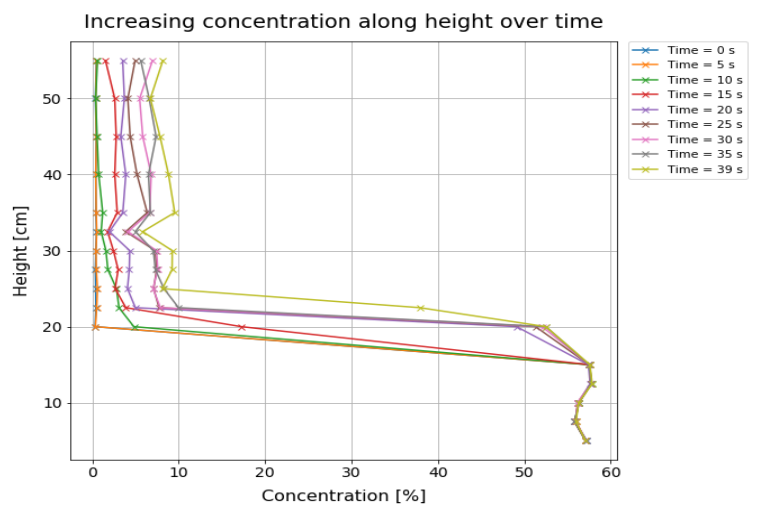
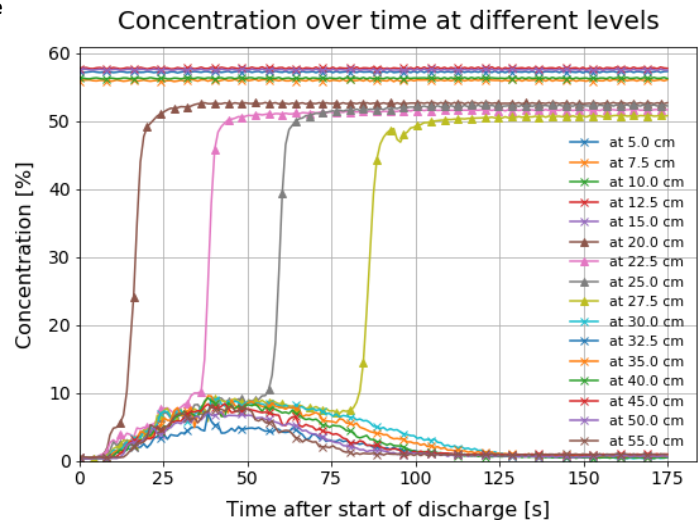


Flotation threshold



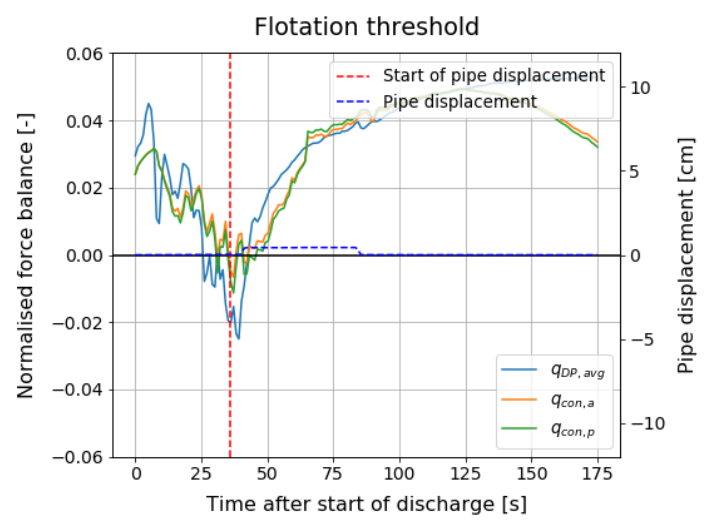
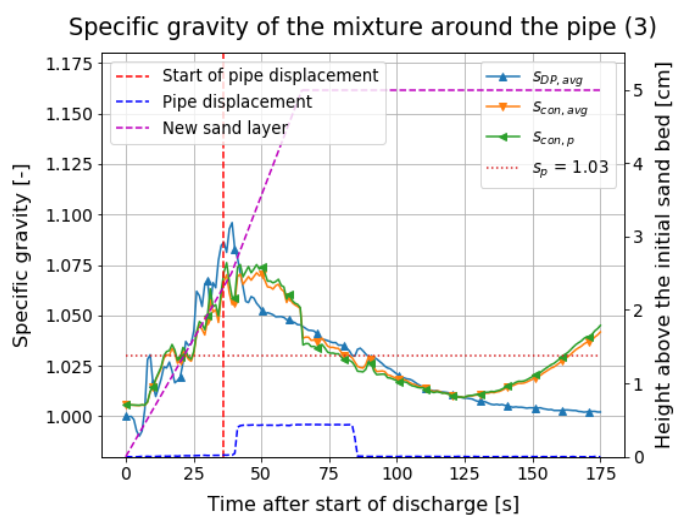
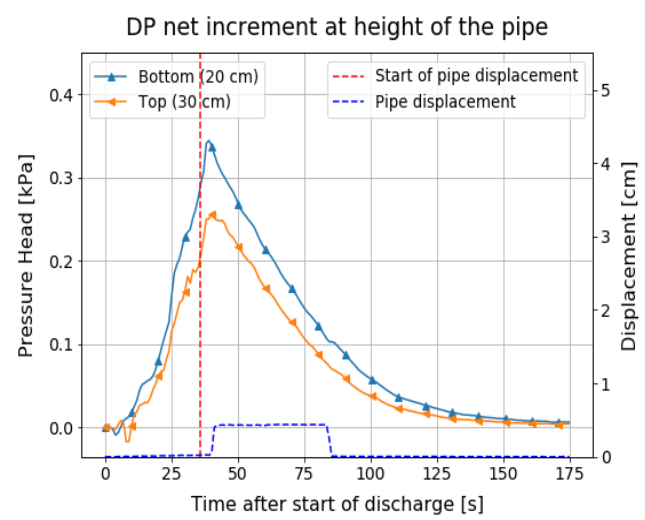
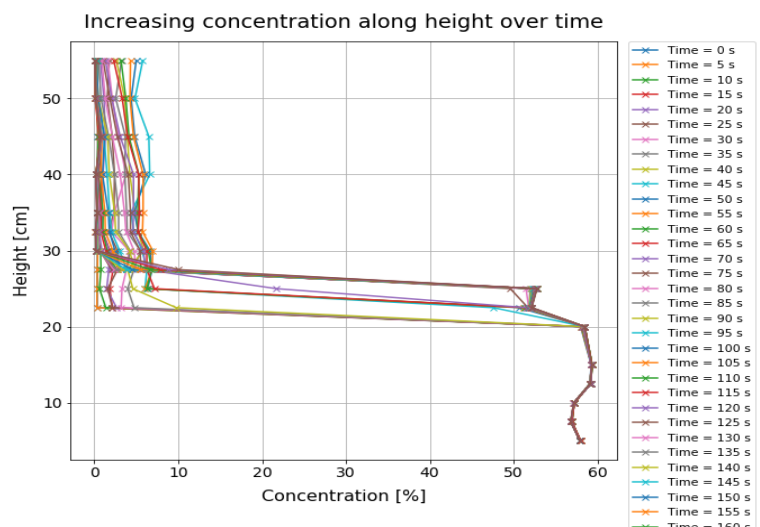
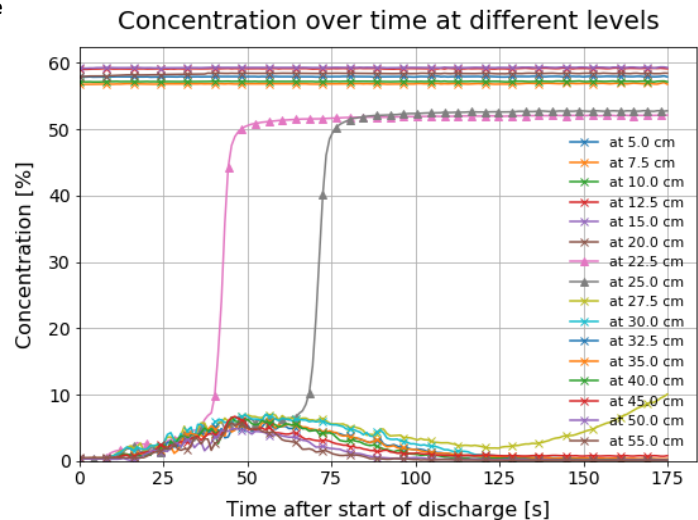
Test	Qcal [L/s]	t <sub>dis</sub> [s]	Δh [cm]	c <sub>dis</sub> [%]	c <sub>max</sub> [%]	S <sub>pipe</sub>	S <sub>dp</sub>	S <sub>con,a</sub>	Flotation	dis,max [cm]	ΔP <sub>dp,bottom</sub> [kPa]	ΔP <sub>dp,top</sub> [kPa]
VNL13	2,02	39	8,03	30,2%	9,6%	1,03	1,122	1,107	Yes	11,6	0,516	0,404

Upwards discharge  
No elevation  
SG<sub>p</sub> = 1.03



Test	Qcal [L/s]	t <sub>dis</sub> [s]	Δh [cm]	c <sub>dis</sub> [%]	c <sub>max</sub> [%]	S <sub>pipe</sub>	S <sub>dp</sub>	S <sub>con,a</sub>	Flotation	dis,max [cm]	ΔP <sub>dp,bottom</sub> [kPa]	ΔP <sub>dp,top</sub> [kPa]
VNL14	1,97	37	5,85	22,9%	7,0%	1,03	1,096	1,071	Semi	4,2	0,345	0,257

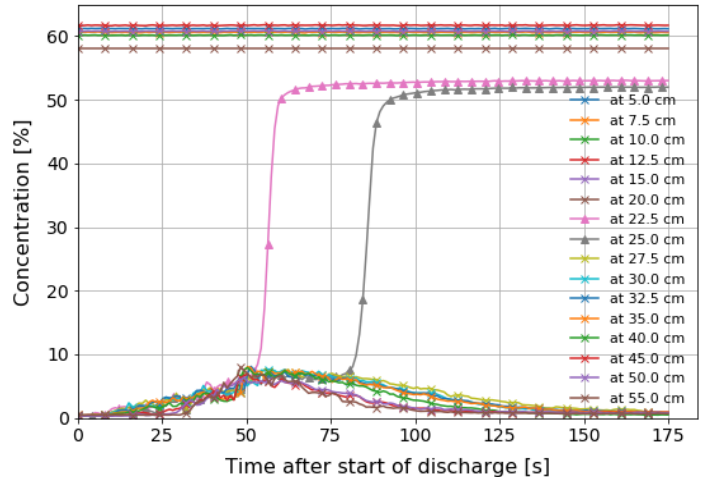
Upwards discharge  
No elevation  
SG<sub>p</sub> = 1.03



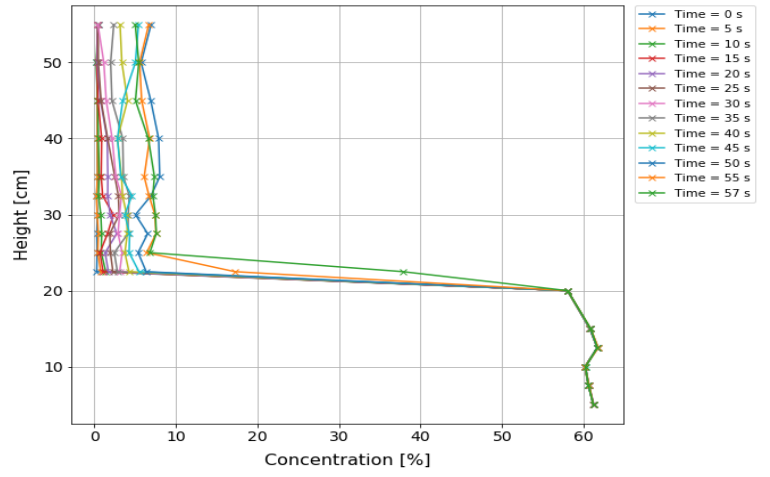
Test	Qcal [L/s]	t <sub>dis</sub> [s]	Δh [cm]	c <sub>dis</sub> [%]	c <sub>max</sub> [%]	Sp <sub>ipe</sub>	S <sub>dp</sub>	S <sub>con,a</sub>	Flotation	dis,max [cm]	ΔP <sub>dp,bottom</sub> [kPa]	ΔP <sub>dp,top</sub> [kPa]
VNL15	1,63	45	5,85	23,8%	7,7%	1,03	1,082	1,087	Yes	8,3	0,351	0,273

Upwards discharge  
No elevation  
SG<sub>p</sub> = 1.03

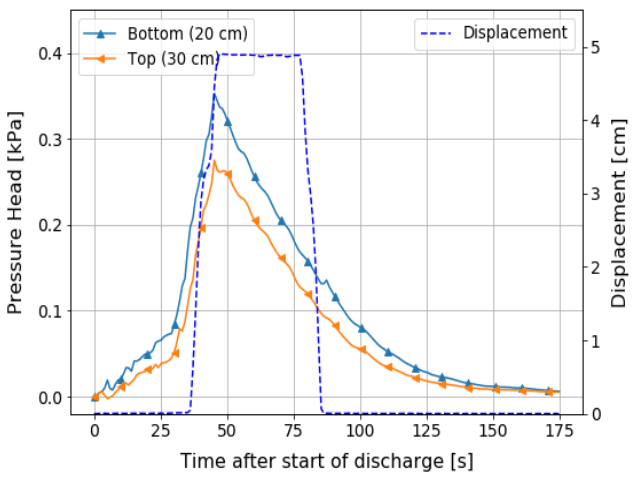
Concentration over time at different levels



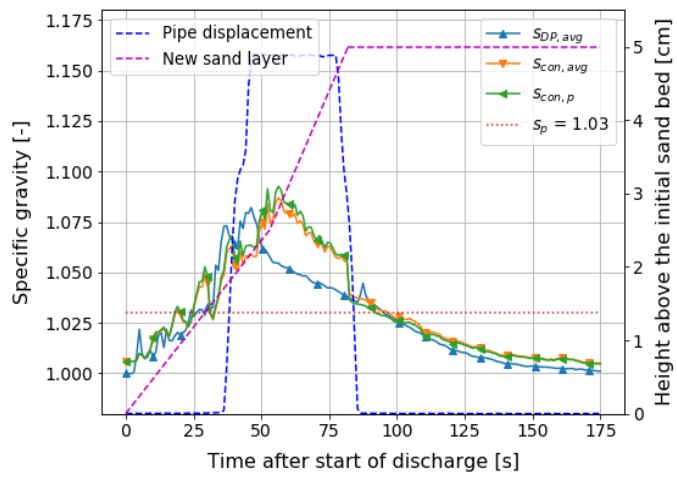
Increasing concentration along height over time



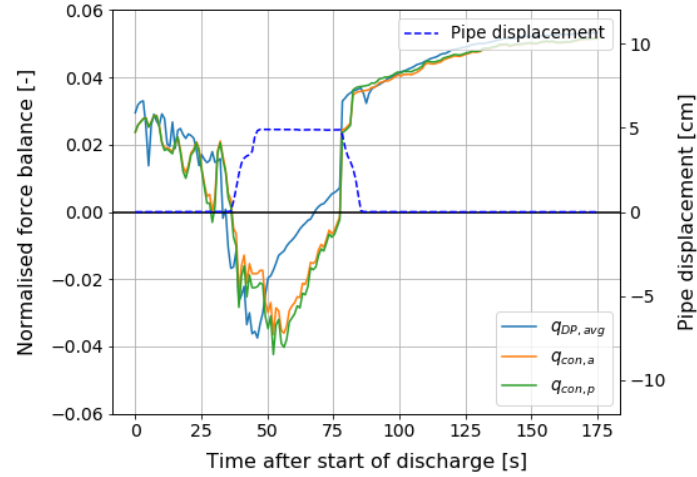
DP net increment at height of the pipe



Specific gravity of the mixture around the pipe (3)



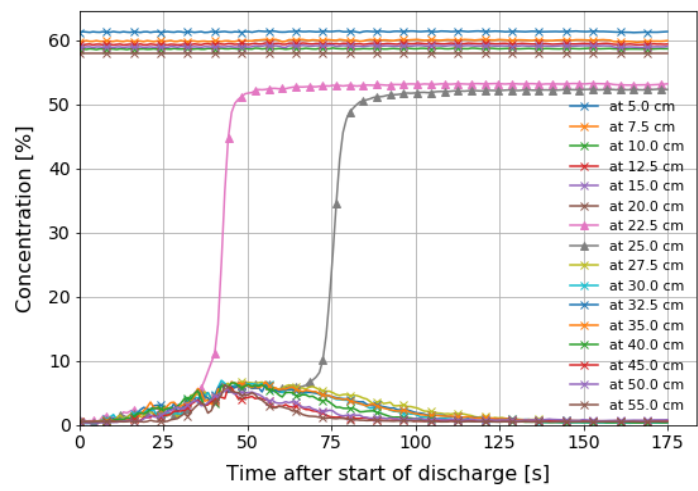
Flotation threshold



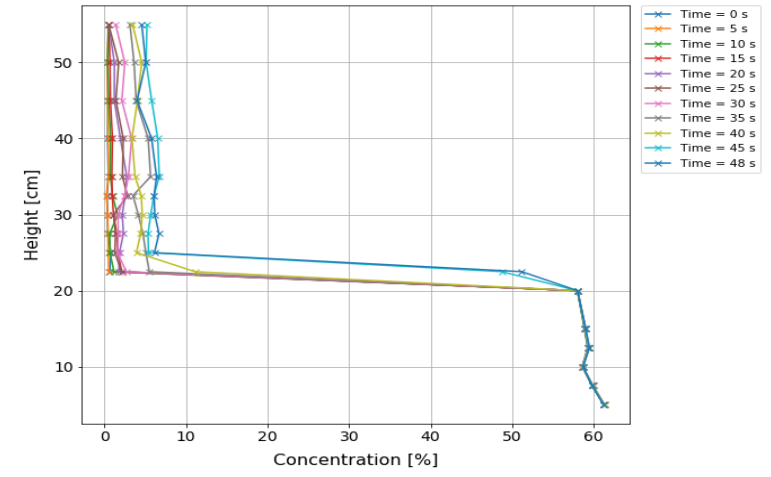
Test	Qcal [L/s]	t <sub>dis</sub> [s]	Δh [cm]	c <sub>dis</sub> [%]	c <sub>max</sub> [%]	Sp <sub>ipe</sub>	S <sub>dp</sub>	S <sub>con,a</sub>	Flotation	dis,max [cm]	ΔP <sub>dp,bottom</sub> [kPa]	ΔP <sub>dp,top</sub> [kPa]
VNL16	1,37	44	4,80	23,7%	7,0%	1,03	?	1,076	Semi	5,8	?	?

Upwards discharge  
No elevation  
SG<sub>p</sub> = 1.03

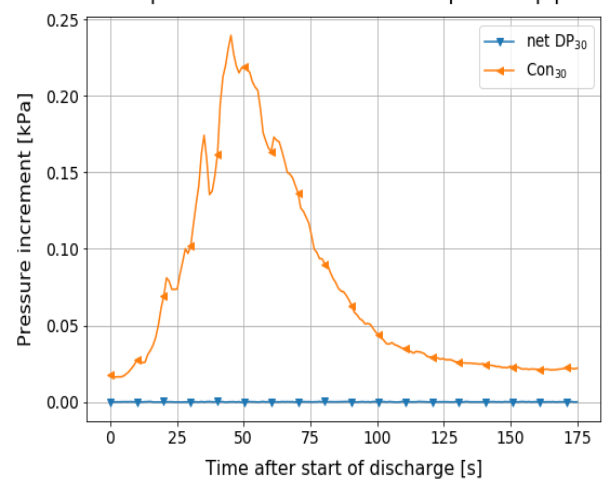
Concentration over time at different levels



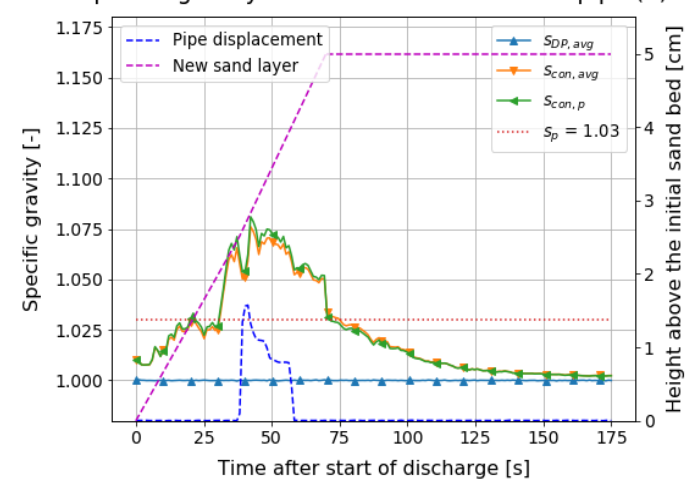
Increasing concentration along height over time



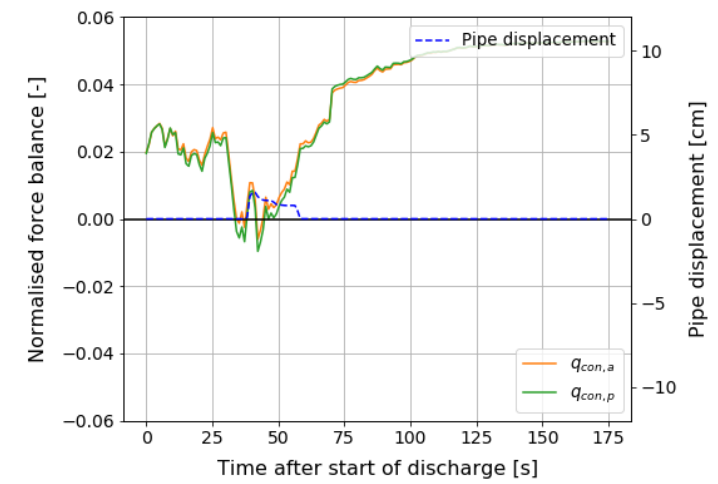
Net pressure increment at the top of the pipe



Specific gravity of the mixture around the pipe (3)



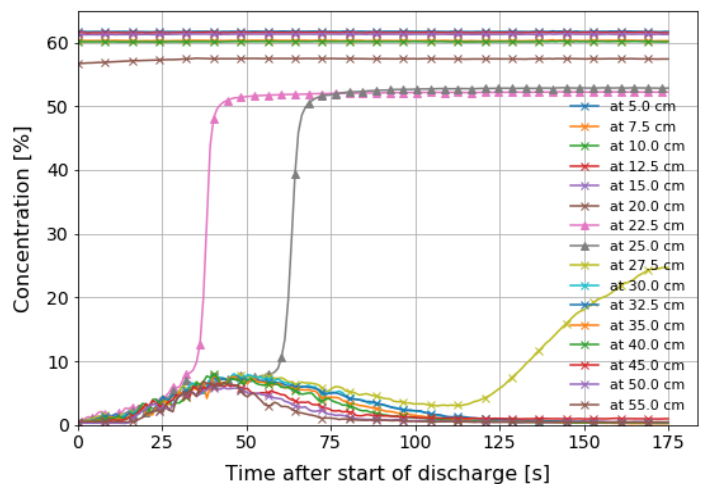
Flotation threshold



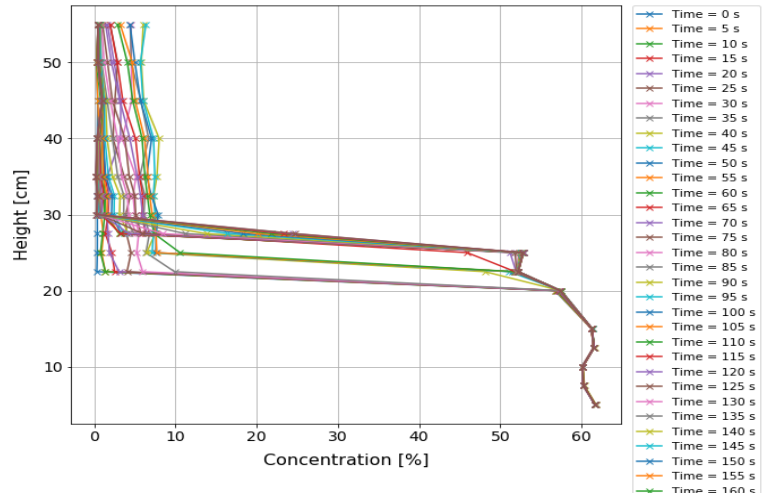
Test	Qcal [L/s]	t <sub>dis</sub> [s]	Δh [cm]	c <sub>dis</sub> [%]	c <sub>max</sub> [%]	Sp <sub>ipe</sub>	S <sub>dp</sub>	S <sub>con,a</sub>	Flotation	dis,max [cm]	ΔP <sub>dp,bottom</sub> [kPa]	ΔP <sub>dp,top</sub> [kPa]
VNL17	1,63	43	6,30	24,9%	8,0%	1,03	1,092	1,081	Yes	10,8	0,348	0,264

Upwards discharge  
No elevation  
SG<sub>p</sub> = 1.03

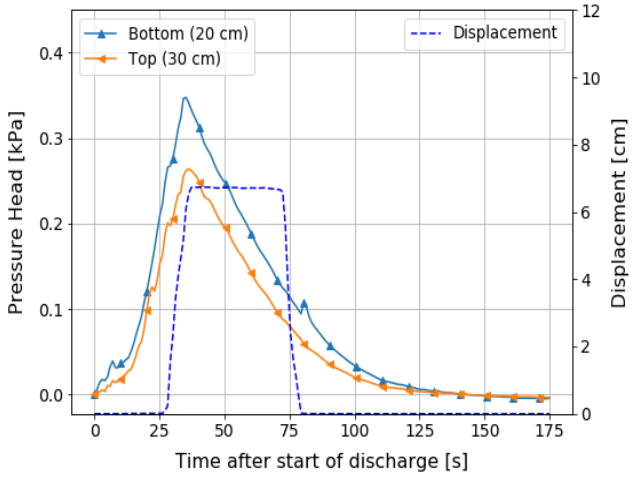
Concentration over time at different levels



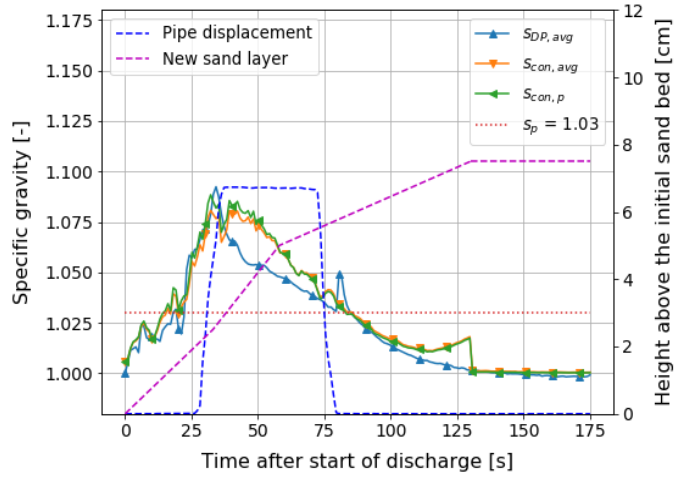
Increasing concentration along height over time



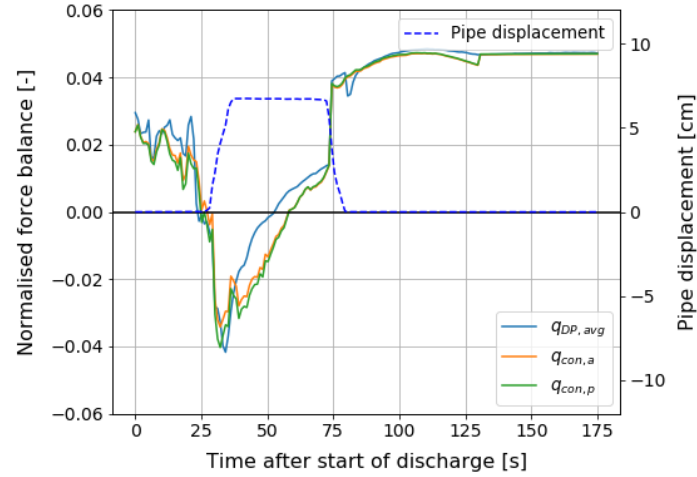
DP net increment at height of the pipe



Specific gravity of the mixture around the pipe (3)



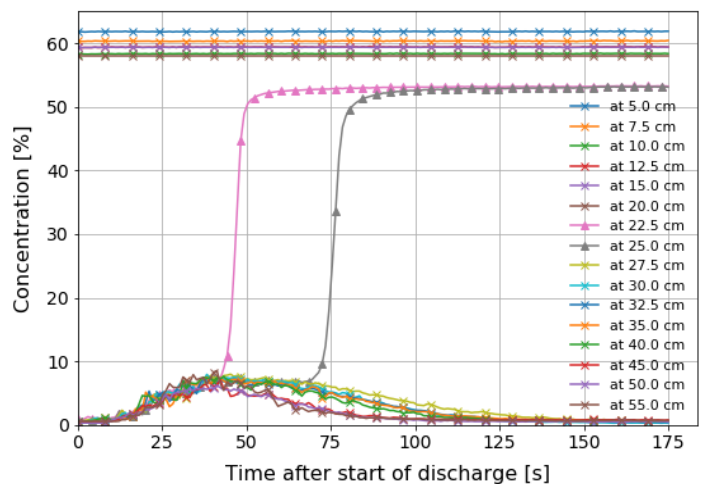
Flotation threshold



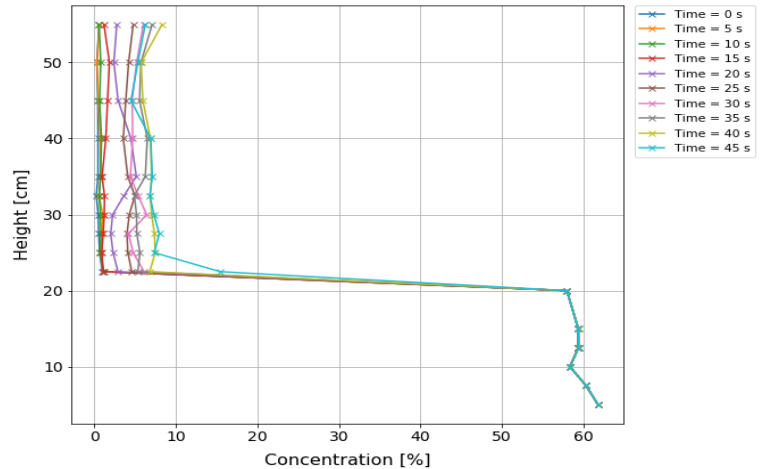
Test	Qcal [L/s]	t <sub>dis</sub> [s]	Δh [cm]	c <sub>dis</sub> [%]	c <sub>max</sub> [%]	Sp <sub>ipe</sub>	S <sub>dp</sub>	S <sub>con,a</sub>	Flotation	dis,max [cm]	ΔP <sub>dp,bottom</sub> [kPa]	ΔP <sub>dp,top</sub> [kPa]
VNL18	1,65	43	6,13	25,2%	8,5%	1,03	1,086	1,093	Yes	11,6	0,347	0,273

Upwards discharge  
No elevation  
SG<sub>p</sub> = 1.03

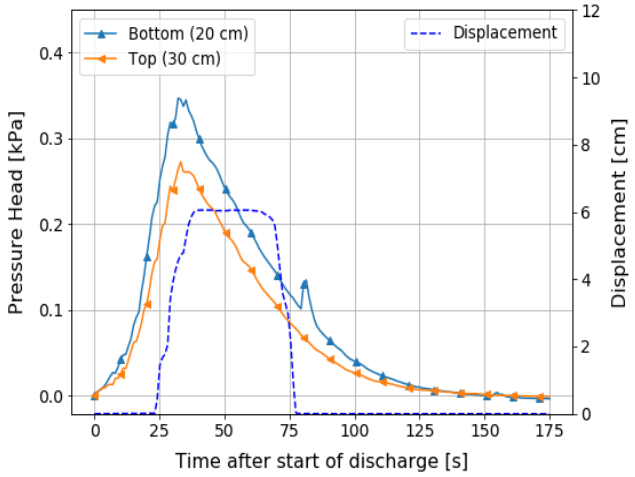
Concentration over time at different levels



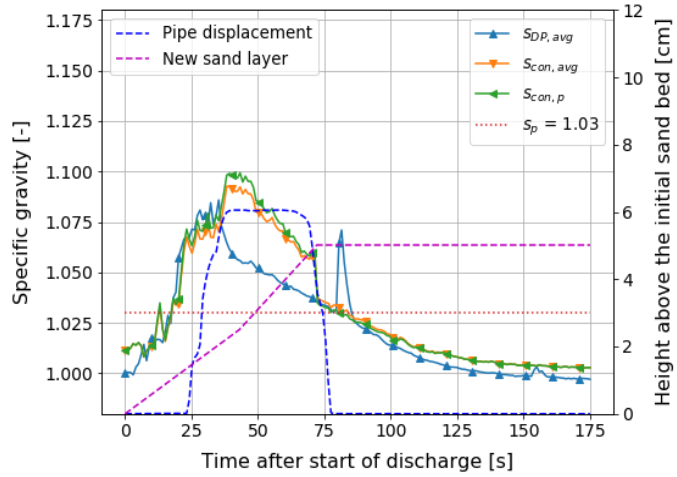
Increasing concentration along height over time



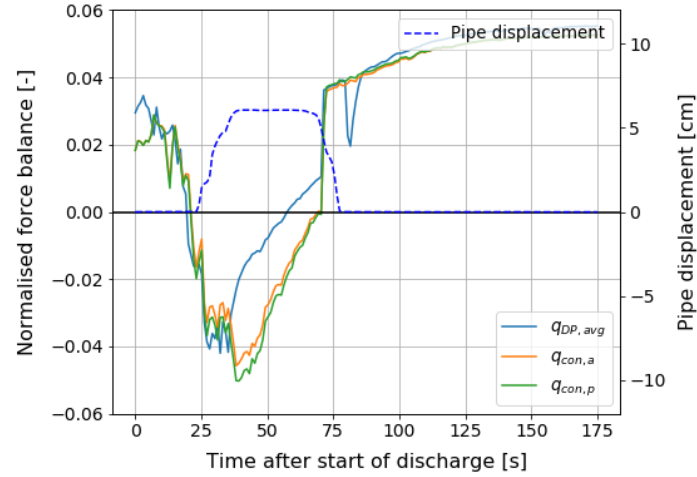
DP net increment at height of the pipe



Specific gravity of the mixture around the pipe (3)



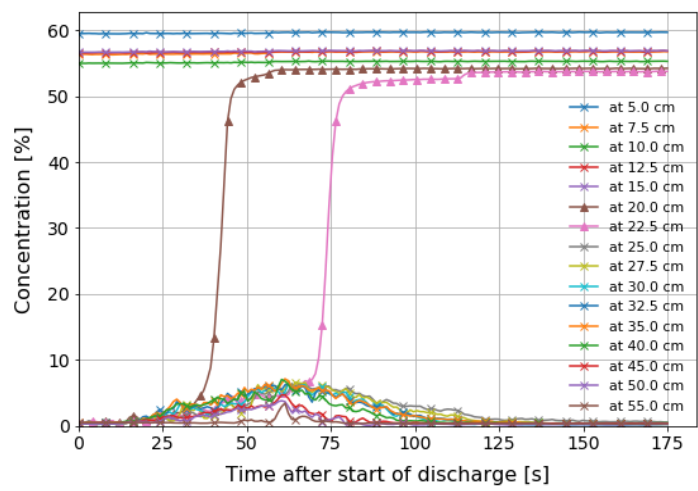
Flotation threshold



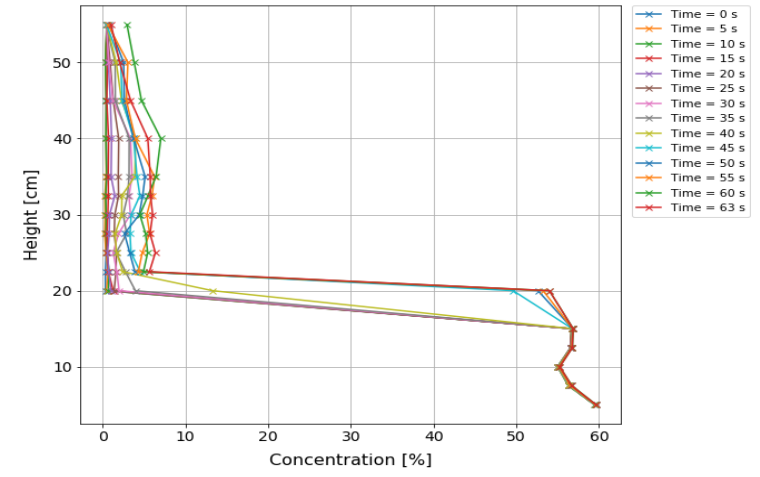
Test	Qcal [L/s]	t <sub>dis</sub> [s]	Δh [cm]	c <sub>dis</sub> [%]	c <sub>max</sub> [%]	S <sub>pipe</sub>	S <sub>dp</sub>	S <sub>con,a</sub>	Flotation	dis,max [cm]	ΔP <sub>dp,bottom</sub> [kPa]	ΔP <sub>dp,top</sub> [kPa]
VNL19	1,01	60	4,70	21,9%	7,1%	1,03	1,108	1,083	No	0	0,224	0,127

Upwards discharge  
No elevation  
SG<sub>p</sub> = 1.03

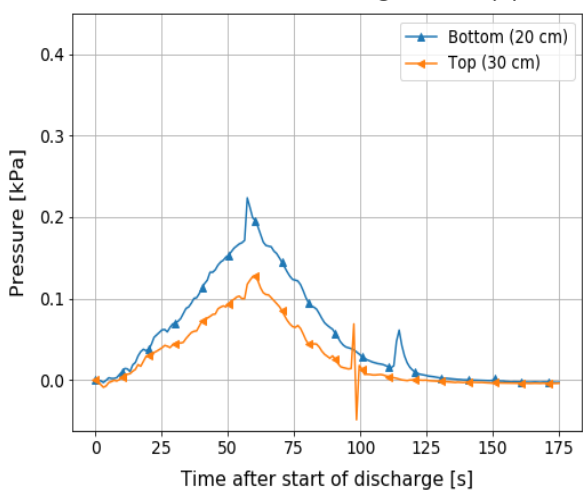
Concentration over time at different levels



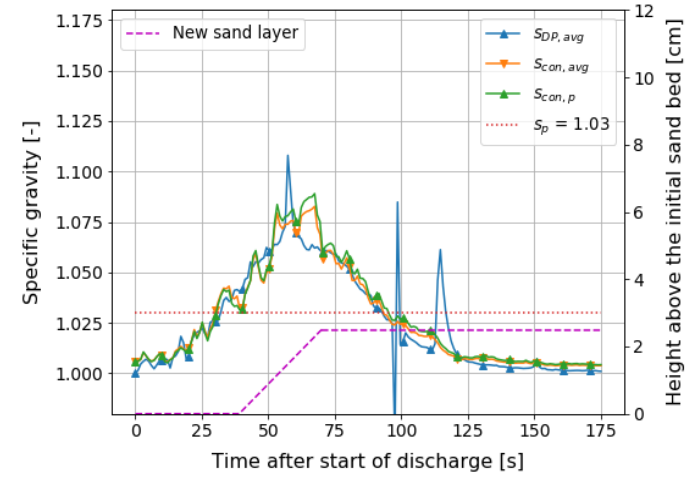
Increasing concentration along height over time



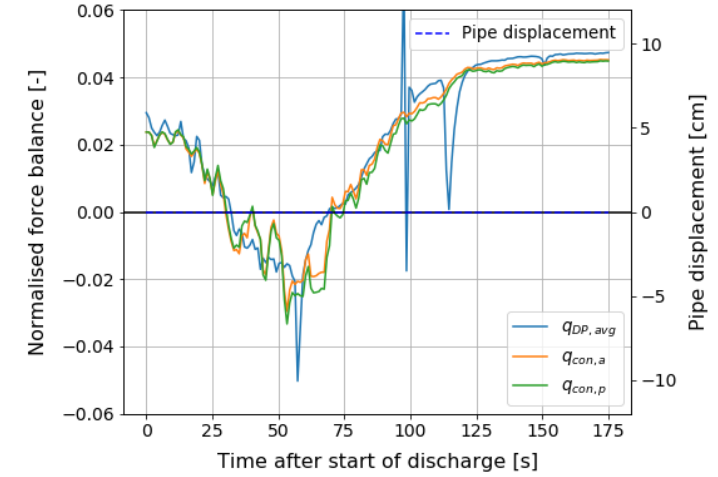
DP net increment at height of the pipe



Specific gravity of the mixture around the pipe



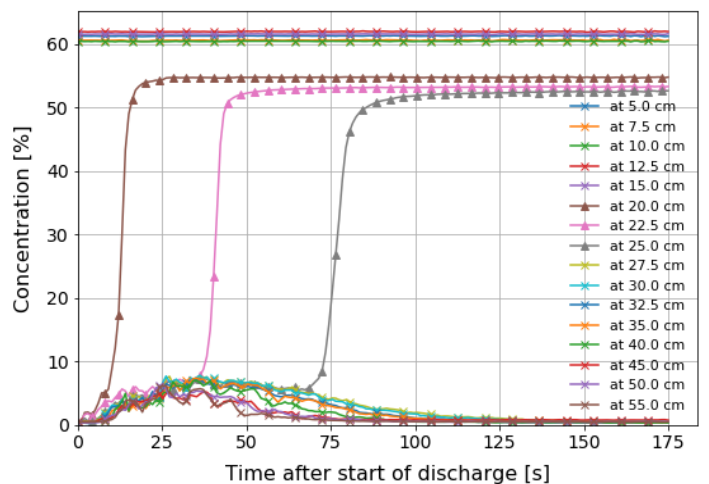
Flotation threshold



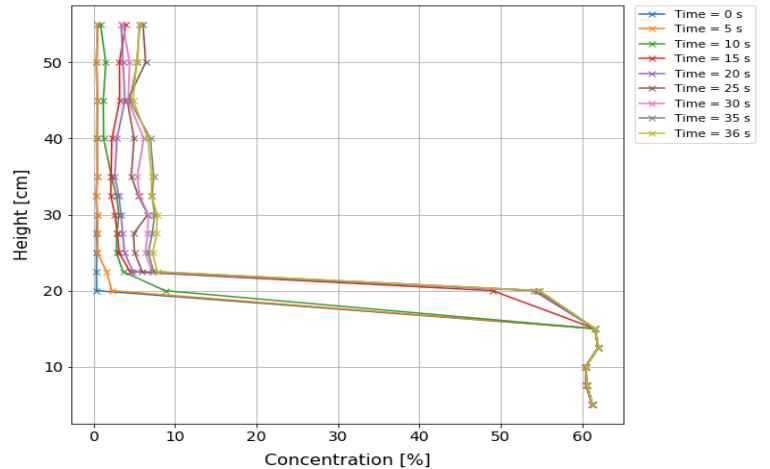
Test	Qcal [L/s]	t <sub>dis</sub> [s]	Δh [cm]	c <sub>dis</sub> [%]	c <sub>max</sub> [%]	Sp <sub>ipe</sub>	S <sub>dp</sub>	S <sub>con,a</sub>	Flotation	dis,max [cm]	ΔP <sub>dp,bottom</sub> [kPa]	ΔP <sub>dp,top</sub> [kPa]
VNL20	2,04	23	4,90	29,7%	7,8%	1,03	1,904	1,986	Yes	12,0	0,337	0,249

Upwards discharge  
No elevation  
SG<sub>p</sub> = 1.03

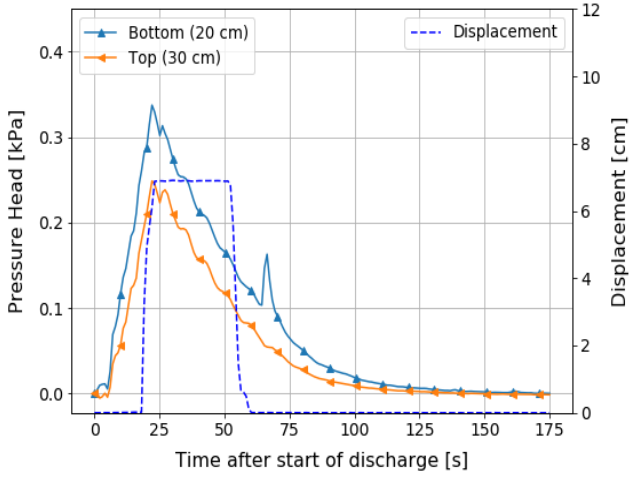
Concentration over time at different levels



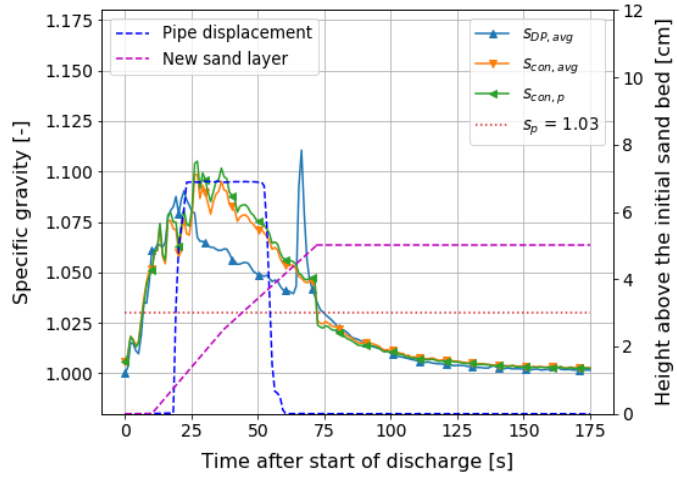
Increasing concentration along height over time



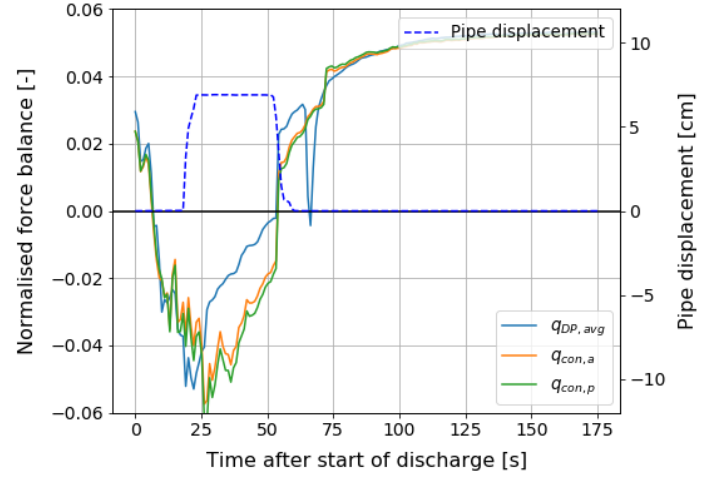
DP net increment at height of the pipe



Specific gravity of the mixture around the pipe (3)



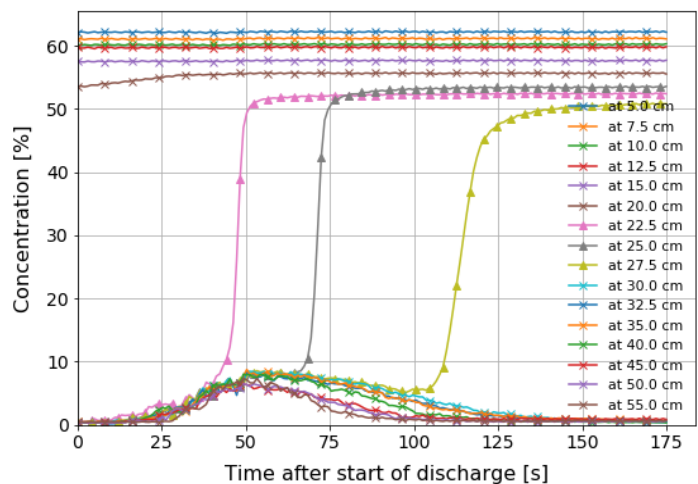
Flotation threshold



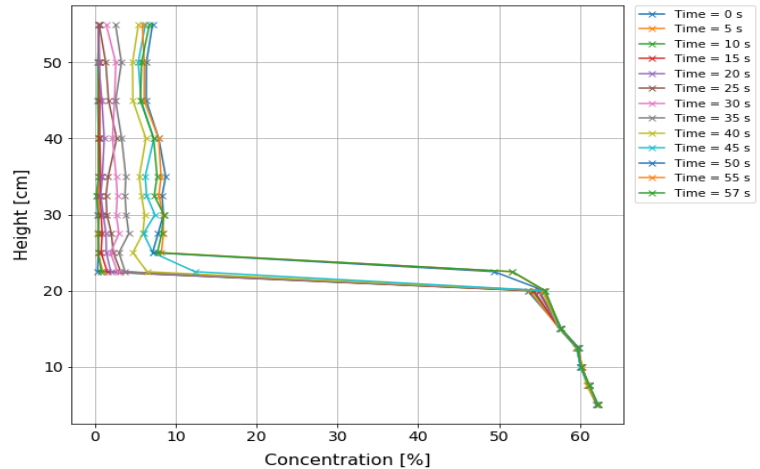
Test	Qcal [L/s]	t <sub>dis</sub> [s]	Δh [cm]	c <sub>dis</sub> [%]	c <sub>max</sub> [%]	S <sub>pipe</sub>	S <sub>dp</sub>	S <sub>con,a</sub>	Flotation	dis,max [cm]	ΔP <sub>dp,bottom</sub> [kPa]	ΔP <sub>dp,top</sub> [kPa]
VNL21	1,57	45	6,83	27,8%	8,8%	1,03	1,106	1,090	Yes	9,1	0,392	0,292

Upwards discharge  
No elevation  
SG<sub>p</sub> = 1.03

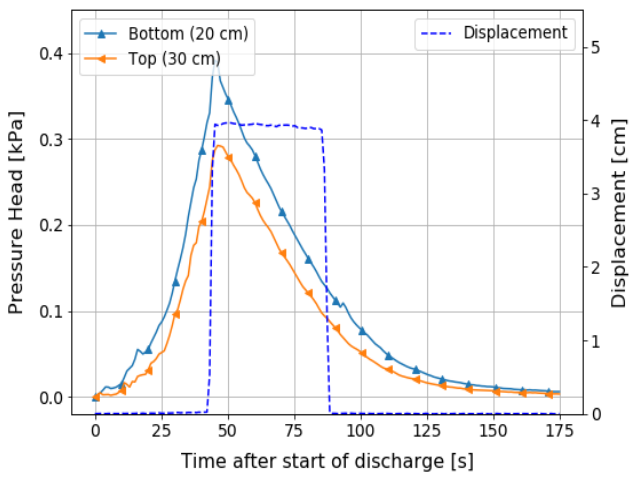
Concentration over time at different levels



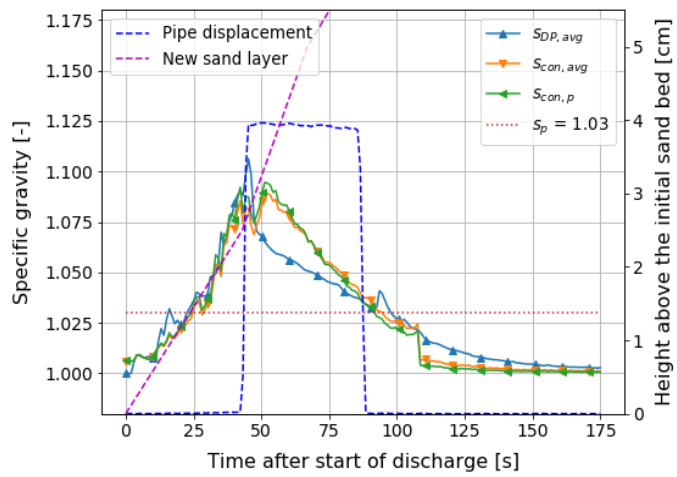
Increasing concentration along height over time



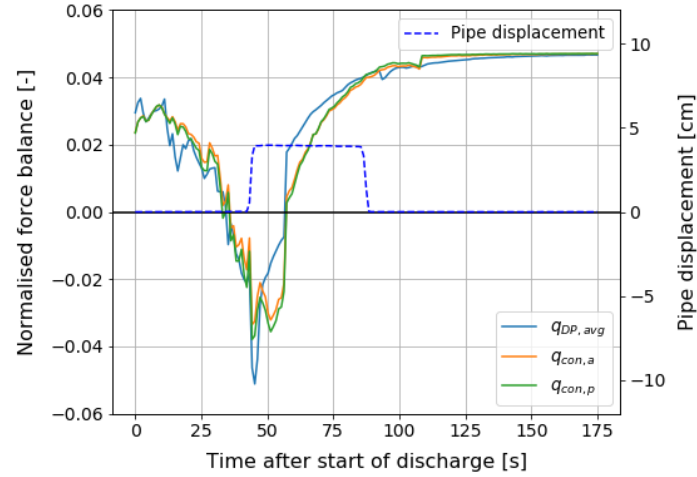
DP net increment at height of the pipe



Specific gravity of the mixture around the pipe (3)



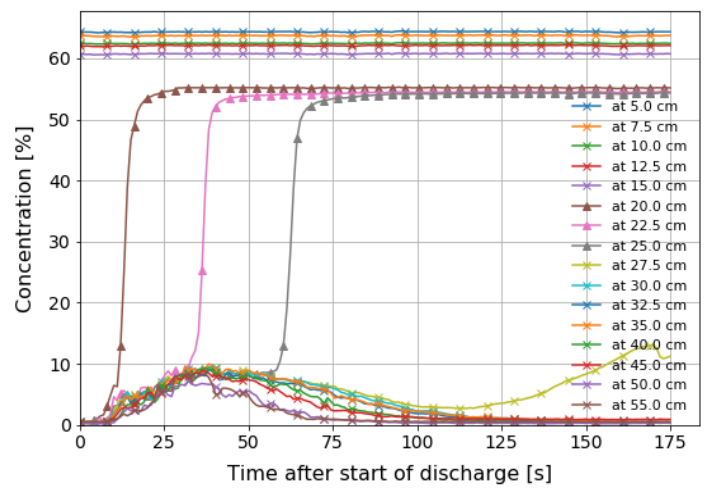
Flotation threshold



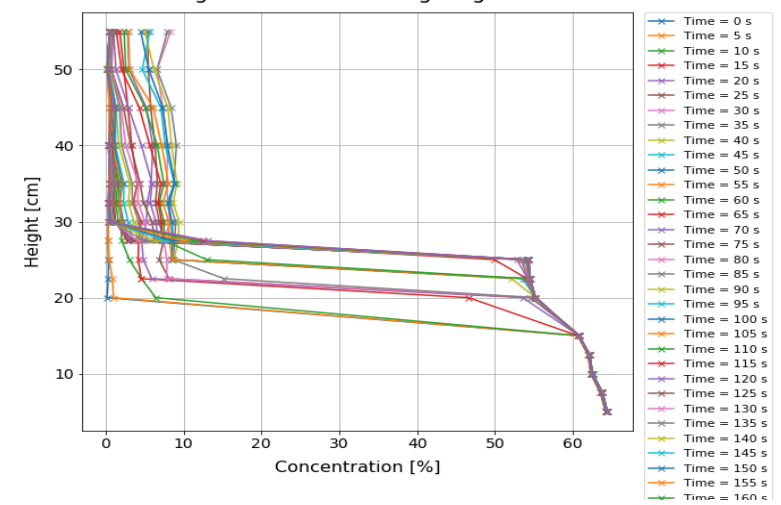
Test	Qcal [L/s]	t <sub>dis</sub> [s]	Δh [cm]	c <sub>dis</sub> [%]	c <sub>max</sub> [%]	Sp <sub>ipe</sub>	S <sub>dp</sub>	S <sub>con,a</sub>	Flotation	dis,max [cm]	ΔP <sub>dp,bottom</sub> [kPa]	ΔP <sub>dp,top</sub> [kPa]
VNL22	1,94	31	5,78	26,9%	10,0%	1,03	1,113	1,115	Yes	11,6	0,395	0,291

Upwards discharge  
No elevation  
SG<sub>p</sub> = 1.03

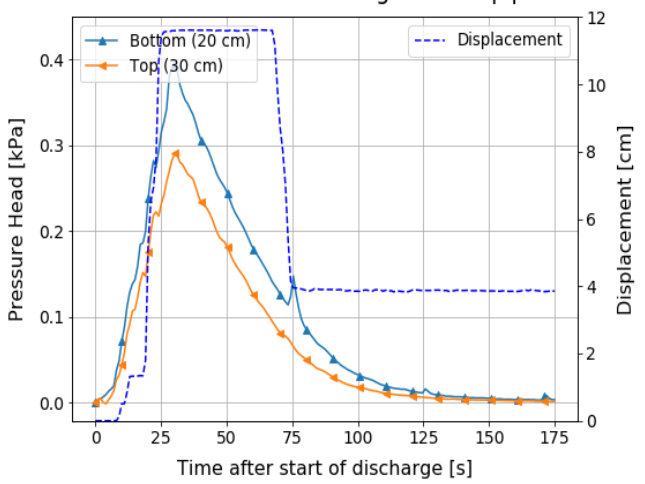
Concentration over time at different levels



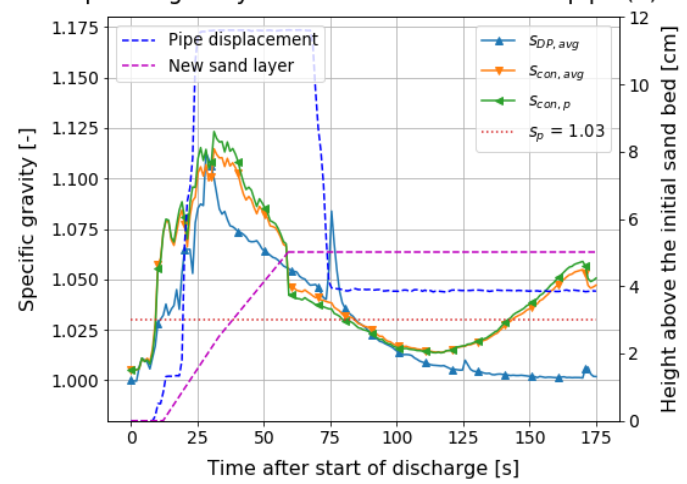
Increasing concentration along height over time



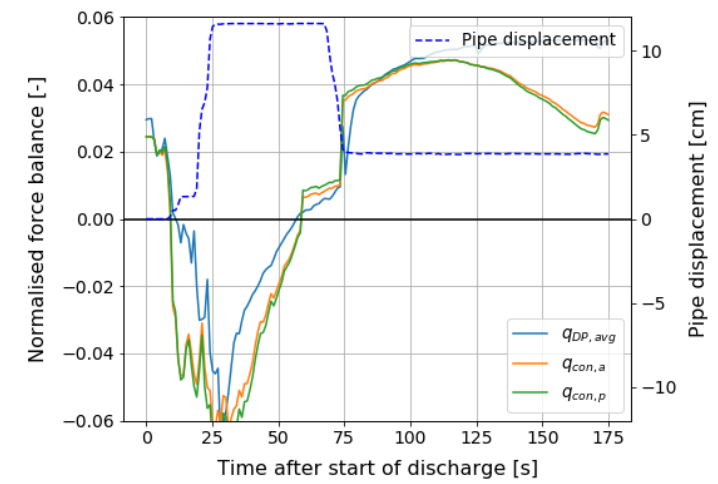
DP net increment at height of the pipe



Specific gravity of the mixture around the pipe (3)



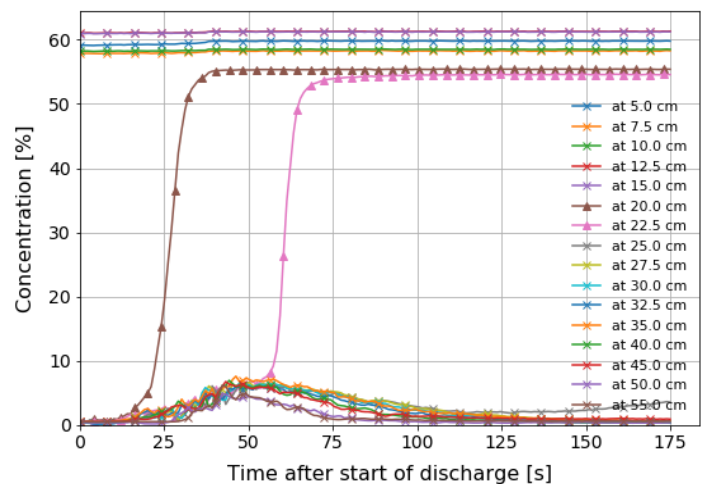
Flotation threshold



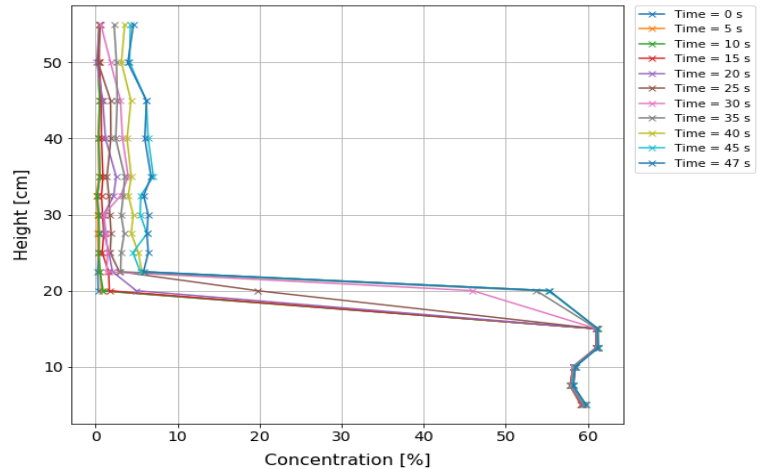
Test	Qcal [L/s]	t <sub>dis</sub> [s]	Δh [cm]	c <sub>dis</sub> [%]	c <sub>max</sub> [%]	Sp <sub>ipe</sub>	S <sub>dp</sub>	S <sub>con,a</sub>	Flotation	dis,max [cm]	ΔP <sub>dp,bottom</sub> [kPa]	ΔP <sub>dp,top</sub> [kPa]
VNL23	1,22	41	4,45	25,8%	7,6%	1,03	1,057	1,084	Semi	1,7	0,226	0,171

Upwards discharge  
No elevation  
SG<sub>p</sub> = 1.03

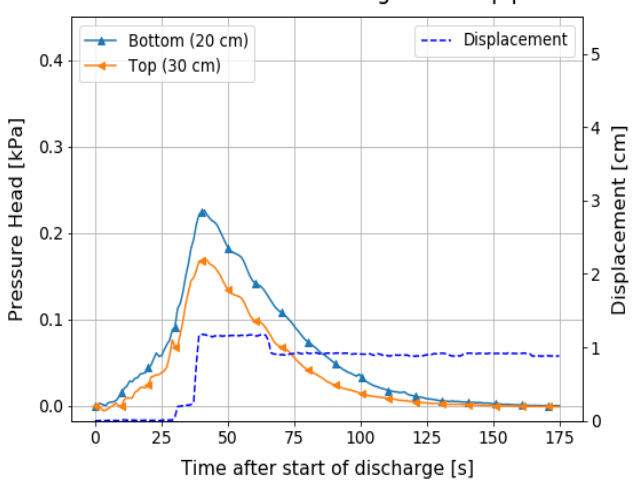
Concentration over time at different levels



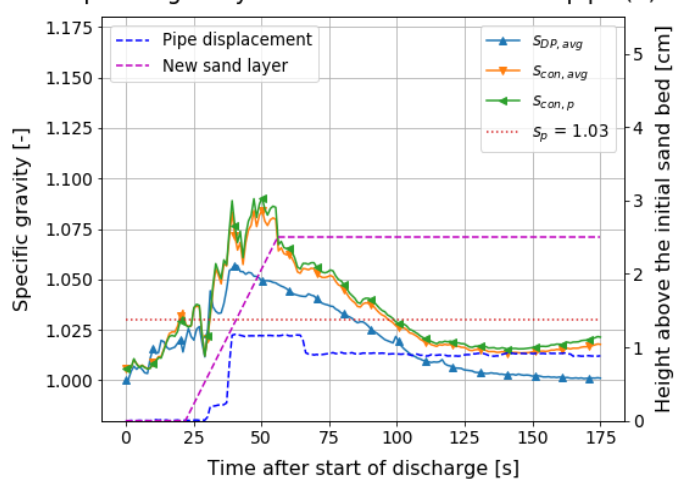
Increasing concentration along height over time



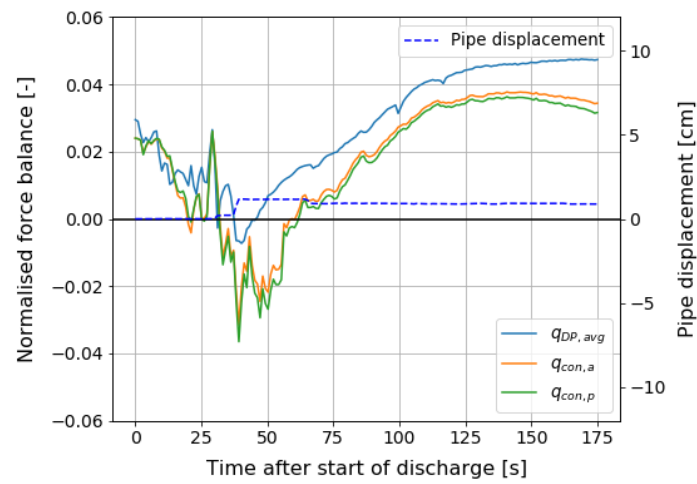
DP net increment at height of the pipe



Specific gravity of the mixture around the pipe (3)



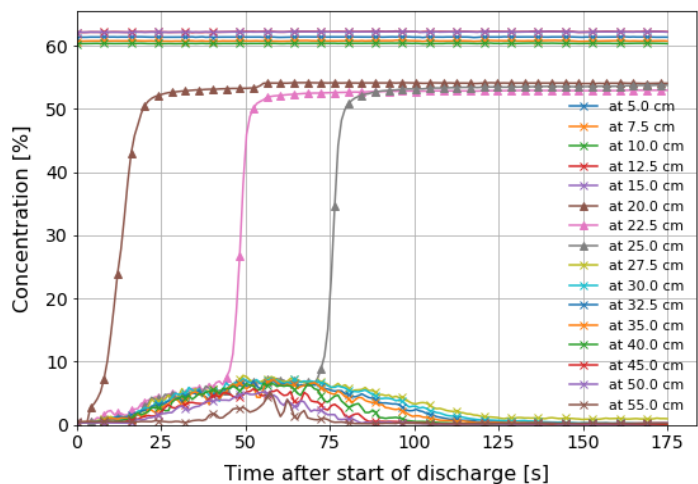
Flotation threshold



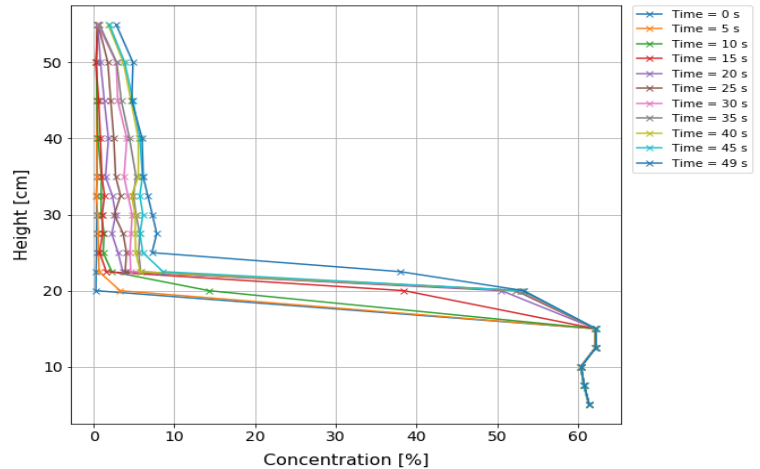
Test	Qcal [L/s]	t <sub>dis</sub> [s]	Δh [cm]	c <sub>dis</sub> [%]	c <sub>max</sub> [%]	S <sub>pipe</sub>	S <sub>dp</sub>	S <sub>con,a</sub>	Flotation	dis,max [cm]	ΔP <sub>dp,bottom</sub> [kPa]	ΔP <sub>dp,top</sub> [kPa]
VSL24	1,27	56	6,55	25,8%	7,8%	1,03	1,100	1,088	Yes	11,2	0,307	0,212

Upwards discharge  
Elevation = 1 cm  
SG<sub>p</sub> = 1.03

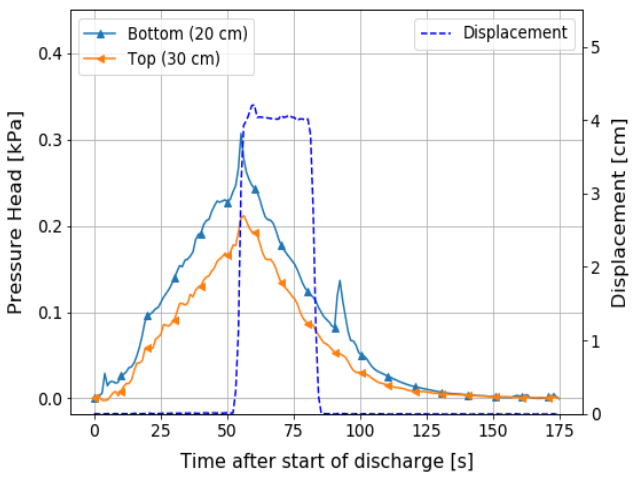
Concentration over time at different levels



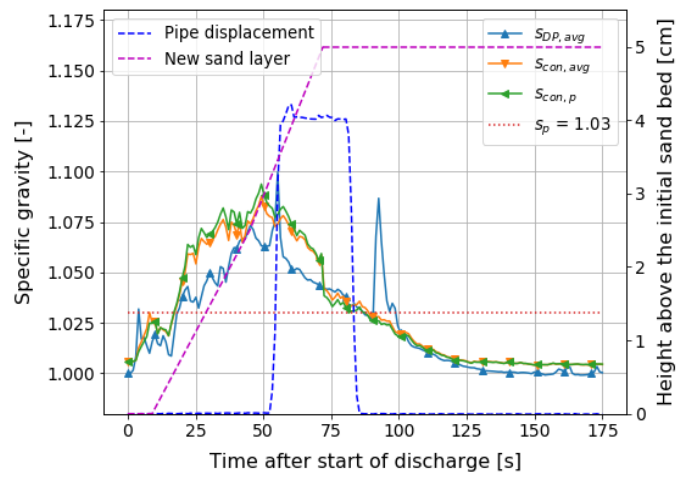
Increasing concentration along height over time



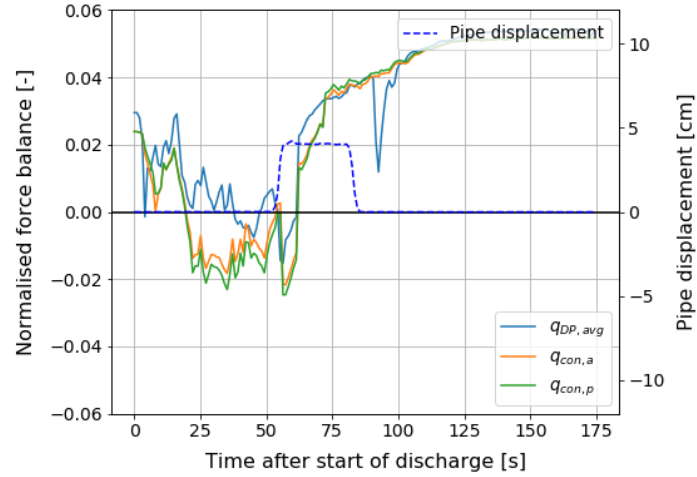
DP net increment at height of the pipe



Specific gravity of the mixture around the pipe (3)



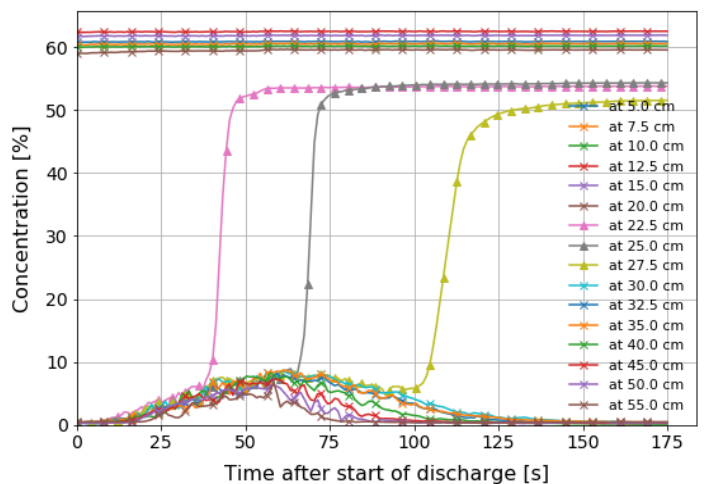
Flotation threshold



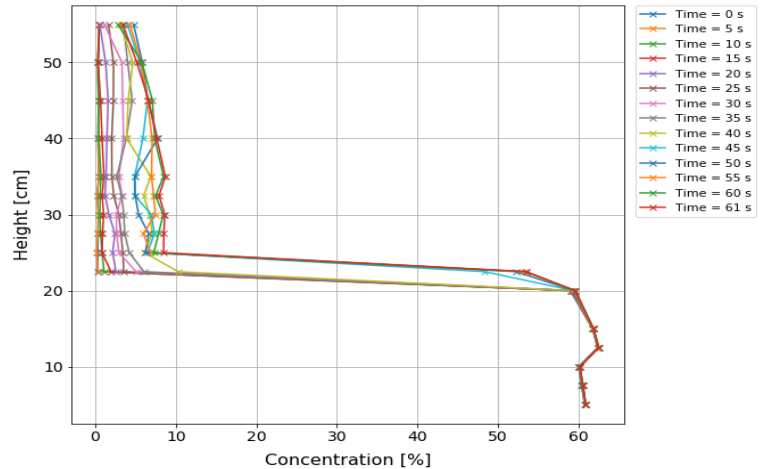
Test	Qcal [L/s]	t <sub>dis</sub> [s]	Δh [cm]	c <sub>dis</sub> [%]	c <sub>max</sub> [%]	S <sub>pipe</sub>	S <sub>dp</sub>	S <sub>con,a</sub>	Flotation	dis,max [cm]	ΔP <sub>dp,bottom</sub> [kPa]	ΔP <sub>dp,top</sub> [kPa]
VSL25	1,32	55	6,83	26,7%	8,7%	1,03	1,079	1,081	Yes	8,3	0,307	0,234

Upwards discharge  
Elevation = 1 cm  
SG<sub>p</sub> = 1.03

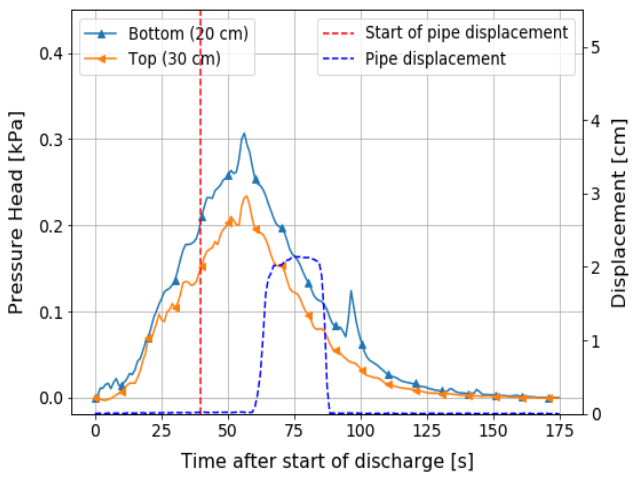
Concentration over time at different levels



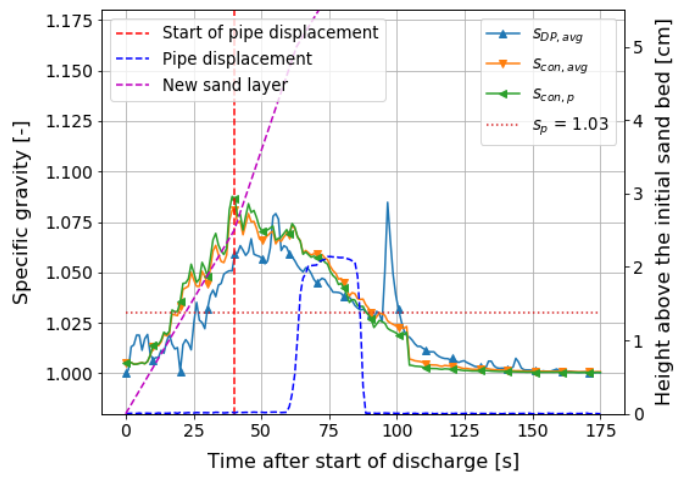
Increasing concentration along height over time



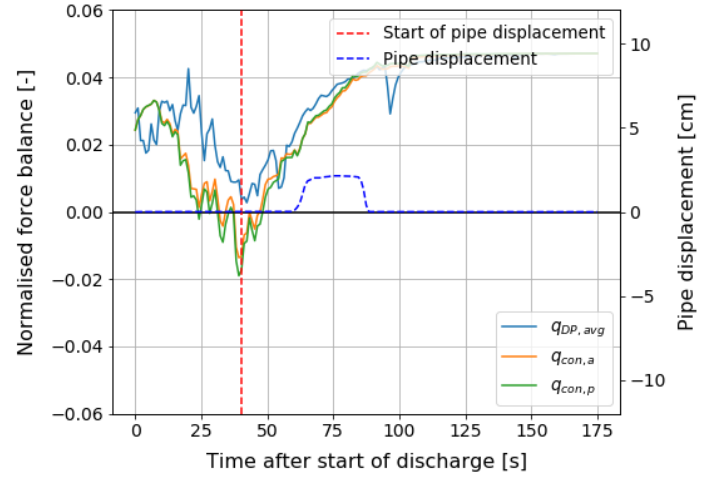
DP net increment at height of the pipe



Specific gravity of the mixture around the pipe (3)



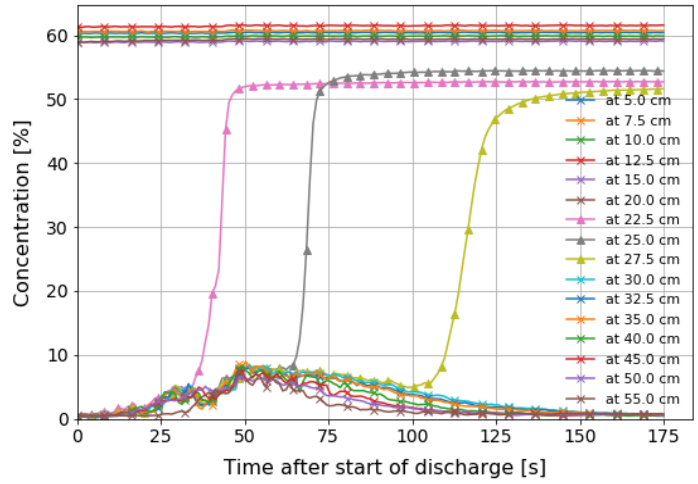
Flotation threshold



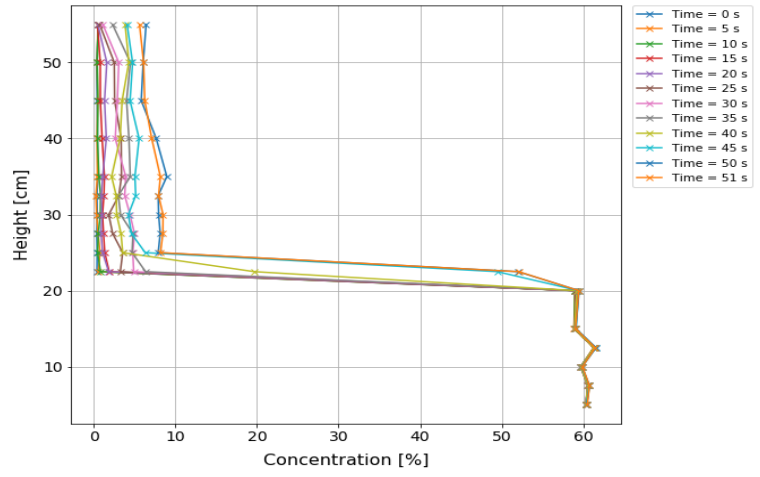
Test	Qcal [L/s]	t <sub>dis</sub> [s]	Δh [cm]	c <sub>dis</sub> [%]	c <sub>max</sub> [%]	Sp <sub>ipe</sub>	S <sub>dp</sub>	S <sub>con,a</sub>	Flotation	dis,max [cm]	ΔP <sub>dp,bottom</sub> [kPa]	ΔP <sub>dp,top</sub> [kPa]
VSL26	1,49	46	6,38	26,5%	8,9%	1,03	1,084	1,086	Yes	9,5	0,326	0,258

Upwards discharge  
Elevation = 1 cm  
SG<sub>p</sub> = 1.03

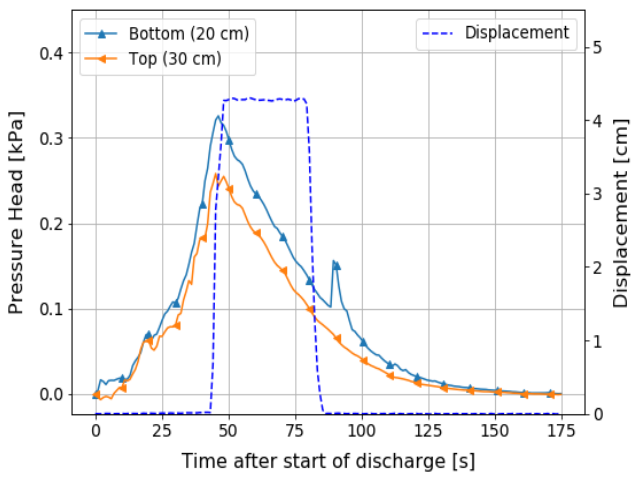
Concentration over time at different levels



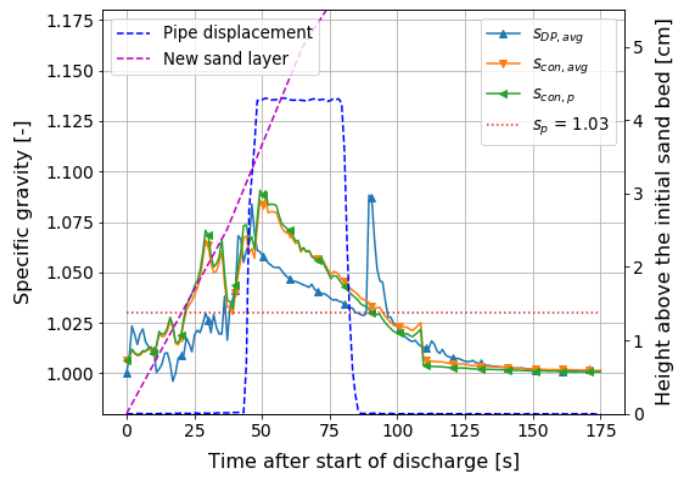
Increasing concentration along height over time



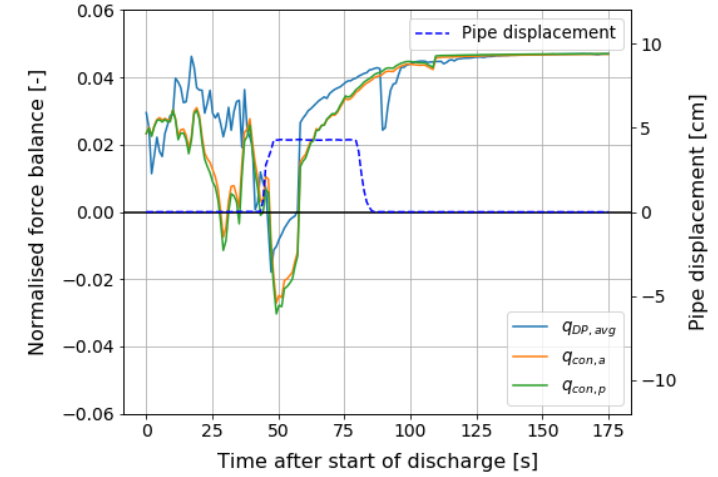
DP net increment at height of the pipe



Specific gravity of the mixture around the pipe (3)



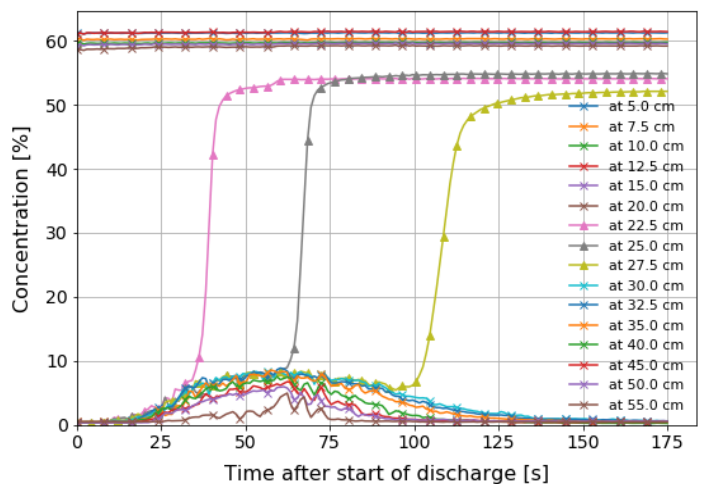
Flotation threshold



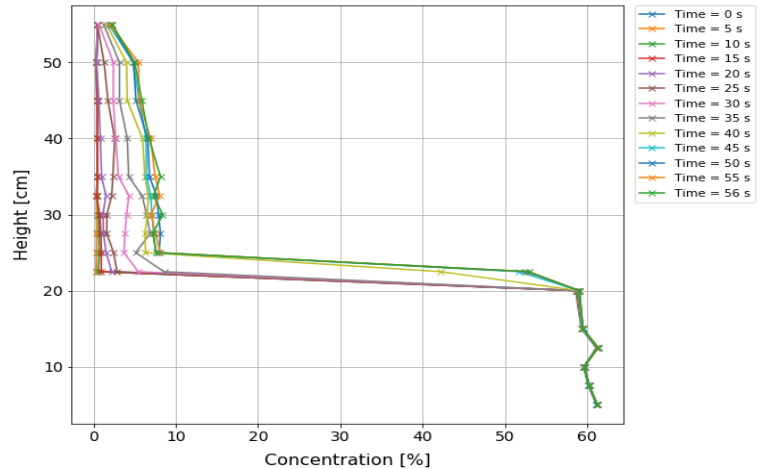
Test	Qcal [L/s]	t <sub>dis</sub> [s]	Δh [cm]	c <sub>dis</sub> [%]	c <sub>max</sub> [%]	S <sub>pipe</sub>	S <sub>dp</sub>	S <sub>con,a</sub>	Flotation	dis,max [cm]	ΔP <sub>dp,bottom</sub> [kPa]	ΔP <sub>dp,top</sub> [kPa]
VSL27	1,12	58	6,05	26,0%	8,9%	1,03	1,087	1,085	Yes	9,5	0,276	0,190

Upwards discharge  
Elevation = 1 cm  
SG<sub>p</sub> = 1.03

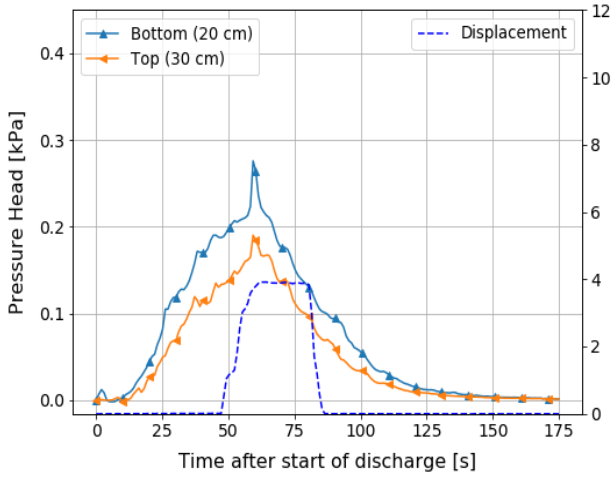
Concentration over time at different levels



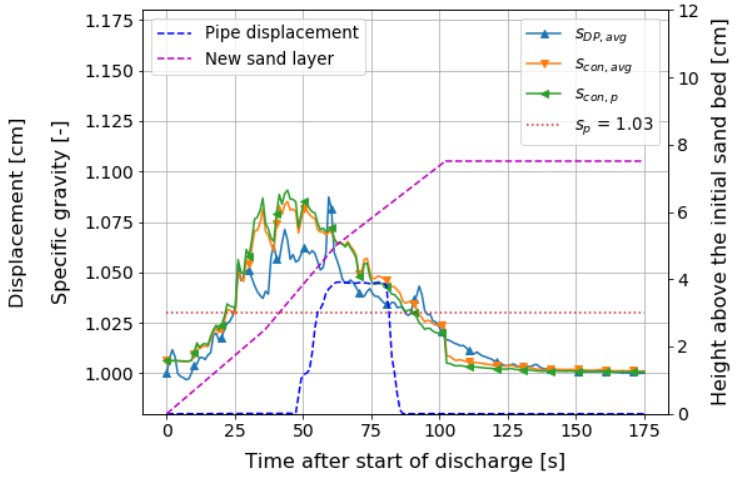
Increasing concentration along height over time



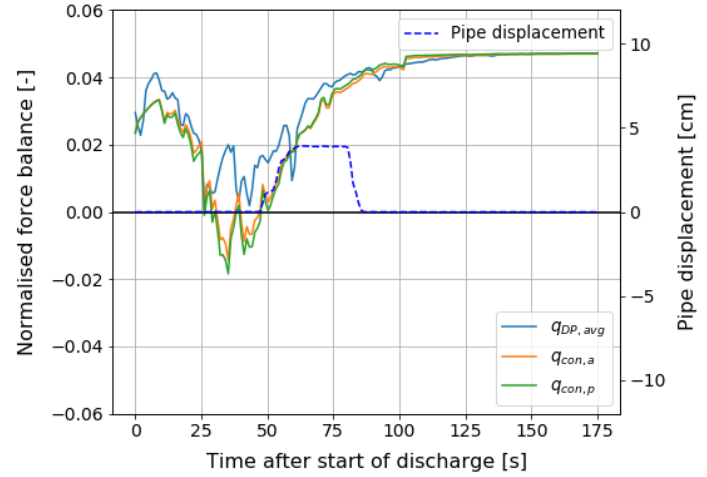
DP net increment at height of the pipe



Specific gravity of the mixture around the pipe (3)



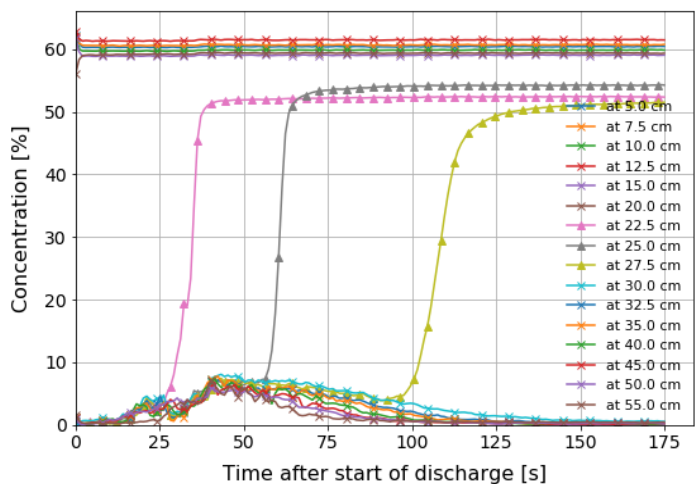
Flotation threshold



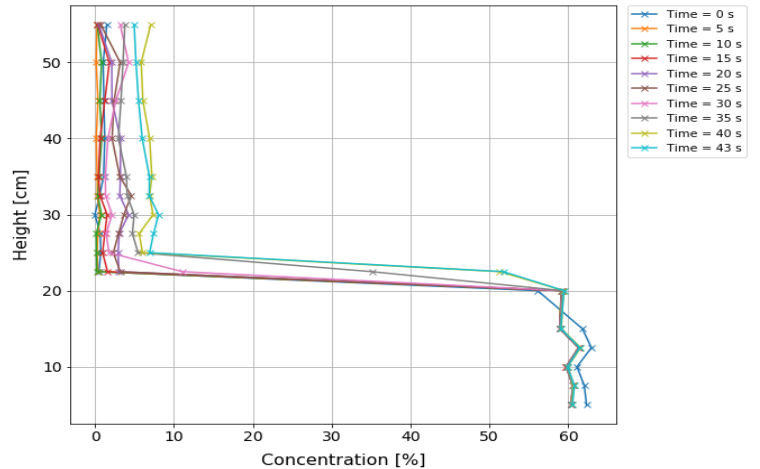
Test	Qcal [L/s]	t <sub>dis</sub> [s]	Δh [cm]	c <sub>dis</sub> [%]	c <sub>max</sub> [%]	S <sub>pipe</sub>	S <sub>dp</sub>	S <sub>con,a</sub>	Flotation	dis,max [cm]	ΔP <sub>dp,bottom</sub> [kPa]	ΔP <sub>dp,top</sub> [kPa]
VSL28	1,38	40	4,68	24,0%	8,1%	1,03	1,079	1,077	Semi	4,4	0,323	0,262

Upwards discharge  
Elevation = 1 cm  
SG<sub>p</sub> = 1.03

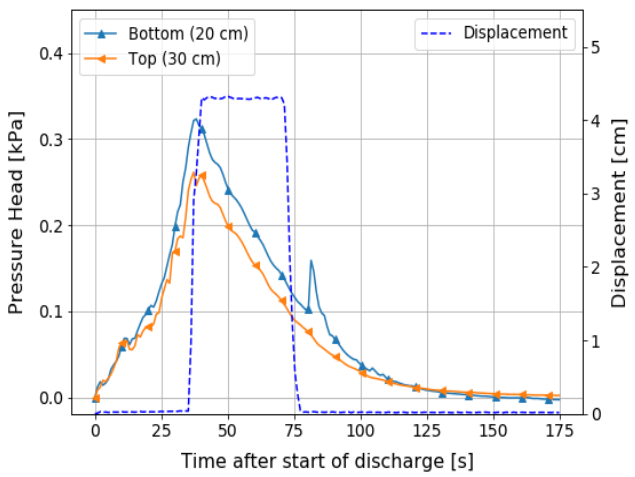
Concentration over time at different levels



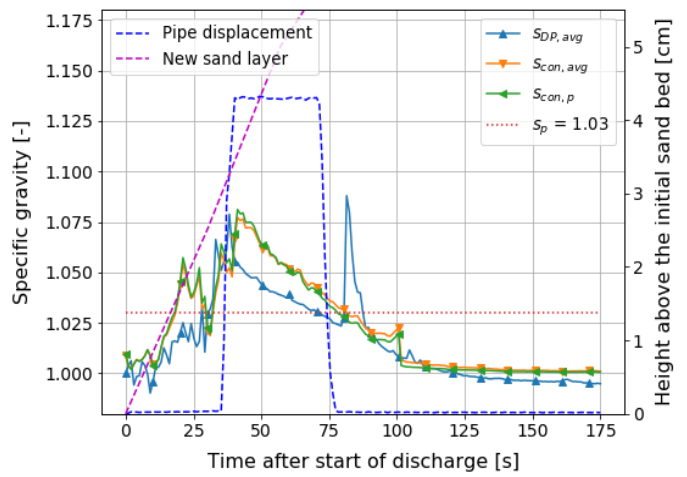
Increasing concentration along height over time



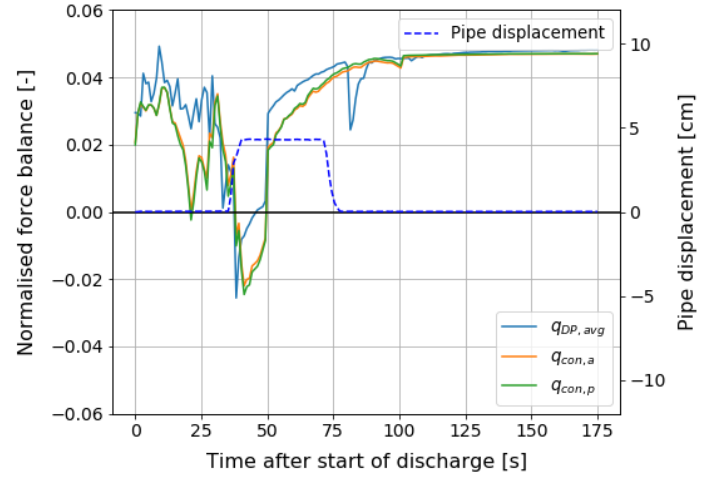
DP net increment at height of the pipe



Specific gravity of the mixture around the pipe (3)



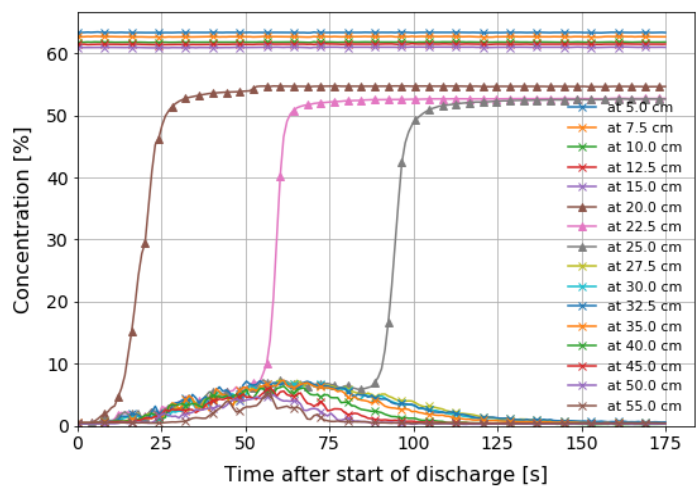
Flotation threshold



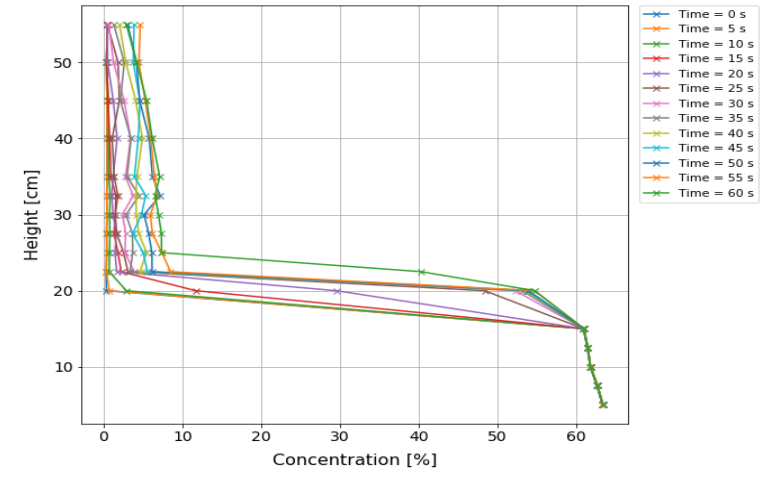
Test	Qcal [L/s]	t <sub>dis</sub> [s]	Δh [cm]	c <sub>dis</sub> [%]	c <sub>max</sub> [%]	S <sub>pipe</sub>	S <sub>dp</sub>	S <sub>con,a</sub>	Flotation	dis,max [cm]	ΔP <sub>dp,bottom</sub> [kPa]	ΔP <sub>dp,top</sub> [kPa]
VML29	1,16	55	5,50	24,4%	7,4%	1,03	1,084	1,086	Semi	2,5	0,270	0,203

Upwards discharge  
Elevation = 2 cm  
SG<sub>p</sub> = 1.03

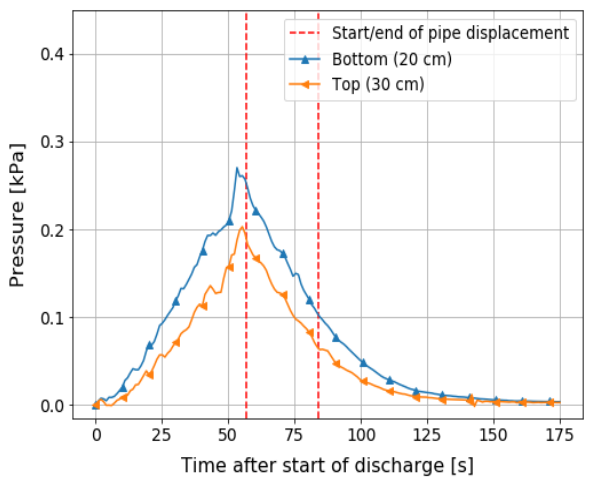
Concentration over time at different levels



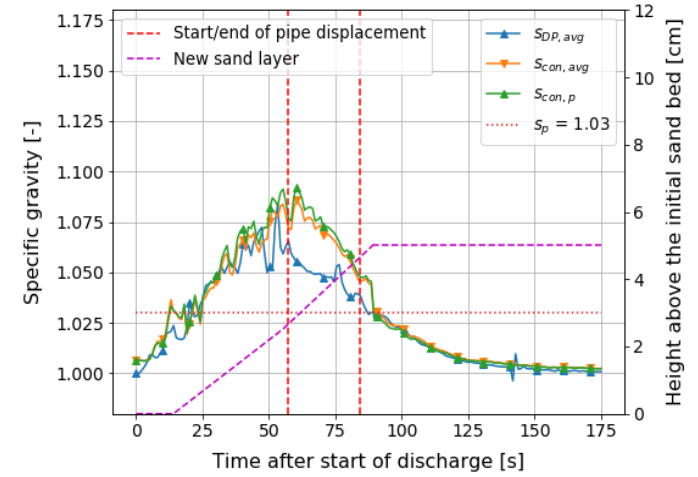
Increasing concentration along height over time



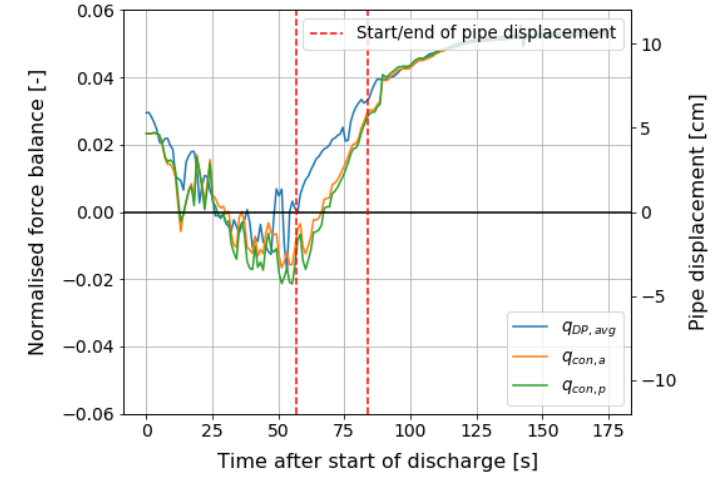
DP net increment at height of the pipe



Specific gravity of the mixture around the pipe



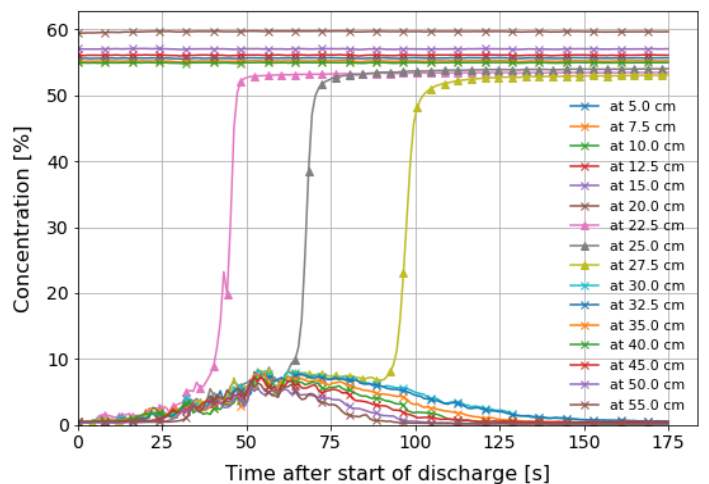
Flotation threshold



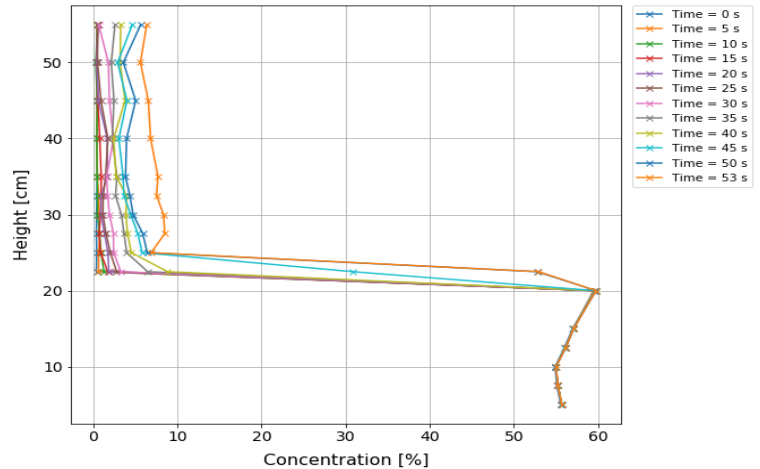
Test	Qcal [L/s]	t <sub>dis</sub> [s]	Δh [cm]	c <sub>dis</sub> [%]	c <sub>max</sub> [%]	S <sub>pipe</sub>	S <sub>dp</sub>	S <sub>con,a</sub>	Flotation	dis,max [cm]	ΔP <sub>dp,bottom</sub> [kPa]	ΔP <sub>dp,top</sub> [kPa]
VML30	1,62	49	7,68	27,5%	8,6%	1,03	1,101	1,079	Yes	10,0	0,444	0,346

Upwards discharge  
Elevation = 2 cm  
SG<sub>p</sub> = 1.03

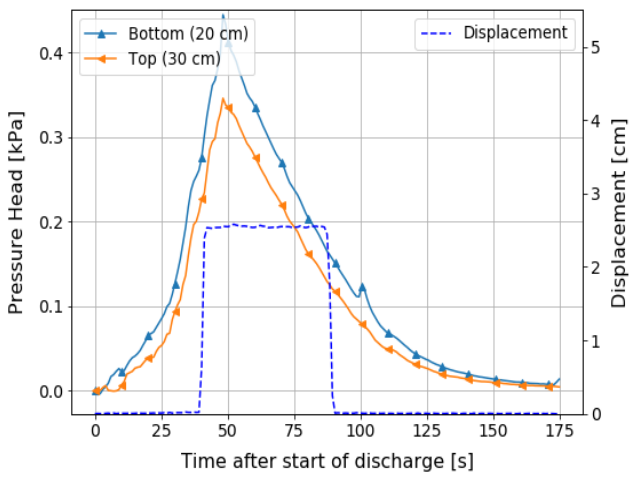
Concentration over time at different levels



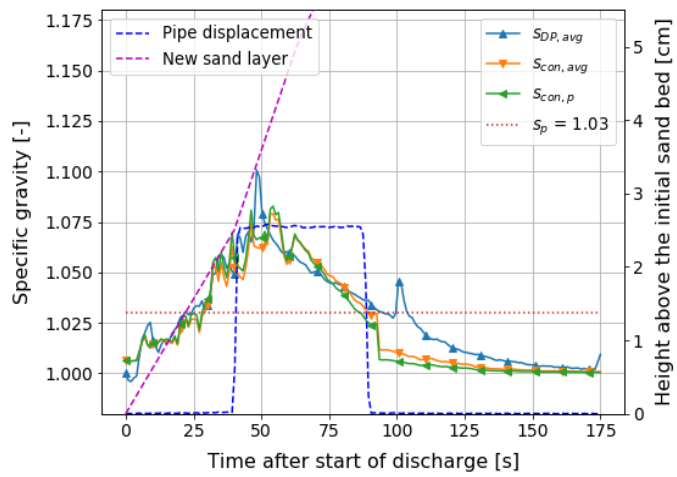
Increasing concentration along height over time



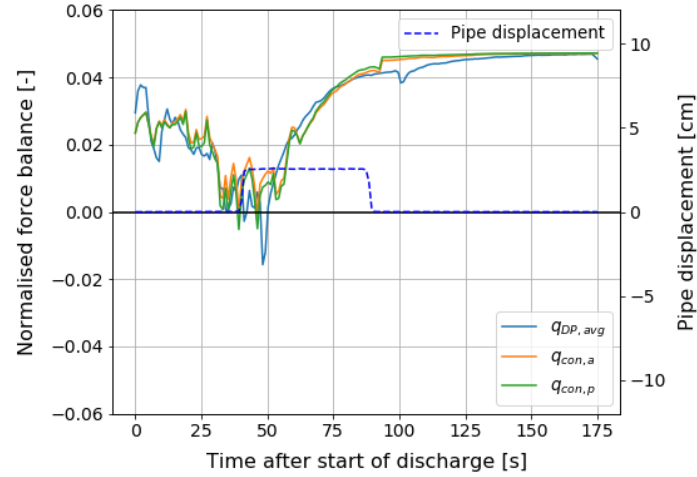
DP net increment at height of the pipe



Specific gravity of the mixture around the pipe (3)



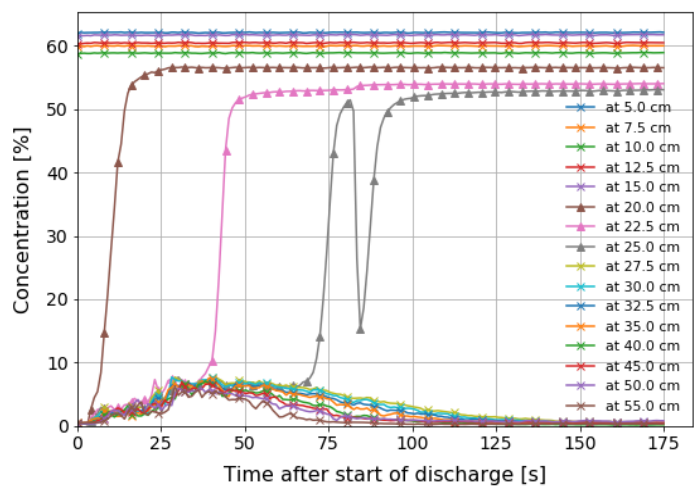
Flotation threshold



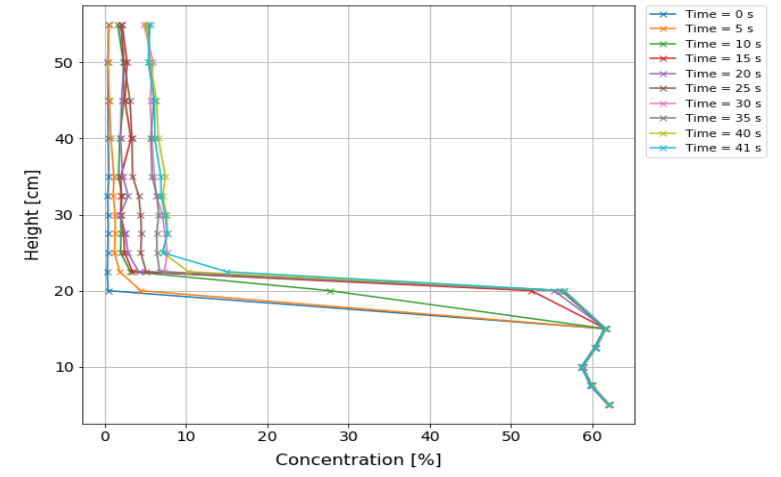
Test	Qcal [L/s]	t <sub>dis</sub> [s]	Δh [cm]	c <sub>dis</sub> [%]	c <sub>max</sub> [%]	S <sub>pipe</sub>	S <sub>dp</sub>	S <sub>con,a</sub>	Flotation	dis,max [cm]	ΔP <sub>dp,bottom</sub> [kPa]	ΔP <sub>dp,top</sub> [kPa]
VML31	2,16	29	5,78	25,9%	7,7%	1,03	1,087	1,100	Yes	10,0	0,368	0,284

Upwards discharge  
Elevation = 2 cm  
SG<sub>p</sub> = 1.03

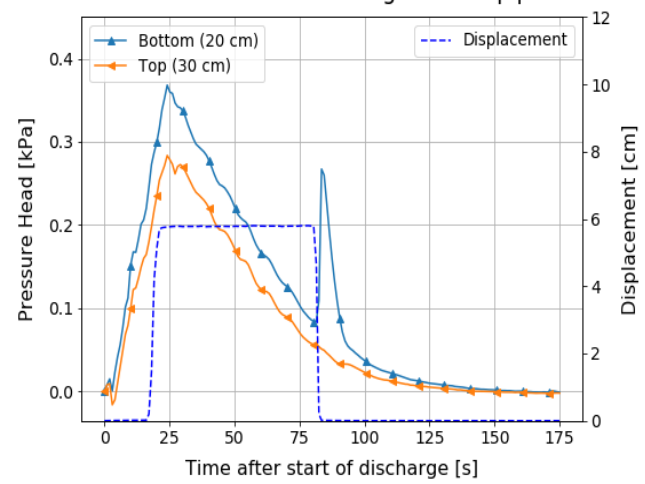
Concentration over time at different levels



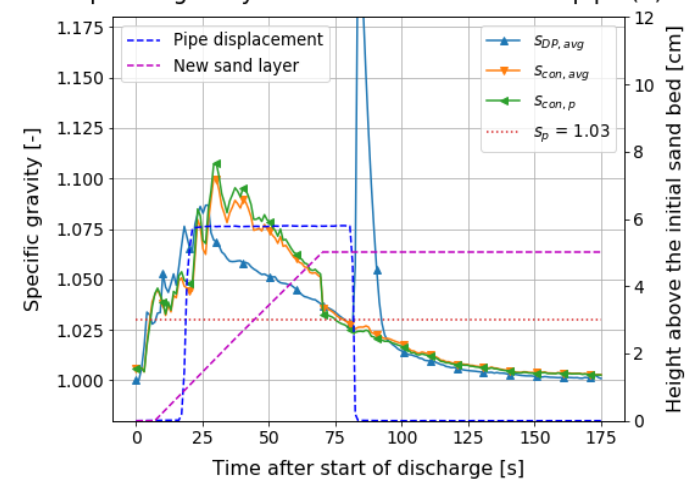
Increasing concentration along height over time



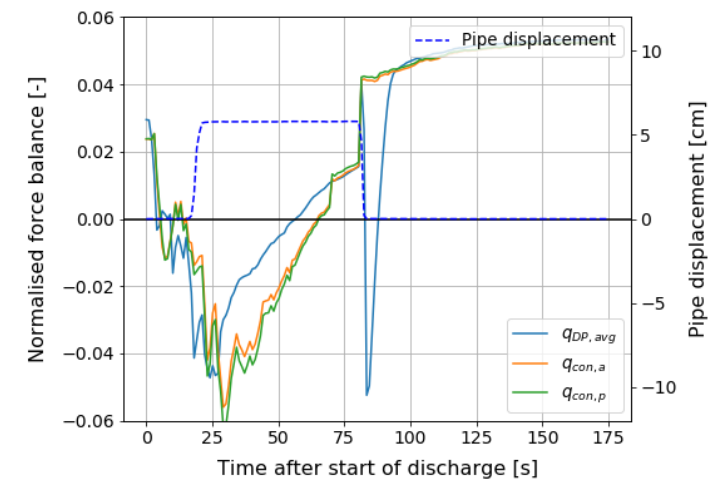
DP net increment at height of the pipe



Specific gravity of the mixture around the pipe (3)



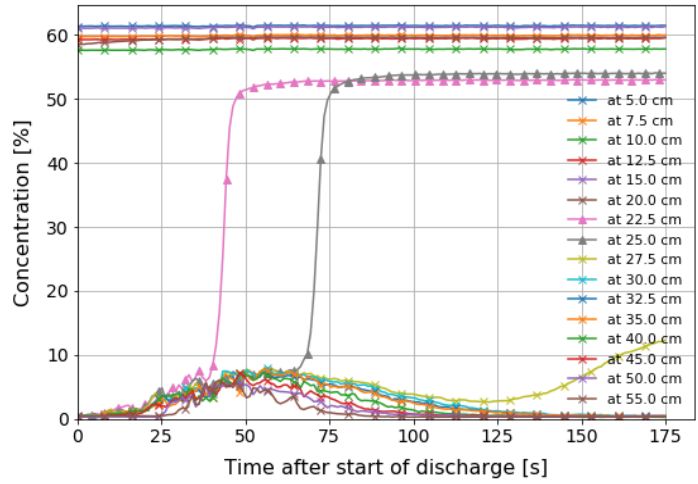
Flotation threshold



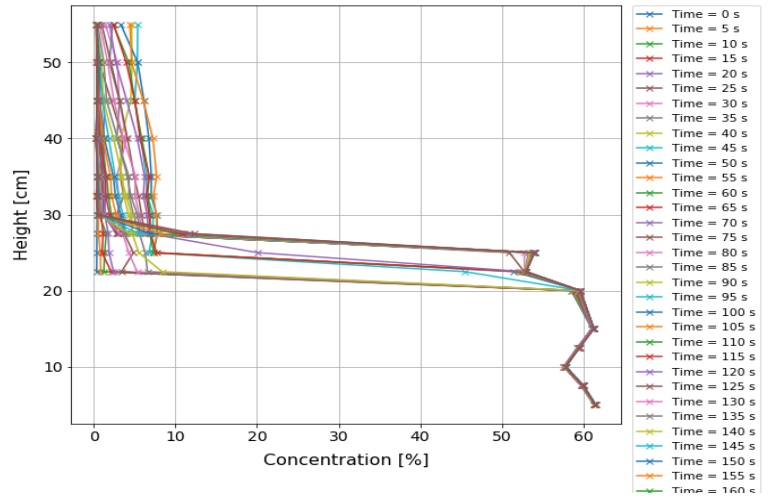
Test	Qcal [L/s]	t <sub>dis</sub> [s]	Δh [cm]	c <sub>dis</sub> [%]	c <sub>max</sub> [%]	S <sub>pipe</sub>	S <sub>dp</sub>	S <sub>con,a</sub>	Flotation	dis,max [cm]	ΔP <sub>dp,bottom</sub> [kPa]	ΔP <sub>dp,top</sub> [kPa]
VML32	1,46	43	5,95	26,8%	8,0%	1,03	1,081	1,082	Yes	10,0	0,345	0,266

Upwards discharge  
Elevation = 2 cm  
SG<sub>p</sub> = 1.03

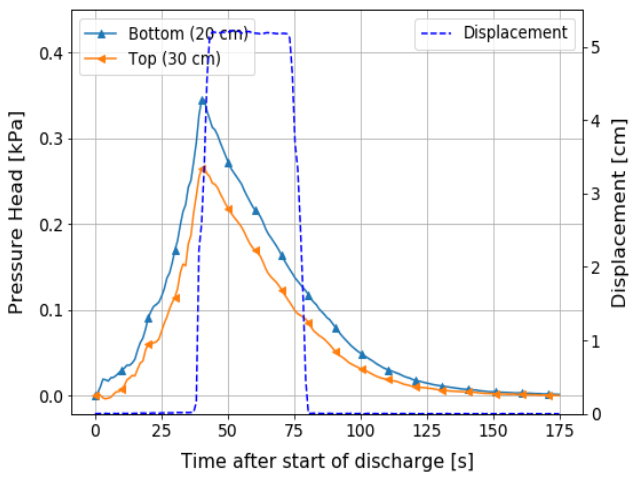
Concentration over time at different levels



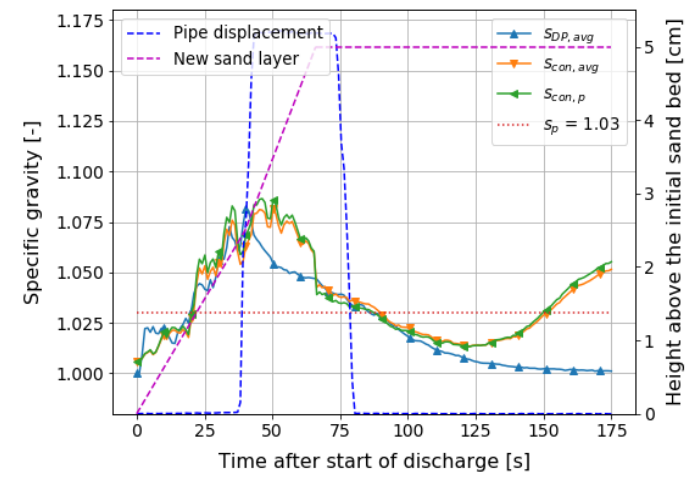
Increasing concentration along height over time



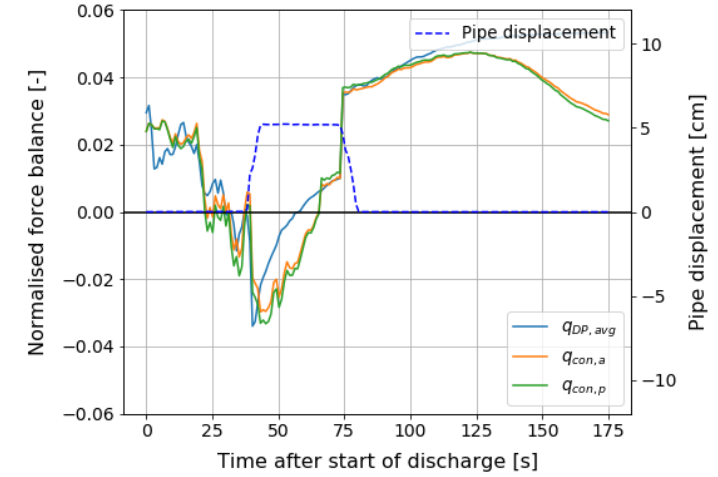
DP net increment at height of the pipe



Specific gravity of the mixture around the pipe (3)



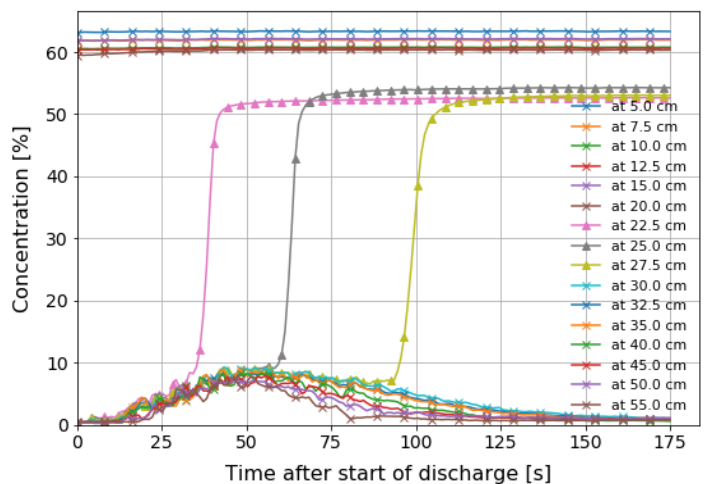
Flotation threshold



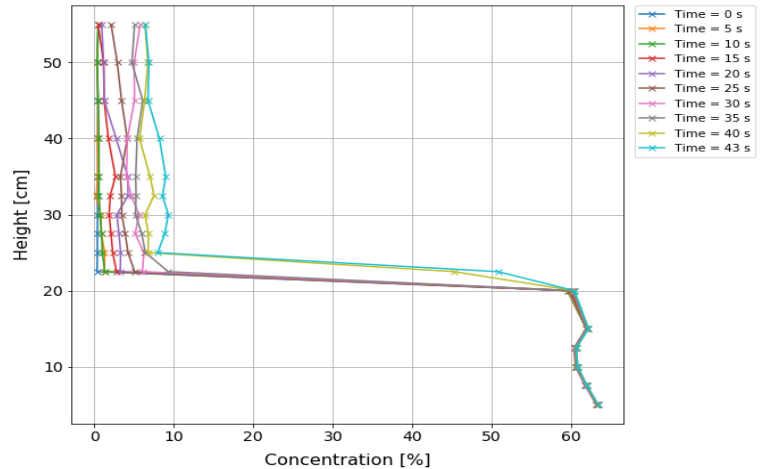
Test	Qcal [L/s]	t <sub>dis</sub> [s]	Δh [cm]	c <sub>dis</sub> [%]	c <sub>max</sub> [%]	Sp <sub>ipe</sub>	S <sub>dp</sub>	S <sub>con,a</sub>	Flotation	dis,max [cm]	ΔP <sub>dp,bottom</sub> [kPa]	ΔP <sub>dp,top</sub> [kPa]
VML33	1,90	38	6,95	27,0%	9,3%	1,03	1,107	1,093	Yes	8,3	0,409	0,304

Upwards discharge  
Elevation = 2 cm  
SG<sub>p</sub> = 1.03

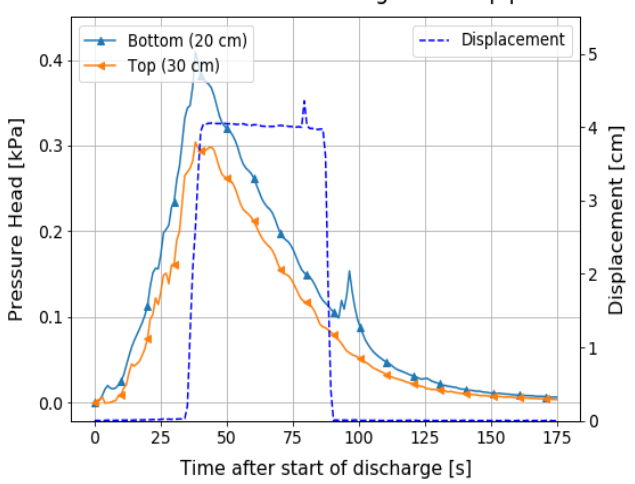
Concentration over time at different levels



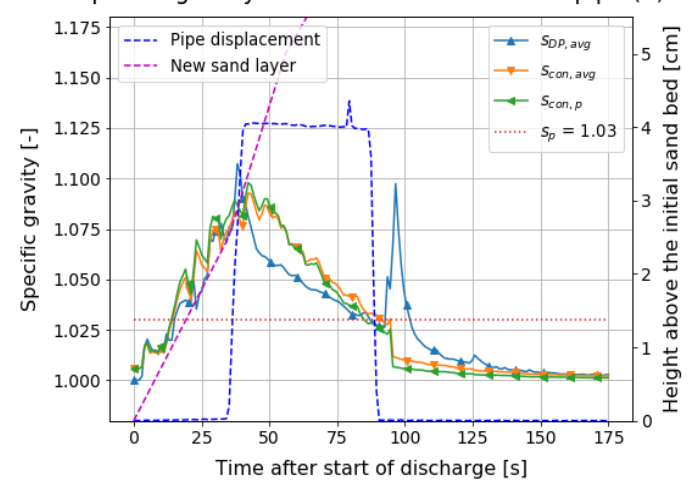
Increasing concentration along height over time



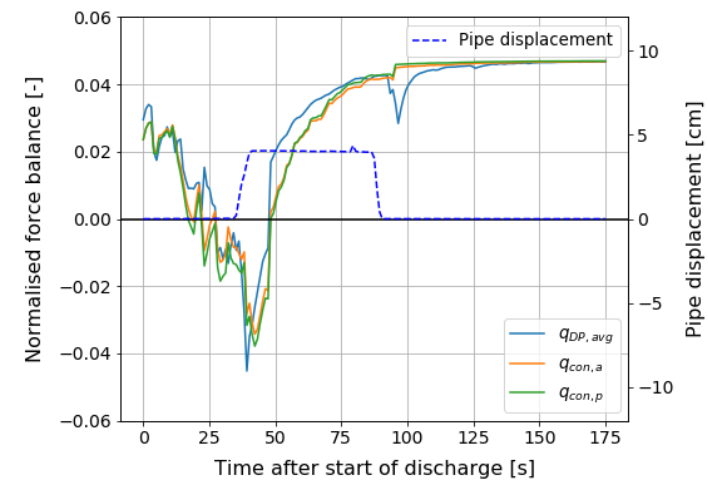
DP net increment at height of the pipe



Specific gravity of the mixture around the pipe (3)



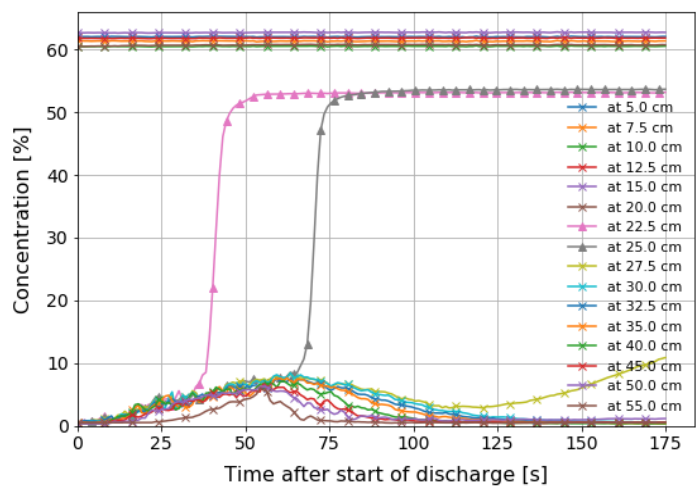
Flotation threshold



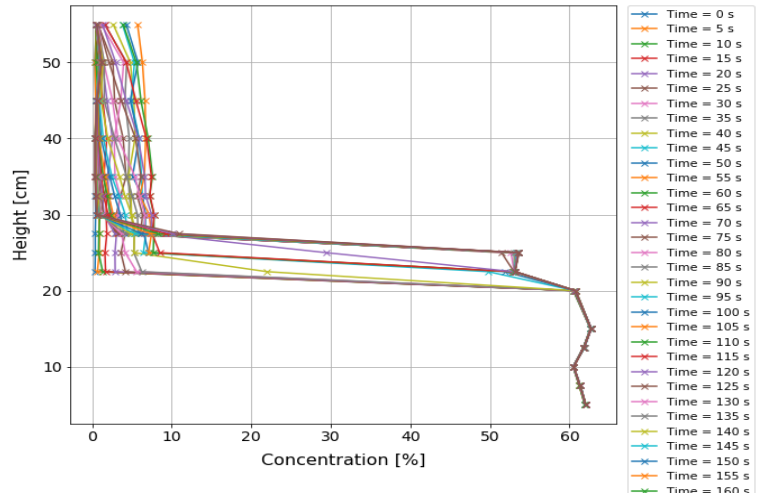
Test	Qcal [L/s]	t <sub>dis</sub> [s]	Δh [cm]	c <sub>dis</sub> [%]	c <sub>max</sub> [%]	S <sub>pipe</sub>	S <sub>dp</sub>	S <sub>con,a</sub>	Flotation	dis,max [cm]	ΔP <sub>dp,bottom</sub> [kPa]	ΔP <sub>dp,top</sub> [kPa]
VML34	1,27	53	6,03	25,4%	8,4%	1,03	1,077	1,075	Semi	1,7	0,275	0,208

Upwards discharge  
Elevation = 2 cm  
SG<sub>p</sub> = 1.03

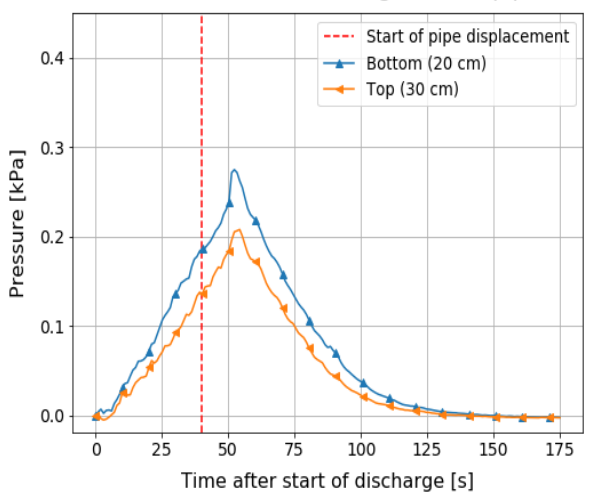
Concentration over time at different levels



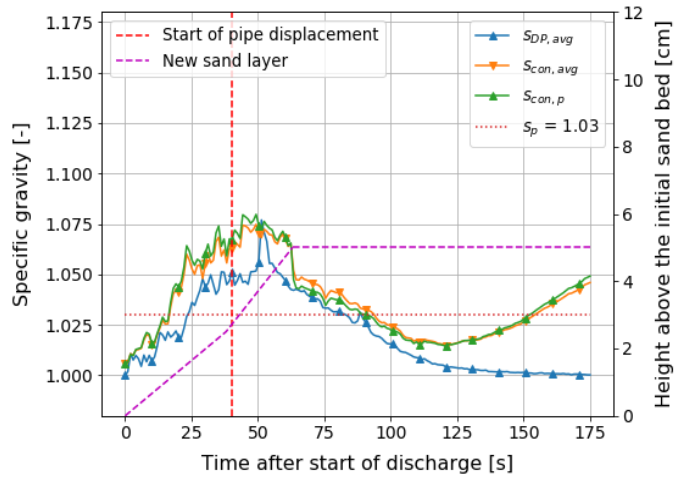
Increasing concentration along height over time



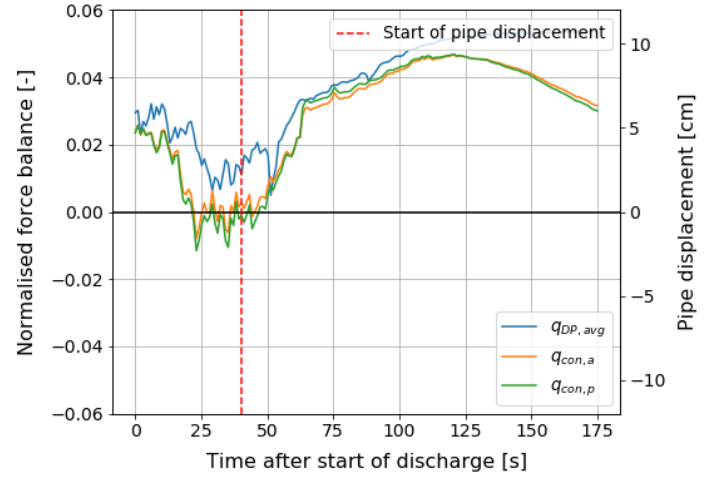
DP net increment at height of the pipe



Specific gravity of the mixture around the pipe



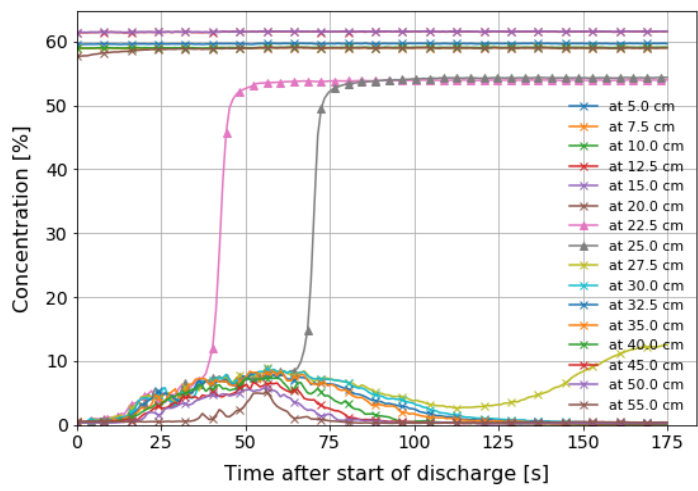
Flotation threshold



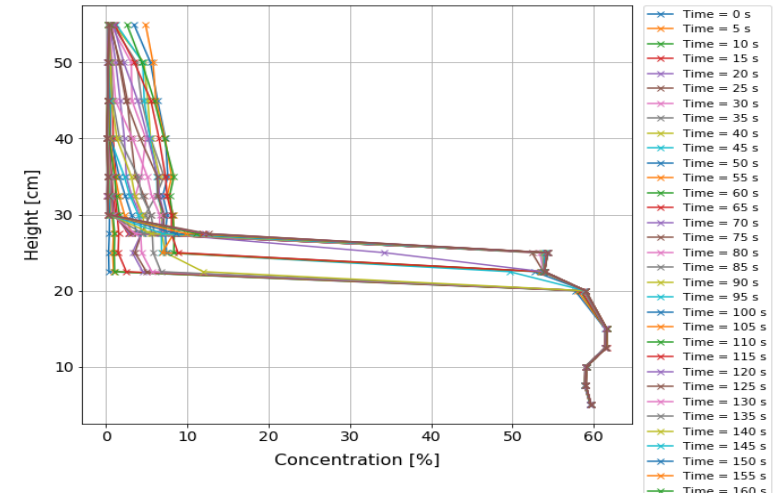
Test	Qcal [L/s]	t <sub>dis</sub> [s]	Δh [cm]	c <sub>dis</sub> [%]	c <sub>max</sub> [%]	S <sub>pipe</sub>	S <sub>dp</sub>	S <sub>con,a</sub>	Flotation	dis,max [cm]	ΔP <sub>dp,bottom</sub> [kPa]	ΔP <sub>dp,top</sub> [kPa]
VVL35	1,24	53	6,08	26,1%	9,1%	1,03	1,081	1,089	Yes	8,3	0,284	0,204

Upwards discharge  
Elevation = 4 cm  
SG<sub>p</sub> = 1.03

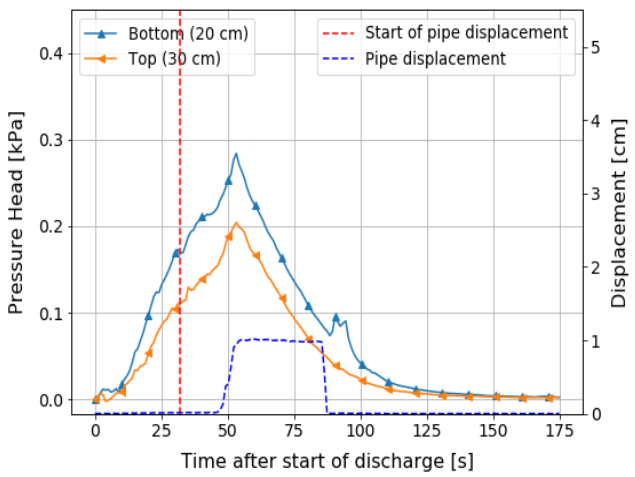
Concentration over time at different levels



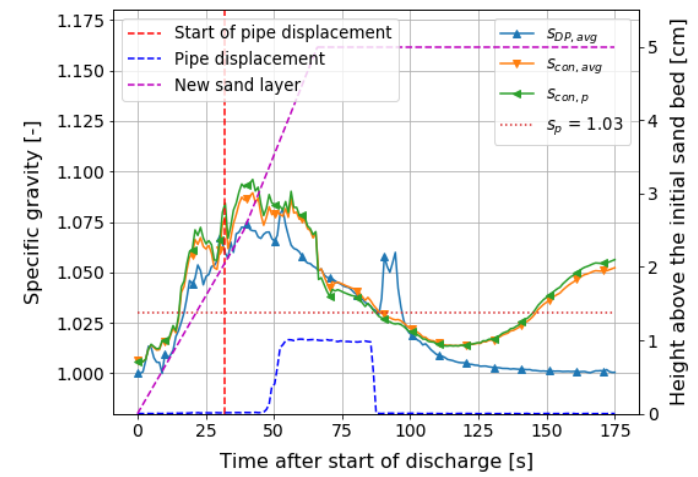
Increasing concentration along height over time



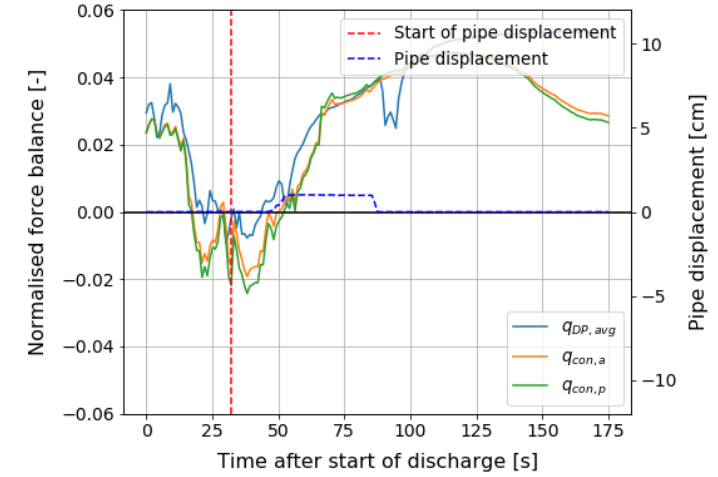
DP net increment at height of the pipe



Specific gravity of the mixture around the pipe (3)



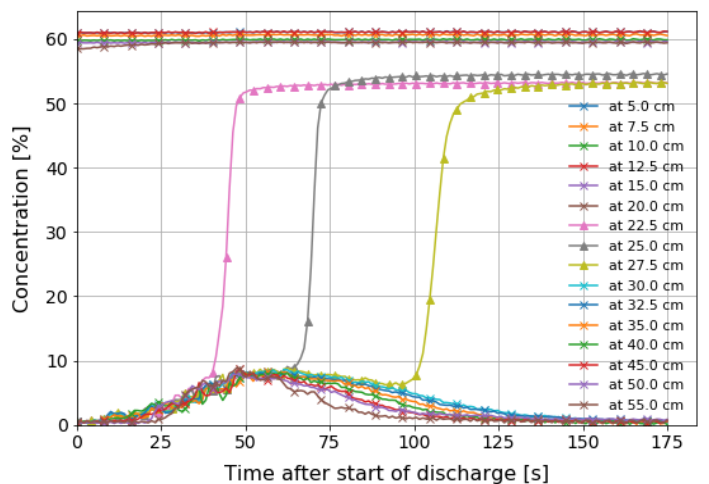
Flotation threshold



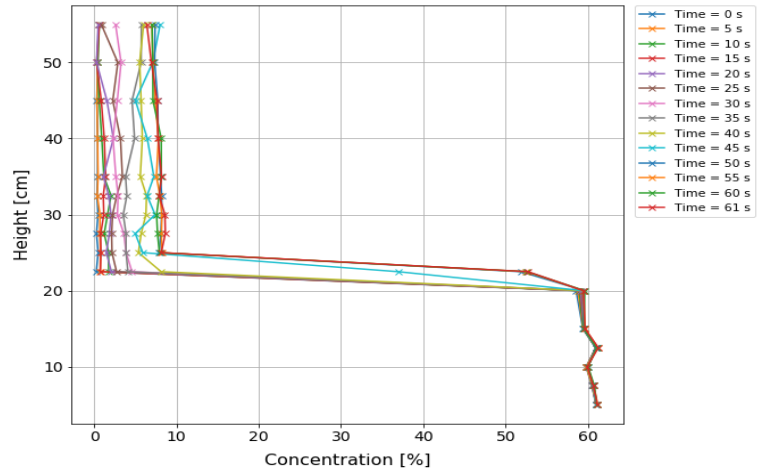
Test	Qcal [L/s]	t <sub>dis</sub> [s]	Δh [cm]	c <sub>dis</sub> [%]	c <sub>max</sub> [%]	S <sub>pipe</sub>	S <sub>dp</sub>	S <sub>con,a</sub>	Flotation	dis,max [cm]	ΔP <sub>dp,bottom</sub> [kPa]	ΔP <sub>dp,top</sub> [kPa]
VVL36	1,64	43	6,68	26,5%	8,8%	1,03	?	1,091	Yes	8,3	?	0,314

Upwards discharge  
Elevation = 4 cm  
SG<sub>p</sub> = 1.03

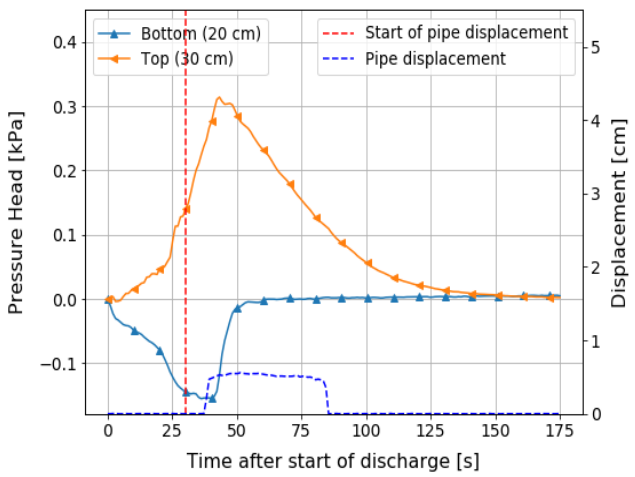
Concentration over time at different levels



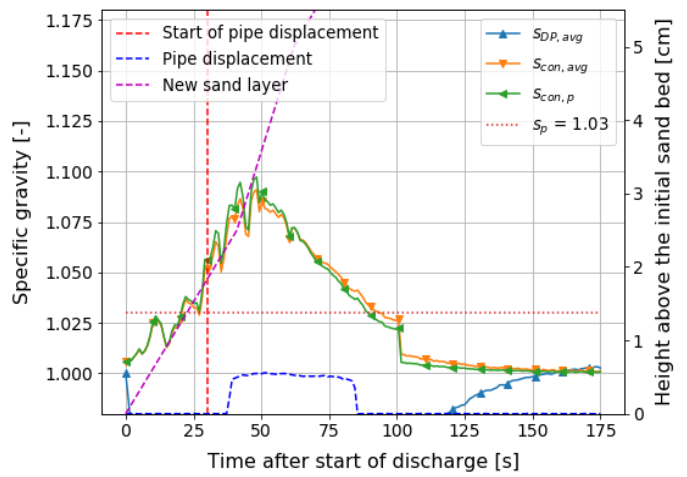
Increasing concentration along height over time



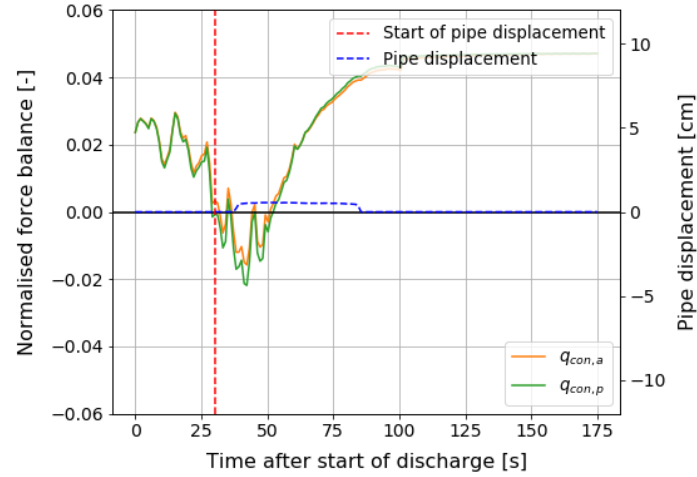
DP net increment at height of the pipe



Specific gravity of the mixture around the pipe (3)

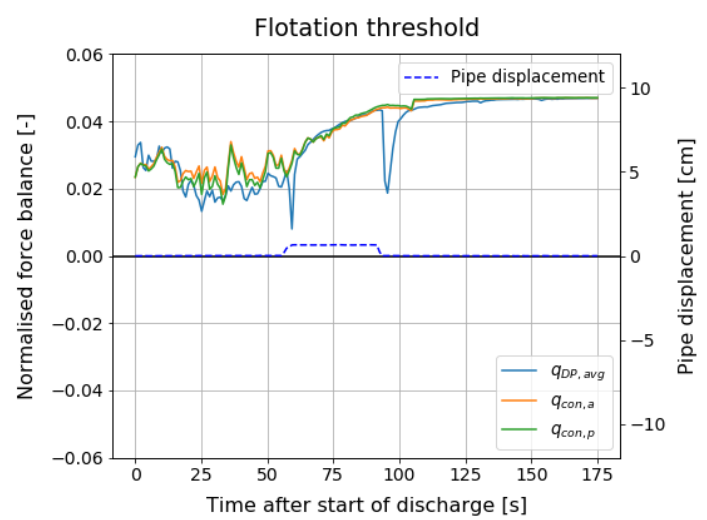
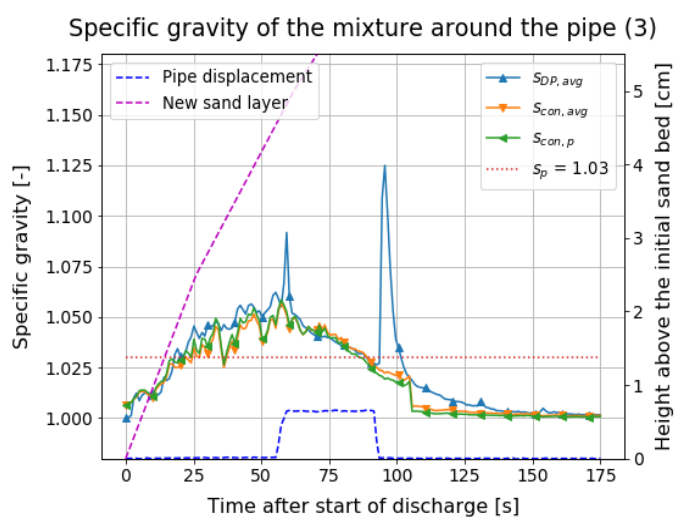
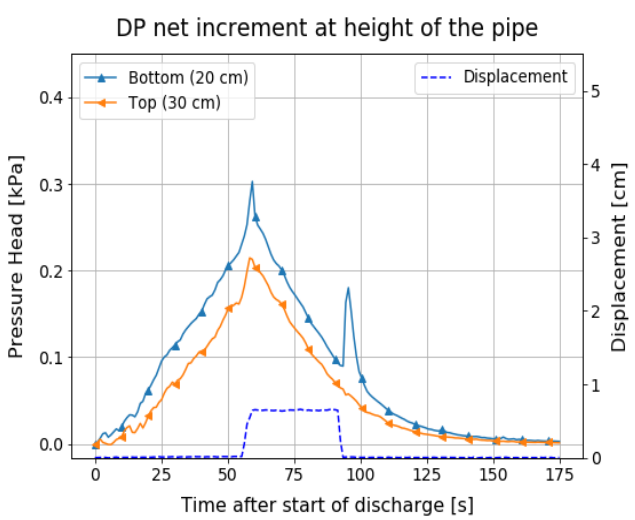
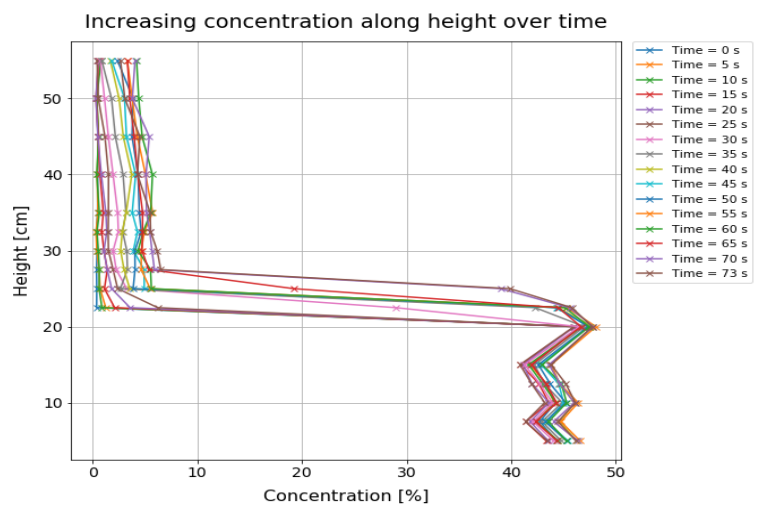
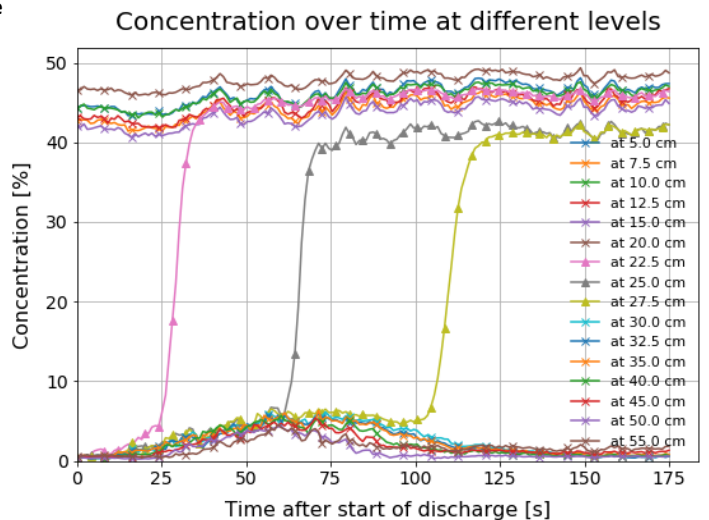


Flotation threshold



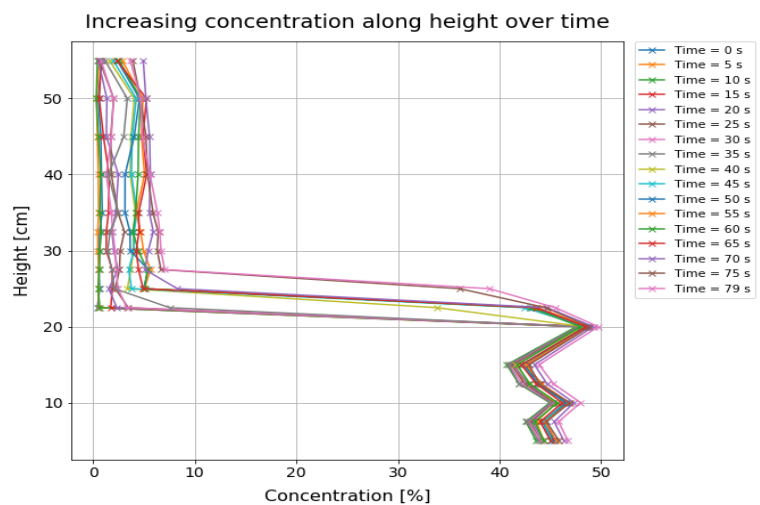
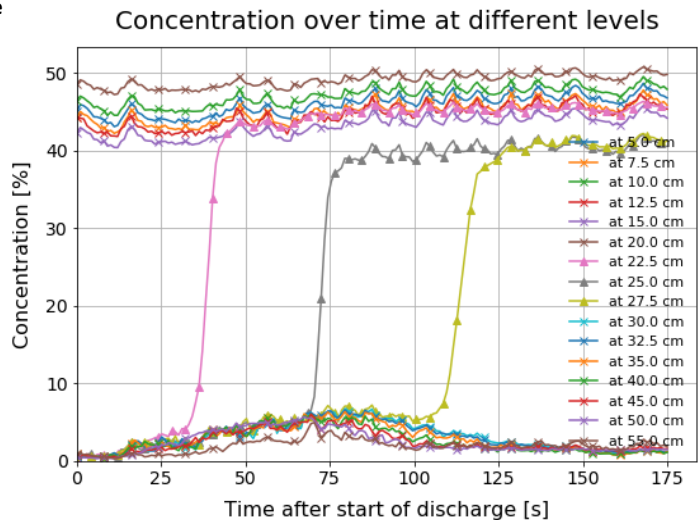
Test	Qcal [L/s]	t <sub>dis</sub> [s]	Δh [cm]	c <sub>dis</sub> [%]	c <sub>max</sub> [%]	S <sub>pipe</sub>	S <sub>dp</sub>	S <sub>con,a</sub>	Flotation	dis,max [cm]	ΔP <sub>dp,bottom</sub> [kPa]	ΔP <sub>dp,top</sub> [kPa]
VVL37	1,22	58	6,13	24,6%	6,7%	1,03	1,092	1,057	Yes	8,3	0,303	0,215

Upwards discharge  
Elevation = 4 cm  
SG<sub>p</sub> = 1.03

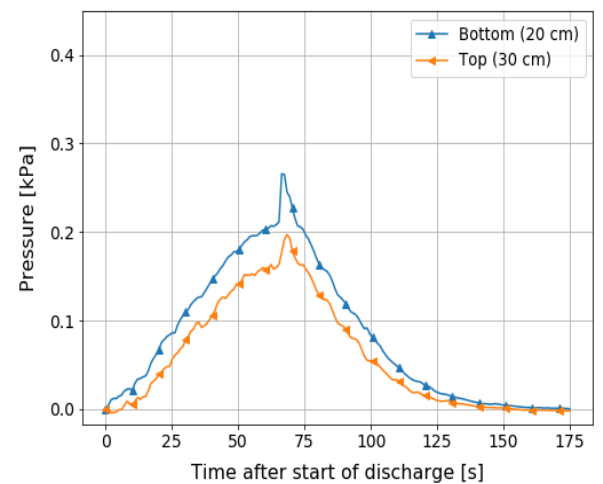


Test	Qcal [L/s]	t <sub>dis</sub> [s]	Δh [cm]	c <sub>dis</sub> [%]	c <sub>max</sub> [%]	S <sub>pipe</sub>	S <sub>dp</sub>	S <sub>con,a</sub>	Flotation	dis,max [cm]	ΔP <sub>dp,bottom</sub> [kPa]	ΔP <sub>dp,top</sub> [kPa]
VVL38	1,22	66	6,40	22,3%	7,2%	1,03	1,091	1,055	Yes	6,6	0,266	0,197

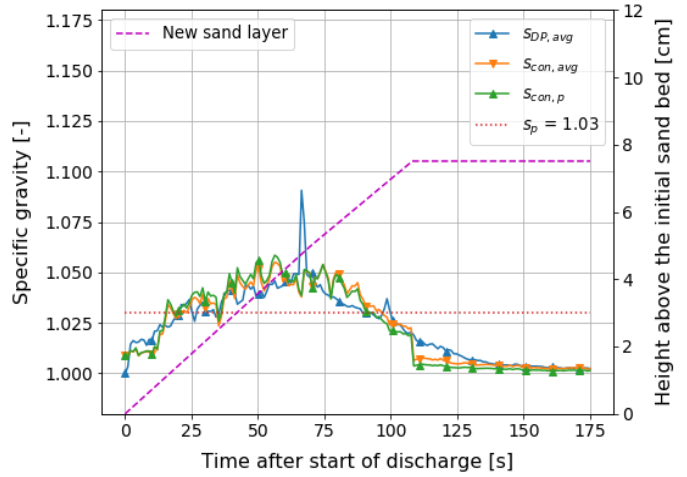
Upwards discharge  
Elevation = 4 cm  
SG<sub>p</sub> = 1.03



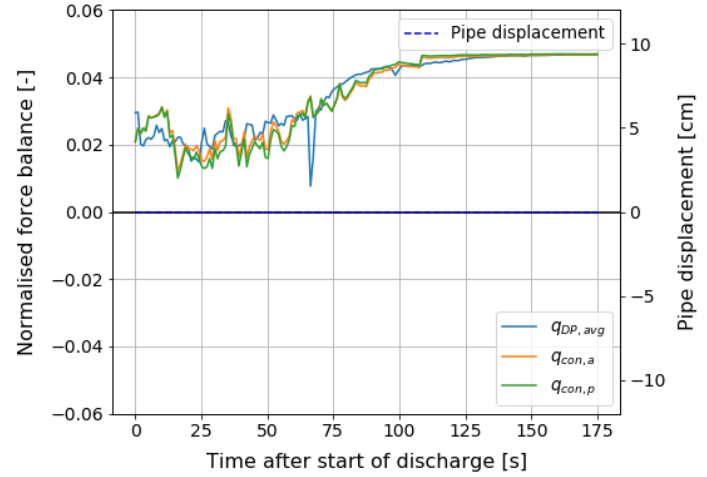
DP net increment at height of the pipe



Specific gravity of the mixture around the pipe



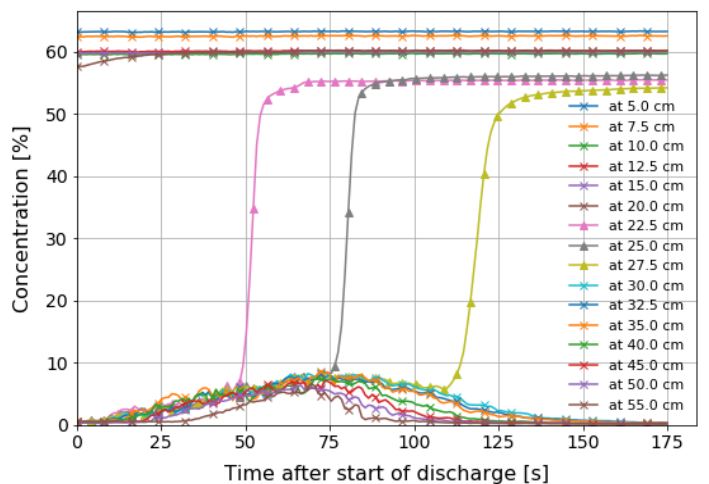
Flotation threshold



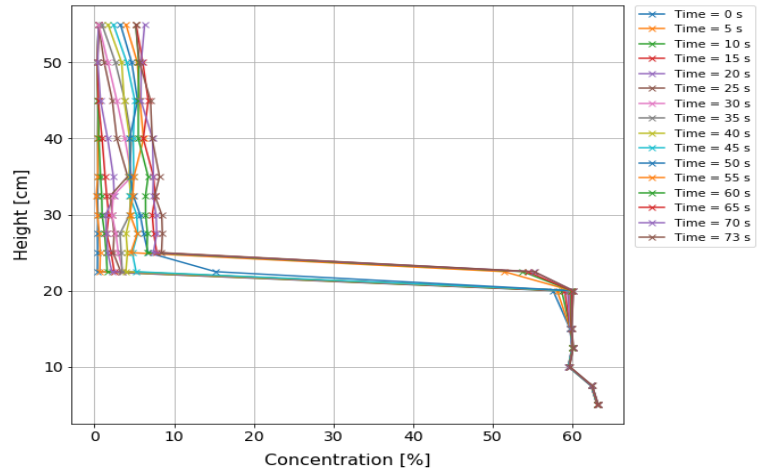
Test	Qcal [L/s]	t <sub>dis</sub> [s]	Δh [cm]	c <sub>dis</sub> [%]	c <sub>max</sub> [%]	S <sub>pipe</sub>	S <sub>dp</sub>	S <sub>con,a</sub>	Flotation	dis,max [cm]	ΔP <sub>dp,bottom</sub> [kPa]	ΔP <sub>dp,top</sub> [kPa]
VVL39	1,25	67	7,28	24,7%	8,7%	1,03	1,118	1,078	Yes	7,5	0,347	0,244

Upwards discharge  
Elevation = 4 cm  
SG<sub>p</sub> = 1.03

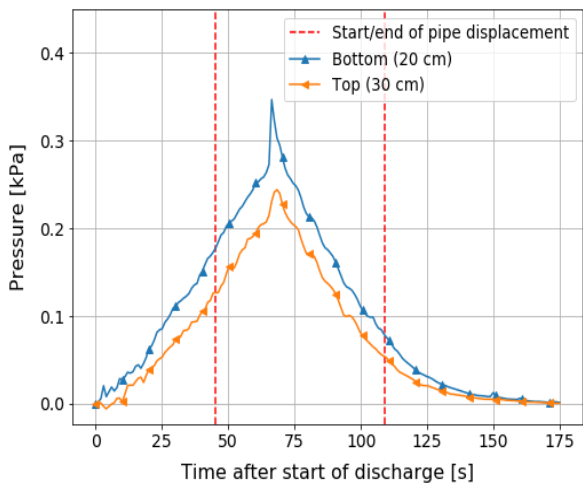
Concentration over time at different levels



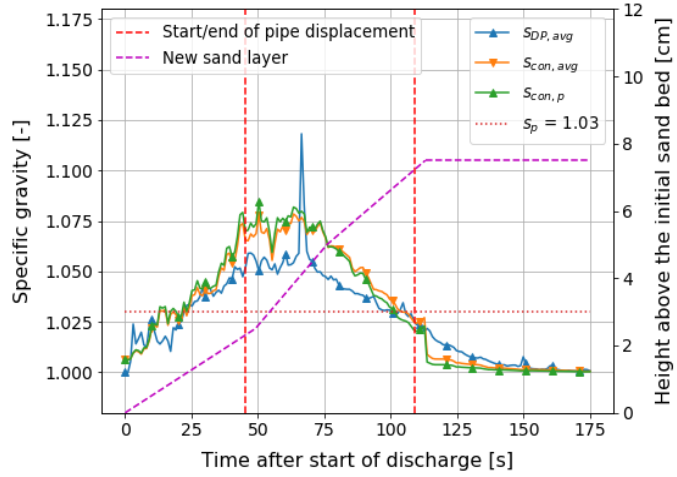
Increasing concentration along height over time



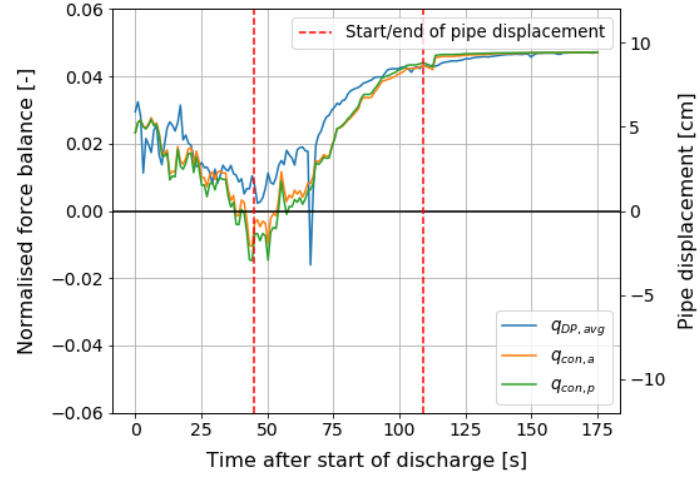
DP net increment at height of the pipe



Specific gravity of the mixture around the pipe



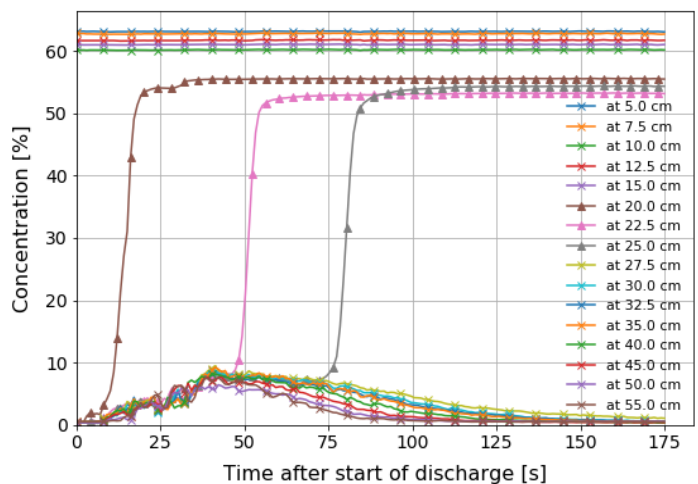
Flotation threshold



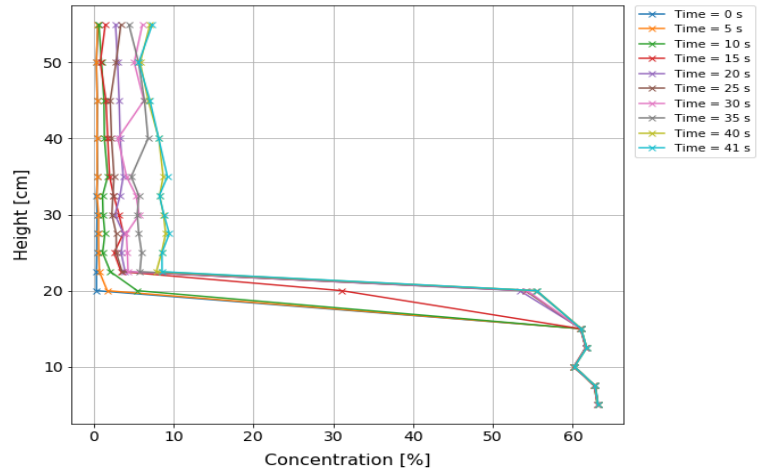
Test	Qcal [L/s]	t <sub>dis</sub> [s]	Δh [cm]	c <sub>dis</sub> [%]	c <sub>max</sub> [%]	S <sub>pipe</sub>	S <sub>dp</sub>	S <sub>con,a</sub>	Flotation	dis,max [cm]	ΔP <sub>dp,bottom</sub> [kPa]	ΔP <sub>dp,top</sub> [kPa]
VVL40	2,18	34	6,38	24,4%	9,5%	1,03	1,073	1,117	Yes	7,1	0,377	0,310

Upwards discharge  
Elevation = 4 cm  
SG<sub>p</sub> = 1.03

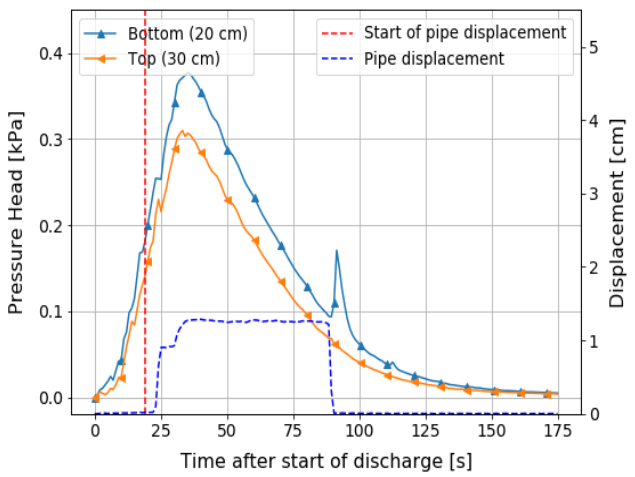
Concentration over time at different levels



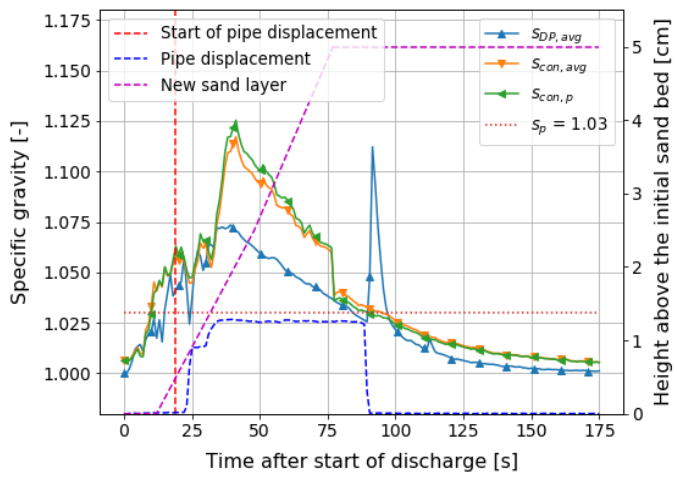
Increasing concentration along height over time



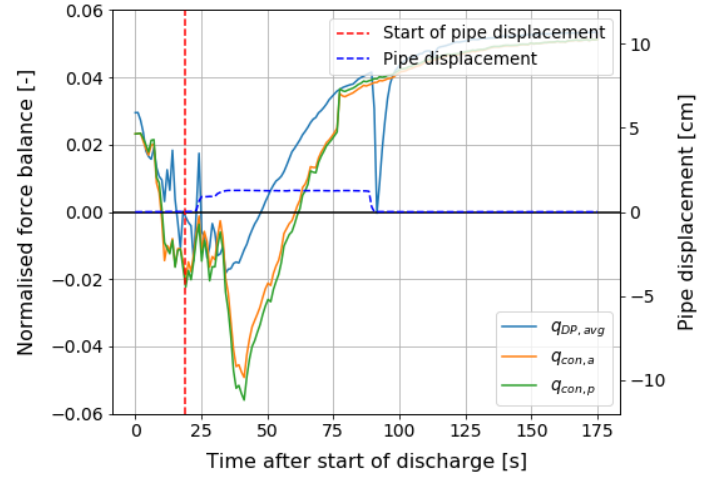
DP net increment at height of the pipe



Specific gravity of the mixture around the pipe (3)



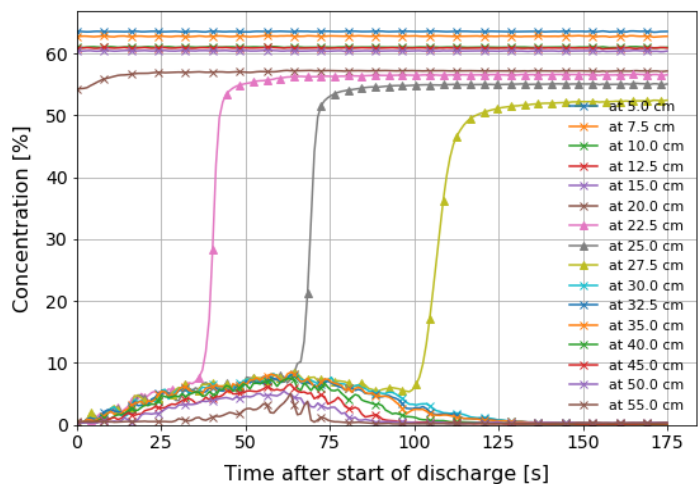
Flotation threshold



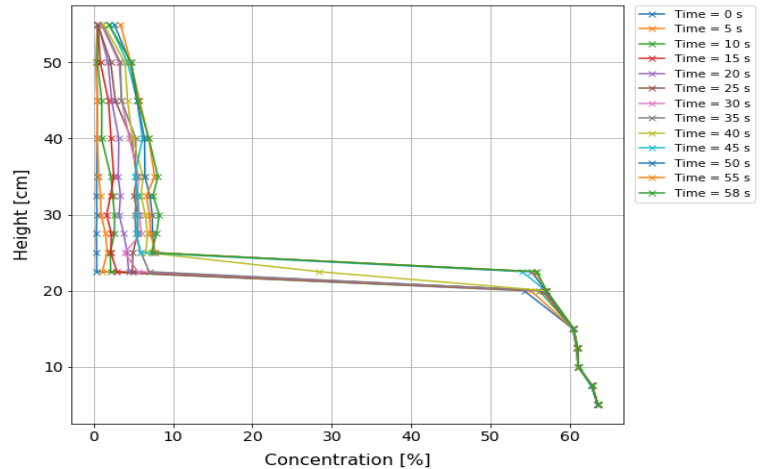
Test	Qcal [L/s]	t <sub>dis</sub> [s]	Δh [cm]	c <sub>dis</sub> [%]	c <sub>max</sub> [%]	S <sub>pipe</sub>	S <sub>dp</sub>	S <sub>con,a</sub>	Flotation	dis,max [cm]	ΔP <sub>dp,bottom</sub> [kPa]	ΔP <sub>dp,top</sub> [kPa]
VVL41	1,34	60	7,10	24,7%	8,5%	1,03	1,095	1,082	Yes	8,3	0,300	0,209

Upwards discharge  
Elevation = 4 cm  
SG<sub>p</sub> = 1.03

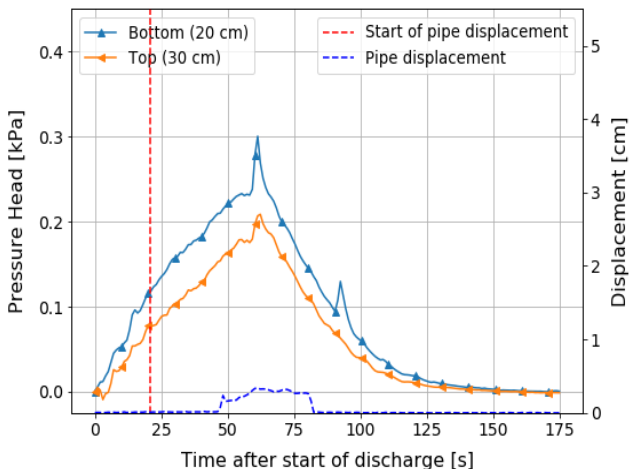
Concentration over time at different levels



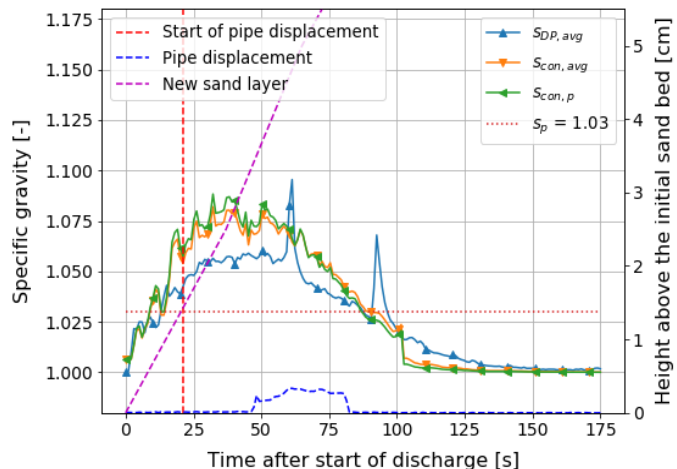
Increasing concentration along height over time



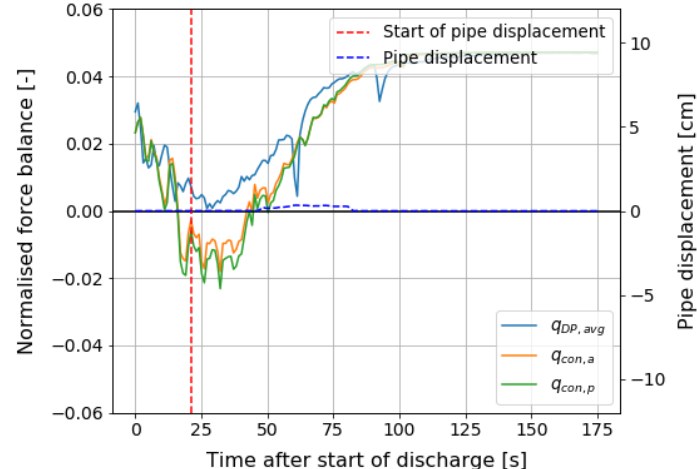
DP net increment at height of the pipe



Specific gravity of the mixture around the pipe (3)



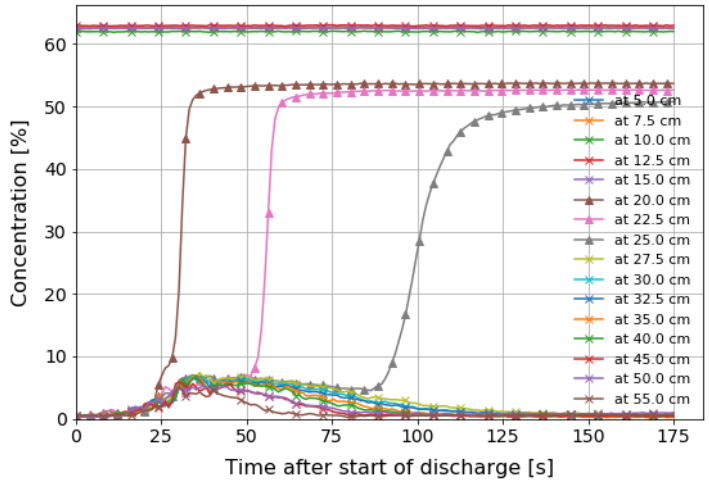
Flotation threshold



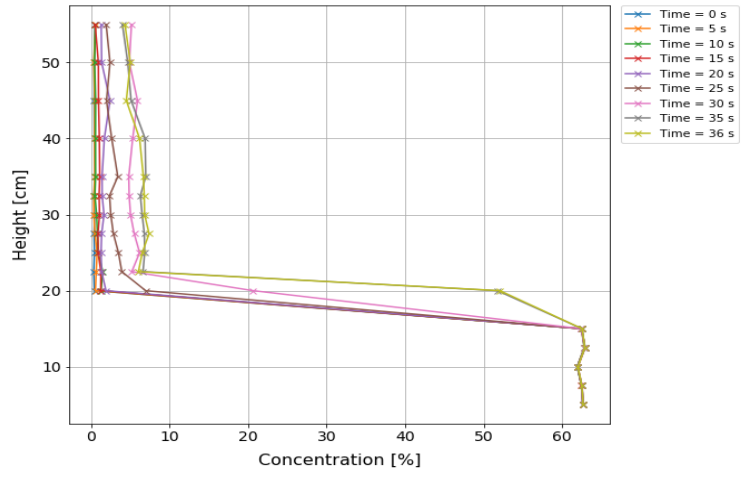
Test	Qcal [L/s]	t <sub>dis</sub> [s]	Δh [cm]	c <sub>dis</sub> [%]	c <sub>max</sub> [%]	S <sub>pipe</sub>	S <sub>dp</sub>	S <sub>con,a</sub>	Flotation	dis,max [cm]	ΔP <sub>dp,bottom</sub> [kPa]	ΔP <sub>dp,top</sub> [kPa]
VNW42	1,77	32	4,68	22,9%	7,4%	1,08	1,072	1,101	No	0	0,273	0,212

Upwards discharge  
No elevation  
SG<sub>p</sub> = 1.08

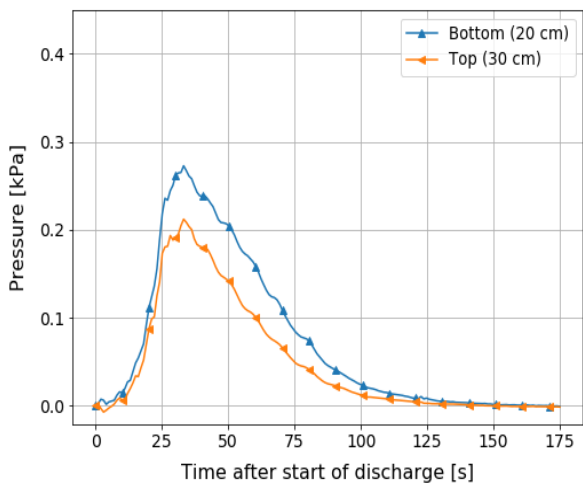
Concentration over time at different levels



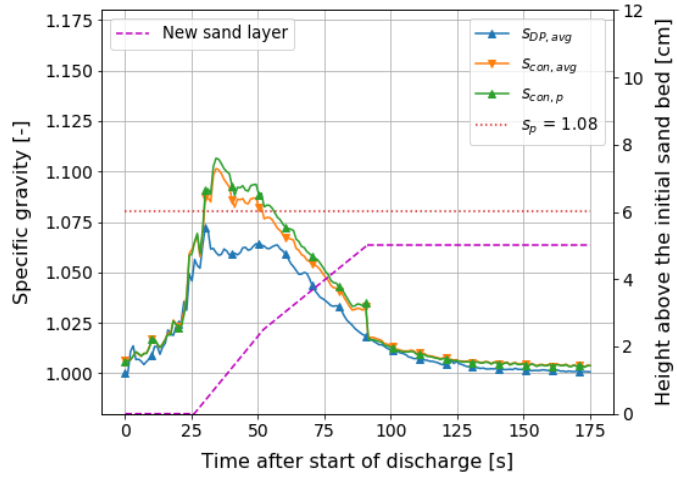
Increasing concentration along height over time



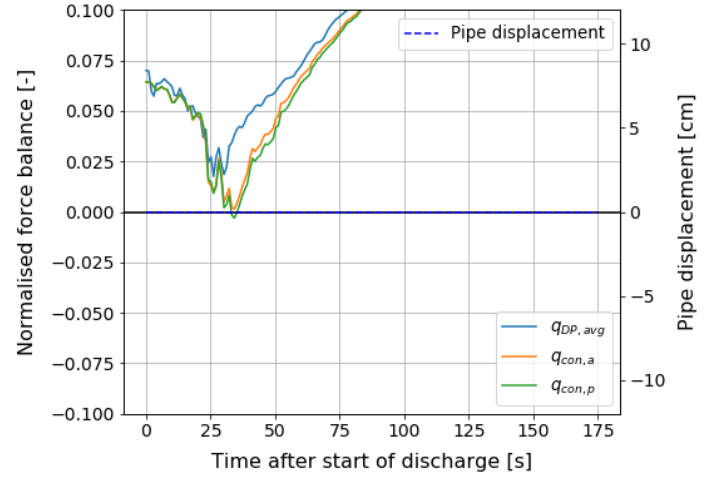
DP net increment at height of the pipe



Specific gravity of the mixture around the pipe



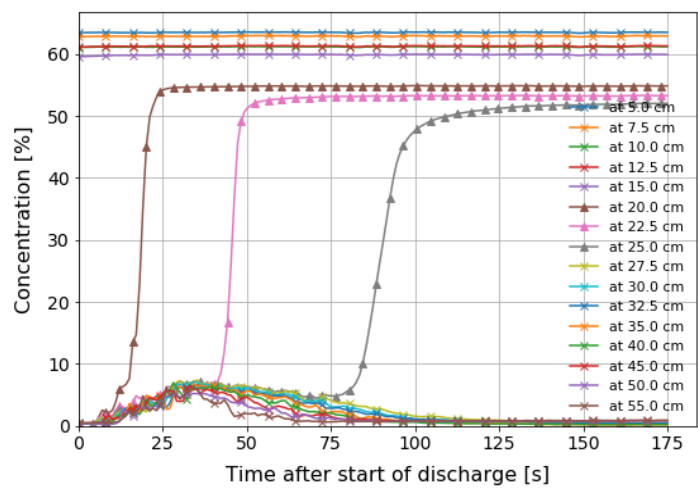
Flotation threshold



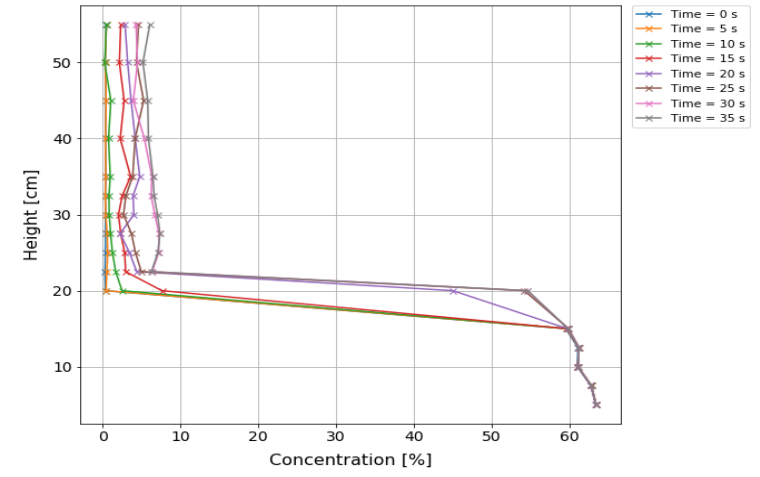
Test	Qcal [L/s]	t <sub>dis</sub> [s]	Δh [cm]	c <sub>dis</sub> [%]	c <sub>max</sub> [%]	S <sub>pipe</sub>	S <sub>dp</sub>	S <sub>con,a</sub>	Flotation	dis,max [cm]	ΔP <sub>dp,bottom</sub> [kPa]	ΔP <sub>dp,top</sub> [kPa]
VNW43	1,90	25	4,35	25,9%	7,4%	1,08	1,068	1,098	No	0,4	0,273	0,213

Upwards discharge  
No elevation  
SG<sub>p</sub> = 1.08

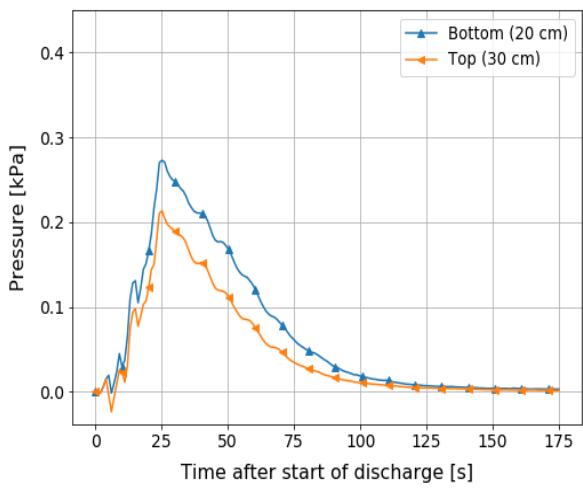
Concentration over time at different levels



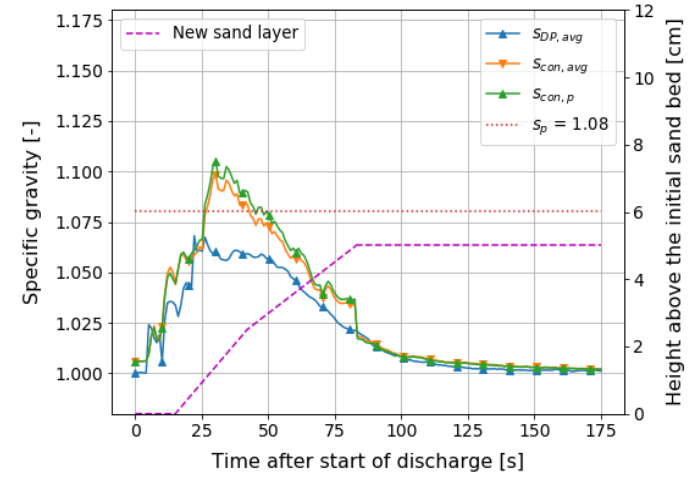
Increasing concentration along height over time



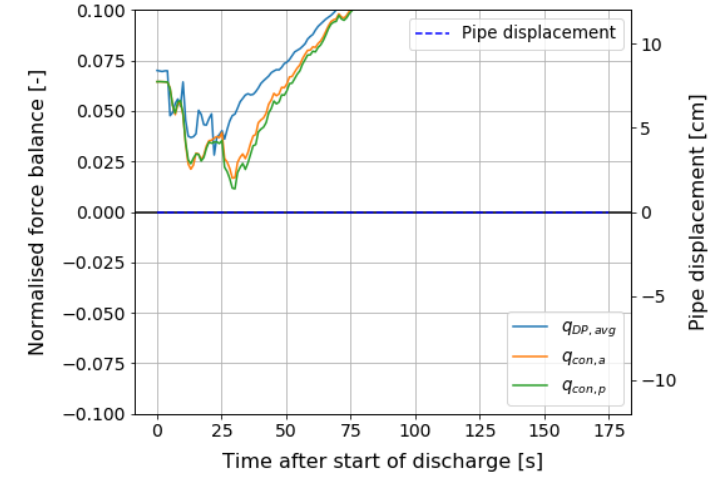
DP net increment at height of the pipe



Specific gravity of the mixture around the pipe



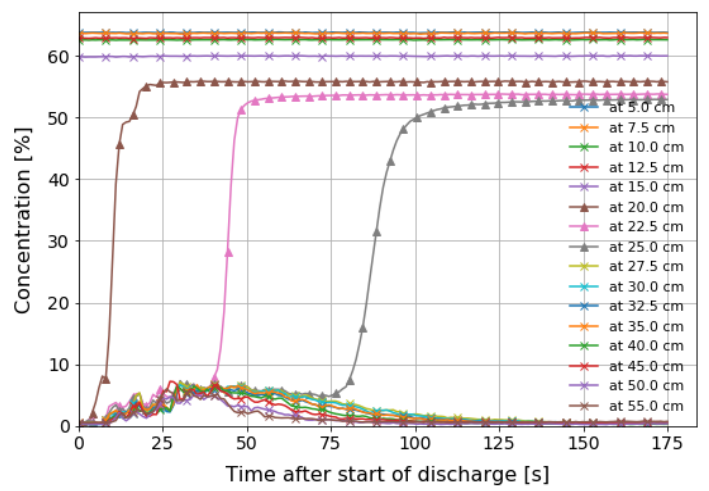
Flotation threshold



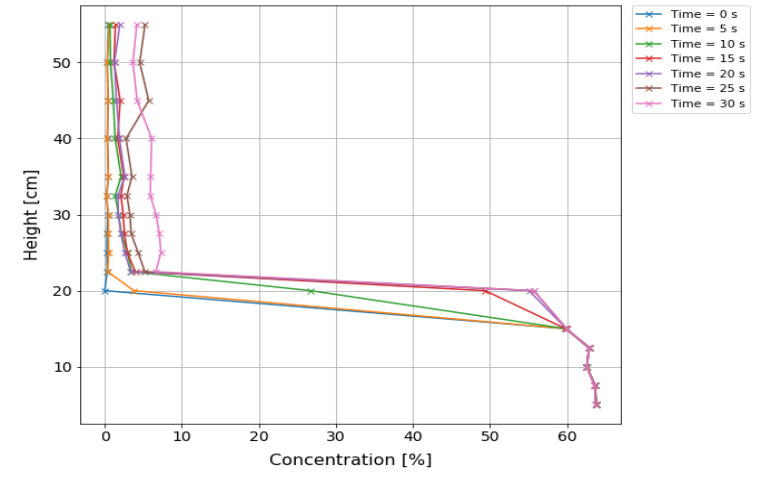
Test	Qcal [L/s]	tdis [s]	$\Delta h$ [cm]	cdis [%]	cmax [%]	Spipe	Sdp	Scon,a	Flotation	dis,max [cm]	$\Delta Pdp, \text{bottom}$ [kPa]	$\Delta Pdp, \text{top}$ [kPa]
VNW44	1,98	26	4,30	23,1%	7,3%	1,08	1,080	1,095	No	0	0,276	0,211

Upwards discharge  
No elevation  
SGp = 1.08

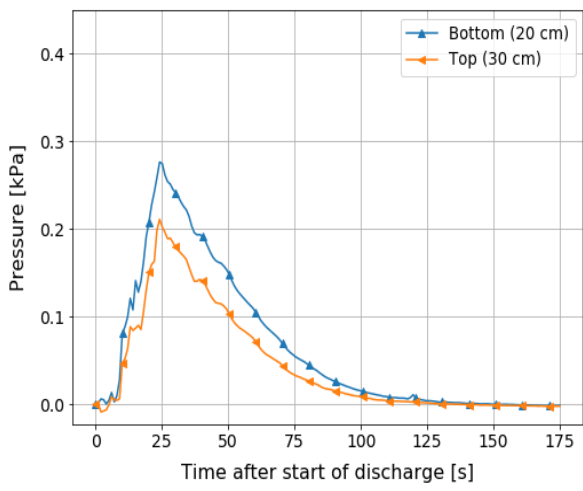
Concentration over time at different levels



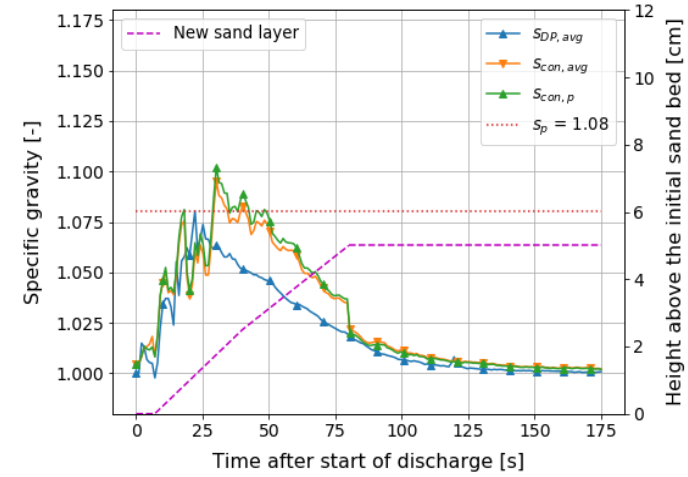
Increasing concentration along height over time



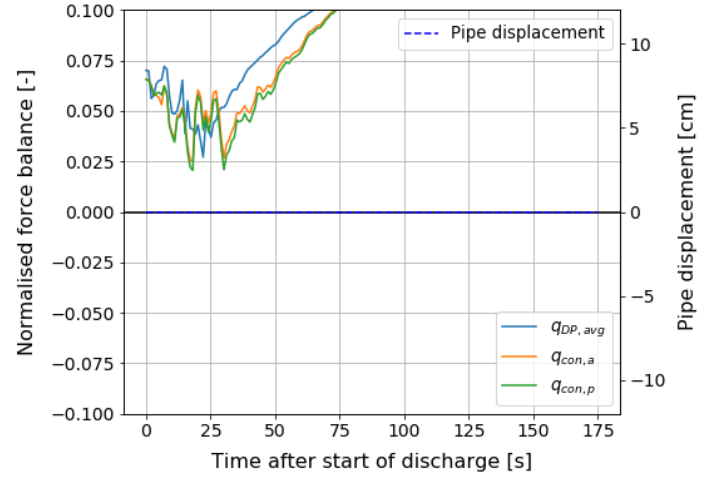
DP net increment at height of the pipe



Specific gravity of the mixture around the pipe



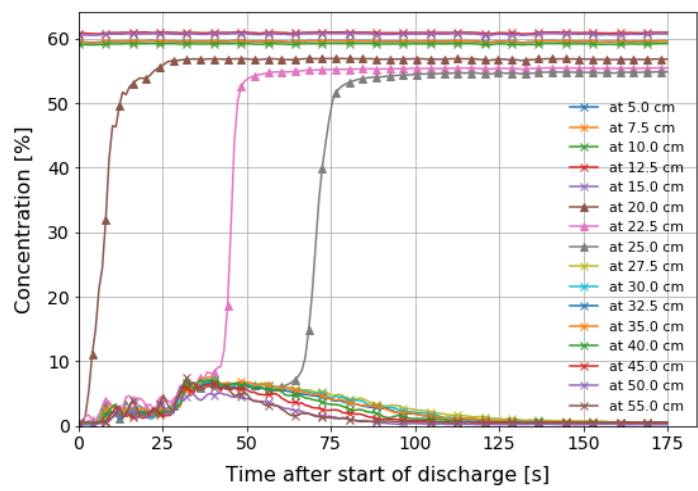
Flotation threshold



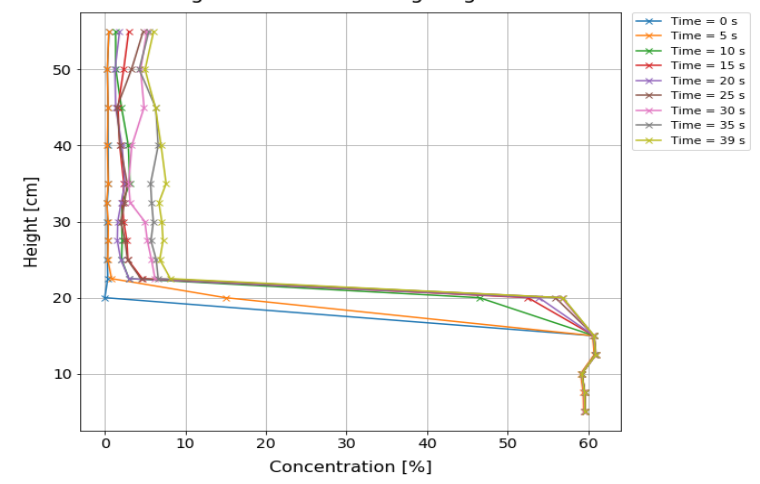
Test	Qcal [L/s]	tdis [s]	$\Delta h$ [cm]	cdis [%]	cmax [%]	Spipe	Sdp	Scon,a	Flotation	dis,max [cm]	$\Delta Pdp, \text{bottom}$ [kPa]	$\Delta Pdp, \text{top}$ [kPa]
VNW45	2,08	30	5,10	23,2%	7,6%	1,08	1,079	1,087	No	0,4	0,318	0,245

Upwards discharge  
No elevation  
SGp = 1.08

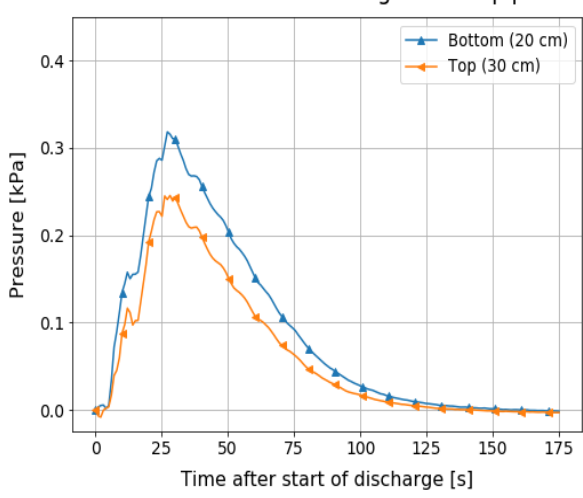
Concentration over time at different levels



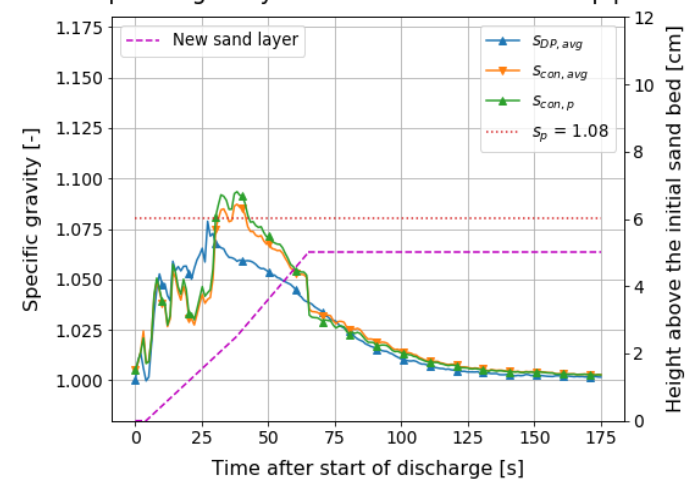
Increasing concentration along height over time



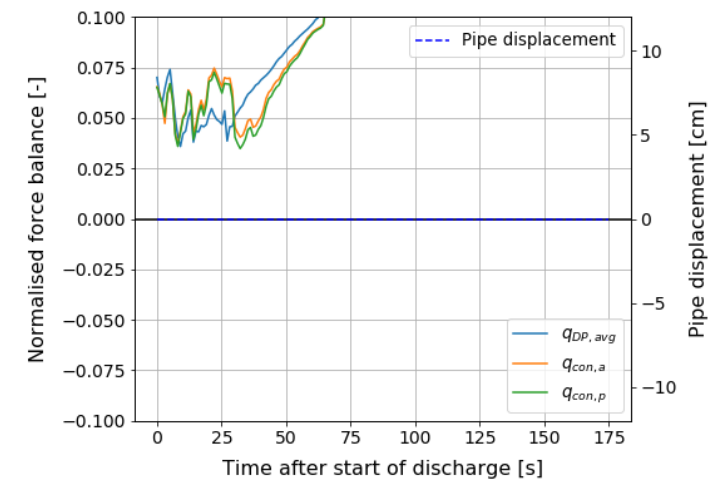
DP net increment at height of the pipe



Specific gravity of the mixture around the pipe



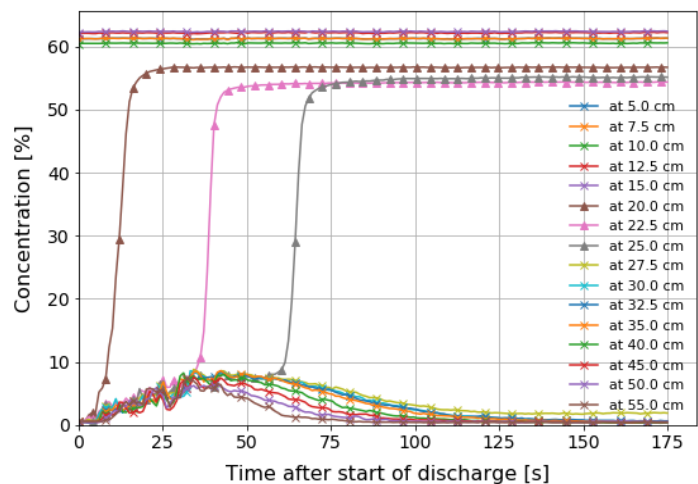
Flotation threshold



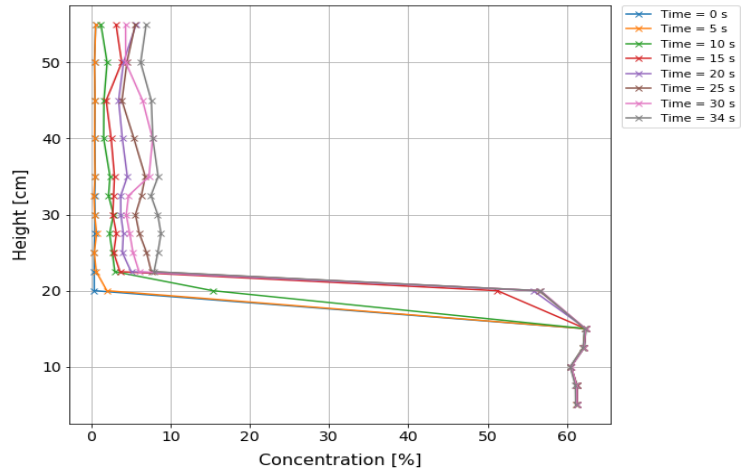
Test	Qcal [L/s]	tdis [s]	$\Delta h$ [cm]	cdis [%]	cmax [%]	Spipe	Sdp	Scon,a	Flotation	dis,max [cm]	$\Delta Pdp, \text{bottom}$ [kPa]	$\Delta Pdp, \text{top}$ [kPa]
VNW46	2,01	30	5,65	26,5%	8,8%	1,08	1,097	1,106	No	0	0,378	0,283

Upwards discharge  
No elevation  
SGp = 1.08

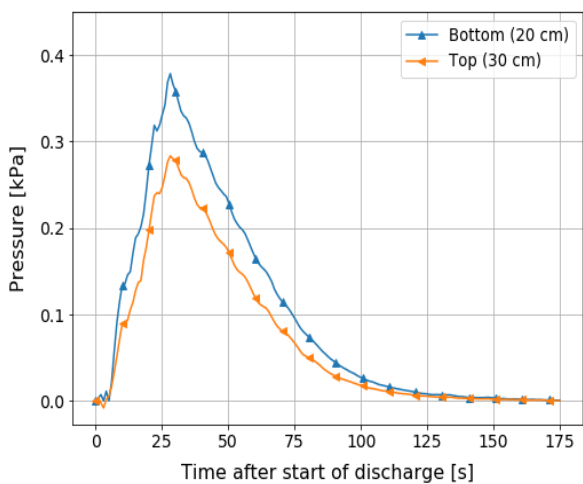
Concentration over time at different levels



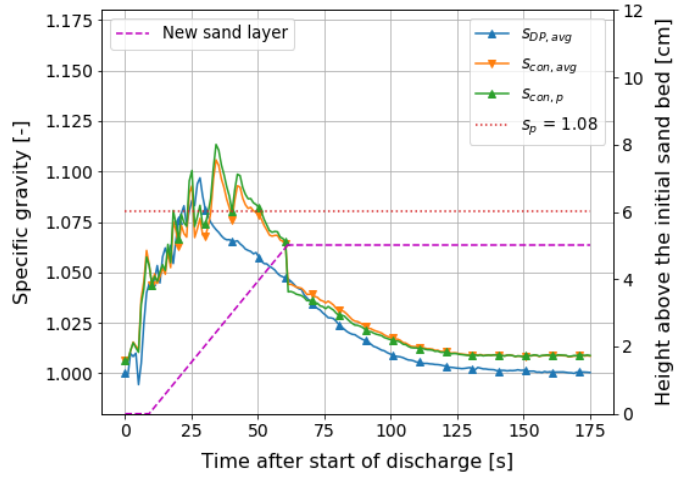
Increasing concentration along height over time



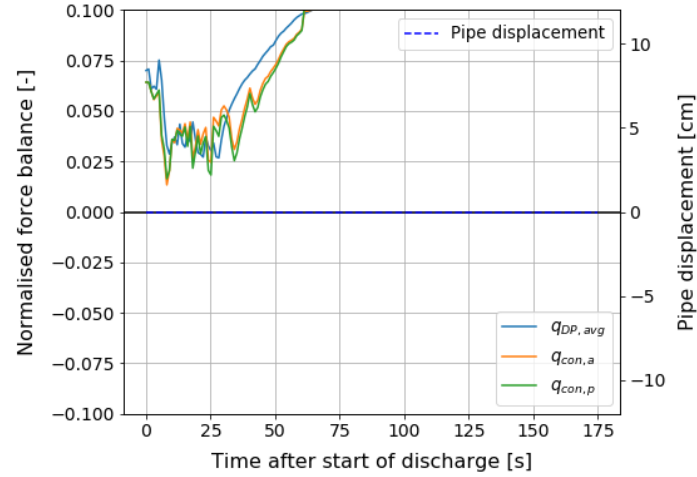
DP net increment at height of the pipe



Specific gravity of the mixture around the pipe



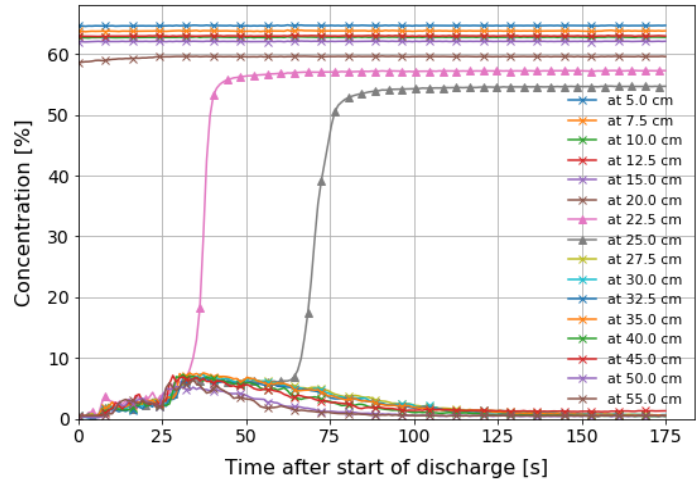
Flotation threshold



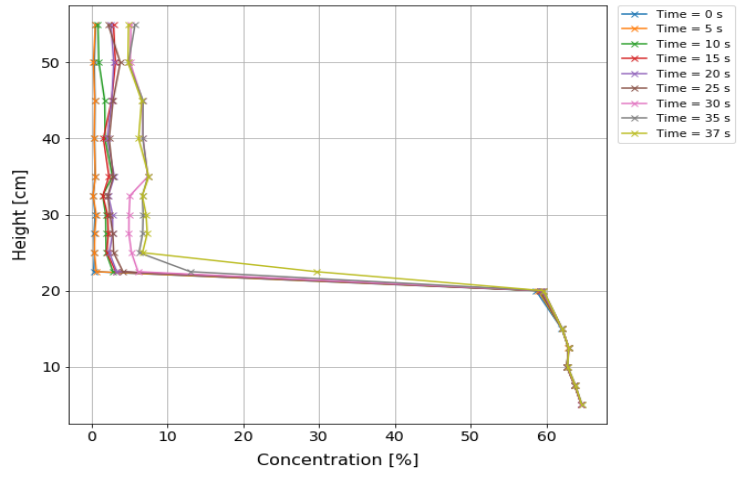
Test	Qcal [L/s]	t <sub>dis</sub> [s]	Δh [cm]	c <sub>dis</sub> [%]	c <sub>max</sub> [%]	S <sub>pipe</sub>	S <sub>dp</sub>	S <sub>con,a</sub>	Flotation	dis,max [cm]	ΔP <sub>dp,bottom</sub> [kPa]	ΔP <sub>dp,top</sub> [kPa]
VNH47	2,09	26	4,55	24,0%	7,6%	1,12	1,072	1,083	No	0	0,294	0,224

Upwards discharge  
No elevation  
SG<sub>p</sub> = 1.12

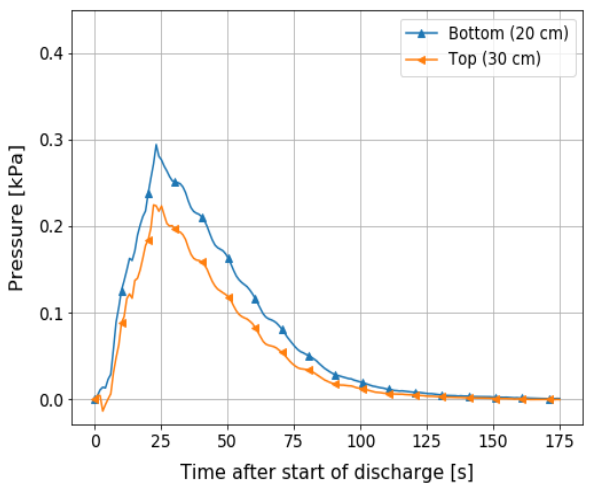
Concentration over time at different levels



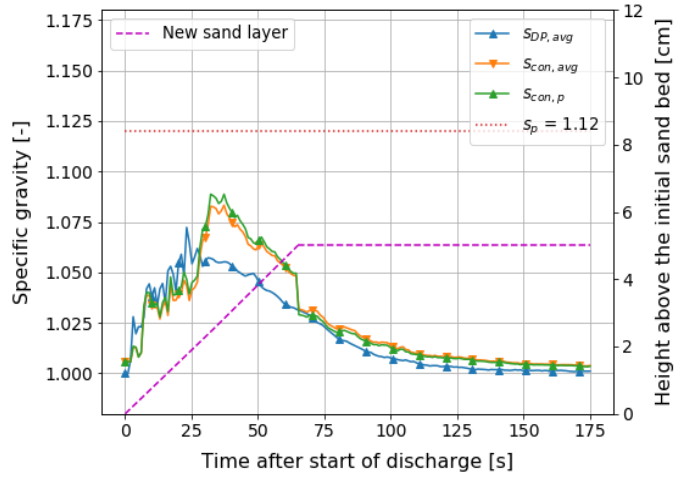
Increasing concentration along height over time



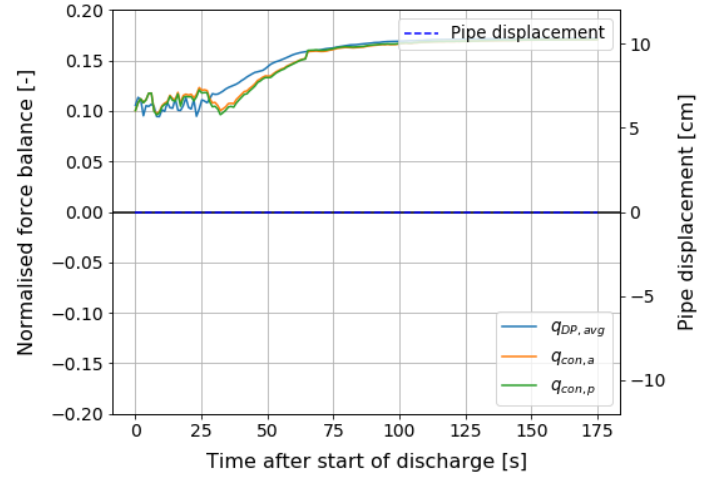
DP net increment at height of the pipe



Specific gravity of the mixture around the pipe



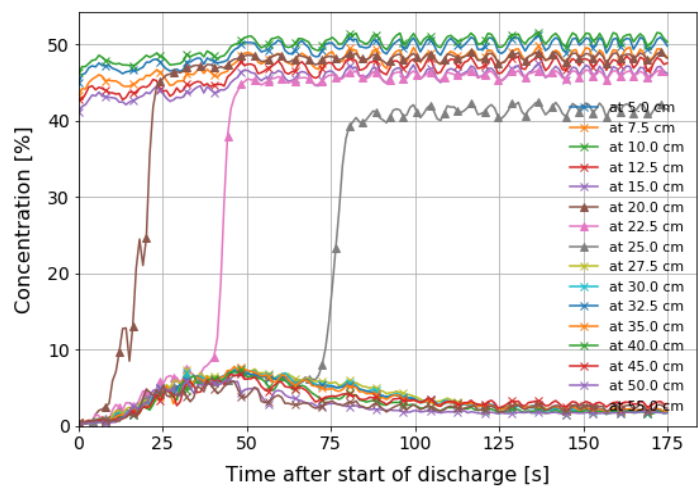
Flotation threshold



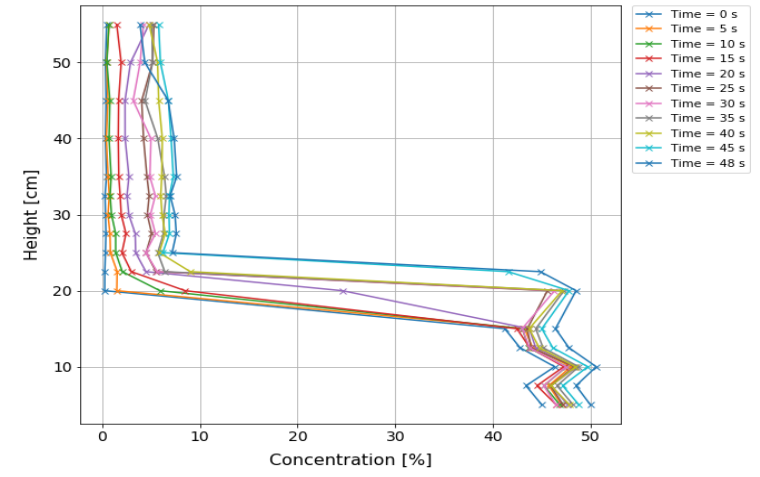
Test	Qcal [L/s]	t <sub>dis</sub> [s]	Δh [cm]	c <sub>dis</sub> [%]	c <sub>max</sub> [%]	S <sub>pipe</sub>	S <sub>dp</sub>	S <sub>con,a</sub>	Flotation	dis,max [cm]	ΔP <sub>dp,bottom</sub> [kPa]	ΔP <sub>dp,top</sub> [kPa]
VNH48	1,90	30	5,00	24,3%	7,8%	1,12	1,086	1,094	No	0	0,314	0,230

Upwards discharge  
No elevation  
SG<sub>p</sub> = 1.12

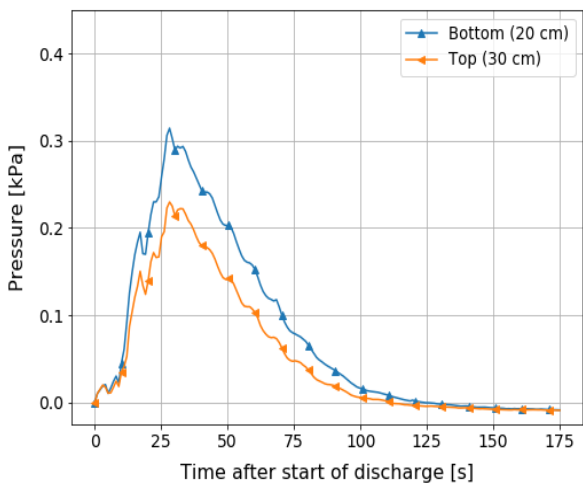
Concentration over time at different levels



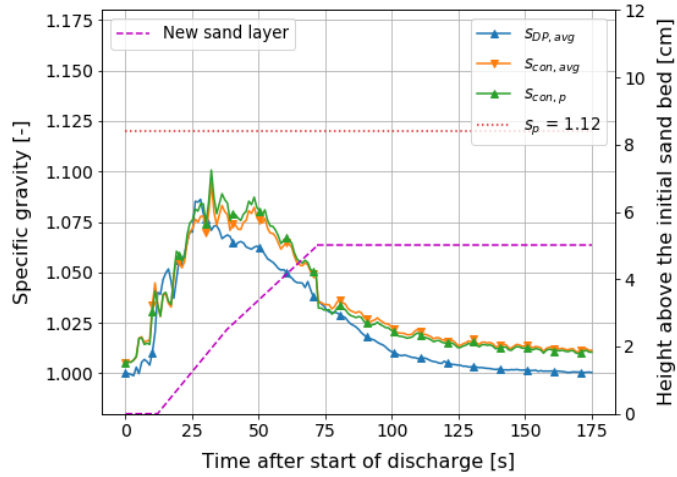
Increasing concentration along height over time



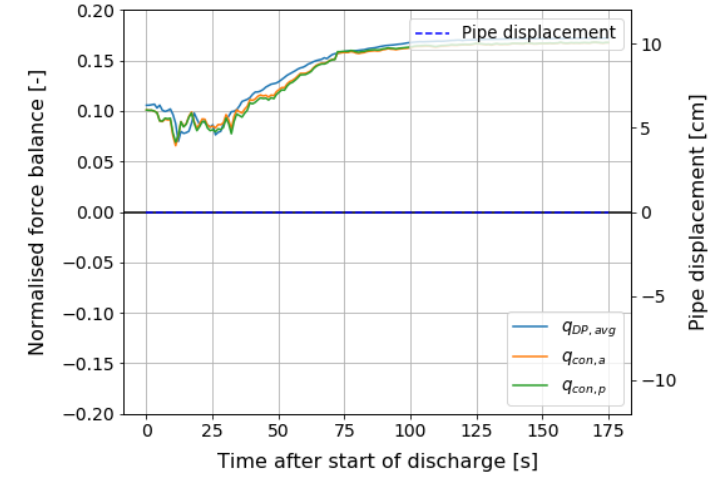
DP net increment at height of the pipe



Specific gravity of the mixture around the pipe



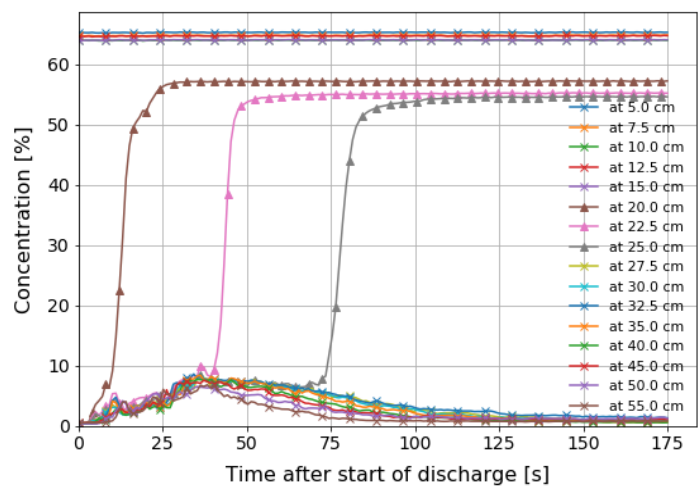
Flotation threshold



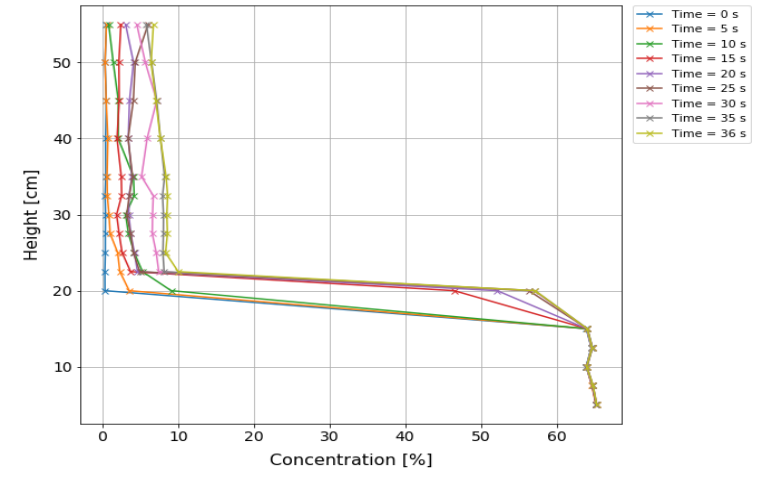
Test	Qcal [L/s]	tdis [s]	$\Delta h$ [cm]	cdis [%]	cmax [%]	Spipe	Sdp	Scon,a	Flotation	dis,max [cm]	$\Delta Pdp, bottom$ [kPa]	$\Delta Pdp, top$ [kPa]
VNH49	2,18	26	5,08	24,8%	8,6%	1,12	1,076	1,105	No	0	0,335	0,260

Upwards discharge  
No elevation  
SGp = 1.12

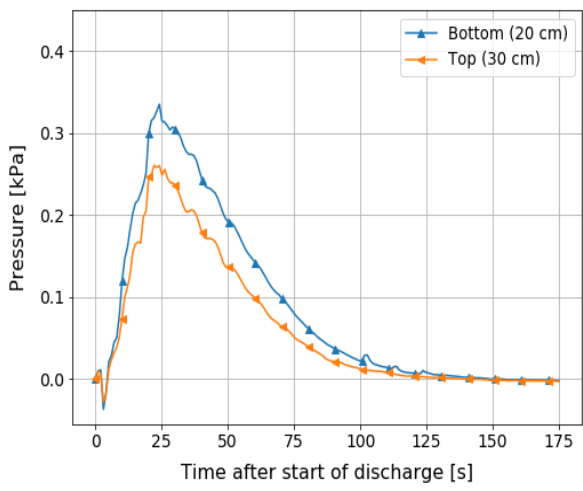
Concentration over time at different levels



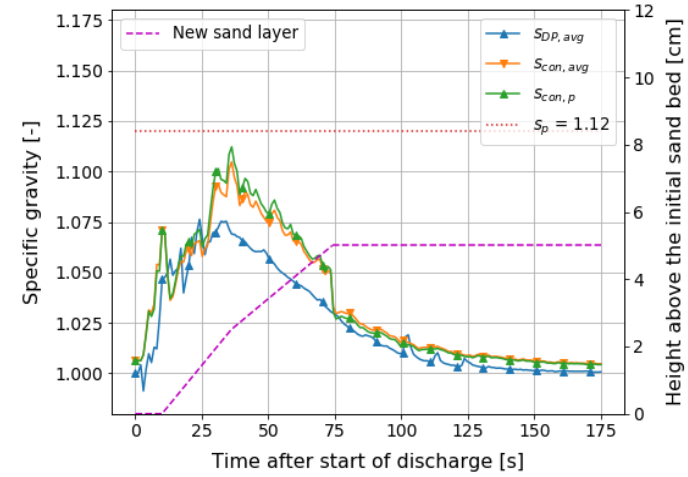
Increasing concentration along height over time



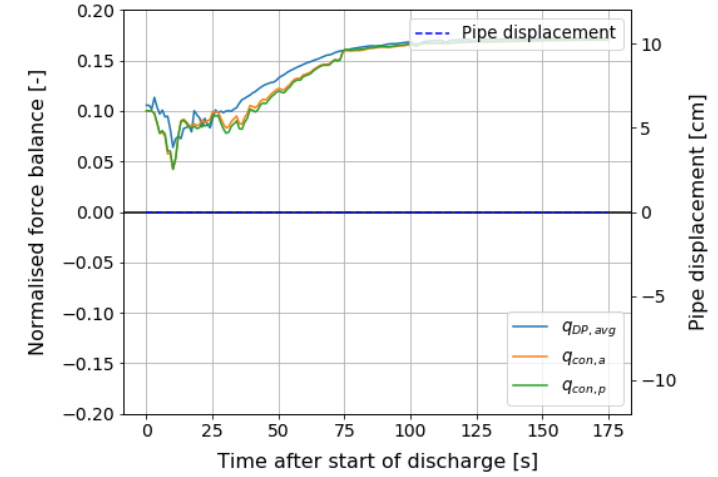
DP net increment at height of the pipe



Specific gravity of the mixture around the pipe



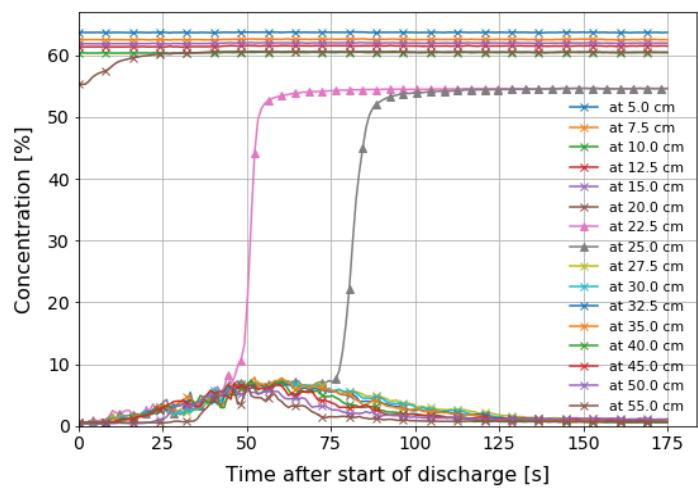
Flotation threshold



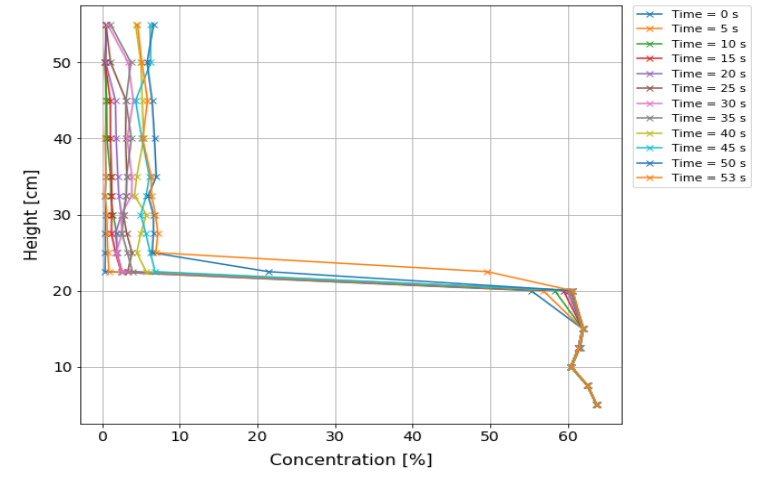
Test	Qcal [L/s]	t <sub>dis</sub> [s]	Δh [cm]	c <sub>dis</sub> [%]	c <sub>max</sub> [%]	S <sub>pipe</sub>	S <sub>dp</sub>	S <sub>con,a</sub>	Flotation	dis,max [cm]	ΔP <sub>dp,bottom</sub> [kPa]	ΔP <sub>dp,top</sub> [kPa]
VNH50	1,23	44	5,08	26,4%	7,9%	1,12	1,125	1,084	No	0	0,302	0,183

Upwards discharge  
No elevation  
SG<sub>p</sub> = 1.12

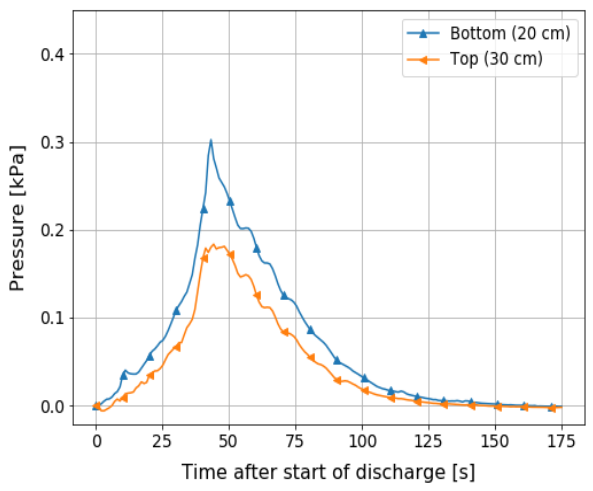
Concentration over time at different levels



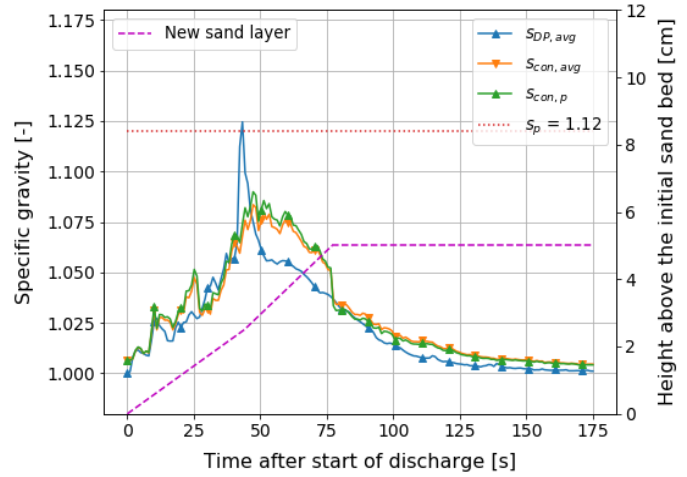
Increasing concentration along height over time



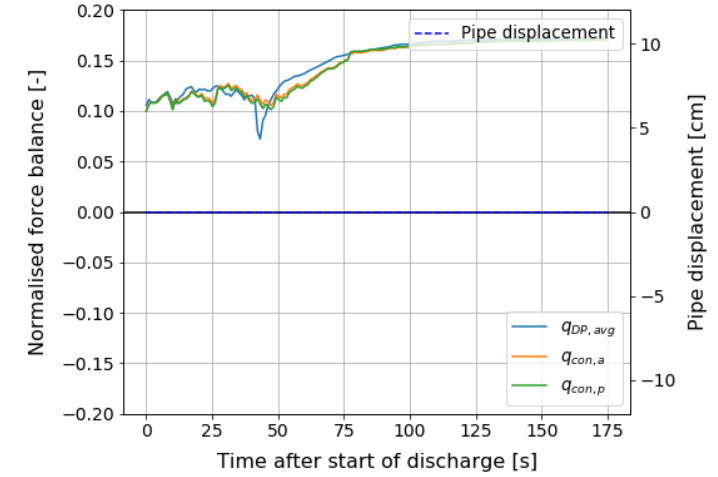
DP net increment at height of the pipe



Specific gravity of the mixture around the pipe



Flotation threshold

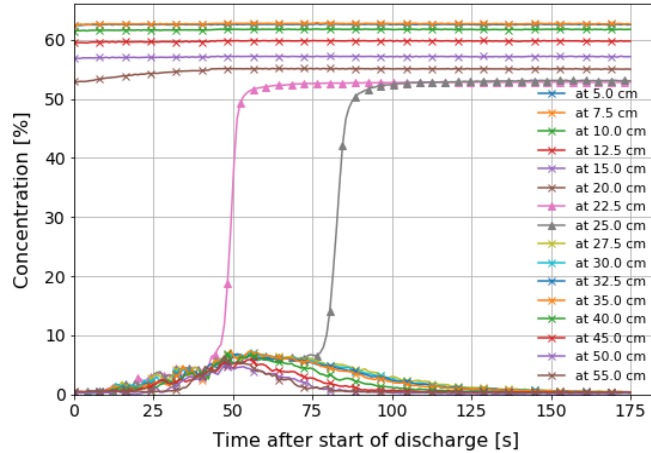


# Pure deposition tests

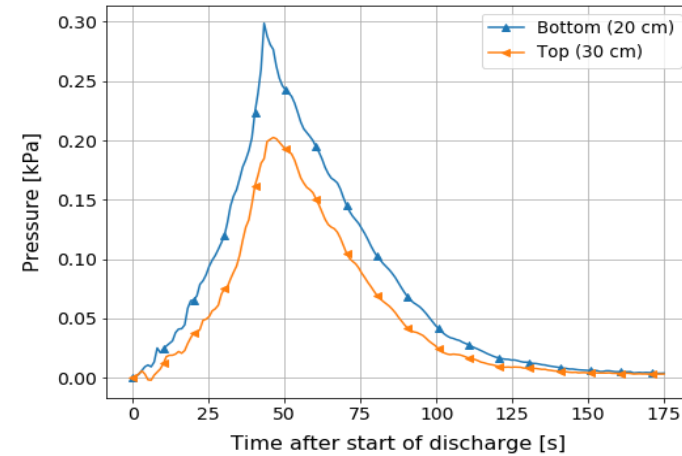
Test	Qcal [L/s]	time dis [s]	$\Delta h$ [cm]	cdis [%]	cmax [%]	Sdp	Scon,a	$\Delta P_{dp,bottom}$ [kPa]	$\Delta P_{dp,top}$ [kPa]
1	1,25	45	4,88	24,0%	7,5%	1,116	1,079	0,299	0,203
2	1,24	57	6,25	24,8%	7,5%	1,089	1,078	0,301	0,222
3	1,20	50	4,95	23,4%	7,5%	1,073	1,074	0,268	0,196
4	1,33	54	7,33	29,1%	8,1%	1,124	1,083	0,377	0,265

Test	Qcal [L/s]	time dis [s]	$\Delta h$ [cm]	cdis [%]	cmax [%]	Sdp	Scon,a	$\Delta Pdp, bottom$ [kPa]	$\Delta Pdp, top$ [kPa]
1	1,25	45	4,88	24,0%	7,5%	1,116	1,079	0,299	0,203

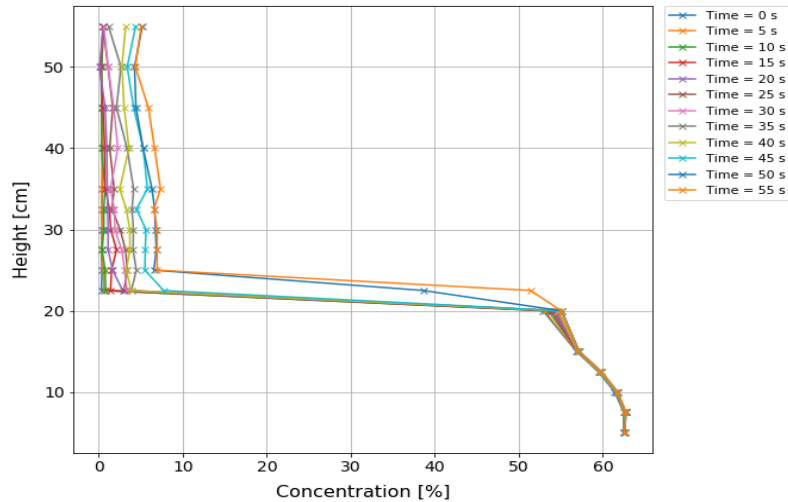
Concentration over time at different levels



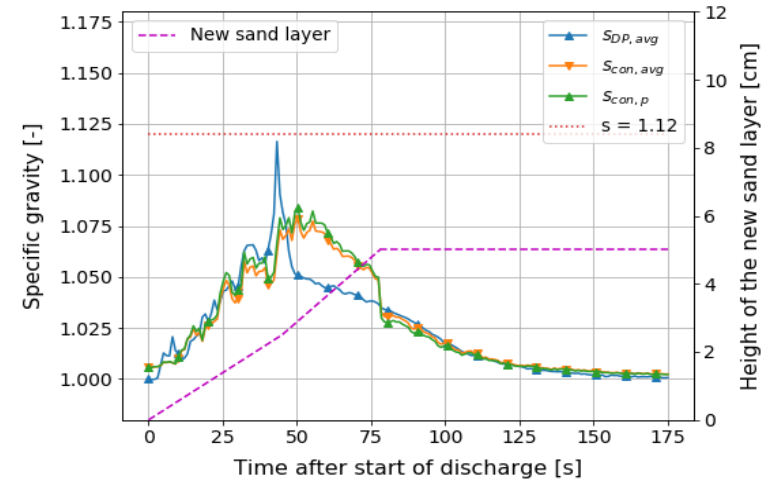
DP net increment at height of the pipe



Increasing concentration along height over time

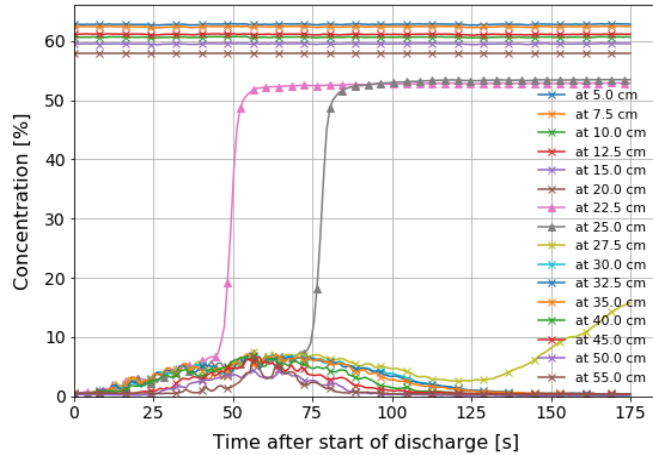


Specific gravity of the mixture around the pipe

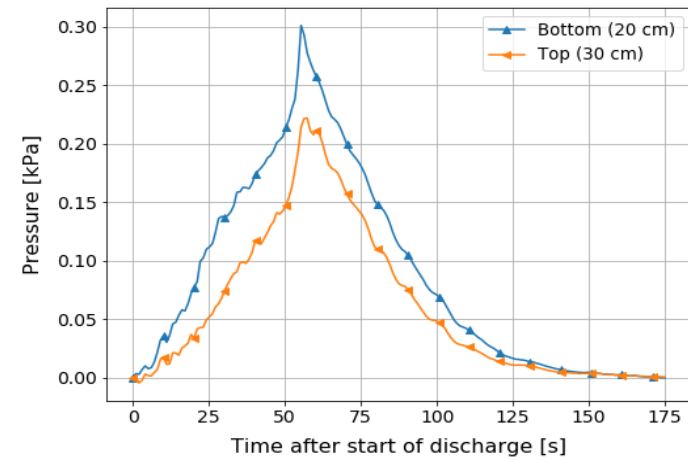


Test	Qcal [L/s]	time dis [s]	$\Delta h$ [cm]	cdis [%]	cmax [%]	Sdp	Scon,a	$\Delta Pdp, \text{bottom}$ [kPa]	$\Delta Pdp, \text{top}$ [kPa]
2	1,24	57	6,25	24,8%	7,5%	1,089	1,078	0,301	0,222

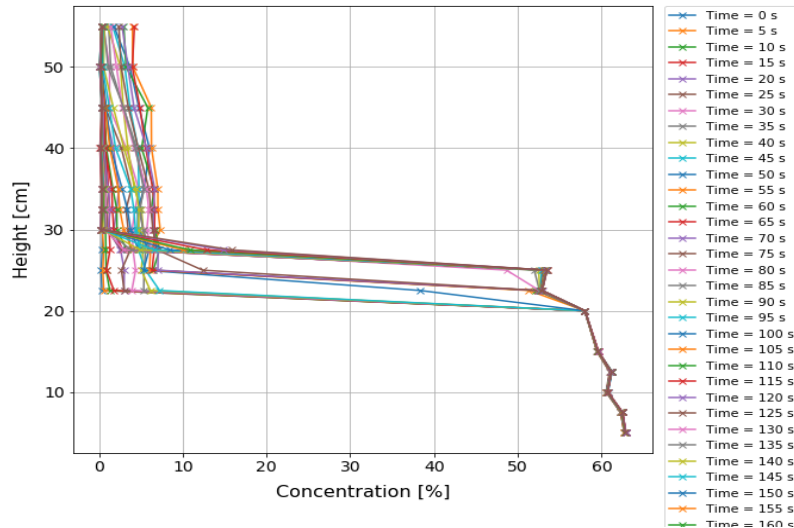
Concentration over time at different levels



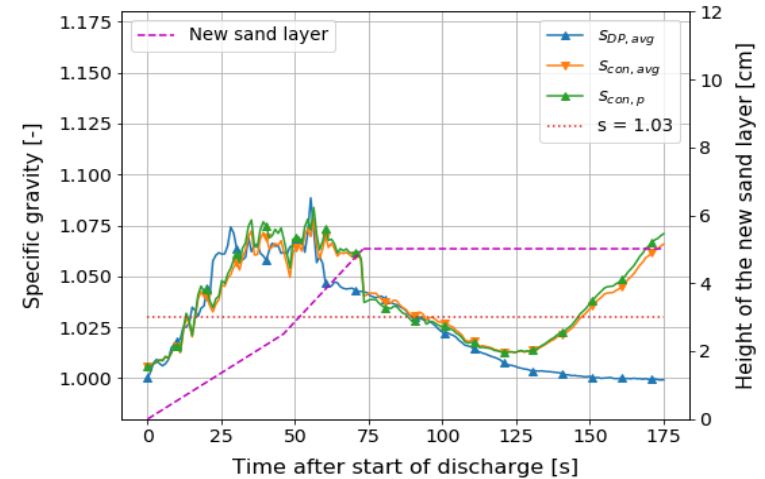
DP net increment at height of the pipe



Increasing concentration along height over time

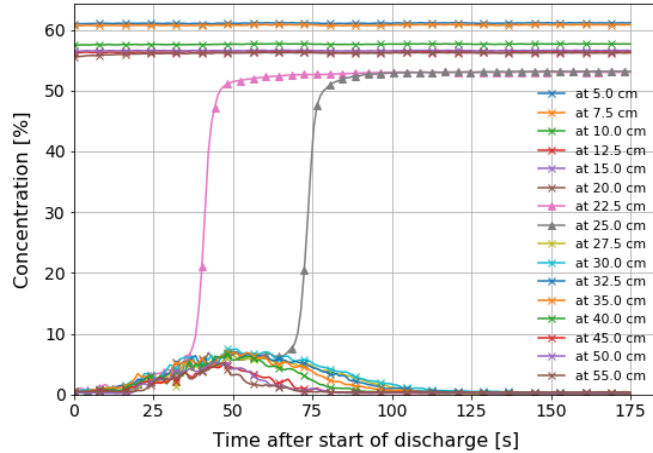


Specific gravity of the mixture around the pipe

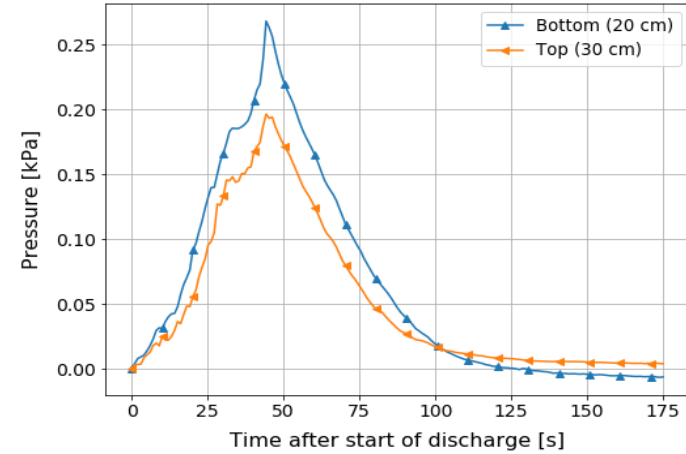


Test	Qcal [L/s]	time dis [s]	$\Delta h$ [cm]	cdis [%]	cmax [%]	Sdp	Scon,a	$\Delta Pdp, bottom$ [kPa]	$\Delta Pdp, top$ [kPa]
3	1,20	50	4,95	23,4%	7,5%	1,073	1,074	0,268	0,196

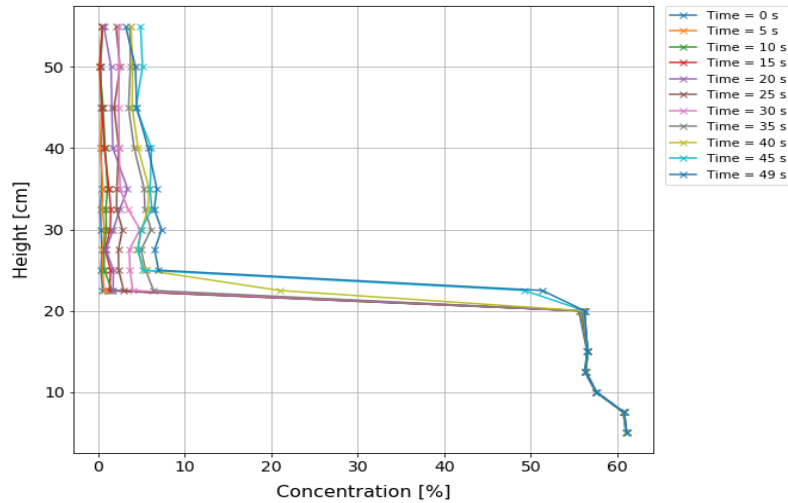
Concentration over time at different levels



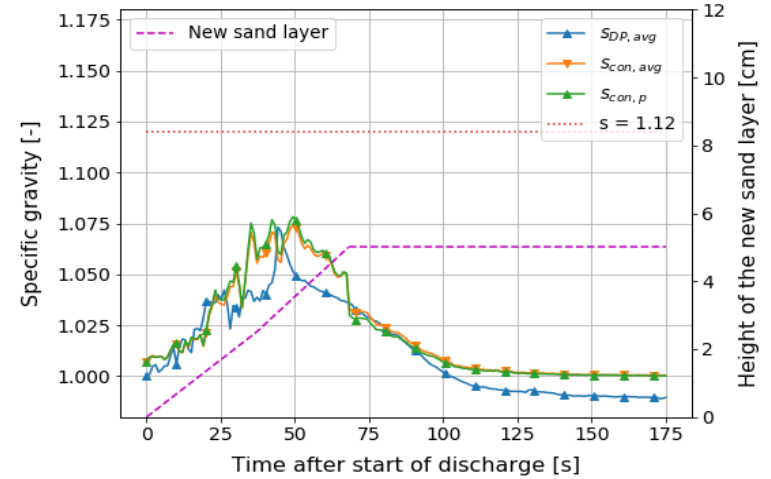
DP net increment at height of the pipe



Increasing concentration along height over time

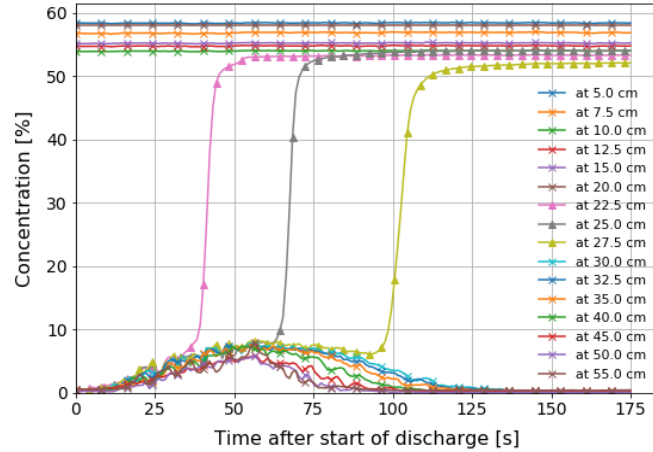


Specific gravity of the mixture around the pipe

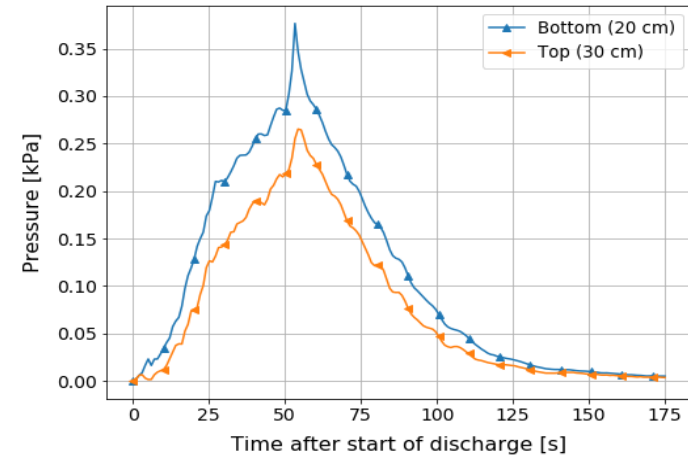


Test	Qcal [L/s]	time dis [s]	$\Delta h$ [cm]	cdis [%]	cmax [%]	Sdp	Scon,a	$\Delta Pdp, bottom$ [kPa]	$\Delta Pdp, top$ [kPa]
4	1,33	54	7,33	29,1%	8,1%	1,124	1,083	0,377	0,265

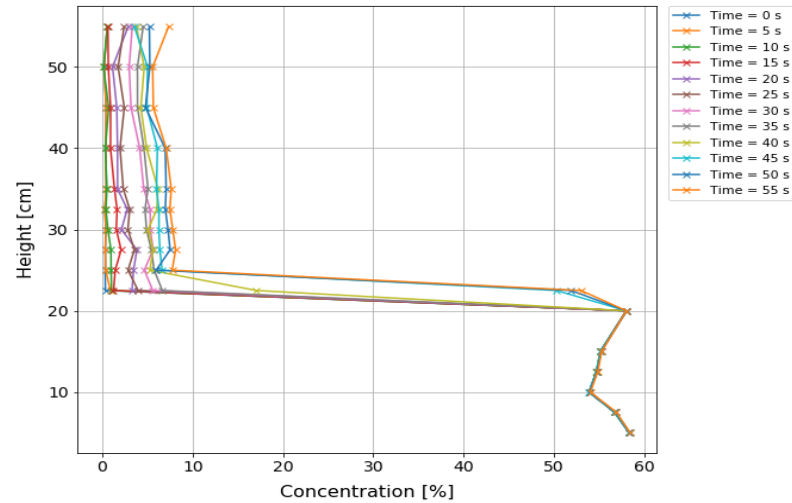
Concentration over time at different levels



DP net increment at height of the pipe



Increasing concentration along height over time



Specific gravity of the mixture around the pipe

